DESIGN AND DEVELOPMENT OF NEW INDOLE BASED SENSITIZERS FOR DYE-SENSITIZED SOLAR CELLS

Thesis

Submitted in partial fulfillment of the requirements for the degree of

DOCTOR OF PHILOSOPHY

by

DICKSON D. BABU

DEPARTMENT OF CHEMISTRY

NATIONAL INSTITUTE OF TECHNOLOGY KARNATAKA

SURATHKAL, MANGALORE - 575 025

February, 2016

DECLARATION

By the Ph.D. Research Scholar

I hereby declare that the Research Thesis entitled **"Design and Development of New Indole Based Sensitizers for Dye Sensitized Solar Cells"** which is being submitted to the **National Institute of Technology Karnataka, Surathkal** in partial fulfillment of the requirements for the award of the degree of **Doctor of Philosophy** in **Chemistry** is a *bonafide report of the research work carried out by me*. The material contained in this Research Thesis has not been submitted to any University or Institution for the award of any degree.

Dickson D. Babu

Reg. No. CY12F01

Department of Chemistry

Place: NITK -Surathkal

Date:

CERTIFICATE

This is to *certify* that the Research Thesis entitled **"Design and Development of New Indole Based Sensitizers for Dye Sensitized Solar Cells"** submitted by **Mr. Dickson D. Babu** (Register Number: CY12F01) as the record of the research work carried out by him is *accepted as the Research Thesis submission* in partial fulfillment of the requirements for the award of degree of Doctor of Philosophy.

Prof. A. Vasudeva Adhikari

Research Guide

Date:

Chairman - DRPC

Date:

DEDICATED TO MY

BELOVED PARENTS

ACKNOWLEDGEMENTS

Although only my name appears on the cover of this thesis, a lot of people have made their sincere contributions towards this research. I am grateful to every individual who has contributed in their own capacities to make this dissertation possible. First and foremost, I thank the almighty **GOD** for instilling a curious sprit in me and giving me the patience, wisdom and strength to successfully complete this thesis.

I would like to express my deep sense of gratitude to my research supervisor **Prof. A. Vasudeva Adhikari**, Department of Chemistry, NITK for his invaluable guidance and help rendered throughout the course of this investigation. He has given me the freedom to explore the research topic on my own and did the appropriate course correction when my steps faltered. The direction he gave and knowledge he shared in each and every single step of this work made it all possible. I am extremely thankful to him for all the help he provided during my research.

I express my earnest thanks to the RPAC members, **Prof. B.R. Bhat**, Chemistry Department and **Dr. P. E. Jagadeeshbabu**, Chemical Engineering Department, NITK for their insightful comments and constructive criticism towards the improvement of research quality.

I sincerely thank **Prof. Swapan Bhattacharya**, Director, NITK and **Prof. B.R. Bhat**, Head, Chemistry Department for providing necessary facilities to carry out this research work. I am also thankful to the all the **Faculty** and **Non-teaching Staff** of the department for their constant support and encouragement.

My special thanks to **Dr. Joshy Joseph**, Scientist, CSIR-National Institute for Intersdisciplinary Science and Technology (CSIR-NIIST) for extending his lab facilities; **MIT, Manipal** for providing ^{1}H NMR and ^{13}C NMR. I remain thankful to **Prof. Ahmed El-Shafei**, North Carolina state university, USA and **Prof. S. Anandan**, National Institute of Technology, Trichy for providing DSSC fabrication studies.

I also thank my group members Dr. Vishnumurthy K.A., Dr. Shrikant, Dr. Ahipa T. N., Mr. Naveenchandra, Mr. Praveen Naik, Ms. Rajalakshmi K, and Mr. Vinayakumar for their regular help, suggestions and company. I am also grateful to my friend **Mr. Shameel T.** for all his help during the course of this work. Also, I would like to thank all the research scholar friends of Chemistry Department, NITK, for their constant help and support.

I would like to place it on record that, no combination of twenty-six alphabets can express my gratitude towards my father, **Mr**. **Babu D. T**. and mother, **Mrs. Lillykutty Babu,** for instilling in me the virtues of perseverance and commitment and relentlessly encouraging me to strive for excellence. I also thank my brother, **Mr. Jipson D. Babu** for his constant support, encouragement, love and bearing with all my idiosyncrasies. Finally, I thank all my **family members** and **friends** for their love and constant support.

Dickson D. Babu

ABSTRACT

Solar energy is regarded as the holy grail of renewables owing to its abundant availability and pollution-free character. The conversion efficiency of Si based cells is currently around 20%. But these cells are expensive and involve energy-intensive fabrication process. Further, their rigid shape confines them to specific applications. Ever since the pioneering report by O'Regan and Graztel in 1991, dye-sensitized solar cells (DSSCs) have emerged as credible alternative to conventional silicon-based solar cells due to their low cost, moderate efficiency and easy fabrication techniques. At present, there is a considerable interest among the researchers to develop new and efficient sensitizers for DSSC application. In this context, it was contemplated to design, synthesize and to investigate the photovoltaic performance of new indole based sensitizers and co-sensitizers.

Based on the detailed literature survey, new indole sensitizers were designed as potential sensitizers/co-sensitizers. They were later successfully synthesized following the appropriate synthetic routes. Further, their synthetic methods as well as purification techniques were established and their yields were optimized. Furthermore, their structures were confirmed by various spectral techniques. Finally, the target compounds were characterized for their optical, electrochemical and photovoltaic performance studies. The photovoltaic performance studies of the newly synthesized sensitizers reveal that molecules carrying 4-aminobenzoic acid exhibit better photovoltaic performance than their cyanoacetic acid based counterparts. Further, the devices fabricated by incorporating the aforementioned co-sensitizers exhibit superior performance than the cells fabricated using only the ruthenium based sensitizer. In addition, the effect of anchoring groups on the co-sensitizer performance has been investigated. The highest efficiency obtained by the sensitizers synthesized in this work is **4.12 %**, whereas, the highest efficiency obtained by a co-sensitized cell is **10.68%.**To sum up, new indole derivatives appeared as active templates for highly efficient metal-free sensitizers/co-sensitizers.

Keywords: DSSC; Indole; Suzuki coupling; Sensitizers; Co-sensitizers; Anchoring moieties; Photovoltaic; DFT.

CONTENTS

CHAPTER 1 **Page No.**

INTRODUCTION

PART A: AN OVERVIEW OF DYE SENSITIZED SOLAR CELLS 1

1.1 INTRODUCTION TO PHOTOVOLTAICS 1

1.2 SOLAR SPECTRUM 2

1.3 TYPES OF SOLAR CELLS 4

1.4 CURRENT PHOTOVOLTAIC TECHNOLOGY 5

1.5 DYE SENSITIZED SOLAR CELL (DSSC) 5

1.5.1 A brief history of DSSC 5

1.5.2 Working principles of DSSC 8

1.5.2.1 Short circuit photocurrent (J_{sc}) 10

1.5.2.2 Open circuit photovoltage (V_{oc}) 10

1.5.2.3 Fill factor (*ff*) 10

1.5.2.4 Incident photon to current conversion efficiency (IPCE) 10

1.5.2.5 Solar energy to electricity conversion efficiency (η) 11

1.5.3 Light harvesting 12

1.5.4 Electron injection 13

1.5.5 Charge transport 14

1.5.6 Charge recombination 15

1.5.6.1 Dye cation recombination 15

1.5.6.2 Redox mediator recombination 15

1.5.7 Charge collection 16

1.5.8 Efficiency of DSSC 17

1.6 COMPONENTS OF DSSC 17

1.6.1 Photosensitizers 17

1.6.2 Semiconductor photoanode 18

1.6.3 Transparent conducting substrate 20

1.6.4 Electrolyte 20

1.6.5 Counter electrode 22

1.7 CHARACTERIZATION OF DSSC 22

1.7.1 DSSC fabrication 22
1.7.2 Photovoltaic characterization 23
1.7.3 Electrochemical impedance spectroscopy characterization 23
1.7.4 Cyclic voltammetric measurements 23
1.7.5 FT-IR analysis: anchoring studies of the dyes on TiO_2 24
1.8 THEORETICAL CALCULATIONS 24
PART B: LITERATURE REVIEW, SCOPE, OBJECTIVES AND DESIGN OF NEW INDOLE BASED SENSITIZERS 24
1.9 LITERATURE REVIEW 24
1.9.1 Ruthenium based chromophores 25
1.9.2 Organic chromophores 27
1.9.2.1 Indole based sensitizers 28
1.9.2.2 Triphenylamine based sensitizers 31
1.9.2.3 Indoline based sensitizers 33
1.9.2.4 Cyanovinylene based sensitizers 35
1.9.2.5 Relay dyes 36
1.9.2.6 Co-sensitization 37
1.10 SCOPE AND OBJECTIVES OF THE PRESENT WORK 39
1.11 DYE DESIGN STRATEGY 40
CHAPTER 2
INDOLE BASED DYES WITH D-π-A CONFIGURATION: SYNTHESIS, CHARACTERIZATION AND PERFORMANCE STUDIES
2.1 INTRODUCTION 51
2.2 EXPERIMENTAL 52
2.2.1 Materials and methods 52
2.2.2 Synthesis of sensitizers **D_{1-3}** 52
2.2.3 Optical and electrochemical measurements 54
2.2.4 Theoretical calculations 54
2.2.5 DSSC fabrication 55
2.2.6 Synthetic methods 55
2.3 RESULTS AND DISCUSSION 59
2.3.1 Structural characterization 59
2.3.2 Crystal structure analysis 61

2.3.3 Photophysical properties 63
2.3.4 Molecular modeling 65
2.3.5 Electrochemical characterization 66
2.3.6 Photovoltaic device characterization 67
2.3.7 Electrochemical impedance spectroscopy characterization 69
2.4 CONCLUSIONS 71

CHAPTER 3

5-METHOXYINDOLE BASED DYES WITH D-D-A-π-A ARCHITECTURE: SYNTHESIS, CHARACTERIZATION AND PERFORMANCE STUDIES

3.1 INTRODUCTION 73
3.2 EXPERIMENTAL 74
3.2.1 Materials and methods 74
3.2.2 Synthesis of sensitizers **E_{1-3}** 74
3.2.3 Optical and electrochemical measurement 76
3.2.4 Theoretical calculations 76
3.2.5 DSSC fabrication 77
3.2.6 Synthetic methods 78
3.3 RESULTS AND DISCUSSION 81
3.3.1 Structural characterization 81
3.3.2 Photophysical properties 84
3.3.3 Molecular modeling 87
3.3.4 Electrochemical characterization 90
3.3.5 Photovoltaic device characterization 91
3.3.6 Electrochemical impedance spectroscopy characterization 94
3.3.7 FT-IR analysis: anchoring studies of the dyes on TiO_2 96
3.4 CONCLUSIONS 98

CHAPTER 4

5-NITROINDOLE BASED CHOMOPHORES WITH A-D-A-π-A CONFIGURATION: SYNTHESIS, CHARACTERIZATION AND PERFORMANCE EVALUATION

4.1 INTRODUCTION 99
4.2 EXPERIMENTAL 100
4.2.1 Materials and methods 100

4.2.2 Synthesis of sensitizers $\mathbf{N_{1-3}}$ 100
4.2.3 Optical, electrochemical and theoretical studies 102
4.2.4 DSSC fabrication 102
4.2.5 Synthetic methods 102
4.3 RESULTS AND DISCUSSION 106
4.3.1 Structural characterization 106
4.3.2 Photophysical properties 109
4.3.3 Molecular modeling 113
4.3.4 Electrochemical characterization 116
4.3.5 Photovoltaic device characterization 118
4.3.6 Electrochemical impedance spectroscopy characterization 124
4.3.7 FT-IR analysis: anchoring studies of the dyes on TiO_2 126
4.4 CONCLUSIONS 128

CHAPTER 5

INDOLE BASED SENSITIZERS CARRYING TRIPHENYL AMINE MOIETY: SYNTHESIS, CHARACTERIZATION AND PERFORMANCE EVALUATION

5.1 INTRODUCTION 129
5.2 EXPERIMENTAL 130
5.2.1 Materials and methods 130
5.2.2 Synthesis of co-sensitizers 130
5.2.3 Optical, electrochemical and theoretical studies 132
5.2.4 DSSC fabrication 132
5.2.5 Synthetic methods 132
5.3 RESULTS AND DISCUSSION 135
5.3.1 Structural characterization 135
5.3.2 Crystal structure analysis 139
5.3.3 Photophysical properties 141
5.3.4 Molecular modeling 145
5.3.5 Electrochemical characterization 147
5.3.6 Photovoltaic device characterization 149
5.3.7 Electrochemical impedance spectroscopy characterization 155
5.3.8 FT-IR analysis: anchoring studies of the dyes on TiO_2 156

5.4 CONCLUSIONS 159

CHAPTER 6

INDOLE BASED CO-SENSITIZERS WITH D-D-A CONFIGURATION: SYNTHESIS, CHARACTERIZATION AND PERFORMANCE STUDIES

6.1 INTRODUCTION 161

6.2 EXPERIMENTAL 162

6.2.1 Materials and methods 162

6.2.2 Synthesis of co-sensitizers 162

6.2.3 Optical, electrochemical and theoretical studies 164

6.2.4 DSSC fabrication 164

6.2.5 Synthetic methods 164

6.3 RESULTS AND DISCUSSION 168

6.3.1 Structural characterization 168

6.3.2 Photophysical properties 171

6.3.3 Molecular modeling 173

6.3.4 Electrochemical characterization 176

6.3.5 Photovoltaic device characterization 178

6.3.6 Electrochemical impedance spectroscopy characterization 181

6.4 CONCLUSIONS 183

CHAPTER 7

AN INDOLE BASED CO-SENSITIZER CARRYING DUAL ANCHORING GROUPS: SYNTHESIS, CHARACTERIZATION AND PHOTOVOLTAIC EVALUATION

7.1 INTRODUCTION 185

7.2 EXPERIMENTAL 186

7.2.1 Materials and methods 186

7.2.2 Synthesis of co-sensitizer 186

7.2.3 Optical, electrochemical and theoretical studies 187

7.2.4 DSSC fabrication 188

7.2.5 Synthetic methods 188

7.3 RESULTS AND DISCUSSION 190

7.3.1 Structural characterization 190

7.3.2 Photophysical properties 193

7.3.3 Molecular modeling 196
7.3.4 Electrochemical characterization 199
7.3.5 Photovoltaic device characterization 200
4.3.6 Electrochemical impedance spectroscopy characterization 203
7.4 CONCLUSIONS 205

CHAPTER 8
SUMMARY AND CONCLUSIONS

8.1 SUMMARY 207
8.2 CONCLUSIONS 209
8.3 SCOPE FOR FUTURE WORK 211

REFERENCES 213
LIST OF PUBLICATIONS 229
CURICULUM VITAE 231

LIST OF ABBREVIATIONS

ACN	Acetonitrile
CV	Cyclic voltammetry
$CHCl_3$	Chloroform
DFT	Density functional theory
DMF	*N*, *N*-Dimethylformamide
DMSO	Dimethyl sulfoxide
DSSC	Dye-sensitized solar cell
EIS	Electrochemical Impedance spectroscopy
FTIR	Fourier transform infrared spectroscopy
FTO	Fluorine doped tin oxide
HOMO	Highest occupied molecular orbital
IPCE	Incident photon to current conversion efficiency
J_{sc}	Short circuit current
LHE	Light harvesting efficiency
LUMO	Lowest unoccupied molecular orbital
MS	Mass spectrometry
NMR	Nuclear magnetic resonance
PV	Photovoltaics
RT	Room temperature
RTIL	Room temperature ionic liquids
SCXRD	Single crystal X-ray diffraction
TDFT	Time-dependent density functional theory
THF	Tetrahydrofuran
V_{oc}	Open circuit voltage

CHAPTER 1

INTRODUCTION

Abstract

Chapter 1 *begins with a brief introduction to photovoltaics followed by an account on dye-sensitized solar cells. Also, it covers description on various components of DSSCs. Further, it includes a concise account of reported literature on design and synthesis of various types of sensitizers and co-sensitizers. Furthermore, the chapter covers scope and objectives of the present research work, arrived at on the basis of detailed literature survey. Finally, it comprises a brief account on design of new sensitizers and co-sensitizers.*

PART A: AN OVERVIEW OF DYE SENSITIZED SOLAR CELLS

1.1 INTRODUCTION TO PHOTOVOLTAICS

Ever increasing energy demand, continuous depletion of non-renewable resources, and the drastic climate changes across the globe have forced us to start looking for alternative, abundant and clean sources of energy; and what better way of producing energy than harvesting it directly from the biggest nuclear reactor of our solar system – Sun. As the need for alternative sources of energy is increasing, photovoltaic energy conversion provides the best option. Solar radiation amounts to 3.8 million EJ/year (1EJ=1018J) which is approximately 10000 times that of the present energy needs (Hasan and Sumathy 2010). The phenomenon of this conversion from photons to electricity is known as the photovoltaic effect. Alexandre-Edmond Becquerel observed it in liquid phase electrochemical cell in the year 1839. Charles Fritts, in 1883, succeeded in making the first solar cell from a selenium/gold junction and reported an efficiency of about 1%. Later on, in 1905 Sir Albert Einstein explained photovoltaic effect for which he was awarded the Nobel prize.

Photovoltaic (PV) technology offers an attractive alternative energy source as it draws power from a renewable source and is environmental friendly. Further, a country like India, which receives a remarkable amount of sunlight throughout the year due to its geographical position, PV becomes a viable alternative to supply power to the remote areas. However, the Achilles heel in the case of PV technology is the comparatively high cost

involved in its processing and manufacturing, when compared to the conventional sources of energy. The challenge before the research community today is to develop cost-effective methods and technologies and thereby making photovoltaic technology more lucrative. If the scientific community successfully overcomes the aforesaid challenges, it will help mankind to tap into a vast energy resource in order to satisfy the current and future global energy requirements.

1.2 SOLAR SPECTRUM

The irradiation from the sun are similar to that from a black body at 5800 K, which is the approximate temperature of the Sun's surface following Planck's distribution. **Fig. 1.1** depicts the solar irradiance spectrum. From this spectrum it is very clear that the maximum energy in the solar spectrum exists in the infra-red region (~55%), followed by the visible region (~42%) and very little within the UV region (~3%). Which means that, for better efficiency the solar cells must strive to absorb in the visible and IR region of the solar spectrum.

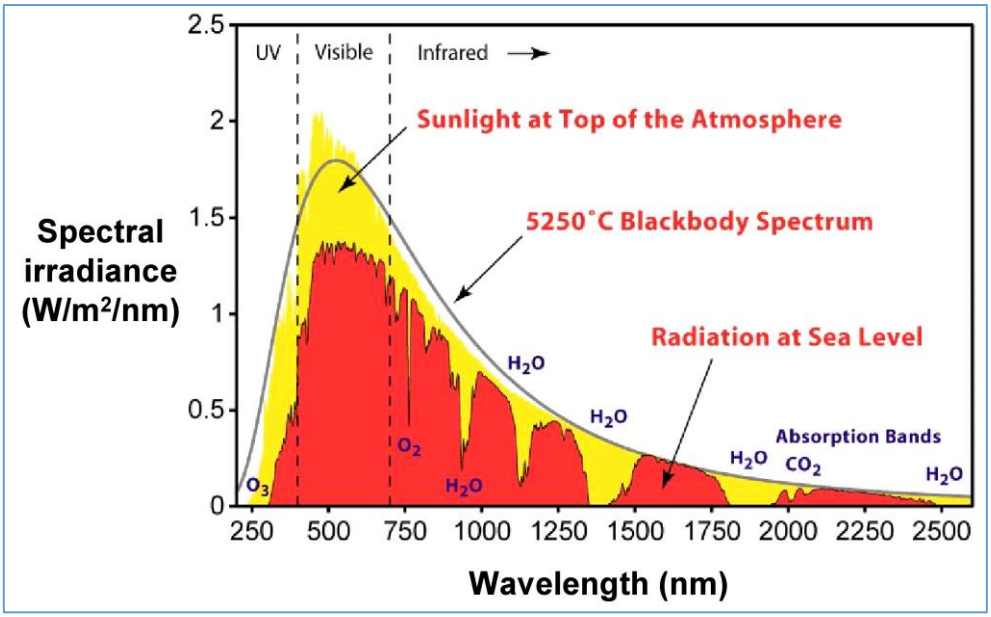

Fig.1.1 Solar irradiance spectrum

To certify consistent test conditions, the American Society for Testing and Materials (ASTM) has set forth some important parameters for solar irradiance. These include AM 0, which is the solar irradiance outside the earth's atmosphere, AM 1.5, the standard solar spectrum and the black body spectrum. The values for these are

$I_{AM\,0} = 1366.1\ Wm^{-2}$ $I_{AM\,1.5} = 1000.4\ Wm^{-2}$

The decline in the solar irradiance on the earth's surface is due to absorption, scattering and reflection. Absorption increases with the increase in the path length *via* atmosphere. The relation between the path length (*l)* for the radiation passing through the atmosphere with an atmospheric thickness of l_o, making an angle α with the normal to the earth's surface is given by $l = l_0 / cos\alpha$. Air mass coefficient (AM) is given by the ratio l/l_o.

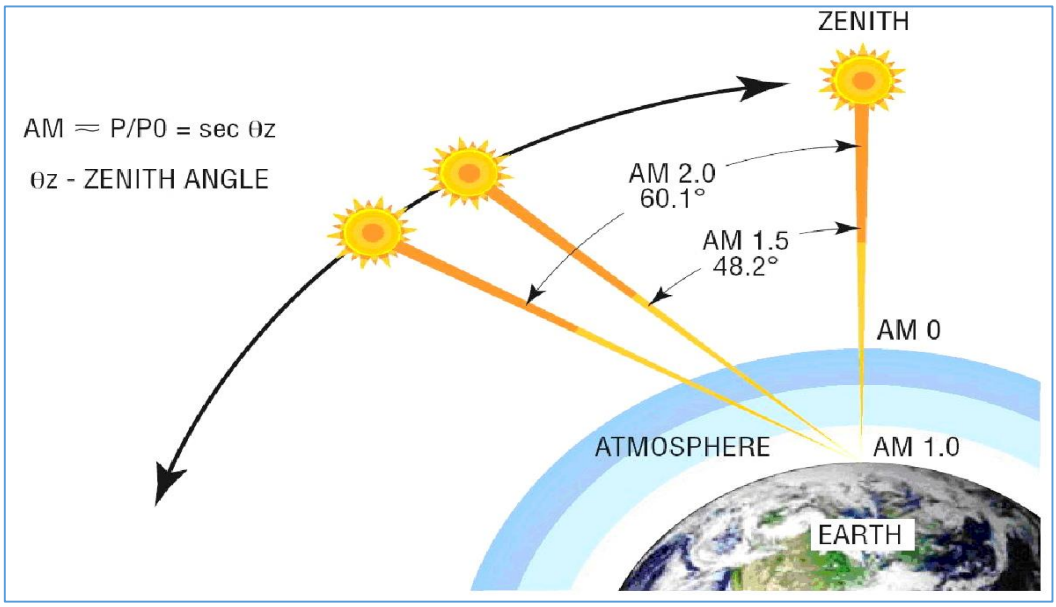

Fig.1.2 Illustration of various air mass (AM) positions and the zenith point.

The spectrum outside the earth's atmosphere is labelled as AM 0, the AM 1, also known as the zenith point, denotes the spectrum on the surface of the earth for normal

incidence, *i.e.* 90º. Whereas, AM 1.5 G represents the complete global irradiance under specified atmospheric conditions at an incidence angle of 48.2º.

1.3 TYPES OF SOLAR CELLS

Typically, solar cells are categorized into three generations based on their performance, material used as well as cost to efficiency ratio. Among these, the first generation of solar cells have a comparatively higher efficiency and are most widely deployed. These cells are manufactured using the second most abundant element in earth`s crust, *i.e.* Silicon (Si). Photovoltaic effect in silicon diode was discovered at Bell Labs by D.M. Chapin, C.S. Fuller and G.L. Pearson in 1954 which marked the beginning of modern photovoltaic technology. Ever since, Si based solar cells have emerged as the most mature photovoltaic technology and account for about 90% of the current photovoltaic market worldwide. The biggest chink in the armor for silicon based solar cells is the high manufacturing cost and challenging purification steps to obtain high quality silicon.

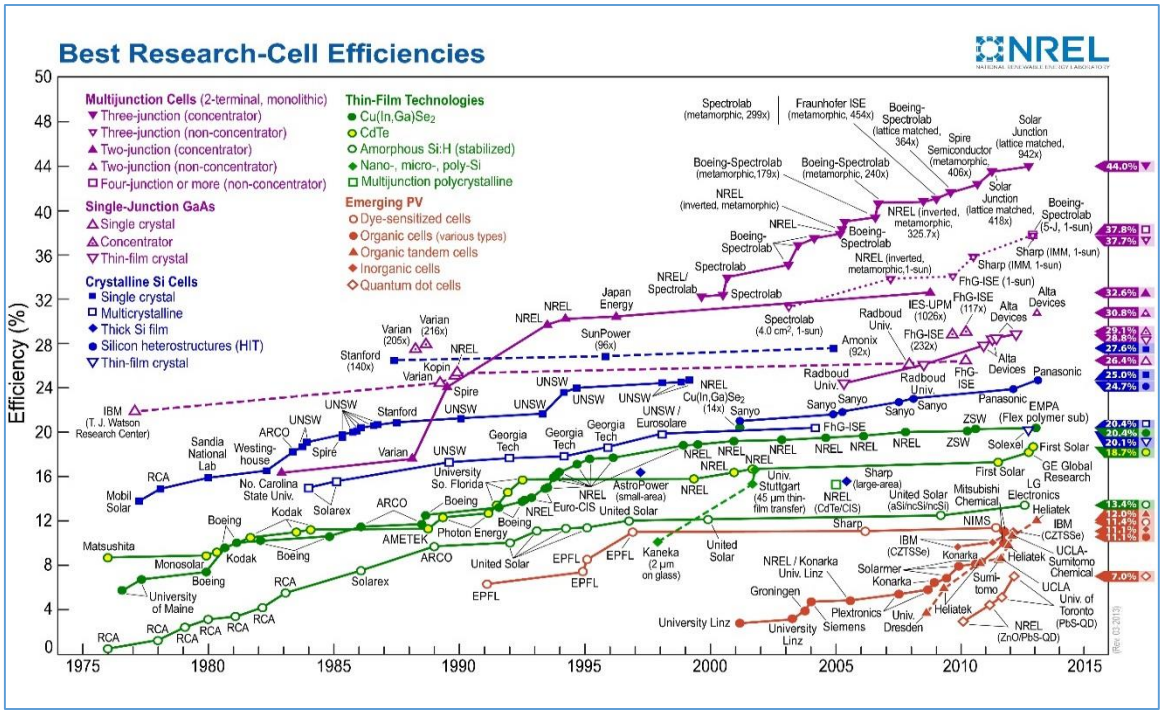

Fig.1.3 Current best photovoltaic research-cell efficiencies (National Renewable Energy Laboratory)

The second generation cells constitute thin film solar cells based on cadmium telluride (CdTe) or copper indium galliumdiselenide (CIGS), and thin film cells based on crystalline silicon. Although they display low efficiency, the motivation behind the development of thin film solar cells has been their low manufacturing cost. The conundrum with the first and second generation solar cells is that they are restricted by the Shockley-Queisser theoretical limit for a single *p*-*n* junction. The third generation solar cells comprise of all the cells that aren't grouped under the first two generations. Most of the cells in this generation are not yet commercialized and are under extensive research. DSSC is a part of third generation solar cells. **Fig.1.3** displays the state-of-the-art for different photovoltaic cells and technologies throughout the world.

1.4 CURRENT PHOTOVOLTAIC TECHNOLOGY

The current photovoltaic market is dominated by silicon based devices which include both monocrystalline and polycrystalline devices. These devices are commonly known as *p*-*n* junctions, since they are constructed by bringing two silicon layers, one doped with third group atom (*p*-type) and another doped with group five atom (*n*-type), into close contact. Solar to electrical power conversion efficiency of the best silicon based devices is around 25%. Silicon based PV modules are robust and have a life time of about 25 years. However, the high manufacturing cost of silicon devices is the major drawback. Since 2002, the PV market is growing at the rate of 48% and it is the world's fastest growing technology. In spite of all this, PV technology contributes only 0.1% towards the world's energy demands. The basic reason for this being the high installation and maintenance costs of silicon photovoltaics. Hence, in the recent years utilizing inexpensive organic materials as an alternative to inorganic semiconductor has attracted the interest of researchers. Accordingly, a vast range of research is undertaken to synthesize and optimize new materials for use in solar cells.

1.5 DYE SENSITIZED SOLAR CELL (DSSC)

1.5.1 A brief history

The energy and electron transfer mechanisms involved in photosynthesis and in dye sensitized silver halide emulsions used for photography were the inspiration behind the development of dye sensitized solar cells (DSSCs). In 1887, Moser displayed the first dye-sensitized semiconductor electrode, while using the erythrosin dye on silver halide electrodes. However, until 1960s the operating mechanism involved in the electron injection from a photo-excited dye molecules into the conduction band of the *n*-type semiconductor substrates was not clearly understood. Later, a breakthrough was obtained in the year 1991 by Grätzel and his co-workers, who developed a solar cell by the successful combination of nanostructured electrodes and efficient charge injection dyes in the 'Laboratory of Photonics and Interfaces' in Ecole Polytechnique Federale de Lausanne, Switzerland. The aforementioned breakthrough was the use of sintered mesoporous titanium dioxide (TiO_2) which raised the DSSC efficiency from 1% to 7% and incident photon to electrical current conversion efficiency was approximately 80%. Since then, DSSCs have been subjected to large number of investigations. It falls somewhere between classical regenerative photoelectrochemical cell and solid-state photovoltaics. Of late, many researchers have been successful in achieving high efficiencies (~12%) using porphyrin based dyes. In the aforementioned study, Yella et al. in 2011 obtained an efficiency of 12.3% from a push-pull zinc porphyrin dye (YD2-o-C8) co-sensitized with an organic dye (Y123). This breakthrough discovery started an avalanche of investigations in D-π-A based dyes to develop high-efficiency DSSCs. Continuous efforts are being made to improve the efficiency of DSSC to make it competitive to the other technologies in current market.

The DSSC (**Fig.1.4**), or Grätzel cell, is a complex system where in three different components, *viz.* the dye, the semiconductor and the electrolyte are brought together to generate electric power from light without undergoing any permanent chemical transformation. The system consists of the following:

1) An anode made up of a glass sheet with a transparent conductive layer.
2) A mesoporous semiconductor oxide layer (typically, TiO_2) deposited on the anode, to activate electronic conduction.

3) A monolayer of the chromophore, *i.e.* the sensitizer, attached to the surface of the semiconductor.
4) An electrolyte, usually an organic solvent containing a redox couple, such as iodide/triiodide for the regeneration of the dye.
5) A cathode made up of glass sheet coated with a catalyst (typically, platinum), to facilitate electron collection.

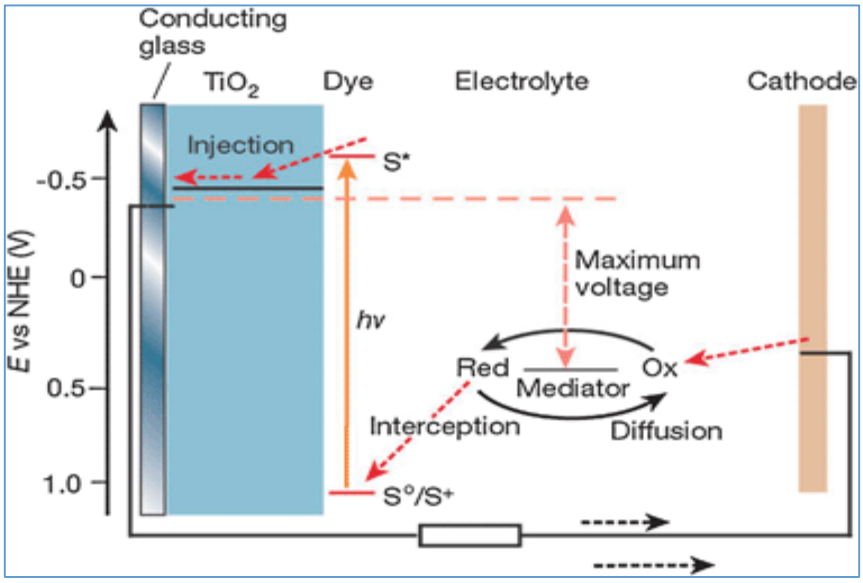

Fig.1.4 A schematic representation of dye sensitized solar cell (Grätzel et al. 2001)

Like photosynthesis, DSSC is a molecular machine that is one of the first of its kind devices to go beyond microelectronics into the realm of nanotechnology, wherein the use of a dye acts as the light harvester to produce excited electrons, TiO_2 replacing carbon dioxide works as the electron acceptor, iodide/triiodide (I^-/I_3^-) replacing water and oxygen function as the electron donor and oxidation product and a multilayer structure similar to the thylakoid membrane works to enhance both the light absorption and electron collection efficiency. When exposed to sunlight, the dye molecule gets excited from ground state (S^0) to excited state (S*) from which an electron is injected into the conduction band of the mesoporous oxide film. These generated electrons diffuse to the anode and are utilized at

the external load before being collected by the electrolyte at cathode surface to complete the cycle. The operating cycle can be summarized in chemical reaction terminology as:

Anode:

$S^0 + h\nu \longrightarrow S^*$ Absorption (1)

$S^* \longrightarrow S^+ + e^-$ Electron injection (2)

$2S^+ + 3I^- \longrightarrow 2S + I^-_3$ Regeneration (3)

Cathode:

$I^-_3 + 2e^- (Pt) \longrightarrow 3I^-$ (4)

Cell:

$e^- (Pt) + h\nu \longrightarrow 3I^-$ (5)

All the operations in the cell are regenerative so none of the chemical substance undergoes any permanent chemical transformations as shown by the cell reaction (5).

1.5.2 Working principles of dye sensitized solar cells

In DSSCs, unlike conventional silicon based devices, charge separation and recombination are exclusively interfacial reactions. Further, due to the weaker van der waals interactions between the organic molecules than those in silicon crystals and a lower dielectric constant, photoexcitation of organic dyes produces a tightly bound neutral Frenkel exciton, whereas the loosely bound Wannier exciton formed when silicon is photoexcited, which are basically considered to be free charges. DSSC cannot produce free charges directly from photoexcitation, but rather requires an additional step for charge separation. Therefore, it can be said that the current generation in DSSC is reliant on three sovereign processes, *viz.* the absorption of light by the dye molecules, the injection of electrons from the excited state of photosensitizer, and its transport through the semiconducting layer. **Fig.1.5** shows the various energy levels present in a typical DSSC and also the electron flow within the solar cell. Upon illumination, the dye molecule is photoexcited in a few femtoseconds followed by ultrafast injection from D* to TiO_2 on the sub picosecond time scale (intramolecular relaxation of the excited sensitizer might complicate the injection process), wherein they are rapidly(less than 10fs) thermalized by

lattice collisions and phonon emissions. The fairly slow rate (nanosecond) of dye (D*) relaxation ensures that, the injection efficiency is 100%. The ground state of the chromophore is then recuperated by the electrolyte in the microsecond domain, successfully annihilating D^+ and seizing the recombination of electron in TiO_2 with D^+, that happens in the millisecond time range. This is followed by two processes, *viz.* electron percolation through the semiconducting film and reduction of the triiodide at the counter electrode, completing the circuit.

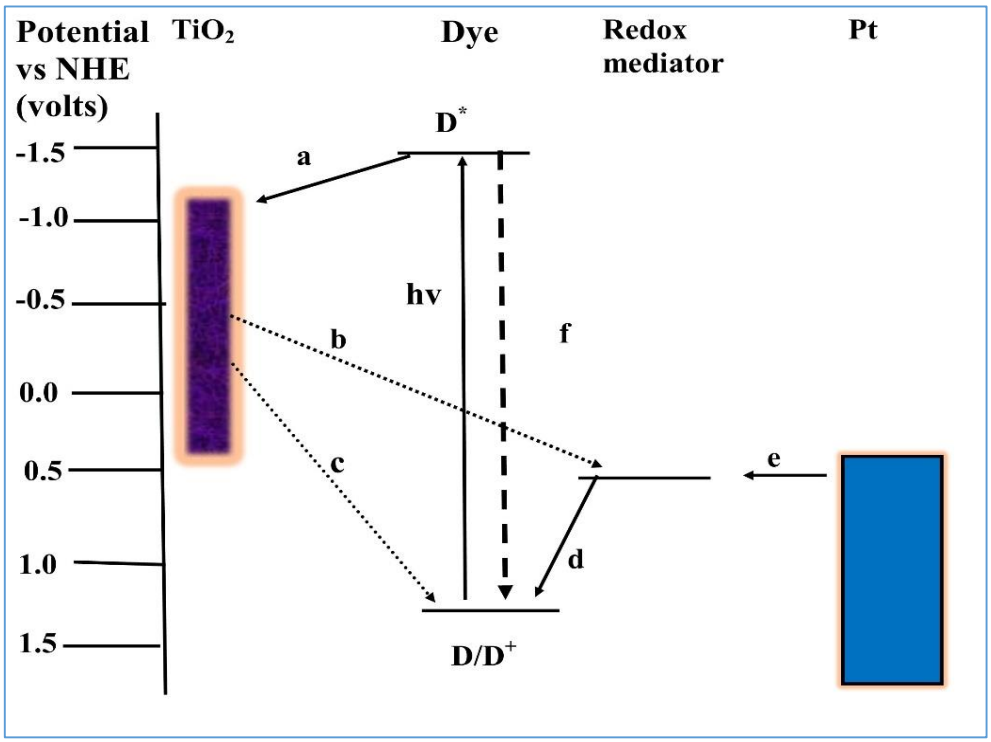

Fig.1.5 Schematic illustration of the energy levels in a typical DSSC specifying the various competing photophysical pathways. These comprises (a) electron injection (b) electron recombination with the acceptor species in the electrolyte (c) with dye cations (d) regeneration of dye cations by the electrolyte (e) reduction of the electrolyte at the counter electrode (f) relaxation of the dye molecule from the excited state

The proficiency of the solar cells can be enumerated with parameters such as incident photon to current efficiency (IPCE), open circuit photovoltage (V_{oc}), short circuit current (J_{sc}) and overall efficiency of the solar cell (η_{cell}).

1.5.2.1 Short circuit photocurrent (J_{sc})

Short circuit photocurrent is defined as the photocurrent per unit area (mA/cm^2) when an illuminated cell is short circuited. The factors influencing J_{sc} are light intensity, injection efficiency, light absorption, and regeneration of the oxidized dye molecule. **Fig. 1.6** displays a current-voltage characteristics of an illuminated cell under an external load going from zero load (open-circuit condition) to infinite load (short circuit condition).

1.5.2.2 Open circuit photovoltage (V_{oc})

The open circuit photovoltage is the difference in potential between the two terminals in the cell under light illumination when the circuit is open. It is reliant on both the level of dark current as well as Fermi level of the semiconductor. V_{oc} is measured when the current through the cell is equal to zero (open circuit condition). Its theoretical maximum can be obtained from the difference between the Fermi level of the semiconductor and the redox potential of the hole-conductor.

1.5.2.3 Fill factor (*ff*)

The fill factor is defined as the ratio of the maximum power output per unit area to the product of V_{oc} and J_{sc}. The value of *ff* determines the ideality of the device. Fill factor can be obtained from the equation 6.

$$ff = \frac{J_{max} \times V_{max}}{J_{sc} \times V_{oc}} = \frac{P_{max}}{J_{sc} \times V_{oc}} \quad (6)$$

Where P_{max} is maximum power. The closer *ff* is to 1, the more power a cell can provide.

1.5.2.4 Incident photon to current conversion efficiency (IPCE)

IPCE is one of the key measurements to evaluate the performance of the solar cell. The aforesaid is also known as external quantum efficiency and defines how efficiently the light of a particular wavelength is converted to current. The IPCE is calculated by employing equation 7.

$$\text{IPCE } (\%) = \frac{1240 \times J_{sc}}{\lambda \times \Phi_{inj}} \times 100 \quad (7)$$

Where, J_{sc} is the short circuit photocurrent density for monochromatic irradiation and λ and Φ are the wavelength and the intensity, respectively. IPCE corresponds to the

measure of photocurrent (electron flux) compared to the photon flux that strikes the cell. It is basically a combination of the quantum yields for these four processes as articulated in equation 8.

$$IPCE\ (\lambda) = LHE\ (\lambda)\ \Phi_{inj}\ \eta_{coll}\ \Phi_{reg} \quad (8)$$

Where, LHE (λ) is the light harvesting efficiency for photons of wavelength λ, Φ_{inj} is the quantum yield for the electron injection, η_{coll} is the electron collection efficiency at the back contact and Φ_{reg} is the quantum yield of regeneration.

1.5.2.5 Solar energy to electricity conversion efficiency *(η)*

The overall solar energy to electricity conversion efficiency *(η)* of a solar cell is defined as the maximum output of the cell divided by the power of the incident light. It can be determined from the photocurrent density measured at short circuit (J_{sc}), the open circuit photovoltage (V_{oc}), the fill factor of the cell (*ff*), and the intensity of the incident light (I_o) as shown in equation 10. Since, it is dependent on all the three aforesaid factors under standard conditions, it is of great importance to optimize each one of them for high overall efficiency. Therefore, efficiency η can be written as:

$$\eta = \frac{j_{sc} \times V_{oc} \times FF}{I_o} \quad (10)$$

The proficiency of DSSC can be limited by any of the competing processes mentioned in the **Fig.1.5**, which affect the photo induced electron density in the semiconductor film. Therefore, to improve the efficiency of DSSC it is a prerequisite to have a detailed knowledge of all these processes.

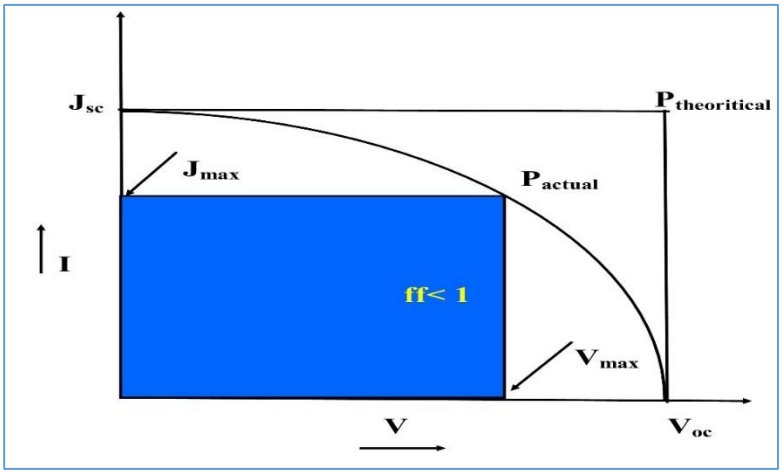

Fig.1.6 A typical I-V curve

1.5.3 Light harvesting

The fraction of the photons absorbed by the dye to the total number of incident photons is known as the light harvesting efficiency (LHE, λ) of a dye. This can be obtained from equation 11.

$$\mathrm{LHE}(\lambda) = 1 - e^{-\alpha_{abs} d} \qquad (11)$$

Where, α_{abs} is the inverse absorption length, and d is the thickness of the dye layer. α_{abs} can be determined from equation 12.

$$\alpha_{abs} = N_A \, \sigma_{abs} \, C_{dye} \qquad (12)$$

Wherein, N_A is the Avogadro number, σ_{abs}, is the absorption cross section per dye molecule, and C_{dye}, is the dye surface concentration. For most of the dyes the value of σ_{abs} is much lower than the geometric area they occupy on the semiconductor surface. As a result, C_{dye} and by extension σ_{abs} will end up having very low values for a monolayer of dye absorbed to the semiconductor surface, which results in a very poor light harvesting efficiency. To dodge this, nanostructured mesoporous semiconductor electrodes with a surface roughness factor (internal surface area normalized to the geometric area) of the order $10^3$are usually employed, which guarantees that, each incident photon crosses several hundred dye molecules as it passes through the chromophore film.

However, for substantial light harvesting efficiency, semiconductor films of significant thickness is still a necessity. This prerequisite places a noteworthy constraint on

the DSSC design. One limitation is, for the proper filling of the nanopores throughout the film the viscosity of the electrolyte must be low and since such solvents are usually organic and volatile, they create a conundrum with the sealing and long term stability of the device. Further, the dyes which are highly susceptible to recombination are not viable in thicker films, as the larger surface area promotes the interfacial electron transfer reactions.

Another germane issue with the light harvesting ability of DSSCs is the fact that significant areas of the solar irradiance spectrum are not covered by the absorption spectrum of most dyes, predominantly in the region beyond 700 nm. Henceforth, it constraining the maximum photocurrent that can be obtained from the DSSC. Numerous tactics have been explored in an attempt to overcome this hurdle. These include, synthetic modifications of the dye to reduce the energy gap between the highest occupied molecular orbital (HOMO) and lowest unoccupied molecular orbital (LUMO) and thereby shifting the absorption onset of the dye, merging multiple sensitizers with complimentary absorption spectra on the same semiconductor electrode, engaging multichromophore antenna dyes which substantially amplify the extinction coefficient.

1.5.4 Electron injection

Once photoexcited, the dye must inject an electron into the conduction band of the semiconductor before it eases back to the ground state. This is arguably the crucial mechanistic step in achieving proficient charge generation in DSSCs. The quantum yield for electron injection (Φ_{inj}), can be determined by knowing the competition among the rates for injection and other pathways (equation 13).

$$\Phi_{inj} = K_{inj} / (K_{inj} + K_{deact}) \qquad (13)$$

Wherein, $K_{inj,}$ the rate constant for electron injection and K_{deact} is the combined rate constant for all the other deactivation pathways. For attaining a high injection yield, the electron injection rate should be an order of magnitude faster than the competing deactivation of the dye excited state. However, given the ultrafast rate of electron injection, it was not surprising that the dynamics of electron injection were not clearly understood until the introduction of femtosecond laser spectroscopy in 1996. Ever since, a lot of studies have been carried out to improve the efficiency of electron injection. It was understood

that, the structure of the dyes plays a pivotal role in injection efficiency. The nature of the substituent groups, the position of the substituents with respect to the chromophore, the nature of the anchoring groups which offer the electron linkage between the chromophore and the semiconducting oxide, the extent of conjugation are the other key factors which affect the electron injection efficiency of a particular dye. Further, it was observed that the dyes with an electron acceptor component close to the semiconducting layer and electron donor component furthest from the semiconducting film guarantees that the electron density in the excited state is concentrated in the vicinity of the TiO_2, boosting injection and localizing the subsequent positive charge away from the interface.

A wide range of additives are also used to improve the efficiency of electron injection by blocking aggregation in the dye layer, which disengages the excited state of the dye through a self-quenching mechanism. Species such as chenodeoxycholic acid which do not interact with the other species in the electrolyte are usually employed for this purpose. Orientation of the dye on the surface of semiconductor is also perceived to play a pivotal role in the electron injection efficiency. Researchers have also speculated that, if the dye molecules are bound to the surface with a distribution of angles, then there is a possibility that, in a certain proportion of the dye the electron transfer may occur directly through space, without any assistance from the linker group.

1.5.5 Charge transport

The space-charge layer, where the charge distribution is unlike from that in the bulk of the material, generates an electric field to drive the electron and hole separation. It is produced as a result of electron flux across the interface of a semiconductor placed in contact with an electrolyte until the Fermi level of electrons in the semiconductor is equal to the electrolyte redox potential. However, due to their smaller size, the nanocrystalline semiconductor particles are unable to sustain any significant charge imbalance between the surface and bulk of the particle. Moreover, due to the porous nature of the semiconductor, each particle will be surrounded by the electrolyte throughout the entire film thickness, curtailing any electric fields that may be present between sintered particles. Therefore, charge transport in DSSC is dominated by diffusion, or more precisely by ambipolar

diffusion, a phenomena where electrons and associated cations on the film surface move through the film simultaneously. Although, now it is widely putative that, the trap states in the semiconductor govern the charge transport behavior. According to this theory, the electronic states in the semiconductor are a mix of conduction band states which permit unrestricted flow of electrons, and intra band trap states, which constrain the free flow of electrons by trapping and later releasing them to the conduction band. Hence, the entrapment of electrons in these traps and their successive escape into the conduction band, governs the charge transport in DSSC.

1.5.6 Charge recombination

To reestablish equilibrium, the electrons in the TiO_2 may recombine with the dye cation or the oxidized form of redox mediator. But, such recombinations are highly detrimental to the overall efficiency of the solar cells, because of them the electrons will no longer be available in external circuit. It is possible to study these two recombination pathways independently as we can add or remove the redox mediator from the electrolyte to engage or disengage this pathway.

1.5.6.1 Dye cation recombination

Given the proximity in which the dye cations exist, it is not surprising to see that, they happen to be the prime cause of potential recombination in a DSSC. However, redox mediators are assigned the job to remove these dye cations by restoring the ground state of the dye and hence annihilating the possible recombination between the electrons and the dye cations. Therefore, it is safe to say that, the kinetic competition between the dye recombination and its regeneration by the redox mediator decides the degree to which recombination will affect the competence of a DSSC. Typically, it is observed that the kinetics of dye regeneration by the redox mediator is much higher (about 10 times) than the recombination between electrons present in semiconductor and dye cation.

1.5.6.2 Redox mediator recombination

As the electrolyte percolates through the whole semiconductor film, recombination can occur at numerous interfaces. Although the electrons present in the semiconductor and

the redox mediator are at a distance of only a few nanometers, it is quite baffling that it takes about 1ms-1sec for the recombination to occur. This might explain why DSSCs have high power conversion proficiency. The precise mechanism for the redox mediator, I_3^- recombination is still a mystery, but the slow recombination rates are attributed to the two electron I_3^- reduction demanding substantial amount of energy to continue. Replacement of this with a one electron system leads to a considerable acceleration in the rate of recombination and hence by default lowering the efficiency of solar cells. A wide range of substances have been used to block this recombination, which include polymers, co-adsorbers, organic acids, dense titania etc.

1.5.7 Charge collection

Once the electrons are injected to the semiconductor from the sensitizer, it travels through the external circuit and has to be collected at the counter electrode. The charge collection efficiency, η_{coll} is given by the ratio of electrons collected at the FTO contact to the overall number of electrons injected into the semiconductor. The efficiency of electron collection can be determined by using equation 14.

$$\eta_{coll} = 1 - \tau_r / \tau_{coll} \qquad (14)$$

Where τ_r, is the time constant for electron recombination (electron lifetime) and τ_{coll} is the time constant for electron withdrawal into external circuit after injection. Moreover, as the charge transport in solar cells is controlled by the process of diffusion, value of L, the length of electron diffusion (average distance travelled by an electron *via* semiconductor before recombination) will also affect the η_{coll}. L can be determined knowing the values of D_0 (electron diffusion length) and τ_r (electron lifetime inside a semiconductor electrode) and substituting them in equation 15

$$L = \sqrt{(D_o \tau_r)} \qquad (15)$$

For a higher efficiency of charge collection, L should be longer than the thickness of the semiconducting film. For the standard ruthenium based dyes the diffusion length is between 20-100 µm, compared to the 15 µm thick semiconducting film, leading to a high η_{coll} values.

1.5.8 Efficiency of DSSCs

For a single junction DSSC having semiconductor with a band gap of 1.1ev, the maximum efficiency that can be obtained under AM 1.5 is proved to be 32%, which is known as Shockely-Queisser limit. But, given the different kinds of charge recombinations which are possible in solar cells this efficiency comes down considerably.

The absorption spectrum for the concerned dye must be known, in order to precisely predict the limit of a DSSC. Although, theoretically the maximum obtainable efficiency from a DSSC is about 32%, making realistic assumptions for all the parameters involved such as the absorption onset of about 900 nm, and loss of potential of about 550 nm, the practically obtainable efficiency stands at 17.6%.

1.6 COMPONENTS OF DSSC

DSSC primarily consist of a sensitizer, a photoelectrode, a wide band gap semiconductor, a redox electrolyte and a counter electrode.

1.6.1 Photosensitizers

The sensitizers play a vital role in generating electron-hole pairs. An efficient photosensitizer should possess certain requirements such as:

- The sensitizer should be capable of absorbing all incident light below the near-IR wavelength of approximately 920 nm.
- It should carry a carboxylate or phosphonate group for strong adsorption onto the semiconductor surface.
- The lowest unoccupied molecular orbital (LUMO) of the sensitizer must be close to the edge of the conduction band of the oxide for efficient electron injection into the conduction band of TiO_2.
- To accept electron donation from an electrolyte or a hole conductive material the highest occupied orbital (HOMO) of the sensitizer must be sufficiently low.

- Electrons and holes in the dye must be quickly separated and injected into the respective photoanodes before being recombined. This basically means that, the quantum yield for charge injection must be close to 1.
- The sensitizer should be stable enough and should not undergo any degradation.

Further, a detailed account on the different kind of sensitizers have been described under literature review (**Section 1.9**).

1.6.2 Semiconductor photoanode

Photoanode consists of wide band gap semiconductors such as TiO_2, ZnO, SnO_2, and chalcogenides. Due to their wide application in energy storage they have been under extensive investigation. Further, they act as sensitizers to facilitate light induced redox process due to the presence of the electronic structure, referred to as valance band and conduction band. Amongst them, TiO_2 has been found to be suited for application in DSSCs. The surface area available for dye chemisorption in mesoporous (minutely structured materials with an enormous internal surface area) TiO_2, is over a thousand folds higher than that of a flat, unstructured electrode of the same size. If a monomolecular layer of the dye is adsorbed on the surface, enough can be retained on a given area of electrode to provide absorption of basically all the incident light. The necessity for DSSC to absorb far more of the incident light was the driving force behind the development of mesoscopic semiconductor material.

TiO_2 occurs in three crystalline forms, *viz.* rutile, anatase and brookite. Among these, anatase is perceived to be the most chemically active when used in DSSCs. The high dielectric constant of TiO_2 (80 for anatase) provides a good electrostatic shielding of the injected electron from the oxidized dye molecules attached to the TiO_2, hence preventing their recombination before reduction of the dye by the redox electrolyte. High refractive index of TiO_2 (2.5 for anatase) leads to efficient diffused scattering of light inside the porous photoelectrode, which remarkably enhances the light absorption. The band-gap of anatase is 3.2 eV at an absorption edge of 388 nm. Moreover, the conduction band edge of anatase is 0.1eV above than that of the rutile phase; hence the maximum open circuit

voltage (V_{oc}) of rutile photoanode is lower than anatase photoanode. It has also been observed that, the intrinsic electrical properties of TiO_2 are profoundly affected by the crystal structure. The other major parameter which affects the carrier concentration and mobility of transition metal oxides is the type and concentration of cation and anion defects. Among these point defects, the oxygen vacancy has been identified as the one which affects the performance of solar cells. Studies done by Meng et al. (2003) on the electron and hole dynamics shows that oxygen vacancy on TiO_2 surface stabilizes the dye adsorption.

Due to the strong bond between dye and the semiconductor, charge injection will be enhanced. Moreover, when the oxygen vacancy is present on the surface of TiO_2, back electron transfer becomes more predominant, as the HOMO and LUMO of the redox species are shifted to higher energy levels. In addition, the electrons that are injected from the dye molecule migrate through TiO_2 *via* hopping without the support of built in potential. Extensive research has be done to improve the carrier transport and dye adsorption by surface modification of TiO_2 nanoparticles. Exploratory research on doped TiO_2 and various other metal oxides has been done extensively to improve the surface properties and electronic structure of the photoanode. Further, ZnO is often considered as promising materials to replace TiO_2 as photoanode, due to its similar conduction band edge, work function and higher carrier mobility. But, surprisingly the performance of ZnO is found to be consistently lower than that of TiO_2. This is attributed to the vulnerability of ZnO surface to the acidic environment and thereby breaking its chemical bond with the dye to form the dye aggregates that dissipates the energy of absorbed photons. The common techniques employed in the preparation of TiO_2 films include the doctor blade technique, electrophoretic deposition, tape casting, and screen printing methods. Of late, sensitization of *p*-type semiconductors have witnessed a growing interest. This is mainly attributed to the perspective of fabricating tandem DSSCs when efficient *p*-type dye-sensitized solar cells (*p*- DSSCs) will be developed. Further, *p*-type DSSCs are almost exclusively made of nickel oxide. However, the conversion efficiencies have remained low and thus keeping the prospects for the aforesaid class of DSSCs grim.

1.6.3 Transparent conducting substrate

Apart from semiconductor oxide film, the transparent conducting substrates such as FTO, also play a key role in deciding the DSSC performance. They function as current collector and a support of the semiconductor layer in DSSCs. High optical transparency allows natural sunlight to pass through to the beneath of the active material avoiding unwanted absorption of the solar spectrum and the low electrical resistivity which reduces energy loss and facilitates electron transfer process.

1.6.4 Electrolyte

The electrolyte is a key component of all DSSCs. The benchmarks for an efficient electrolyte are following:

- The photoexcited dye loses an electron before it reacts with the electrolyte.
- The oxidized dye molecule has to be reduced by the electrolyte rather than recombined with the electrons from the neighboring dye molecule.
- The reduced electrolyte reacts slowly with electrons in both TiO_2 and TCO layers.
- The reduction rate of the oxidized ion at the cathode is rapid.

The very critical constituent of the liquid electrolyte is a redox couple. The electrolyte used in DSSC mostly contains I^-/I_3^- redox ions; it functions as a charge carrier collecting electrons at cathode and transporting electrons back to the dye molecules. The electrolyte is a neutral sink of I^- and I_3^- maintaining the redox potential in the bulk of the electrolyte *via* the fast redox reaction of the I^-/I_3^- pair. A lithium cation is also a desirable constituent of the liquid electrolyte, because the adsorption of the lithium ion on the surface of the semiconductor nanoparticles considerably increases J_{sc} and slightly decreases V_{oc}. The adsorbed lithium ion on TiO_2 nanoparticles changes the flat band on the surface of the photoanode and lowers the acceptor state of TiO_2. This in turn makes the electron injection energetically more favorable, though there is a slight decrease in V_{oc}. Also the adsorption of lithium ion expands dark current under positive bias, since the screening effect of electrons in conduction band is reduced.

The redox reaction involved is a two electron reaction.

$$3I^- \longrightarrow I_3^- + 2e^-$$

Which is composed of a series of successive reactions:

$$(I^- \longrightarrow I + e^-) \times 2 \text{ charge transfer reaction}$$

$$2I \longrightarrow I_2 \text{ fast chemical reaction}$$

$$I_2 + I^- \longrightarrow I_3^- \text{ fast chemical reaction}$$

At the TiO_2 electrode, the oxidized dye left behind by the electron injected to the TiO_2, is regenerated by I^- in the electrolyte in the reaction while at the counter electrode, I_3^- is reduced to I^- in the reaction. Bromine (Br^-/Br_2) and hydroquinone have also been used as redox electrolyte for DSSC; but the iodine redox electrolyte gives the best performance. Liquid electrolyte usually have high ionic conductivity and excellent interfacial contact property. However, the main drawback with them is the leakage and volatility of the solvent which affect the long term performance of DSSCs. To overcome these disadvantages non-traditional electrolytes, *e.g.* room temperature ionic liquids (RTILs), quasi-solid state and solid state electrolytes have been under extensive investigation. RTILs have shown promising potential to serve as alternative electrolytes, they are a group of organic salts containing cations such as imidazolium, pyridinium and anions from the halide or pseudo-halide family. It is expected that RTILs could solve the sealing problem and enhance the stability by virtue of their inherent characteristics such as good chemical and thermal stability, negligible vapor pressure, non-flammability and high ionic conductivity. When incorporated into DSSCs, they serve both as a source of iodide and the solvent itself. Quasi-solid electrolytes are another class of electrolytes wherein both liquid and solid electrolytes can be combined to form a quasi-solid electrolyte, or gel electrolyte. Apparently there are several advantages of using gel electrolyte such as relatively high ambient ionic conductivity, intimate interfacial contact with TiO_2 and remarkable electrolyte stability. However, the high viscosity of ionic liquids and quasi-solid

electrolytes severely affects the mass transfer *via* ion-diffusion and the completeness of pore filling, which in turn hampers the cell performance.

1.6.5 Counter electrode

Low charge transfer resistance and high exchange current densities are the prerequisites of a material to be used as counter electrode in DSSC, because it is responsible for the reduction of the oxidized form of the charge mediator. Electrons arriving from the external circuit are transferred back to the redox electrolyte by the counter electrode. Since it is an excellent catalyst for I_3^- reduction, platinum (Pt) has been the most suitable material for the counter electrode. But the recent studies have shown that, carbon can be used as an alternative to Pt because it combines sufficient electrical conductivity and heat resistance as well as corrosion resistance and electro catalytic activity for the I_3^- reduction.

1.7 CHARACTERIZATION OF DSSCs

1.7.1 DSSC fabrication

There are several methods available for DSSC Fabrication. A typical protocol followed for the fabrication of DSSCs includes the following steps:

The Fluorine-doped tin oxide (FTO) coated glasses are washed with detergent, water, and acetone. After this thoroughly cleaned plates are immersed into an aqueous solution containing of $TiCl_4$ and maintained at 70 °C for 30 minutes and subsequently washed with water and ethanol. A thin layer (8-12 μm thick) of TiO_2 is deposited on transparent conducting glass by squeegee printing followed by drying at suitable temperatures. After cooling to room temperature, the TiO_2 electrodes were treated with 40 mM aqueous solution of $TiCl_4$ at 70 °C for 30 minutes and then washed with water and ethanol. Generally, the dye solutions is prepared by dissolving the dye in suitable solvents. The electrodes are immersed in the dye solution and then kept at 25 °C for 20 hours to adsorb the dye onto the TiO_2 surface. The counter electrodes are obtained using platinum. The dye sensitized TiO_2 electrode is sandwiched with Pt counter electrode and the

electrolyte is then injected into the cell, while the two electrodes are held together with the clips.

1.7.2 Photovoltaic characterization

Current-voltage plots of DSSCs are obtained using a Keithley 2400 source meter under illumination of AM 1.5 G solar light from solar simulator (SOL3A, Oriel), coupled with a 450 W xenon lamp (91160, Oriel). A reference Si solar cell (Newport Oriel, 91150V) is used to calibrate the incident light intensity to 1 Sun (100 mW cm^{-2}). The measurement are fully controlled under Oriel IV Test Station software. Further, IPCE (incident monochromatic photon to current conversion efficiency) experiments are performed using a system (QEX10, PV Measurements, USA) equipped with a 75 W short arc xenon lamp (UXL-75XE, USHIO, Japan) as a light source linked to a monochromater. Calibrations of incident light are performed before measurements using a silicone photodiode (IF035, PV Measurements). All the measurements are carried out without the use of anti-reflecting film.

1.7.3 Electrochemical impedance spectroscopy characterization

Electrochemical impedance spectroscopy (EIS) successfully models the charge transfer and chemical capacitance at the interface of TiO_2/dye/electrolyte and Pt/eletrolyte in DSSC under operational conditions (Wang et al. 2005). A typical EIS measurements result in Nyquist and Bode plots. In Nyquist plot, intermediate frequecny semicirlce is related to electron transport through mesoporous TiO_2 and back electron transfer from TiO_2 to electrolyte. Bigger the radius of middle semicircle, higher is the charge recombination resistance (R_{ct}) from TiO_2 to electrolyte (Han et al. 2006) corresponding to Nernst impedance. Further, from Bode frequency plots, lifetime for injected electrons into conduction band of TiO_2 can be determined by using the the relation ($\tau = 1/2\pi f$), where τ is the lifetime of electrons in TiO_2 and f is the mid frequency peak in Bode plots.

1.7.4 Cyclic voltammetric measurements

A cyclic voltammetry (CV) study helps to determine the electrode potentials of the sensitizers and thereby to estimate the position of HOMO and LUMO levels of the dyes.

These values are useful to find out the thermodynamic feasibility of electron injection into the conduction band of the semiconductor from the HOMO level of dye molecule and dye regeneration by the electrolyte.

1.7.5 FT-IR analysis: anchoring studies of the dyes on TiO_2

FT-IR spectroscopy is widely applied in order to gain an insight into the nature of anchoring groups and the mode of their interaction with the TiO_2 substrate. By implementing this technique one can elucidate the absorption states of the sensitizers and/or bonds formed upon adsorption on the TiO_2 nanoparticles using a set of rules developed by Deacon and Phillips.

1.8 THEORETICAL CALCULATIONS

TURBOMOLE is a quantum chemical program package, developed by Prof. Dr. Reinhart Ahlrichs at the University of Karlsruhe. It is an extremely optimized software package for large-scale quantum chemical simulations of clusters, molecules, and periodic solids. Turbomole utilizes Gaussian basis sets and specializes on predictive electronic structure methods with admirable cost to performance characteristics. The methods include time-dependent density functional theory (TDDFT), explicitly correlated coupled cluster (CC) methods. The aforementioned methods combined with ultra-efficient and numerically stable algorithms such as resolution-of-the-identity, integral-direct and Laplace transform methods.

PART B: LITERATURE REVIEW, SCOPE, OBJECTIVES AND DESIGN OF NEW INDOLE BASED SENSITIZERS

1.9 LITERATURE REVIEW

This section covers a detailed literature review of different kinds of sensitizers. Further, it also describes the influence of structure on different photovoltaic parameters. In fact, the sensitizer is the pivotal component in any DSSC. Therefore, in addition to the high temperature stability and broad spectral range of absorption, the sensitizer should be efficient in electron injection. For efficient carrier injection from the dye to the semiconducting photoanode a proximal contact required. To achieve this, the functional groups of the dyes have been modified accordingly at the molecular level. In particular,

an anchoring group that attaches the dye onto the nanoparticles of the photoanode is vital. Carboxylic acid and phosphonic acid are generally used as anchoring groups. But studies reveal that, due to the difference in proximity the electrons move through the carboxylic acid anchor two times faster than through the phosphonic anchor group. The polarity of the dye-semiconductor interface plays a crucial role in controlling the charge injection. The dipole formed at the interface can accelerate the transition of charge carrier, *i.e.* electron. Since the aggregation will reduce the charge injection efficiency, another facet to be considered while designing a dye is to minimize aggregation within the photoanode. Therefore, proper structure is critical in preventing aggregation, for example dye molecules with lesser number of carboxyl group have less chance to form intermolecular aggregates, which results from hydrogen bonding between the carboxyl groups of the dye molecules. Another factor which plays a pivotal role is the geometry of the anchoring *i.e.* the bonding structure between the dye and the semiconductor. For instance, a bridging bidentate type bonding is more stable than unidentate type bonding and a chelating type bonding.

1.9.1 Ruthenium based chromophores

The photovoltaic performance in terms of both conversion yield and long term stability achieved with polypyridyl complexes of ruthenium (**N3**, **N719** and **'*Black dye*'**), developed by the Grätzel group was almost unparalleled till recently. These dyes have shown record solar energy to electricity conversion efficiencies (η) of 11%. It has an absorption threshold around 800 nm covering the visible to the near-infra red region of solar spectrum. In addition, **N3** dye can inject photo-excited electrons into the semiconductor-layer efficiently *via* carboxylate groups, which on one hand firmly attach to the surface of TiO_2 as an electron transfer channel, and on the other hand, link to the bipyridyl moiety to lower the energy of the ligand π^* orbital. Since the molecular electronic transition is a metal-to-ligand charge transfer, this structure synergetically favors in the electron injection process. The performance of **N3** dye as a sensitizer was almost unparalleled until the emergence of **Black dye**.

Table 1.1 Ruthenium based sensitizers

Reference	Sensitizer	J_{sc} (mAcm^{-2})	V_{oc} (V)	*ff*	η (%)
Nazeeruddin et al. (1993)	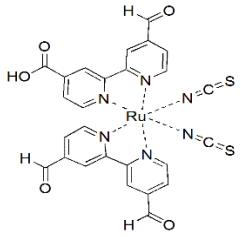 **1.1** (**N3**)	16.80	0.85	0.77	11.03
Wang et al. (2003)	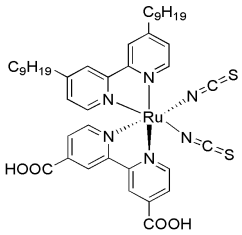 **1.2** (**Z907**)	14.6	0.72	0.69	7.3
Ito et al. (2005)	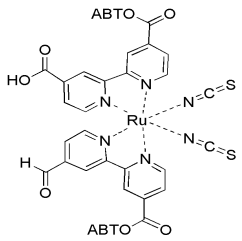 **1.3** (**N719**)	18.7	0.79	0.71	10.6
Chiba et al. (2006)	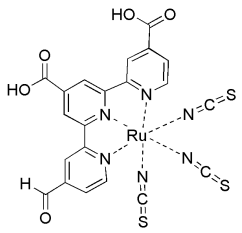 **1.4** (**Black dye**)	20.90	0.73	0.72	11.1

Cheema et al. (2014)	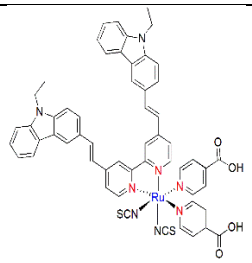 **1.5 (NCSU-10)**	19.58	0.71	0.73	10.19

Nazeeruddin et al. in 1993 first reported the synthesis of **Black dye** which displays the panchromatic sensitization character over the entire visible range extending from the near-IR region up to 920 nm. This expansion in the absorption spectrum of the **Black dye** leads to increase in J_{sc} of DSSCs to be larger than 20 mA cm^{-2}. However, the molar extinction coefficient of it is lower than **N719**, which requires a thicker TiO_2 film to attach the sufficient quantity of the dye molecules on the surface of the photoanode. Apart from the superior light harvesting properties and durability, a significant advantage of these dyes lie in the metal-ligand charge transfer transition through which the photoelectric charge is injected into TiO_2. In Ru complexes, this transfer takes place at a much faster rate than the back reaction, wherein the electron recombines with the oxidized dye molecule rather than flowing through the circuit. **Table 1.1** lists some important ruthenium based sensitizers. Though, ruthenium (II) based dyes have provided a relatively high efficiency, there are several drawbacks of them:

- High cost
- Limited availability of noble metals
- Sophisticated synthesis and purification steps.

To address these issues, metal-free organic dyes have been prepared and applied in DSSCs to replace Ru (II) based dyes as sensitizers.

1.9.2 Organic chromophores

The interest in metal-free organic sensitizers has grown in the past few years. The major merits of the organic dyes over the ruthenium-complex dyes are as follows:

- Larger molar extinction coefficient
- More facile synthesis
- Flexibility in tuning the absorbing light spectrum
- Cost effective

Organic sensitizers contains a framework with an electron donor-acceptor moiety for intramolecular charge transfer and a carboxyl group as an anchoring unit for the attachment onto TiO_2 nanoparticles. This configuration was generalized as donor-π-bridge-acceptor (D-π-A) structure as shown in **Fig.1.7**.

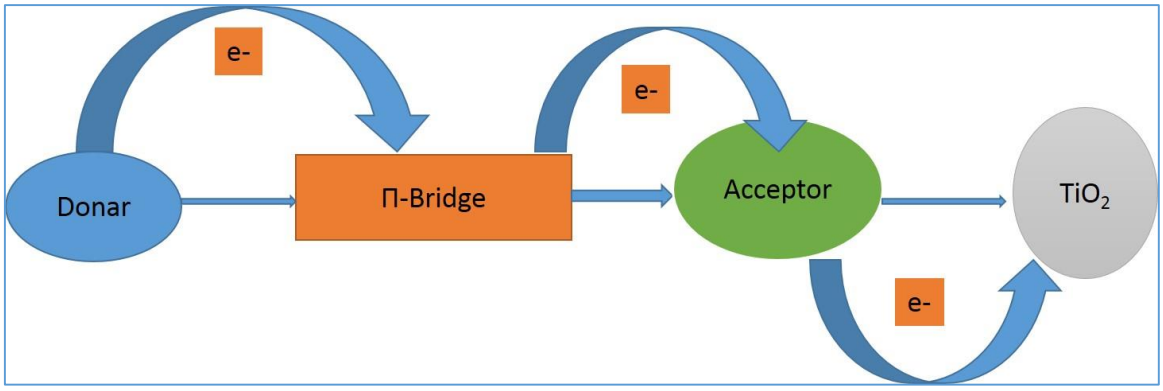

Fig.1.7 General framework of metal-free organic dyes

Generally, the anchoring group is carboxylate, phosphonate or sulphonate. In the literature, various types of metal-free dyes based on coumarin, indole, indoline, cyanine, hemicyanine, merocyanine, perylene, triarylamine, oligoene, thiophene etc have been reported. A brief account of the literature review pertaining to metal-free dyes is given below.

1.9.2.1 Indole based sensitizers

The first indole based sensitizers for DSSC's were designed and synthesized by Li et al. in the year 2009. It is well known that, the copious electronic cloud in indole rings promote the electron flow in the indole based compounds, and the easy functionalization at the third position of indole ring facilitates the fine-tuning of its optoelectronic properties.

Table 1.2 Indole based sensitizers

Reference	Sensitizer	J_{sc} (mAcm^{-2})	V_{oc} (V)	*ff*	η (%)
Li et al. (2009)	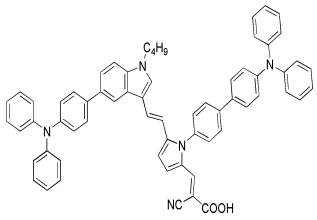 **1.5**	9.46	0.71	0.64	4.31
Li et al. (2009)	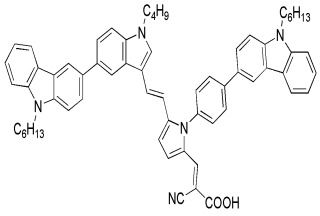 **1.6**	10.25	0.69	0.61	4.31
Zhang et al. (2010)	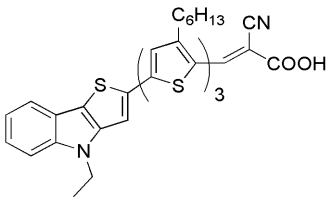 **1.7**	14.60	0.70	0.76	7.80
Liu et al. (2013)	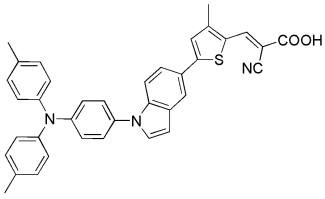 **1.8**	9.78	0.76	0.74	5.53
Cai et al. (2013)	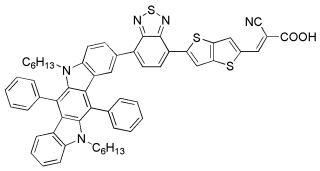 **1.9**	14.81	0.68	0.69	7.03

Reference	Sensitizer	J_{sc} ($mAcm^{-2}$)	V_{oc} (V)	*ff*	η (%)
Hong et al. (2014)	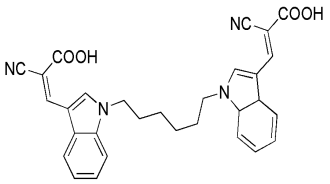 **1.10**	1.91	0.69	0.71	1.19
Hong et al. (2014)	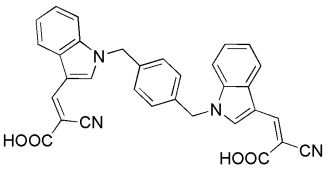 **1.11**	1.63	0.63	0.70	0.91

In the aforementioned report, Li et al. (2009) attached triphenylamine and carbazole moieties to the pyrrole ring through a carbon-nitrogen single bond, in order to suppress the dye-aggregation on the surface of TiO_2. Although, dyes **1.5** and **1.6** displayed same overall conversion efficiency of 4.31%, the values of J_{sc}, V_{oc} and *ff* were found to be different. As expected the dye with triphenylamine substitution displayed enhanced V_{oc} owing to the nonplanar geometry of triphenylamine moiety which helps in suppressing the electron recombinations in the cells. Whereas, the sensitizer **1.6** containing carbazole moiety displayed enhanced J_{sc} values owing to the better light harvesting capability of carbazole moiety.

Similarly, Zhang et al. (2010) designed and synthesized organic dyes containing Thieno[3,2-b]indole donor for efficient DSSCs. An overall conversion efficiency (η) of 7.8% was obtained with the aforesaid sensitizer. Further, Cai et al. (2013) synthesized efficient and stable sensitizers based on substituted dihydroindolo[2,3-b]carbazole donors. The effective conjugation in the new donor moiety led to a high molar extinction coefficient, which enhances the light harvesting capability of the sensitizer. The highest efficiency obtained by using the above-mentioned dye is 7.03%. Further, Hong et al. (2014)

synthesized a series of compounds, wherein double donor-acceptor branches -were linked *via* non-conjugated alkyl or aryl linkages, resulting in two separate light-harvesting units. Furthermore, it was observed that the photovoltaic performance of the cells based on these dyes have been dependent upon the structure of the incorporated linkages, such as the length of alkyl chains and aryl groups. **Table 1.2** comprises the structure and performance parameters of reported indole based dyes.

1.9.2.2 Triphenylamine based sensitizers

The triphenylamine (TPA) moiety is known for its strong electron-donating capability as well as hole-transport properties. Due to this very reason, large number of triarylamine sensitizers were designed and synthesized and majority of them exhibited decent power conversion efficiencies. Kitamura and co-workers in 2004 were the first to introduce TPA based organic dyes and obtained an efficiency of 3.3%.

Chiba and co-workers (2006) synthesized TPA based dye by incorporating thiophene as a π-spacer and achieved an improved efficiency of 5.9% (Chiba et al. 2006). Later, Liang et al. (2007) employed rhodanine-3-acetic acid as acceptor/anchoring group in sensitizer **1.14** and obtained an overall efficiency of 4.32%. Further, Hagberg and co-workers synthesized two TPA dyes (**1.15** and **1.16**). The slightly better efficiency obtained by the sensitizer **1.16** (6.9%) compared to the dye **1.15** (5.9%) can be attributed to the presence of additional electron-donating methoxy groups in the sensitizer **1.16**. This in turn**,** red-shifted the absorption maximum by 30 nm and resulted in an enhanced power conversion efficiency of 6.9% as compared to 5.9% obtained for the sensitizer **1.15**. The aforementioned discovery establishes the influence of alkoxy groups on the V_{oc} and J_{sc} through broadening of spectral response. However, refining the electron-donating capability of TPA, suppressing undersiable charge recombinations and dye-aggregation remain key issues in order to obtain high J_{sc} values. Therefore, designing new push-pull systems for broader and better IPCE response is essential. **Table 1.3** includes the structure and performance parameters of reported TPA based sensitizers.

Table 1.3. Triphenylamine based sensitizers

Reference	Sensitizer	J_{sc} ($mAcm^{-2}$)	V_{oc} (V)	*ff*	η (%)
Kitamura et al. (2004)	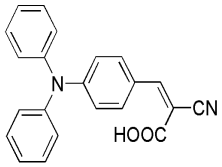 **1.12**	6.3	0.77	0.67	3.30
Chiba et. al (2006)	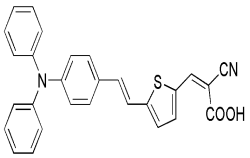 **1.13**	12.0	0.69	0.72	5.90
Liang et. al (2007)	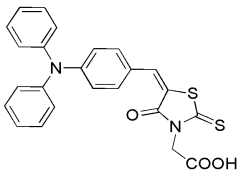 **1.14**	13.0	0.56	0.59	4.32
Hagberg et al. (2007)	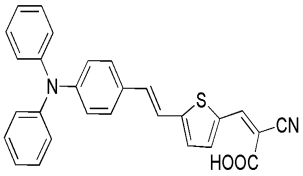 **1.15**	12.8	0.62	0.66	5.20
Hagberg et al. (2008)	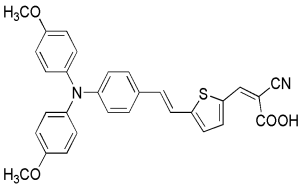 **1.16**	14.0	0.69	0.71	6.90

1.9.2.3 Indoline based sensitizers

Indoline dyes were first reported by Horiuchi and co-workers in the year 2003. A conversion efficiency of 6.1% was obtained with sensitizer **1.17**. Further, it was observed that, in addition to a high PCE efficiency, the aforesaid dye is stable to redox process by cyclic voltammetry (CV) experiments. It was concluded that, the molecular design of the rhodanine ring contributed to the bathochromic shift in the absorption spectrum and improved the overall performance. Ito et al. in 2006, achieved a conversion efficiency of 9% with sensitizer **1.19** after optimizing the semiconductor (TiO_2) films with an antireflection layer, which helped in improving the transmittance of the FTO glass and barred UV light from passing through. Indoline dye **1.20**, bearing an octyl chain instead of ethyl chain as in dye **1.19**, displayed an improved efficiency of 9.5%, which is the highest efficiency obtained so far among DSSCs sensitized using an indoline dye. The enhancement in the overall efficiency can be attributed to effective suppression of dye-aggregation between indoline dye molecules. Unfortunately, the aforesaid indoline derivatives incorporating rhodanine-3-acetic acid as the acceptor/anchoring unit have been plagued with low-stability.

Keeping this in view, Zhu et al. in 2011, synthesized a series of D-A-π-A organic sensitizers. The new design was found to enhance the photo-stability of the sensitizers. The cell based on the sensitizer **1.21** displayed an overall efficiency of 8.7%, but more importantly was found to exhibit good stability with the overall PCE remaining at 94% of the initial value even after 1000 h of visible-light soaking. Although, the indoline dyes exhibit impressive J_{SC} values, their V_{oc} values are comparable or inferior to those of substituted triphenylamine sensitizers, which limits their enhancement in overall efficiency. **Table 1.4** comprises the structure and performance parameters of reported indoline based sensitizers.

Table 1.4 Indoline based sensitizers

Reference	Sensitizer	J_{sc} ($mAcm^{-2}$)	V_{oc} (V)	*ff*	η (%)
Horiuchi et al. (2003)	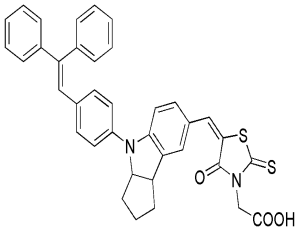 **1.17**	17.8	0.60	0.57	6.1
Horiuchi et al. (2004)	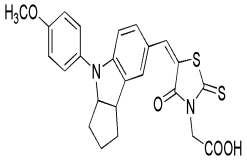 **1.18**	14.8	0.59	0.59	5.1
Ito et al. (2006)	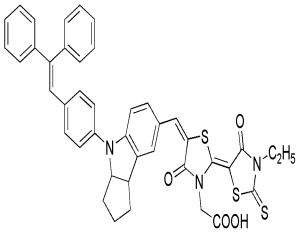 **1.19**	20.0	0.65	0.69	9.0
Ito et al. (2008)	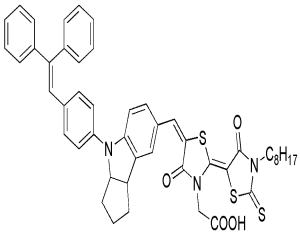 **1.20**	18.6	0.72	0.71	9.5
Zhu et al. (2011)	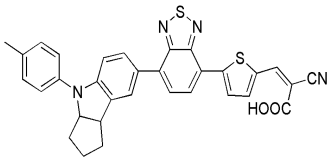 **1.21**	17.70	0.65	0.76	8.70

1.9.2.4 Cyanovinylene based sensitizers

Many researchers have focused on broadening the absorption profile of the dyes in order to enhance the overall efficiency of the cells.

Table 1.5 Cyanovinylene based sensitizers

Reference	Sensitizer	J_{sc} ($mAcm^{-2}$)	V_{oc} (V)	*ff*	η (%)
Wang et al. (2007)	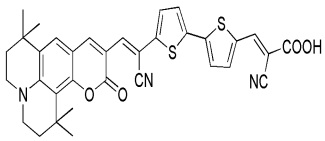 **1.22**	18.80	0.53	0.65	6.50
Mikroyannidis et al. (2010)	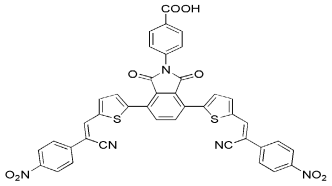 **1.23**	12.15	0.65	0.58	4.58
Sharma et al. (2014)	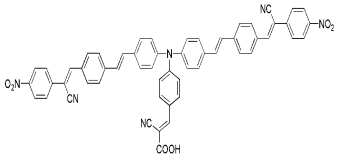 **1.24**	11.86	0.64	0.68	5.16
Sharma et al. (2014)	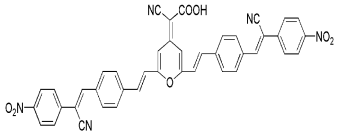 **1.25**	10.92	0.60	0.66	4.42
Gupta et al. (2015)	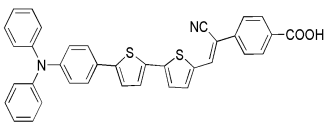 **1.26**	20.0	0.65	0.69	9.00

Generally, the best approach to obtain molecules having broad absorption profiles is to incorporate a statergic arrangement of electron rich (donor) and electron deficient (acceptor) moieties in the dye molecule. Keeping this in view, the introduction of cyanovinylene unit into chromophores is a good approach to expand π-conjugation (reduce band gap) and thereby shifting the absorption maxima to higher wavelengths with enhanced molar extinction coefficients. Wang et al. in 2007 synthesised a dye **1.22** based on coumarin, with a higher values of λ_{max} (552 nm) and molar extinction coefficient (97400 $M^{-1}cm^{-1}$) than the dye without cyanovinylene substitution. The major difference between the two dyes is the presence of a cyanovinylene group in the molecular core of **1.22**, which lead to the reduction in the band gap. Further, Mikroyannidis et al. in 2010 synthesized a novel broadly absorbing sensitizer **1.23** with cyanovinylene group carrying 4-nitrophenyl segments incorporated into the backbone of the molecule. The presence of the aforesaid terminal segments resulted in substantial red-shift in the absorption spectrum and contributed to the enhanced light harvesting efficiency of the fabricated cells.

Later, in 2014 Sharma et al. synthesized a class of new dyes **1.24** and **1.25**. Both the dyes exhibited broad absorption profiles extending up to near infrared region. The higher PCE for the **1.24** as compared to that of **1.25** can be attributed to the reduced charge recombination and greater amount of dye loading on TiO_2. Further, Gupta et al. in 2015 used 4-(cyanomethyl)benzoic acid in the sensitizer **1.26** as a replacement for the conventional cyanoacrylic acid group as an acceptor moiety and obtained an overall conversion efficiency of 9.0%. **Table 1.5** includes the structure and performance parameters of reported cyanovinylene containing sensitizers.

1.9.2.5 Relay dyes

Another recent advancement is the introduction of the concept of relay dyes. Where in the two dyes with different absorption spectra are simultaneously implemented on to the semiconducting layer. Out of the two, only one dye with smaller band gap is anchored to the oxide nanoparticles and the unattached dye with a large HOMO-LUMO gap absorbs high energy light and efficiently transfers the energy to the nearby anchored dye *via* a

dipole-dipole interaction which is known as Forster resonant energy transfer. These type of donor dyes are known as energy relay dyes. The benefit of the resonant energy transfer between two dyes is the broadening of the light absorption spectrum without losing the active dye interface area. It has been observed that, on adding the energy relay dye the efficiency of DSSC went up by 25%. The other way to overlay the light absorption spectra is to attach multiple dyes in the same photoanode. In this scenario, the dye absorbing high energy photons is placed adjacent to the photoanode and the dye absorbing low energy photons is attached to the deep region of the photoanode. Lee et al. (2009) reported that the organic dye molecules with different absorption ranges can be selectively positioned in a mesoporous TiO_2 by mimicking a technique used in column chromatography.

1.9.2.6 Co-sensitization

The metal-free sensitizers exhibit merits such as ease of structural modification, tunable absorption and electrochemical properties, low cost, high molar extinction coefficients, and ease of purification over their metal-based counterparts. However, in order to achieve higher efficiency, the sensitizer is required to possess a wide absorption spectrum. Many researchers around the globe have focused on extending the absorption spectrum of the sensitizer and thereby enhancing the overall efficiency (Takechi et al. 2008). The main dye design philosophy implemented by many research groups to broaden the absorption spectra of the sensitizers is donor-π-bridge-acceptor (D-π-A) strategy (Tang et al. 2010). However, the extension of absorption spectrum comes with its share of parallel limitations. Firstly, red-shifting the absorption spectrum by extending the conjugation may result in sensitization problems, *i.e.* dye aggregation on the semiconductor surface, leading to lower photo-conversion efficiency. Further, it has been reported that extending the π-conjugation of the sensitizer to absorb the near-IR photons can negatively affect its overall efficiency and stability (Hara et al. 2003). Secondly, as a result of broadening of the absorption spectra, a destabilization of the ground state oxidation potential (GSOP) and/or the excited state oxidation potential (ESOP) is required, which decreases the electron injection and dye regeneration thermodynamic driving forces. Because of these limitations, it still remains a challenge for the scientific community to design highly efficient

sensitizers. Keeping all these facts in view, a viable strategy for enhancement of the overall efficiency of DSSCs is the development of new organic compounds which can be used as co-adsorbents in ruthenium based DSSCs (Lan et al. 2012). Hence, infusing the merits of both ruthenium dyes as well as metal-free sensitizers into same DSSC, it is possible to further enhance the overall efficiency of the cell. Generally, the prerequisites for a molecule to become an ideal co-adsorber are : (i) the molecule should possess structural features to avoid competitive adsorption among the sensitizer molecules while efficiently suppressing the dye aggregation on the semiconductor surface, (ii) the co-adsorbers must possess a very high molar extinction coefficient (ε) around 400 nm to recuperate the drop in the IPCE spectra because of tri-iodide species present in the electrolyte, and (iii) it should be capable of forming a compact molecular monolayer on the TiO_2 surface and thereby reducing the electron recombination in the TiO_2 film with the redox species present in electrolyte as well as other acceptor species (Han et al. 2012).

Recently, Michael Graztel and co-workers have achieved an efficiency of 13% through the molecular engineering of porphyrin sensitizers (Mathew et al. 2014). However, the major drawback of porphyrin based dyes is the pretty weak absorption characteristics in the spectral region between the Soret and Q bands. To overcome this drawback, co-sensitization of the photoanode by dyes with complementary absorption profiles has been an established strategy *via* broadening the photoelectric response range. For example, the co-sensitization of the **Black dye** with an organic co-sensitizer **Y1** yielded a considerably improved photocurrent and the device performance attained an efficiency of 11.28% (Han et al. 2012). Further, Han et al. in 2013 utilized a squaraine dye (**HSQ1**) together with **N3** for co-sensitized solar cells and obtained an efficiency over 8.14%. However, the obtained performance of the co-sensitized device was not up to the mark. The relatively inferior performance can be attributed to the weak absorption of squaraine dye below 500 nm, dye aggregation on the TiO_2 surface and fast charge recombinations. From all the aforementioned observation it is evident that, there is a lot of room to further ameliorate the device performances by strategic structural modifications of the organic dyes.

1.10 SCOPE AND OBJECTIVES OF THE PRESENT WORK

Even though significant advances have been made in the field of DSSCs by making use of metal-free sensitizers, there is still a long way to go as far as the chemical and physical property optimization is concerned. The growing interest in the field is quite evident from the review reports by Mishra et al. 2009. Still lots of work need to be carried out for improving the overall efficiency of solar cell such as, efficient light harvesting ability throughout the entire solar spectrum, tuning of the band gap, charge generation and separation, molecular interactions, and studying the effect of different functional groups on the overall performance.

From the literature review it is clear that there are number of factors influencing the efficiency of DSSC. Without a doubt, DSSC technology has a very bright future but there is still room to ameliorate performance. It is fair to say that, the overall performance of the solar cells depends on a number of parameters, ranging from the different materials used as electrodes, the semiconductor, the counter electrode, electrolyte etc., but from a synthetic chemist's point of view, the geometry and electronic structure of the dye play a pivotal role. Therefore, it is an immediate challenge and requirement to design and synthesize appropriate and efficient dyes for DSSC application.

Based on the above facts and the detailed literature survey, the following main objectives have been intended in the present research work:

1) Design and synthesis of new indole based sensitizers/co-sensitizers with different donor, π-conjugation and acceptor (D-π-A) configurations, carrying substituted indole systems as electron donor and cyanovinylene/thiophene groups as linkers and cyanoacetic acid/rhodanine-3-acetic/4-aminobenzoic acid /barbituric acid as acceptors /anchoring groups.
2) Characterization of new intermediates and target compounds by FTIR, ^{1}H-NMR, ^{13}C-NMR and mass spectral techniques followed by elemental analysis, and finally by single crystal X-ray study.

3) Evaluation of linear optical properties by means of UV absorption spectroscopy and fluorescence emission spectroscopy.
4) Determination of electrochemical properties, charge carrying properties and bandgaps using cyclic voltammetric studies.
5) Evaluation of electronic distribution in HOMO-LUMO levels of newly synthesized target compounds, by DFT studies.
6) Fabrication of DSSC device and quantify the performance of the newly synthesized sensitizers /co-sensitizers with parameters such as incident photon to current efficiency (IPCE), short circuit photocurrent (J_{sc}), open circuit photovoltage (V_{oc}), fill factor (*ff*) and the overall efficiency of the photovoltaic cell (η).
7) Assessment of charge recombination processes at TiO_2 / dye / electrolyte interfaces by EIS studies

Conclusively, the present research investigation is aimed at design, synthesis and characterization of new donor-π-acceptor (D-π-A) type sensitizers/co-sensitizers carrying different donors, linkers and acceptors. It has been planned to fabricate DSSC using the newly synthesized dyes and to study and understand the influence of different groups on the efficiency of solar cells.

1.11 DYE DESIGN STRATEGY

A detailed literature survey reveals that metal-free dyes offer DSSCs an attractive alternative with some substantial enhancements over the organometallic counterparts. The attributes which make these dyes more desirable are: low cost of production, high extinction coefficients, ease of synthesis and absence of heavy metals, making it eco-friendly. Among various D-π-A sensitizers reported in the literature, dyes based on carbazole (Tang et al. 2010, Koumura et al. 2006, Wang et al. 2008, and Lai et al. 2012), coumarin (Hara et al. 2005, Wang et al. 2007), fluorine (Kim et al. 2006, Jung et al. 2007), triphenylamine (Xu et al. 2008, Liu et al. 2008, and Hagberg et al. 2007), phenothiazine (Tian et al. 2007, Marszalek et al. 2011, Tsao et al. 2011, and Wan et al. 2012) and indoline (Ito et al. 2006, Liu et al. 2012, Tefashe et al. 2012, and Jose et al. 2008) have been shown to be the most promising candidates with respectable conversion efficiencies, mainly

because of their favorable electronic structures to act as good electron donor moieties. However, from the literature survey it is evident that, indole based sensitizers are under-explored when compared to the sensitizers based on triphenylamine, diphenylamine, coumarin, indoline etc. Further, the literature suggests that indole based dyes are promising materials, due to their ease of synthesis, chemical stability, processability, readiness of functionalities and solubility in common organic solvents. Against this background, our new designs have been centered on substituted indole derivatives.

Design of indole based sensitizers (Series 1; D_{1-3})

The indole ring is known to promote the electron flow in the indole-based compounds due to ample amount of electronic cloud possessed by it. Further, the ease of functionalization at the third position of indole ring facilitates the fine-tuning of its optoelectronic properties. On the other hand, thiophene is found to exhibit excellent charge transporting capability (Mishra et al. 2009). In addition, thiophene derivatives have been widely used as building blocks for sensitizers because of their well-known polarizabilty, as well as tunable spectroscopic and electrochemical properties. Their presence in between the donor and acceptor groups not only enhances the π-conjugation but also increases the overall stability of the resulting molecules. Whereas, introduction of cyanovinylene unit into chromophores is a good approach to expand π-conjugation (reduce band gap) and thereby shift the absorption maxima to higher wavelengths with enhanced molar extinction coefficients (Wang et al. 2007).

Apart from the electron donor moiety, the acceptor segment is also recognized for its significance in performance control of DSSC. In this context, certain functionalized acids such as cyanoacetic acid, rhodanine-3-acetic acid and 4-aminobenzoic acid have been adopted as efficient electron acceptors in most cases, mainly due to their strong electron-withdrawing properties and anchoring capabilities on the TiO_2 surface through an ester linkage. Keeping these facts in view, three new dyes (**D_{1-3}**) with a general D-π-A configuration have been designed. In the new design, the indole ring acts as an electron donor, thiophene and cyanovinylene linkers function as the π-conjugation bridge, while

cyanoacetic acid, rhodanine-3-acetic acid and 4-aminobenzoic acid behave as different electron acceptors. The design of **series 1** is depicted in **Fig.1.8**.

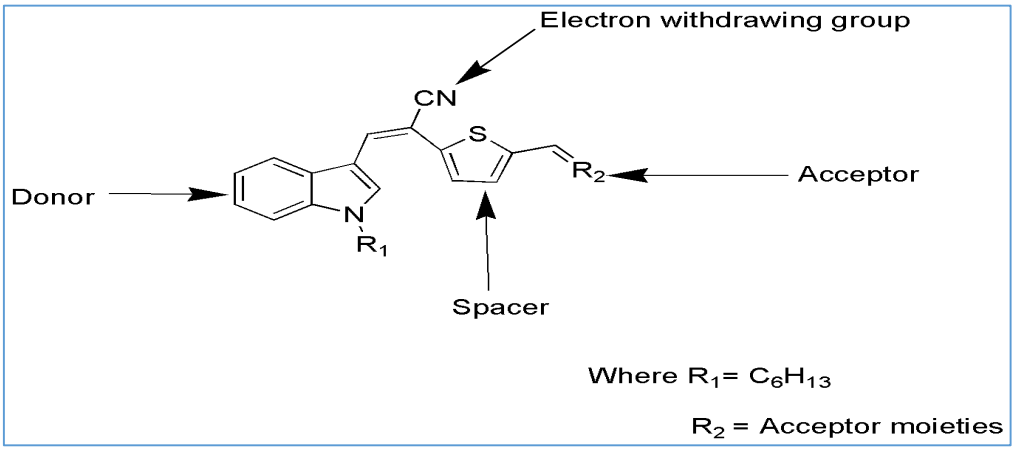

Fig.1.8 Design of **series 1** sensitizers

Design of 5-methoxy indole based sensitizers (Series 2; E_{1-3})

In the literature various dye design philosophies have been explored for the enhancement of overall efficiency of the cell. These include, donor-π-conjugation bridge-acceptor (D-π-A) (Ning and Tian 2009), with auxiliary acceptors (D-π-A-π-A) (Shi et al. 2012), (D-A-π-A) (He et al. 2012) and auxiliary donors (D-π-D-π-A) (Yang et al. 2012), or (D-D-A-π-A) (Hagberg et al. 2008) configuration. Among these, D-D-A-π-A configuration is receiving a lot of attention lately. In this approach, an auxiliary electron donor and electron withdrawing moieties are incorporated into the erstwhile common D-π-A architecture. Generally, the auxiliary donor enhances the electron donating capability of the principal donor moiety and thereby inducing a bathochromic shift in the absorption that results in the increase of photocurrent. Whereas, an auxiliary acceptor acts as an electron trap to separate charges and also facilitates the migration of electrons to the main acceptor (Ding et al. 2013). Moreover, this helps in broadening the absorption spectrum of the sensitizers for better light harvesting. It has been reported that the presence of electron accepting moieties such as diketeopyrrolopyrrole (Qu et al. 2012), benzotriazole (Mao et

al. 2012), cyanovinyl (Huang et al. 2008), plays an active role of auxiliary acceptors and they serve as effective charge transporters between the donor and acceptor (Lin et al. 2009).

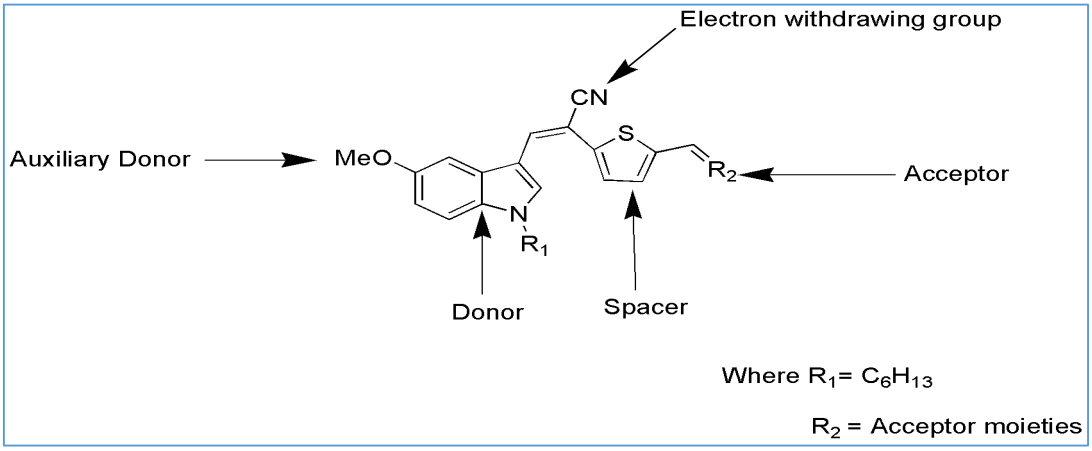

Fig.1.9 Design of **series 2** sensitizers

Typically, thiophene and its derivatives have been successfully utilized as π-conjugation bridges in the molecular design of organic dyes, due to their polarizability and overall stability (Mishra et al. 2009). Usually, the main acceptors used in DSSC include cyanoacrylic acid, rhodanine acetic acid etc. Further, many researchers have shown that introduction of long alkyl chain enhances the electron lifetime in DSSC due to their shielding effect, which suppresses the approach of triiodide ions in the electrolyte to the titanium dioxide surface and hence results in lower dark current (Koumura et al. 2006). This phenomenon directly translates into enhancement in open circuit voltage (V_{oc}) and thereby increasing the overall efficiency of cell.

Against this background, new methoxy substituted indole based sensitizers (**series 2**) have been designed and investigated for the effect of structural variation on their photovoltaic performance. In the new architecture methoxy group acts as an auxiliary donor, indole moiety works as a principal donor segment and the attached hexyl chain serves as a shield against electron recombination as well as dye aggregation. Further, cyanovinylene segment functions as an auxiliary acceptor while thiophene performs the function of a π-conjugation bridge in order to facilitate red shift in the absorption spectrum and to enhance the molar extinction coefficient (ε) of the dye, which may result in enhanced

light harvesting efficiency (Zhang et al. 2011). Whereas, cyanoacetic acid, rhodamine-3-acetic acid, and 4-aminobenzoic acid have been used as potential acceptors and anchoring units in **E_{1-3}**, respectively. **Fig.1.9** depicts the design of **series 2** sensitizers.

Design of 5-nitroindole based co-sensitizers (Series 3; N_{1-3})

In **series 3**, three new organic co-sensitizers having an indole core, and thiophene π-bridge attached to different acceptor units (**N_{1-3}**) with A-D-A-π-A (acceptor-donor-acceptor-π-bridge-acceptor) architecture have been designed. Greenwald et al. (1996) reported that, by incorporating electron acceptors such as a nitro group in the sensitizer, the photocurrents in photovoltaic devices can been enhanced. Further, cyanovinylene segment has been reported to increase the electrochemical stability of the molecule. Also, the presence of cyanovinylene is known to destabilize the ESOP of the sensitizer and thereby resulting in smaller E_{0-0}, and hence resulting in the broadening of the absorption spectrum. Against this background, cyanovinylene has been incorporated in the present design. Moreover, hexyl chain has been introduced in all the three co-adsorbers **N_{1-3}**, to fine-tune the distance between ruthenium based sensitizer **HD-14** (Cheema et al. 2014) molecules in order to avoid dye aggregation and to enhance the overall efficiency of the cell. **Fig.1.10** shows the design of **series 3** sensitizers carrying nitro group as auxiliary acceptor, indole ring as donor, cyanovinylene group as electron acceptor, thiophene moiety as π-conjugator and various anchoring groups.

The co-adsorbents **N_{1-3}** would enhance the IPCE spectra by counteracting the competitive light absorption due to triiodide species in 400-500 nm range of the visible spectrum. It was shown that, incorporation of electron-withdrawing and donating groups into the sensitizer molecule enhances the charge-transfer characteristics of absorption spectra and thereby giving a wider and higher absorptivity. In addition, anchoring groups are indispensable in DSSCs as they are essential in grafting the dye onto the semiconductor surface, and thereby assisting in achieving better electron injection from the excited state of the sensitizer into the TiO_2 conduction band edge. Therefore, the way in which the sensitizer is anchored on the semiconductor surface plays a pivotal role in determining the efficiency of the electron-injection step at the dye-semiconductor interface. Keeping this

in view, three different anchoring groups have been used in the present study in order to investigate their effect on the coadsorbing properties.

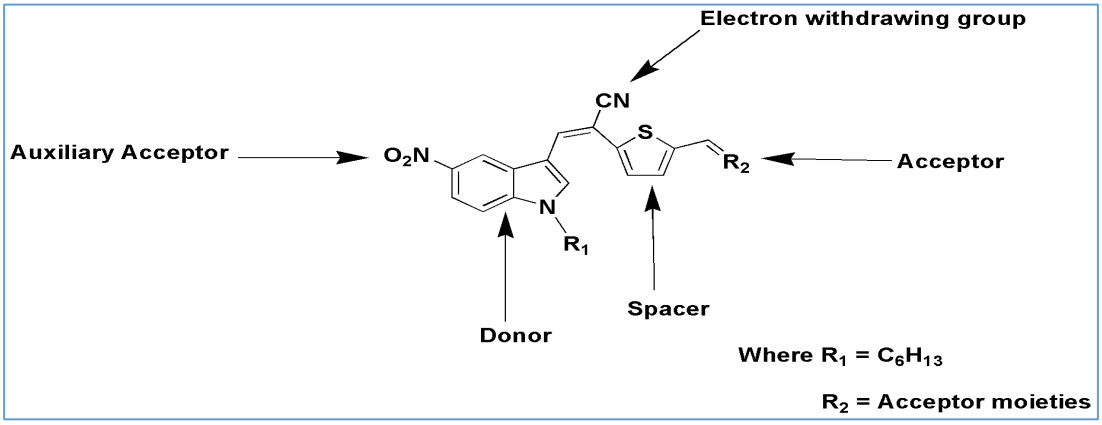

Fig.1.10 Design of **series 3** sensitizers

Design of triphenylamine substituted indole based co-sensitizers (Series 4; DBA-1 and DBA-2)

In the new design, a triphenylamine moiety is attached to an indole π-bridge linked to different acceptor units, leading to the formation of co-sensitizers **DBA-1** and **DBA-2**. Tripheylamine moiety has been introduced into the molecule to diminish the undesirable charge recombinations (Tian et al. 2008). Further, indole moiety has been incorporated in the current design predominantly due to its excellent electron donating capability and exceptional light harvesting proficiency (Jose et al. 2008, Higashijima et al. 2012, Sharma et al. 2013). Furthermore, the aforementioned design prevents the intermolecular π-π stacking of sensitizer molecules and hence, preventing the self-quenching of excited states and thereby enhancing the electron injection efficiency. These compounds, when used as co-adsorbents along with ruthenium based sensitizer **HD-2 (**Cheema et al. 2014), it is expected that, its photovoltaic efficiency would enhance by counteracting the competitive light absorption due to triiodide species in 400-500 nm range of the visible spectrum and also reducing the various undesired recombination processes happening inside the cell. Moreover, in order to avoid dye aggregation and to fine-tune the distance between the ruthenium based sensitizer **HD-2** molecules, hexyl chain has been introduced in the two

co-adsorbers. The presence of the hexyl chain avoids dye aggregation and thereby resulting in the enhancement of overall efficiency of the cell.

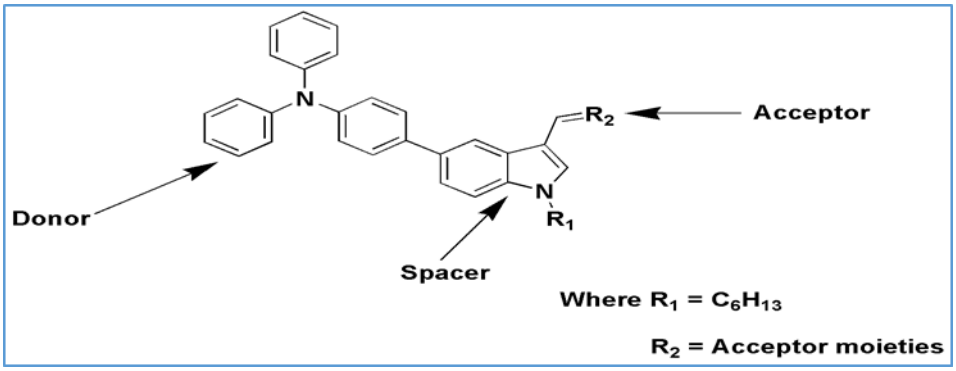

Fig.1.11 Design of **series 4** co-sensitizers

In addition, anchoring groups play a crucial role in DSSCs, as they are quintessential in grafting the sensitizer onto the semiconductor surface, and thereby enhancing the efficiency of electron injection from the excited state of the sensitizer into the conduction band of TiO_2. Keeping this in view, in the present design two different anchoring groups have been used and to comprehend effect on the co-adsorbing characteristics as well as on the overall efficiency of the cell. The design of **series 4** is depicted in **Fig.1.11**.

Design of substituted indole based co-sensitizers (Series 5; DBA-3 to **DBA-5)**

From the literature, it is quite evident that auxiliary donor groups are beneficial in extending the π-conjugation and thereby leading to the broadening of the absorption profile. In recent times, a wide range of strategies were employed to extend the π-electron delocalization and upturn the molar absorptivity coefficient of the materials. In this regard, the incorporation of triphenylamine, carbazole and thiophene moieties in some of the structures proved to be effective strategies for extending the π-conjugation of the chromophore and enhancing the molar absorptivity of the compound. Further, the aforesaid configuration makes the molecule to occupy a larger surface area than a molecule having linear shape and hence leading to the decline of dye loading capacity. Typically, the auxiliary donor groups improve the electron donating proficiency of the principal donor

and thereby leads a bathochromic shift in the absorption spectra that contributes to the enhancement of photocurrent (Babu et al. 2015). The typical moieties employed as auxiliary donors are nonplanar bulky substituted triarylamines with excellent electron-donating capabilities. However, in the present study the linear planar groups such as -methoxy or 4-methoxyphenyl donor group together with the electron-rich indole moiety have been used to provide a seamless electron migration from donor to acceptor. Further, indole moiety is incorporated in the current design predominantly due to its excellent electron donating capability and exceptional light harvesting proficiency (Higashijima et al. 2012). Moreover, in order to avoid dye aggregation and to fine-tune the distance between the ruthenium based sensitizer **NCSU-10** molecules, hexyl chains have been introduced in the two coadsorbers. The presence of these hexyl chains could avoid dye aggregation and thereby resulting in the enhancement of overall efficiency of the cell.

Besides, due to the higher extinction coefficients exhibited by the organic dyes, they can in turn minimize the amount of the dye required to yield appropriate optical density, this can provide enough space on the TiO_2 for the attachment of other sensitizer molecules. Further, due to the size differences between the organic co-sensitizers and the ruthenium based **NCSU-10** dye, the metal-oxide surface can be covered more effectively and efficiently as the small size of the organic dye can get adsorbed onto the gaps between the large **NCSU-10** sensitizer molecules. Against this background, in **series 5**, three new co-sensitizers, *viz.* **DBA-3**, **DBA-4** and **DBA-5** have been designed in order to investigate the effect of various auxiliary donor moieties on the performance of the solar cells. In the present design, anisole and methoxy groups have been incorporated as auxiliary donors, while barbituric acid has been employed as electron acceptor moiety. These compounds are used as co-sensitizers along with ruthenium based sensitizer **NCSU-10** (El-Shafei et al. 2012), to enhance its photovoltaic efficiency by counteracting the competitive light absorption due to triiodide species in 400-500 nm range of the visible spectrum and also reducing the various undesired recombination processes happening inside the cell. Since, the foremost objective of the present study is to comprehend the repercussions of varying the structure and strength of the auxiliary donor group on the co-sensitization properties of

small organic co-sensitizers, the aforementioned dyes have been designed. The design of **series 5** is depicted in **Fig.1.12**.

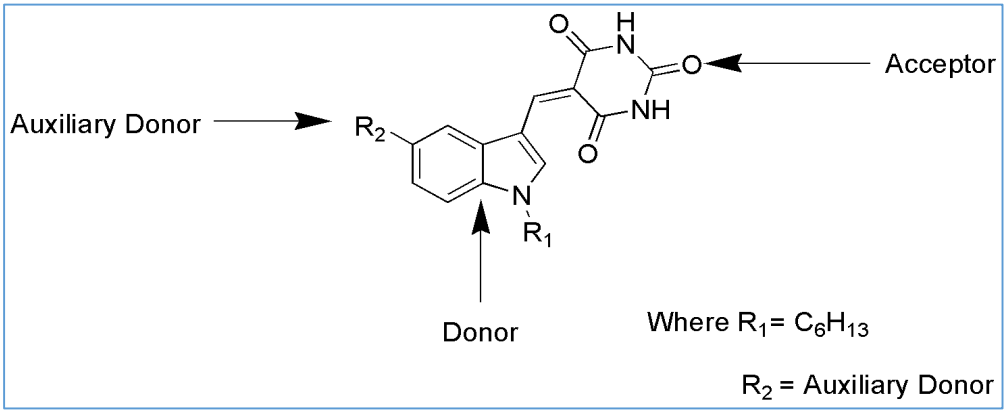

Fig.1.12 Design of **series 5** co-sensitizers

Design of indole based dual anchoring co-sensitizer (Series-6; DBA-8)

Lately, several organic sensitizers containing two anchoring groups were reported in the literature (Sirohi et al. 2012). Most of the dyes are plagued by inefficient charge injection due to the weak force of binding onto the TiO_2 surface. This can be resolved by the usage of bi-anchoring groups in sensitizers. Moreover, this results in broadening of the absorption spectrum of the dye due to the enhancement in the conjugation. These di-anchoring organic sensitizers possess several advantages over their mono-anchoring counter-parts, which include: (i) panchromatic response due to extended π-conjugation (ii) multi binding abilities to TiO_2 nanoparticles (iii) more electron extraction channels (iv) higher efficiency and (v) enhanced stability. Further, the presence of only one anchoring group per molecule in the organic sensitizers may lead to serious impairments with respect to their ruthenium based counter-parts, wherein 1 to 4 anchoring groups are present for the efficient injection of photo-excited electrons into the conduction band of the semiconductor through the anchoring groups by metal to ligand charge transfer (MLCT) process (Hagfeldt and Grätzel 1991). On the other hand, di-anchoring sensitizers are known to exhibit lower open circuit photovoltage (V_{oc}) compared to their mono-anchoring counterparts. The aforesaid trait can be attributed to enhanced charge recombination process in di-anchoring sensitizers (Ren et al. 2012). Therefore, there is a great yearning to optimize the structure

of dual anchoring dyes for more efficient DSSCs. Abbotto and co-workers reported several symmetric di-branched di-anchoring organic dye with A-π–D-π–A architecture. These dyes exhibited improved light harvesting properties as well as higher stability than its mono-anchoring analogs (Abbotto et al. 2011). However, most of the available literature on di-anchoring sensitizers are focused on the symmetric architecture, but reports on the asymmetric di-anchoring dyes are quite rare. In order to obtain high photovoltaic conversion efficiency, the sensitizer must possess a wide absorption characteristics and thereby, efficiently absorbing maximum number of photons from the electromagnetic spectrum. However, researchers have been unsuccessful in synthesizing an organic sensitizer having strong photon absorption throughout the wide range of wavelengths (350-900 nm).

Keeping the aforesaid point in view, co-sensitization strategy was implemented, wherein an organic dye is employed as a co-sensitizer along with a ruthenium based sensitizer with complementary absorption spectra and thus enhancing the overall efficiency of the DSSC (Magne et al. 2013). Further, π-conjugating moieties are known to play a vital role in enhancing electrochemical and spectroscopic properties as well as increasing the overall stability of the resulting molecules. Keeping all this in view, an unsymmetrical di-anchoring organic co-sensitizer **DBA-8** having one donor and two acceptor/anchoring groups to be employed as co-sensitizer along with ruthenium based dye **NCSU-10**, has been designed. In the present design, thiophene has been adopted as π-conjugating moiety due to its excellent charge transporting capability, polarizabilty, as well as tunable electrochemical and spectroscopic properties including enhanced molar extinction coefficients at longer absorption wavelengths. Further, barbituric acid has been employed as acceptors/ anchoring moieties. Furthermore, a hexyl alkyl chain is attached on the indole unit to assist in suppressing the unwanted electron recombination reactions in DSSC and also to improve the solubility of the dye in common solvents. In addition, the following key traits required by an ideal candidate for a co-sensitizer, *i.e.* high molar extinction coefficient around 400 nm region to recuperate the drop in the IPCE spectra due to

competitive light absorption by the tri-iodide species present in the electrolyte (Han et al. 2012) have been successfully instilled. **Fig.1.13** shows the design of co-sensitizer **DBA-8**.

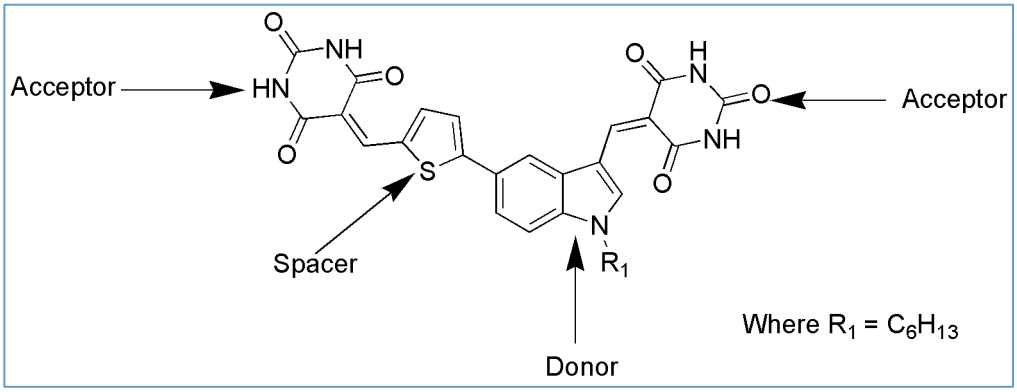

Fig.1.13 Design of **series 6** co-sensitizer

The newly designed sensitizers/co-sensitizers of **series 1-6** have been synthesized by adopting various synthetic techniques as depicted in **Schemes 2.1**, **3.1**, **4.1, 5.1**, **6.1** and **7.1,** respectively. Their preparation methods and experimental conditions have been established. Their purification methods have been developed and the purified compounds are then characterized by various spectroscopic techniques such as FTIR, ^{1}H NMR, ^{13}C NMR and mass spectrometry followed by elemental analysis. Their redox properties have been investigated by cyclic voltammetric studies. Also, they have been evaluated for UV-visible absorption and fluorescence emission spectral studies. Further, density functional theory (DFT) and time dependent density functional theory (TDFT) studies have been carried out to gain an insight into the electronic distribution in the HOMO and LUMO levels of the sensitizer/co-sensitizer molecule and obtain simulated absorption spectra of the newly synthesized molecules. Finally, DSSCs have been fabricated using each of the newly synthesized sensitizer/co-sensitizer molecule and photovoltaic parameters have been obtained. Electrochemical impedance studies have also been carried out to study interfacial charge transfer and the recombination process in DSSCs. A detailed description of the aforementioned studies of **series 1-6** have been discussed in **chapter 2-7**, respectively. Finally, summary and important research outcomes have been highlighted in concluding **chapter 8**.

CHAPTER 2

INDOLE BASED DYES WITH D-π-A CONFIGURATION: SYNTHESIS, CHARACTERIZATION AND PERFORMANCE STUDIES

Abstract

Chapter 2 *covers the experimental protocols pertaining to synthesis, optical and electrochemical studies, and device fabrication studies of newly designed sensitizers* ***D*****$_{1-3}$***. It also involves theoretical calculations of the aforesaid sensitizers. Further, it includes a detailed discussion on the obtained results.*

2.1 INTRODUCTION

Based on the detailed literature survey, three new Donor-π-Acceptor (D-π-A) type dyes **D$_{1-3}$ (series 1)** with three different acceptor units were designed by following the design strategy described in **chapter 1 (Section 1.11)** and synthesized. The new dyes were characterized using various spectral and elemental analyses. Their optical and electrochemical properties were investigated, while their photovoltaic performance was evaluated by a device fabrication study. Further, density functional theory study was carried out to investigate their Frontier Molecular Orbital energy states. Additionally, a single crystal X-ray diffraction study was performed to confirm the structure of a key intermediate. The experimental as well as results and discussion pertaining to the aforementioned series have been covered in this chapter. **Fig.2.1** depicts the chemical structures of the newly designed sensitizers (**E$_{1-3}$**).

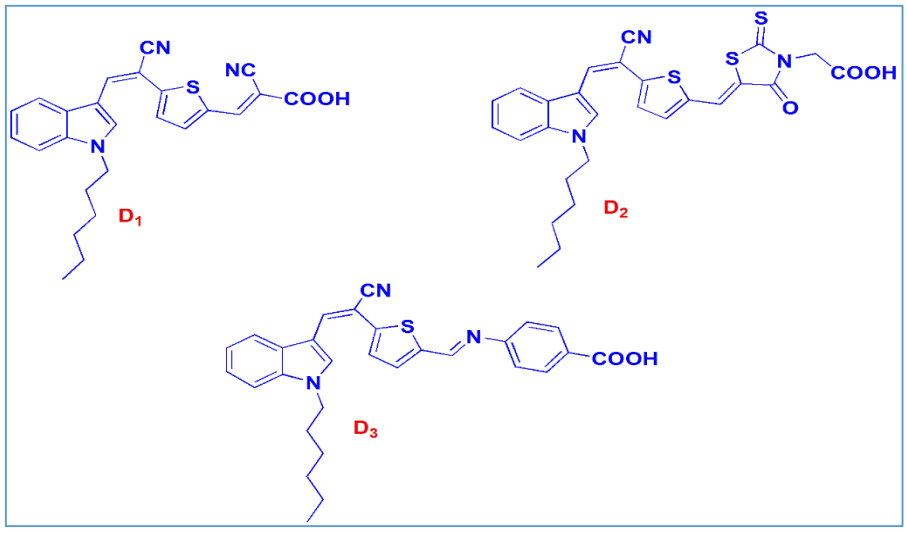

Fig.2.1 Chemical structures of sensitizers **D$_{1-3}$**

2.2 EXPERIMENTAL

2.2.1 Materials and methods

The starting materials indole-3-carbaldehyde, thiophene-2-acetonitrile, 1-bromohexane, cyanoacetic acid, rhodanine-3-acetic acid and 4-aminobenzoic acid were purchased from Sigma-Aldrich and were used without any further purification unless stated otherwise. ^{1}H NMR and ^{13}C NMR spectra were run using a Bruker avance 500MHz and 400MHz spectrometers, using DMSO-d6 and $CDCl_3$ as solvents and TMS as an internal standard. The single crystal X-ray diffraction analysis was conducted using BRUKER APEX DUO. Mass spectra were recorded on thermo scientific- EXACTIVE (ESI-MS). FTIR spectra were run using Nicolet Avatar 5700. Elemental analysis was carried out on a Flash EA1112 CHNS analyzer (Thermo Electron Corporation). PV measurements were performed using oriel PV measurement system.

2.2.2 Synthesis of sensitizers $D_{1\text{-}3}$

The synthetic scheme for the three new sensitizers is depicted in **scheme 2.1**. In the first step, the indole-3-aldehyde was alkylated using 1-bromohexane to yield *N*-hexyl indole derivative **2.1**. The product was then condensed with thiophene-2-acetonitrile in the presence of sodium methoxide to give *3*-(1-hexyl-1*H*-indol-3-yl)-2-(thiophen-2-yl)acrylonitrile **2.2**, *via* a Knoevenagel reaction. Further, the resulting product was subjected to Vilsmeier-haack formylation to form the precursor **2.3**. In the final step, the target compounds $\mathbf{D_{1\text{-}2}}$ were obtained in reasonably good yield by a Knoevenagel condensation of the aldehyde **2.3** with cyanoacetic acid and rhodanine-3-acetic acid in presence of acetic acid and ammonium acetate respectively, whereas compound $\mathbf{D_3}$ was obtained by the condensation of precursor **2.3** with 4-aminobenzoic acid. All the new compounds were characterized using various spectroscopic tools. Details of synthetic methods along with characterization data are provided in **section 2.2.6**.

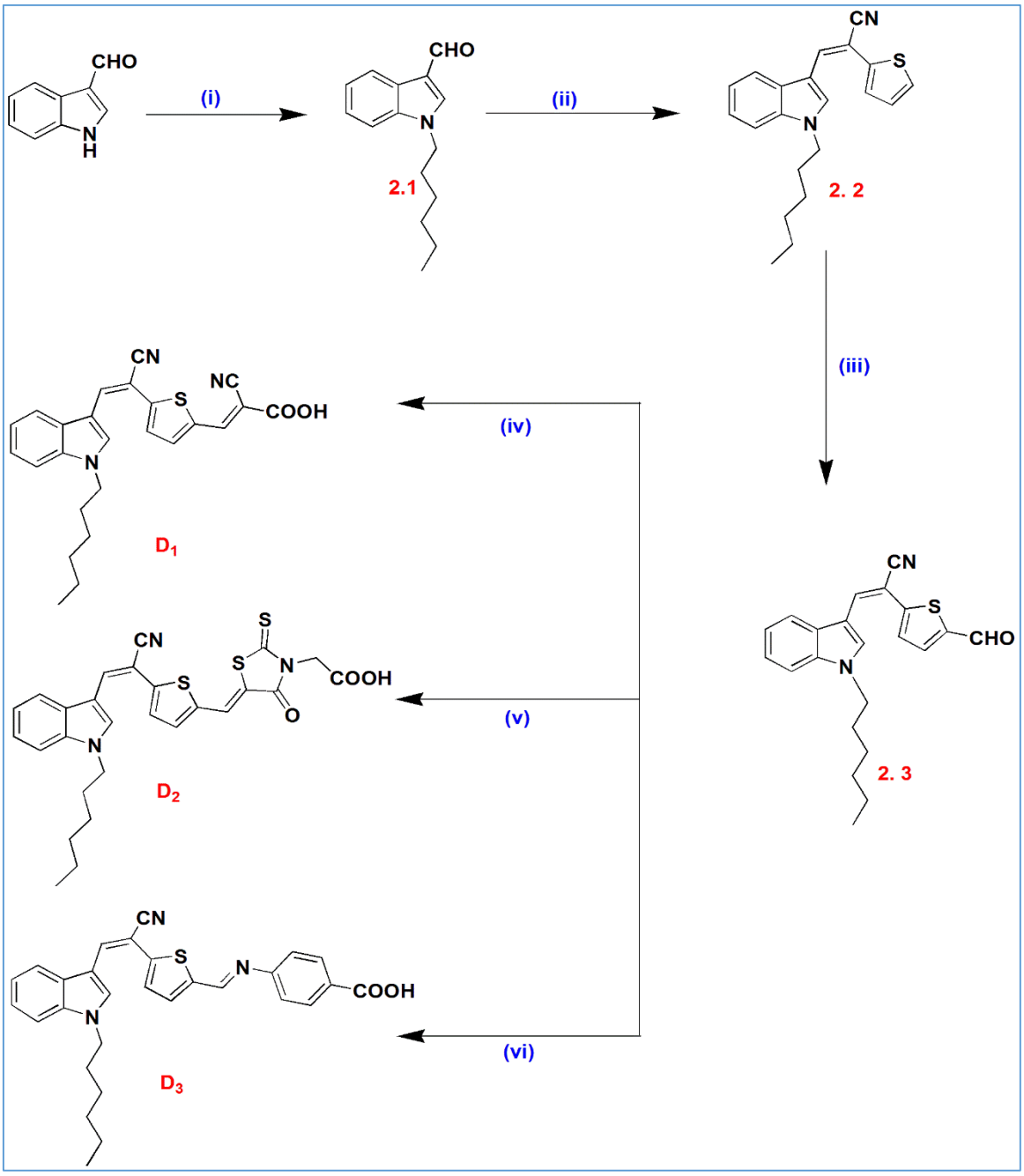

Scheme 2.1. Synthetic route of the sensitizers (i) 1-Bromohexane, K_2CO_3, DMF, RT (ii) 2-(thiophen-2-yl)-acetonitrile, NaOMe, CH_3OH, RT (iii) $POCl_3$, DMF, RT (iv) Cyanoacetic acid, ammonium acetate, glacial CH_3COOH, 110 ^{0}C (v) Rhodanine-3-acetic acid, ammonium acetate, glacial CH_3COOH, 110 ^{0}C (vi) 4-Amino benzoic acid, CH_3OH, 80 ^{0}C

2.2.3 Optical and electrochemical characterization

UV-visible spectra were obtained using GBC Cintra 101. Further, the fluorescence spectra were recorded using Perkin Elmer LS55 fluorescence spectrophotometer. The UV-visible spectra of $\mathbf{D_{1\text{-}3}}$ were recorded in chloroform (3×10^{-5} M) solution and the corresponding spectra are depicted in **Fig.2.6** and the pertaining data is summarized in **Table 2.2**.

The electrochemical studies were performed on AUTOLAB PGSTAT30 by following the three electrode system, consisting of glassy carbon as the working electrode, platinum as counter and Ag/AgCl as a reference electrode. The electrode system was immersed in the electrolyte [0.1 M$(n\text{-Bu})_4N^+(ClO_4)^-$ in acetonitrile] and data were recorded at a scan rate of 100 mV/S. All the measurements were calibrated using ferrocene as standard. The dye solution was drop casted on a glassy carbon electrode and was used as a working electrode. Before recording electrochemical data nitrogen was purged for a few minutes. The data obtained from the electrochemical studies are tabulated in **Table 2.2**.

Further, EIS measurements were done for the fabricated DSSC under 85 mW cm^{-2} light illumination by using an Autolab PGSTAT potentiostat/galvanostat-84610. The impedance spectra were recorded with a frequency ranging between 10 kHz and 1 Hz at their open circuit potential (OCP). The graphs obtained from EIS measurements are depicted in **Fig.2.10**.

2.2.4 Theoretical calculations

In order to gain a better understanding of the electronic and optical properties, density functional theory (DFT) calculations were performed at the def-TZVPP (Schafer et al. 1994) level using Turbomole software package (Ahlrichs et al. 1989, Deglmann et al. 2004). These calculations are used to obtain the electronic distribution in frontier molecular orbitals. All the geometries were first optimized with semi empirical AM1 basis with MOPAC in Tmolex. The aforementioned geometries were further optimized using C_1 point group symmetry at density functional theory level using the BP functional. The default

convergence criteria were used in all the geometry optimization. The resolution of the identity approximation and def-TZVPP basis set were used in all calculations. The optimized geometries and electronic distribution in the HOMO and LUMO levels are depicted in **Fig.2.7**.

2.2.5 DSSC fabrication

DSSC fabrication was done as per the following procedure. Preparation of the TiO_2 nanoparticles was done by following the procedure reported in the literature (Sirimanne and Tributsch 2004). Thus obtained TiO_2 was coated onto the FTO glass plate (1 cm^2) by doctor blade technique. The photoanode was then sensitized by dipping in a dye solution (0.3 mM) for 24 h. The counter electrode was prepared by drop-casting hexachloroplatinic acid in distilled *iso*-propanol solution (50 mM) and subsequent heating at 400 ^oC for 15 min. The two electrodes were held together by using binder clips. A drop of electrolyte (0.05 M I_2 / 0.5 M KI / 0.5 M 4-*tert*-butylpyridine (TBP) in 2-methoxypropionitrile) was introduced between the two electrodes through predrilled holes by vacuum backfilling. The results pertaining to photovoltaic characterization are tabulated in **Table 2.3**.

2.2.6 Synthetic methods

Synthesis of *1-hexyl-1H-indole-3-carbaldehyde (2.1)*

A mixture of 1-bromohexane (0.682 g, 4.13 mmol), indole-3-carbaldehyde (0.5 g, 3.44 mol), potassium carbonate (0.571 g, 4.13 mmol), in DMF (15 mL) was stirred at room temperature for 10 h. The reaction was then neutralized with dil. HCl and the product was extracted using ethyl acetate/water (50 mL × 3). Organic phase was dried using sodium sulfate. The solvent was removed under reduced pressure and the crude oily product obtained was further purified by column chromatography on silica gel using hexane as an eluent. The product was a light brown color liquid. Yield: 85%. (ATR, cm^{-1}): 3103(-C-H aromatic stretching); 2974 (-C-H aliphatic stretching); 1671 (aldehyde –C=O). ^1H NMR (400 MHz, DMSO-d6): δ (ppm) 9.92 (s, 1H), 8.32 (s, 1H), 8.13 (d, *J* = 7.6 Hz, 1H), 7.61 (d, *J* = 8.4 Hz, 1H), 7.33-7.23 (m, 2H), 4.26 (t, *J* = 6.8 Hz, 2H), 1.78 (t, J = 6.5 Hz, 2H),

1.24 (s, 6H), 0.83 (t, *J* = 6.8 Hz, 3H). Anal. Calcd for $C_{15}H_{19}NO$: C, 78.56; H, 8.35; N, 6.11 found: C 78.66; H, 8.43; N, 6.19.

Synthesis of *3-(1-hexyl-1H-indol-3-yl)-2-(thiophen-2-yl)acrylonitrile (2.2)*

To a freshly prepared solution of sodium methoxide (0.132 g, 5.76 mmol of sodium in 10 mL of methanol), 1-hexyl-1*H*-indole-3-carbaldehyde (**2.1**, 1.1 g, 4.8 mmol) was added slowly while stirring. Thiophene-2-acetonitrile (0.709 g, 5.76 mmol) was then added to reaction mass. Stirring was continued for 6h at room temperature. The precipitated yellow solid was collected by filtration, washed with methanol and finally recrystallized from chloroform. Yellow solid, yield 65%, m.p. 91-93 ^{0}C. (ATR, cm^{-1}): 3103(-C-H aromatic stretching); 2974 (-C-H aliphatic stretching); 2207 (-CN stretching). ^{1}H NMR (400 MHz, DMSO-d6): δ (ppm) 8.31 (s, 1H), 8.00 (d, *J* = 7.6 Hz, 1H), 7.96 (s, 1H), 7.61 (d, *J* = 8 Hz, 1H), 7.58 (d, *J* = 4.8 Hz, 1H), 7.40 (s, 1H), 7.30 (t, *J* = 7.2 Hz, 1H), 7.23 (t, *J* = 7.6 Hz, 1H), 7.15 (s, 1H), 4.31 (t, *J* = 6.8 Hz, 2H), 1.78 (s, 2H), 1.27 (s, 6H), 0.83 (t, *J* = 6.4 Hz, 3H). Anal. Calcd. for $C_{21}H_{22}N_2S$: C,75.41; H,6,63; N, 8.38 found: C 73.21; H, 6.69; N, 8.43.

Synthesis of *2-(5-formylthiophen-2-yl)-3-(1-hexyl-1H-indol-3-yl)acrylonitrile (2.3)*

A dry round bottomed flask was charged with freshly distilled DMF (0.32 mL, 3 eq) and $POCl_3$ was added to it drop-wise (0.686 mL, 5 eq) at 0 ^{o}C under nitrogen. The mixture was stirred for 30 min. and to this 3-(1-hexyl-1*H*-indol-3-yl)-2-(thiophen-2-yl)acrylonitrile (**2.2**, 0.5 g, 1.49 mmol) dissolved in dichloroethane (5 mL) was added while stirring and stirring was continued at room temperature for 12 h. The reaction mass was then poured into ice cold water and subsequently basified by using 5M NaOH solution. The precipitated solid was collected by filtration and the crude product was purified by column chromatography on silica gel using ethyl acetate/ hexane (1:5) as mobile phase to give orange colored solid. Yield: 55%, m.p. 99-101^{0}C. IR (ATR, cm^{-1}): 2974 (C-H stretching); 2207 (-CN stretching); 1689 (aldehyde –C=O).^{1}H NMR (500 MHz, $CDCl_3$): δ (ppm) 9.86 (s, 1H), 8.38 (s, 1H), 7.891 (s, 1H), 7.77 (d, *J* = 7.5 Hz, 1H), 7.69 (d, *J* = 4 Hz 1H), 7.41(d, *J* = 8 Hz, 1H), 7.36-7.26 (m, 4H), 4.21 (t, *J* = 7.2 Hz, 2H), 1.353-1.25 (bs,

8H), 0.88 (t, *J* = 6.5Hz, 3H). ^{13}C NMR (125 MHz, $CDCl_3$) δ (ppm): 182.33, 149.85,141.38, 137.34, 136.05, 134.83, 131.14, 128.06, 125.08, 123.57, 121.95, 118.31, 118.25, 110.55, 110.29, 97.20, 47.54, 31.30, 31.23, 29.91, 29.78, 26.53, 26.43, 22.49, 22.45, 13.97. Anal. Calcd. for $C_{22}H_{22}N_2$ OS: C,75.89; H,6.12; N, 7.73 found: C,75.77; H,6.19; N, 7.68. ESI-MS (+ve mode) m/z Calcd for $C_{22}H_{22}N_2OSNa$: 385.15. Found: 385.13 $[M + Na]^+$.

Synthesis of *2-cyano-3-(5-((Z)-1-cyano-2-(1-hexyl-1H-indol-3-yl)vinyl)thiophen-2-yl)acrylic acid (D_1)*

A dried round bottomed flask was charged with 2-(5-formylthiophen-2-yl)-3-(1-hexyl-1*H*-indol-3-yl)acrylonitrile (**2.3**, 0.100 g, 0.275 mmol), cyano acetic acid (0.028 g, 0.331 mmol), and ammonium acetate (0.233 g, 3.03 mmol) and the mixture was dissolved in glacial acetic acid (20 mL) under argon. This mixture was then heated under reflux for 12 h. After completion of the reaction, the mass was cooled to room temperature and was poured into ice cold water. The obtained solid was filtered. The crude product was purified by column chromatography using silica gel and $CHCl_3$: CH_3OH (10:1) as mobile phase to get red color solid. Yield: 41%, m.p. 228-230^{0}C. IR (ATR, cm^{-1}): 3509 (O-H stretching); 2923 (C-H stretching); 2211 (-CN stretching); 1725 (Carboxylic -C=O). ^{1}H NMR (400 MHz, DMSO-d6): δ 8.48 (s, 1H), 8.46 (s, 1H), 8.29 (s, 1H), 8.092 (d, *J* =7.6 Hz, 1H), 8.01 (d, *J* = 4 Hz, 1H), 7.71 (d, *J* = 4 Hz, 1H), 7.65 (d, *J* = 8.4Hz, 1H), 7.35-7.26 (m, 2H), 4.36 (t, *J* = 6.8 Hz, 2H), 1.912 (s, 2H), 1.28-1.22 (bs, 6H), 0.83 (t, *J* = 6.4 Hz, 3H). ^{13}C (100MHz, DMSO-d_6) δ(ppm) : 164.09, 149.47, 146.68, 141.81, 136.42, 134.31, 132.38, 127.96, 125.01, 123.90, 122.12, 119.77, 118.89, 117.03, 111.66, 110.50, 95.93, 46.97, 31.16, 29.91, 26.21, 22.47, 21.52, 14.31. Anal. Calcd. for $C_{25}H_{23}N_3O_2S$: C,69.91; H,5.40; N, 9.78 found: C, 69.79; H, 5.47; N, 9.71. ESI-MS (+ve mode) m/z Calcd for $C_{25}H_{23}N_3O_2SNa$: 452.15. Found: 452.14 $[M + H]^+$.

Synthesis of *2-((Z)-5-((5-((Z)-1-cyano-2-(1-hexyl-1H-indol-3-yl)vinyl)thiophen-2-yl)methylene)-4-oxo-2-thioxothiazolidin-3-yl)acetic acid (D_2)*

A mixture of 2-(5-formylthiophen-2-yl)-3-(1-hexyl-1*H*-indol-3-yl)acrylonitrile (**2.3**, 0.100 g, 0.275 mmol), rhodanine-3-acetic acid (0.063 g, 0.331 mmol), and ammonium

acetate (0.233 g, 3.03 mmol) was taken in a dry RBF and dissolved in glacial acetic acid (20 mL) under argon. This mixture was then heated under reflux for 12 h. After cooling the reaction mixture to room temperature, the reaction mass was poured into ice cold water and the obtained solid was collected by filtration. The crude product was purified by column chromatography using silica gel and $CHCl_3$:CH_3OH (10:1) as a mobile phase. The product was obtained as a dark colored solid. Yield 39%, m.p. 239-240^{0}C. IR (ATR, cm^{-1}): 3466 (O-H stretching); 2953 (C-H stretching); 2216 (-CN stretching); 1700 (Carboxylic -C=O). ^{1}H NMR (400MHz DMSO-d6, ppm): δ 8.42 (s, 1H), 8.22 (s, 1H), 8.13 (s, 2H), 7.80 (s, 1H), 7.64 (d, *J* = 6.8, 1H), 7.59 (s, 1H), 7.33-7.27 (m, 2H), 4.69 (s, 2H), 4.35 (bs, 2H), 1.80 (s, 2H), 1.28 (bs, 6H), 0.84 (s, 3H). ^{13}C (100MHz, DMSO-d_6) δ(ppm) : 192.21, 136.36, 136.27, 135.35, 126.24, 123.83, 121.96, 111.55, 96.43, 46.93, 31.17, 29.93, 26.23, 22.48, 14.31. Anal. Calcd. for $C_{25}H_{23}N_3O_2S$: C,69.91; H,5.40; N, 9.78 found: C, 69.79; H, 5.47; N, 9.71. ESI-MS (+ve mode) m/z Calcd for $C_{27}H_{25}N_3O_3S_3$: 535.11. Found: 535.14 $[M + H]^+$.

Synthesis of *4-((E)-(5-((Z)-1-cyano-2-(1-hexyl-1H-indol-3-yl)vinyl)thiophen-2-yl)methyleneamino)benzoic acid (D_3)*

A mixture of 2-(5-formylthiophen-2-yl)-3-(1-hexyl-1*H*-indol-3-yl)acrylonitrile (**2.3**, 0.100 g, 0.275 mmol) and 4-aminobenzoic acid (0.037 g, 0.275 mmol) was heated under reflux in absolute methanol for 3 h. The separated solid was filtered and recrystallized from methanol to obtain bright orange color solid. Yield 77%, m.p. 233-235^{0}C. IR (ATR, cm^{-1}): 3006 (O-H deformation of carboxyl); 2926 (C-H stretching); 2210 (-CN stretching); 1697 (Carboxylic -C=O). ^{1}H NMR (400MHz DMSO-d_6, ppm): δ 8.82 (s, 1H), 8.44 (s, 1H), 8.17 (s, 1H), 8.11 (d, *J* = 8, 1H), 7.98 (d, *J* = 8, 1H), 7.73 (d, *J* = 3.6, 1H), 7.74 (d, *J* = 8, 1H), 7.43 (d, *J* = 8, 1H), 7.47 (d, *J* = 3.2, 1H), 7.36-7.24 (m, 4H), 4.35 (t, *J* = 6.4, 2H), 1.80 (s, 2H), 1.28 (s, 6H), 0.84 (t, *J* = 6.4, 3H). ^{13}C (100MHz, DMSO-d_6) δ(pmm) : 167.46, 155.38, 154.83, 145.11, 141.18, 136.31, 135.97, 134.89, 131.42, 131.12, 128.66, 127.95, 125.41, 123.69, 121.85, 121.69, 119.69, 118.87, 111.47, 110.32, 97.09, 46.86, 31.17, 29.94, 26.23, 22.47, 14.30. Anal. Calcd. for $C_{29}H_{27}N_3O_2S$: C,72.32; H,5.65;

N, 8.72 found C,72.12; H,5.69; N, 8.75. ESI-MS (+ve mode) m/z Calcd for $C_{29}H_{27}N_3O_2S$: 481.18 Found: 482.18 $[M + H]^+$.

2.3 RESULTS AND DISCUSSION

2.3.1 Structural characterization

The chemical structures of newly synthesized compounds were confirmed by ^1H NMR, ^{13}C NMR spectroscopy and elemental analysis. In ^1H NMR spectrum of compound **D_3**, the aromatic proton at the second position of indole ring appeared as a singlet at δ 8.82 ppm. All the other aromatic protons depicted peaks between 8.44 and 7.24 ppm. Further, two protons of $–NCH_2$ of hexyl chain resonated as a singlet at δ 4.37 ppm, whereas the appearance of signals of primary and secondary protons signals in the range of δ 1.80-0.84 ppm in its ^1H NMR spectrum confirmed the presence of hexyl chain. ^{13}C NMR spectrum of **D_3** showed the characteristic signals obtained at higher frequency (downfield region). The carbonyl carbon atoms in acid group resonated at δ 167.46 ppm, whereas the remaining signals appearing in the region of δ 155.38-97.09 ppm are due to other aromatic carbons. Further, the aliphatic carbons appeared between 46.86-14.30 ppm. Furthermore, its mass spectrum exhibited the $[M+H]^+$ peak at 482.18, which is in agreement with the calculated molecular weight for the formula of $C_{29}H_{27}N_3O_2S$. **Fig.2.2, 2.3** and **2.4** show ^1H NMR, ^{13}C NMR and Mass spectra of compound **D_3**, respectively.

Spectrograms of selected target compounds

^1H NMR, ^{13}C NMR and Mass spectra of representative title compound (**D_3**) are given below

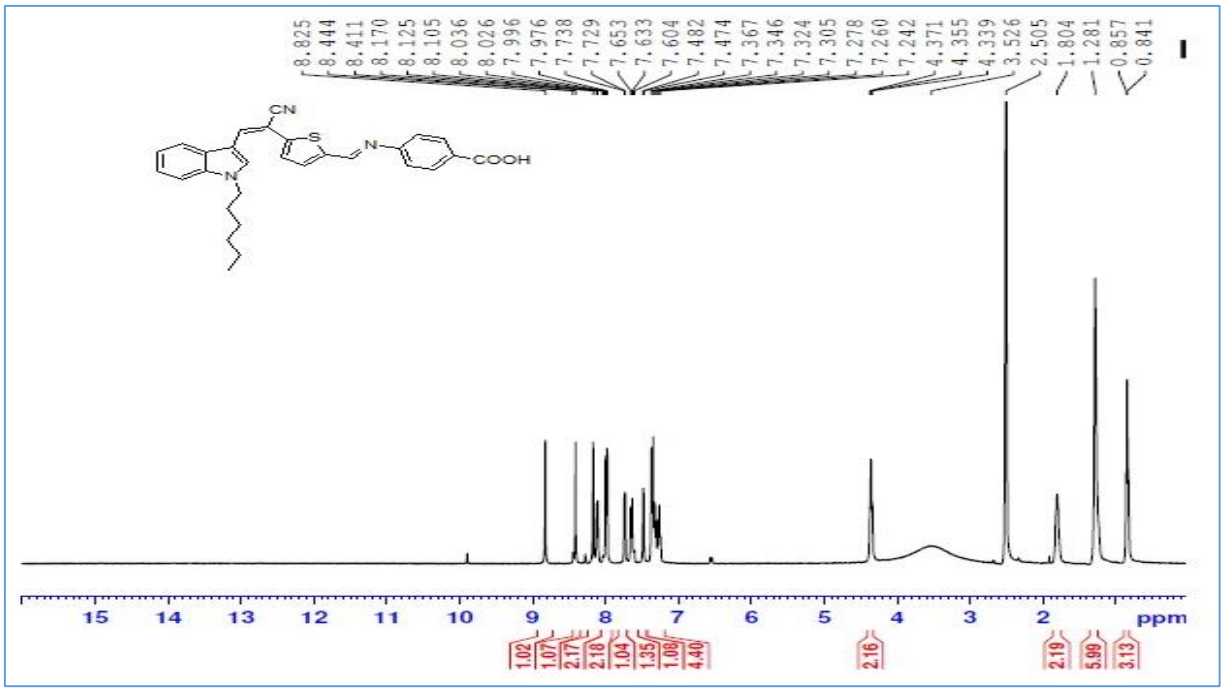

Fig.2.2 ^{1}H NMR spectrum of **D_3** in DMSO-d_6

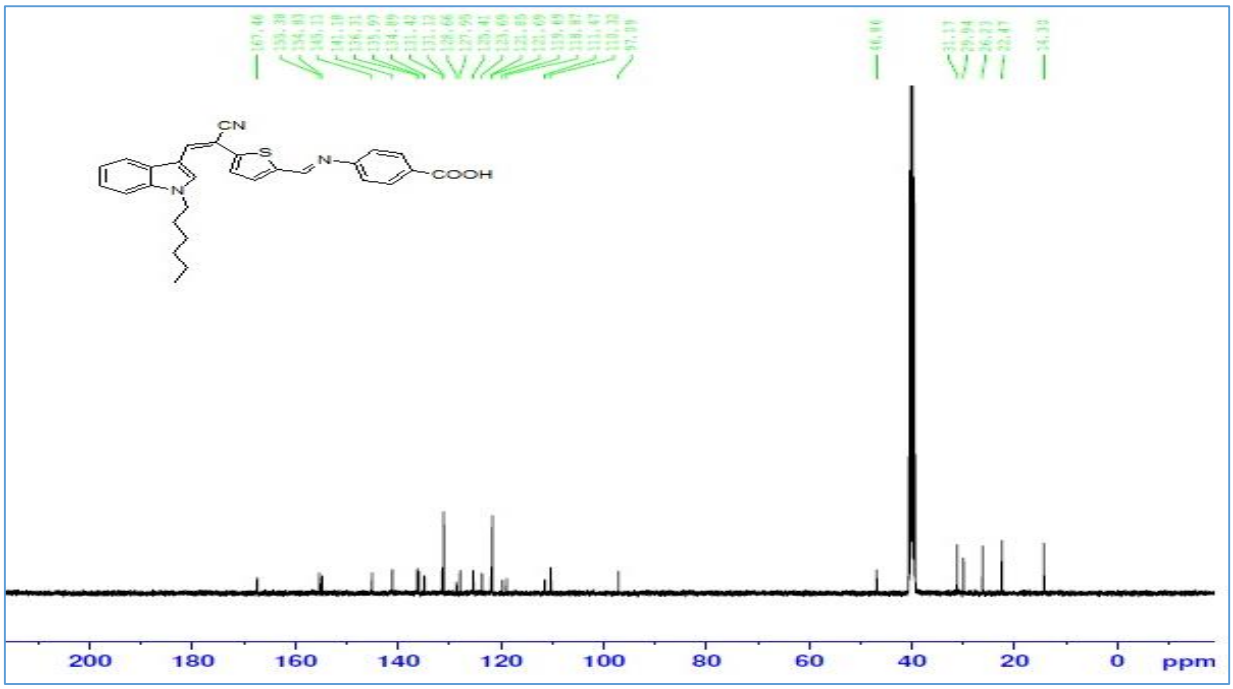

Fig.2.3 ^{13}C NMR spectrum of **D_3** in DMSO- d_6

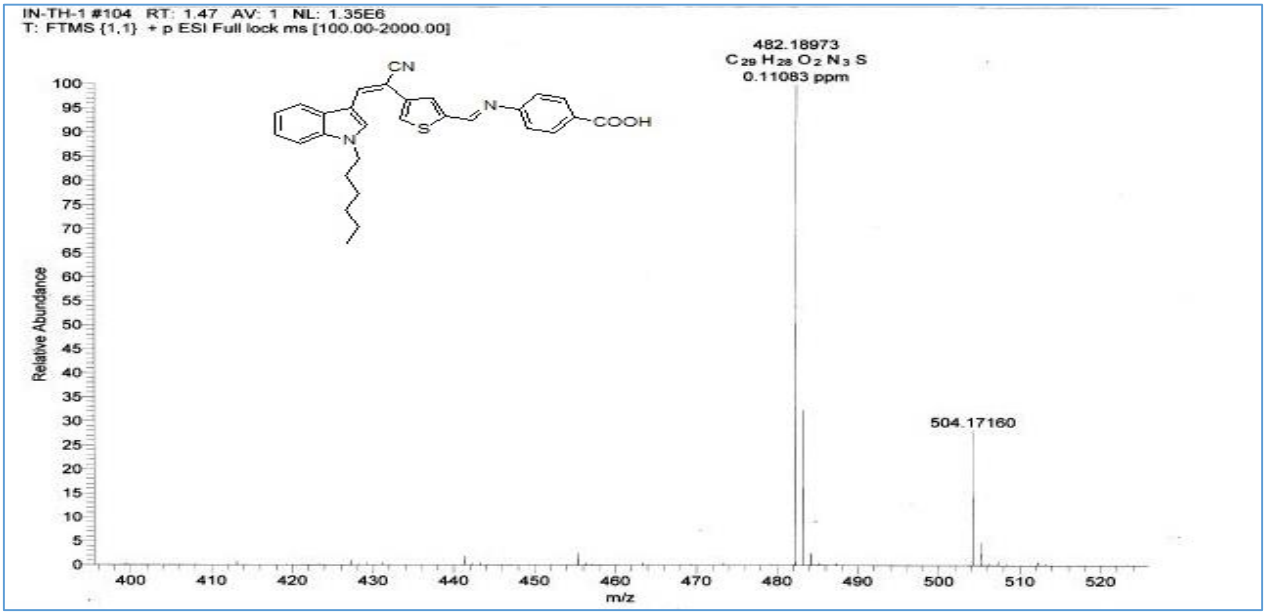

Fig.2.4 Mass spectrum of **D_3**

2.3.2 Crystal structure analysis

It is well known fact that molecules with D-π-A configuration have a low crystallization tendency, this peculiar feature is attributed to the planar nature of these type of molecules leading to aggregation (Menzel et al. 2012). Therefore, in order to have better understanding about the geometry of the dyes, the precursor *2-(5-formylthiophen-2-yl)-3-(1-hexyl-1H-indol-3-yl)acrylonitrile* (**2.3)**, has been crystalized. This has a similar structure as that of the sensitizers except that of the acceptor segment. Single crystals suitable for diffraction were obtained by slow evaporation of its solution prepared from a 1:1 mixture of chloroform and methanol. Data from the single crystal X-ray diffraction analysis are summarized in **Table 2.1**.

The study revealed that the compound crystalizes in triclinic space group P-1 having cell parameters a = 9.8714 (2) (Å), b = 11.0898 (3) Å, c = 9.8714 (2) Å, V = 985.12(4) Å, Z =2, α (^{0}) = 79.4660 (12), β (^{0}) = 79.1550 (11), γ (^{0}) = 69.5580 (11). **Fig.2.5** shows the ORTEP diagram of compound **3**, from which it is quite evident that the

molecule is almost planar. The planarity favors the flow of electron density from the donor segment to the acceptor segment through the π-conjugation bridge and thereby enhancing the overall efficiency of the sensitizers.

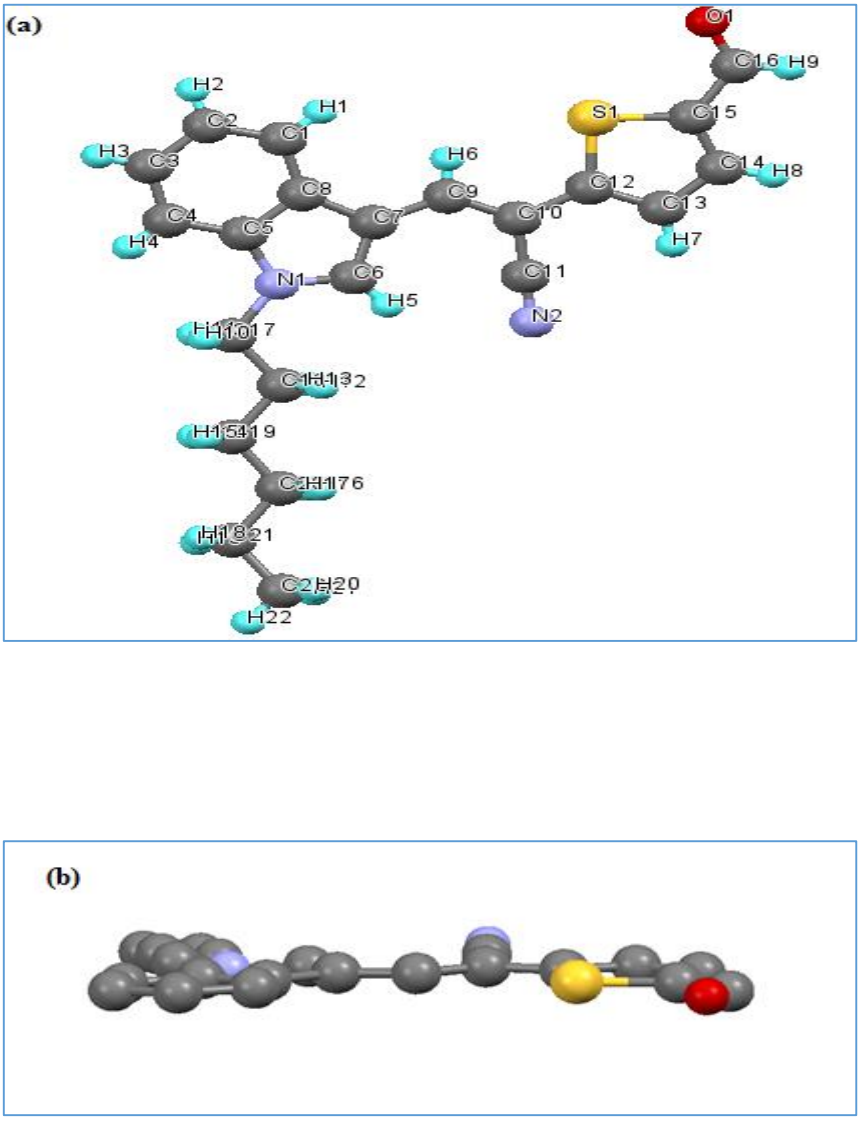

Fig.2.5 (a) ORTEP (50% probability) diagram **2.3** (b) side elevation, H atoms are omitted for clarity.

TABLE 2.1 Crystal and structure refinement data for compound **2.3**

Compound	**2.3**
Formula	$C_{22}H_{22}N_2OS$
Formula weight	362.49
CCDC number	999374
Temperature (K)	296(2)
Crystal form	Block
Colour	Red
Crystal system	Triclinic
Space group	P-1
a (Å)	9.8584(2)
b (Å)	9.8714(2)
c (Å)	11.0898(3)
α (^{0})	79.4660(12)
β (^{0})	79.1550(11)
γ (^{0})	69.5580(11)
Volume ($Å^3$)	985.12(4)
Z	2
Density (g cm^{-3})	1.222
μ(mm^{-1})	0.177
F (000)	384.0
$h_{min, max}$	-12, 12
$k_{min, max}$	-12, 12
$l_{min, max}$	-13, 13
Reflections collected	3871
$R_{_all}$, $R_{_obs}$	0.0468, 0.0372
$wR2_{_all}$, $wR2_{_obs}$	0.1347, 0.1197
GOOF	0.919

2.3.3 Photophysical properties

As depicted in **Fig.2.6 (a)**, all the dyes exhibited two broad peaks in the range of 334-378 nm and 451-511 nm; the low energy peak (451-511 nm) is attributed to intramolecular charge transfer (ICT) from the indole donor to the acceptor, whereas the peak corresponding to higher energy (334-378 nm) is be due to the π-π* transition. It must be noted that both the bands were red shifted while going from cyanoacetic acid to

rhodanine-3-acetic acid as acceptors. This bathochromic shift can be attributed to the extension of π-conjugated system and stronger electron withdrawing capability of rhodanine-3-acetic acid (Park et al. 2009, Tian et al. 2008). This shift is quite desirable as it escalates the light harvesting ability of the sensitizer. Further, the dyes showed relatively high molar extinction coefficient indicating good light harvesting capability. The molar extinction coefficients of all the sensitizers were determined according to Lambert–Beer law, the stock solution of each dye was prepared in chloroform at 10^{-5}-10^{-3} M, then diluted to five different concentrations. The absorbance at the corresponding λ_{max} was recorded for each sample and plotted versus the molar concentration of the solution. The corresponding extinction coefficients were obtained from the slope of the calibration curve between concentration and absorbance.

The values of molar extinction coefficients for **D_1**, **D_2**, and **D_3** are 79000, 56000 and 69000 $M^{-1}cm^{-1}$, respectively. These exceptionally high values of extinction coefficients can be attributed to the presence of cyanovinylene unit in all the dyes. The fluorescence emission spectra of the dyes were recorded upon their excitation wavelengths and the obtained data are summarized in **Table 2.2** and the corresponding spectra are shown in **Fig. 2.6 (b)**. From the results it is clear that the dyes exhibit a strong luminescence maxima in 549-577 nm region. The Stokes shifts were also calculated, ranging from 1380-3975 cm^{-1}. It is interesting to note that among the three sensitizers **D_3** showed the highest value for stokes shift, it may be caused by large changes in the dipole moment in the excited state, as a result of charge transfer from donor to acceptor moiety.

Table 2.2 Optical, electrochemical data and HOMO, LUMO energy levels of **D_{1-3}**

Dye	λ_{abs} [nm]	ε [M^{-1} cm^{-1}]	λ_{ex} [nm]	Δν [cm^{-1}]	Φ_f [%]	E^g_{opt} [eV]	E^o_{red} [V]	HOMO [eV]	LUMO [eV]
D_1	495	79000	577	2871	69.33	2.18	0.87	-5.71	-3.53
D_2	511	56000	549	1380	74.04	2.09	0.83	-5.66	-3.57
D_3	452	67000	551	3975	74.50	2.39	0.88	-5.93	-3.54

Further, the method described by Demas and Crosby was used to determine their fluorescence quantum yields (Φ_f) in solution state, with quinine sulphate in degassed 0.1M sulphuric acid as reference standard (Φ_f=54 %) (Crosby and Demas 1971). All the sensitizers exhibited very good quantum yield in the range of 69-74 % in their solution state (**Table 2.2**).

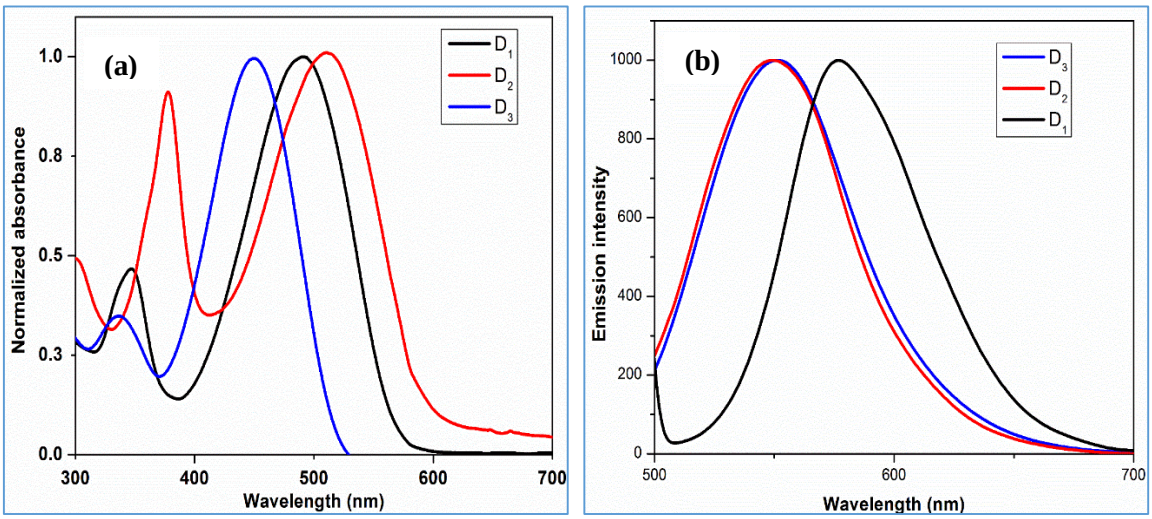

Fig.2.6 (a) UV-Vis spectra of **D_{1-3}** in chloroform (10^{-5} M) **(b)** Fluorescence spectra of **D_{1-3}** in chloroform (10^{-5} M).

2.3.4 Molecular modeling

From the **Fig.2.7**, it is quite clear that all the dyes exhibit similar type of Frontier molecular orbital distributions. It is observed that in the HOMO level the electron density is predominantly localized on the indole donor part and is extended along the thiophene bridge, whereas in the LUMO level the electron cloud shifts towards the acceptor part, via intramolecular charge transfer. This sort of movement in the electron density while going from the HOMO to LUMO level favors the effective injection of electrons in the conduction band of TiO_2. It is worth noting that, in the case of sensitizer **D_2**, the efficiency of electron injection from its LUMO level into the conduction band of the metal oxide is low. This can be explained on the basis of the greater distance between the LUMO of **D_2**

and that of its anchoring group which might be the reason for lower efficiency of DSSC based on **D_2** compared to the other two sensitizers (Jose et al. 2008).

DYE	Optimized geometry	HOMO	LUMO
D_1	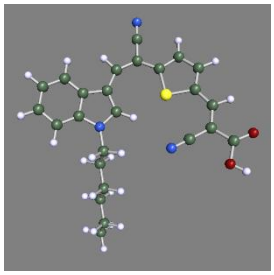	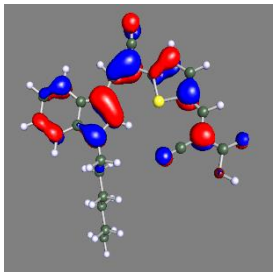	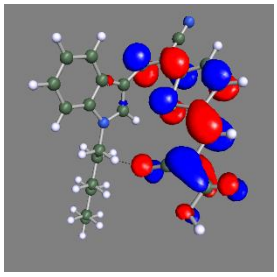
D_2	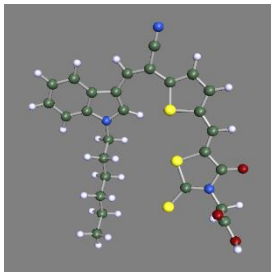	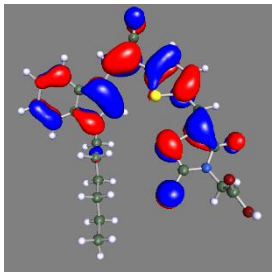	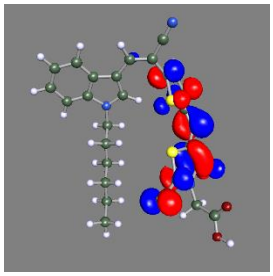
D_3	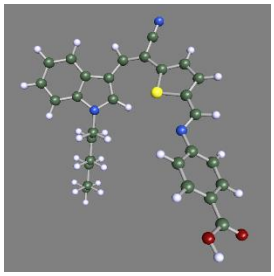	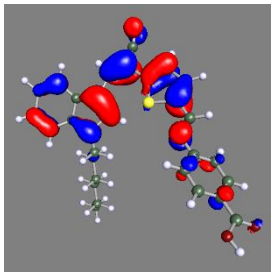	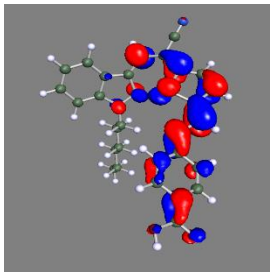

Fig.2.7 Optimized structure and Frontier molecular orbitals of **$D_{1\text{-}3}$**

2.3.5 Electrochemical characterization

A Cyclic voltammetry (CV) study was undertaken to determine the electrode potentials of the new sensitizers **$D_{1\text{-}3}$** and then to estimate the HOMO and LUMO levels of the dyes. These values are useful to find out the thermodynamic feasibility of electron

injection into the conduction band of the metal oxide from the HOMO level of dye molecule and dye regeneration by the electrolyte. For the calculations of LUMO levels the equation, E_{LUMO} = - [E_{red} (onset) - 4.4 eV], where E_{red} (onset) are the onset potential versus standard calomel electrode (SCE) for the reduction of the material referred, was used. The HOMO levels of the sensitizers were calculated by the addition of LUMO energy and $E_{0\text{-}0}$ energy of the dye obtained from the intersection of the absorption and emission spectral curves. The data obtained are tabulated in **Table 2.2**. **Fig.2.8** depicts the representational energy level diagram of the dyes.

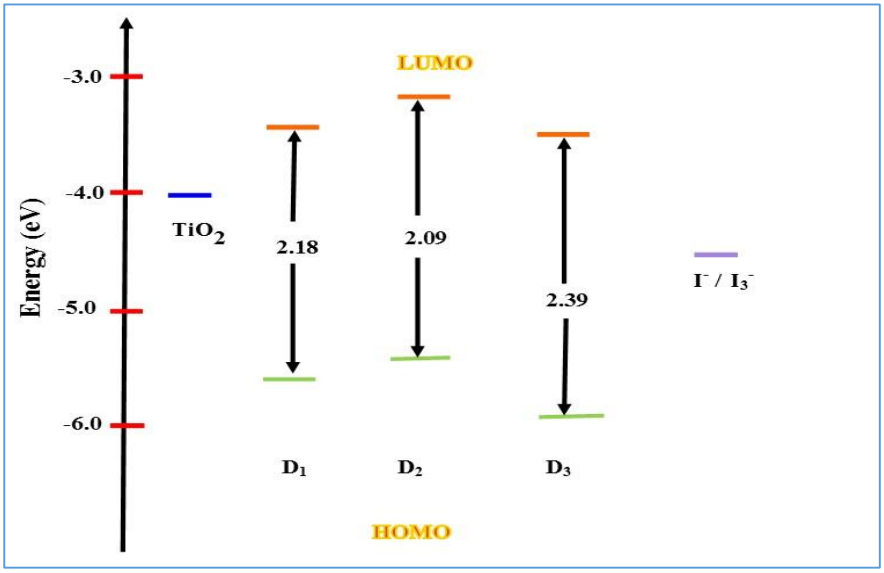

Fig.2.8 Representational energy level diagram of **$D_{1\text{-}3}$**.

2.3.6 Photovoltaic device characterization

Fig. 2.9 shows the photocurrent-voltage (*J-V*) curves of DSSCs based on **$D_{1\text{-}3}$** under AM 1.5 illumination (85 mW cm^{-2}), while **Table 2.3** summarizes the corresponding values of short-circuit photo- current density (J_{SC}), open circuit photovoltage (V_{oc}), fill factor (*ff*) and efficiency (η). The results indicate that the cell sensitized by **D_3** showed highest efficiency with a J_{sc} of 4.24 mA cm^{-2}, a V_{oc} of 640 mV, and a *ff* of 36.9, corresponding to an overall conversion efficiency of 1.18 %. Under similar conditions, cells sensitized by **D_1** and **D_2** exhibited J_{sc} values of 2.89 and 1.24 $mAcm^{-2}$, V_{oc} values of 577.46 and 509.94

mV and a fill factor of 53.0 and 47.6, corresponding to an overall efficiency of 1.04% and 0.35%, respectively. The observed data are summarized in **Table 2.3**.

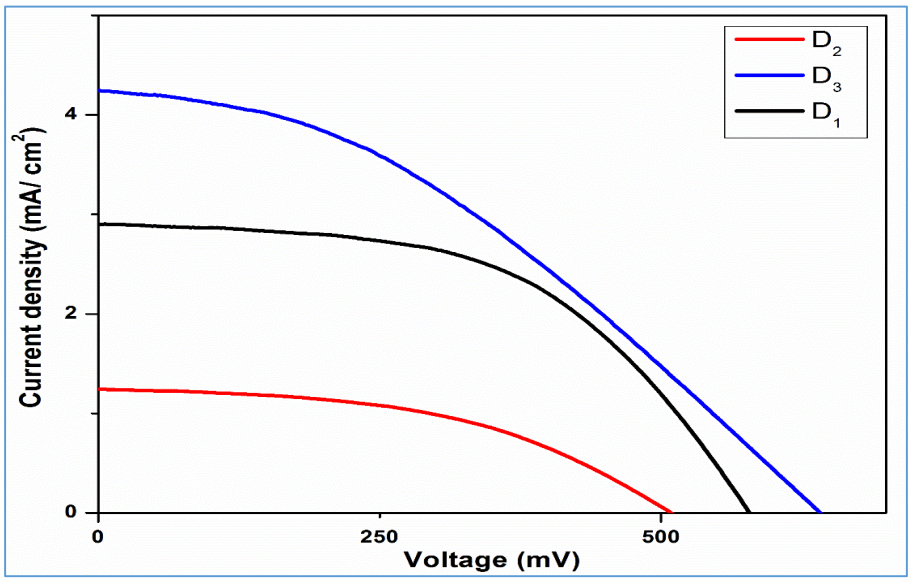

Fig.2.9 *J-V* characteristics of the DSSCs based on **D1-3**

Table 2.3 Photovoltaic performance of DSSCs based on **D1-3**

Dye	J_{sc} (mAcm^{-2})	V_{oc} (mV)	*ff* (%)	η (%)	Surface concentration	Electron lifetime (ms)
D1	2.89	577.46	53.0	1.04	0.92×10^{-5}	9.1
D2	1.24	509.94	47.6	0.35	1.87×10^{-5}	9.0
D3	4.24	640.89	36.9	1.18	2.75×10^{-5}	14.4

As explained earlier, the lower efficiency of **D2** can be attributed to breakage of delocalization leading to the separation of the LUMO from the anchoring group as a consequence of the -CH_2- unit (Tian et al. 2007). Generally, dye loading studies are performed in the quest to understand the difference in efficiency with the variation in the anchoring groups. Keeping this in view, to estimate the total amount of dye adsorbed on the TiO_2 surface, desorption of the dye from the TiO_2 was done using 0.1M NaOH in DMF/H_2O (1:1) mixture. The obtained data are summarized in **Table 2.3**. From the results

it is quite evident that concentration of **D_3** on TiO_2 surface was higher than that of other two. This is in agreement with the experimentally obtained J_{sc} values of **D_3**, which is the highest among the three sensitizers.

2.3.7 Electrochemical impedance spectroscopy characterization

EIS analysis was carried out for the dyes in order to study interfacial charge transfer and the recombination process in DSSCs. EIS measurements were done under 85 $mWcm^{-2}$ light illumination by using an Autolab PGSTAT potentiostat/galvanostat-84610. The impedance spectra were recorded with a frequency ranging between 10 kHz to 1Hz at their open circuit potential (OCP). **Fig.2.10 (a)** shows the generated Nyquist plots for the DSSCs fabricated using **$D_{1\text{-}3}$**. The curve can be divided into three regions; the semicircle in the low frequency region can be attributed to the diffusion process of I^-/ I_3^- in the electrolyte (Warburg diffusion), the middle region can be ascribed to the electron transport at the TiO_2/dye/electrolyte interface, whereas the high frequency region is due to the charge transfer at the Pt/electrolyte interface (Wu et al. 2014). From the Nyquist plots it is apparent that, the diameter of the medium frequency semicircle decreased in the order of **D_3** > **D_2** > **D_1** implying that, the rate of recombination is in the order **D_1**> **D_2** > **D_3**.

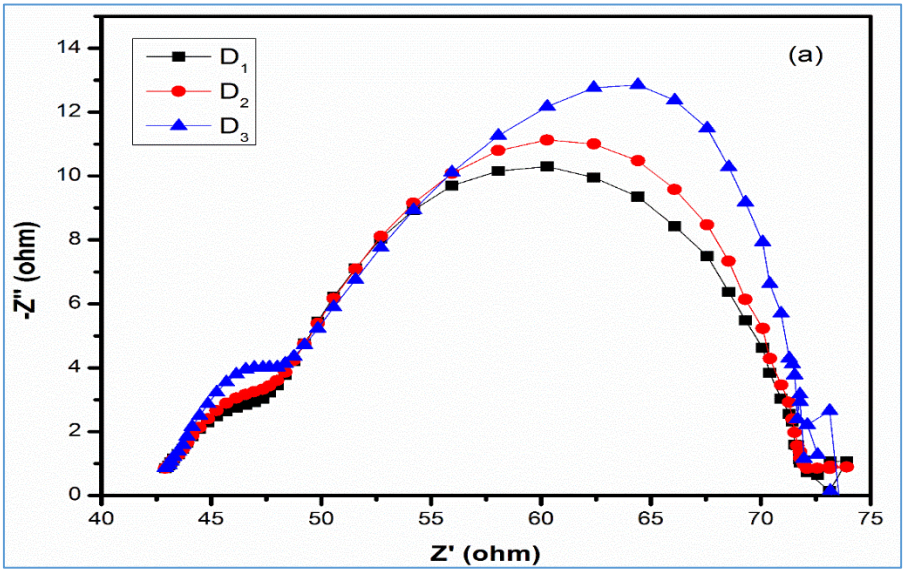

Fig.2.10 (a) Nyquist plots of DSSCs based on dyes measured at V_{oc} 0.85 mW cm^{-2}

The electron lifetimes of **D_1, D_2** and **D_3** are found to be 9.1, 9.0 and 14.4 ms, respectively. Therefore, larger the charge recombination resistance and enhanced electron lifetime maybe the intrinsic reason for the higher V_{oc} value of the DSSC based on **D_3,** but the low electron lifetime and higher the electron recombination of **D_2** dye may be the reason for lower V_{oc}, and it is proportional to the difference between the Fermi level of the TiO_2 electrode and the electrochemical potential of the redox couple. (**Fig.2.8**). From these results **D_3** (640 mV) shows larger V_{oc} value than **D_1** and **D_2**. Further, Bode phase plots (**Fig. 2.10 (b)**) were used to find out the effective lifetime (τ_{CB}) of electrons in the conduction band of TiO_2. τ_{CB} were calculated by making use of the equation: $\tau_{CB} = 1/2\pi f$, wherein, f is the frequency of the corresponding peak in the Bode plot.

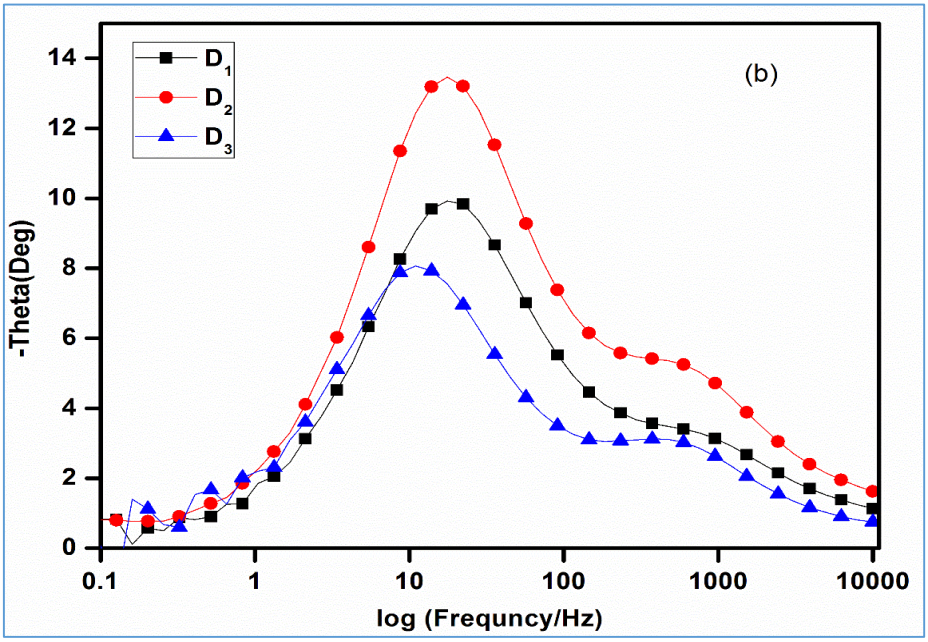

Fig.2.10 (b) Bode plots of DSSCs based on dyes measured at V_{oc} 0.85 $mWcm^{-2}$

The obtained electron lifetimes for DSSC sensitized by **D_1**, **D_2** and **D_3** are 9.1, 9.0 and 14.4 ms, respectively. The observed longer electron lifetime in case of **D_3** could explain its high V_{oc} and also the higher efficiency as well as more effective suppression of dark current than that of the other two dyes. From the experimental results it can be concluded that, the acceptor / anchoring unit plays a pivotal role in the overall efficiency of DSSCs.

2.4 CONCLUSIONS

In summary, three new sensitizers **D_{1-3}** carrying the same donor unit and π-conjugation system but with different electron acceptors, *viz.* 2-cyanoacrylic acid, rhodanine-3-acetic acid and 4-aminobenzoic acid, were designed and synthesized. Their optical, electrochemical and structural characterization were performed and device fabrication studies were carried out. It is interesting to note that although the absorption maxima red shifted in the order **D_3< D_1< D_2**, the device sensitized by **D_3** with 4-aminobenzoic acid as an acceptor displayed the highest efficiency, which is mainly attributed to the longest electron lifetime. The overall conversion efficiency exhibited by **D_3** is 1.18 %. It also indicates that, **D_3** is capable of reducing the electron recombination rates in the TiO_2 more effectively and hence leading to a higher efficiency than the dyes **D_1** and **D_2**. To sum up, by optimizing the acceptor unit of the dye it is possible to further ameliorate the performance of DSSCs.

CHAPTER 3

5-METHOXYINDOLE BASED DYES WITH D-D-A-π-A ARCHITECTURE: SYNTHESIS, CHARACTERIZATION AND PERFORMANCE STUDIES

Abstract

In this chapter, synthetic methods, structural characterization, photophysical and electrochemical studies of newly designed dyes ***E**$_{1-3}$* *have been incorporated. Further, it covers their DFT and TDFT calculations along with photovoltaic characterization studies. Also, a detailed discussion on obtained results has been included.*

3.1 INTRODUCTION

Based on the comprehensive literature survey and by following the design strategy described in **chapter 1 (Section 1.11)**, three new metal-free sensitizers **E$_{1-3}$** **(Series 2)** were synthesized starting from simple organic molecules as promising sensitizers for DSSC application. The new dyes were characterized using various spectral studies, elemental analysis and theoretical calculations. Their photovoltaic performance was evaluated by device fabrication studies. The details of experimental protocols as well as obtained results pertaining to **E$_{1-3}$** have been discussed. **Fig.3.1** depicts the chemical structures of the newly designed sensitizers (**E$_{1-3}$**).

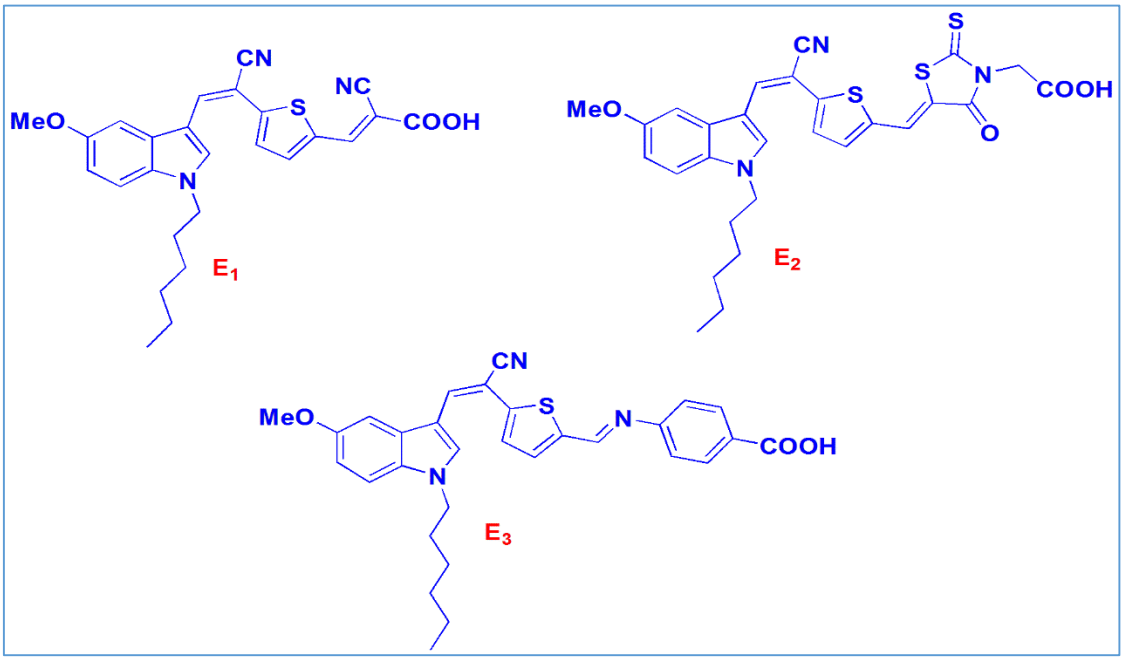

Fig.3.1 Chemical structures of sensitizers **E$_{1-3}$**

3.2 EXPERIMENTAL

3.2.1 Materials and methods

The starting materials 5-methoxy-1*H*-indole-3-carbaldehyde, 1-bromohexane, thiophene-2-acetonitrile, cyanoacetic acid, rhodanine-3-acetic acid and 4-aminobenzoic acid were obtained from Sigma-Aldrich. All the solvents were dried following standard protocols prior to use. The reactions were performed under argon atmosphere and the completion of reaction was monitored by TLC technique. Chromatographic separations were carried out using silica gel (60–120 mesh). ^{1}H NMR and ^{13}C NMR spectra were recorded using a Bruker avance 500 MHz and 400 MHz spectrometers, in DMSO-d_6 or $CDCl_3$ and TMS was used as an internal standard. Mass spectra were recorded on thermo scientific-EXACTIVE (ESI-MS), whereas the elemental analysis was carried out on a Flash EA1112CHNS analyzer (Thermo Electron Corporation).

3.2.2 Synthesis of sensitizers E_{1-3}

The synthetic pathways of the three new sensitizers (**E_{1-3}**) are depicted in **Scheme 3.1**. N-alkylation of 5-methoxy-1*H*-indole-3-carbaldehyde was done using 1-bromohexane to yield compound **3.1**. It was then was coupled with thiophene-2-acetonitrile to obtain 3-(1-hexyl-5-methoxy-1H-indol-3-yl)-2-(thiophen-2-yl)acrylonitrile (**3.2**) *via* Knoevenagel condensation. The compound **3.2** was then subjected to Vilsmeier–Haack formylation protocol to give compound **3.3**. Finally, Knoevenagel condensation of these aldehydes with cyanoacetic acid and rhodanine-3-acetic acid in the presence of ammonium acetate produced the desired dyes **E_1** and **E_2**, respectively; whereas **E_3** was obtained by condensation of aldehyde **3.3** with 4-aminobenzoic acid.

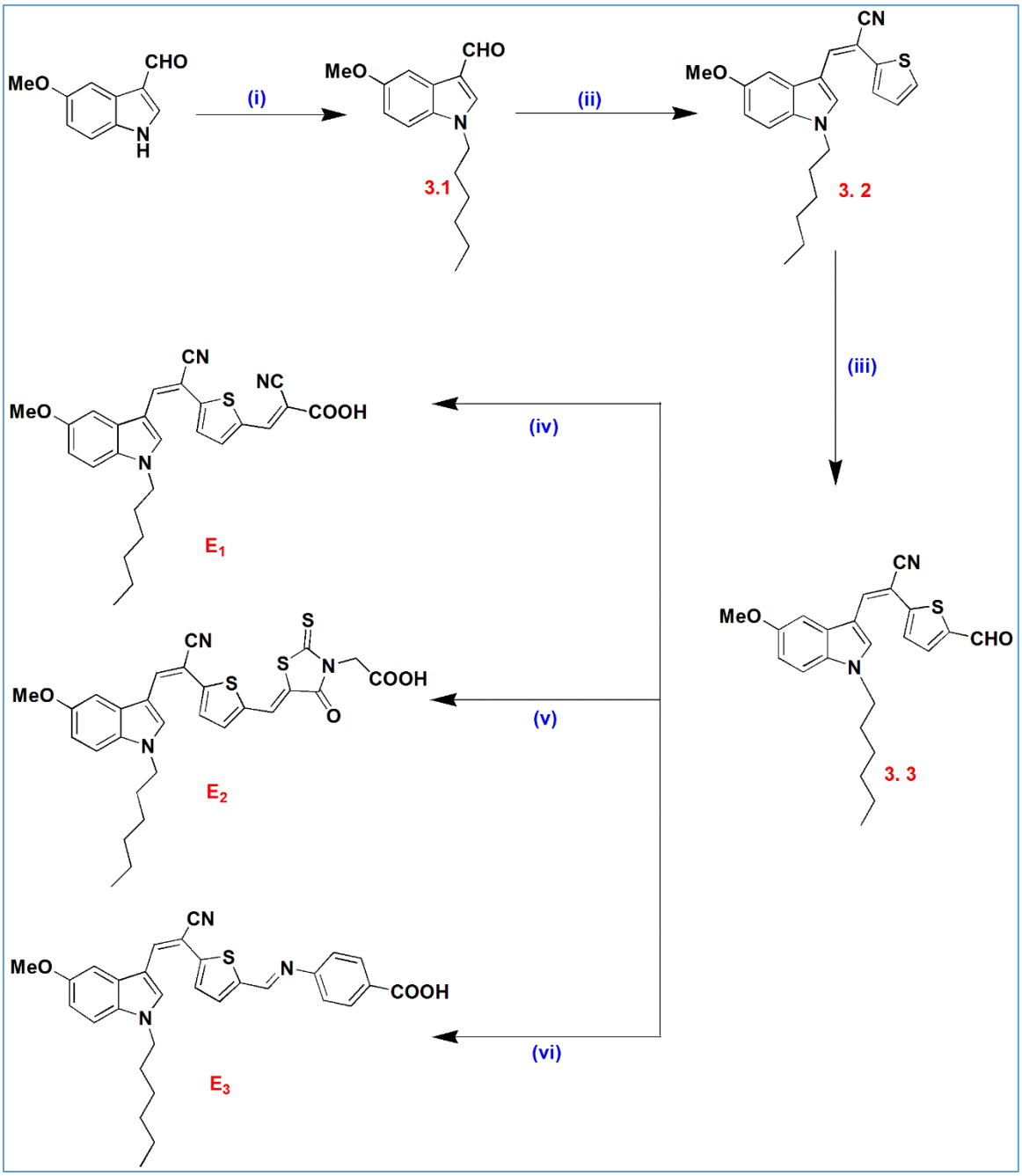

Scheme 3.1 Synthetic route of the sensitizers (i) 1-Bromohexane, K_2CO_3, DMF, RT (ii) 2-(Thiophen-2-yl)-acetonitrile, NaOMe, CH_3OH, RT (iii) $POCl_3$, DMF, RT (iv) Cyanoacetic acid, ammonium acetate, glacial CH_3COOH, 110 ^{0}C (v) Rhodanine-3-acetic acid, ammonium acetate, glacial CH_3COOH, 110 ^{0}C (vi) 4-Aminobenzoic acid, CH_3OH, 80 ^{0}C

3.2.3 Optical and electrochemical measurement

UV-visible spectra of the dyes were recorded at room temperature using SPECORD S 600 spectrophotometer. Further, the fluorescence spectra were recorded using Perkin Elmer LS55 fluorescence spectrophotometer. The absorption and emission spectra of the dyes (**E_{1-3}**) recorded in chloroform (3×10^{-5}M) solutions are displayed in **Fig.3.6 (a)** and **(b)**, respectively; whereas, UV-visible spectra of dyes **E_{1-3}** for solid films while attached to TiO_2 are depicted in **Fig.3.7** and all the pertinent results are summarized in **Table 3.1**.

The cyclic voltammetry (CV) and impedance measurements were performed on Bio-Logic SP-150 electrochemical workstation. The CV measurements were carried out in anhydrous dichloromethane with 0.1 M [TBA][PF_6] as an electrolyte at a scan rate of 50 mVs^{-1}. Glassy carbon was used as the working electrode (WE), Pt wire as counter electrode and Ag/Ag^+ in ACN was used as the reference electrode. Fc/Fc^+ was used as internal reference which was converted to NHE by addition of 0.63 V. The data obtained from the electrochemical studies are depicted in **Fig.3.12**.

The electrochemical impedance spectra were measured with an impedance analyzer potentiostat (Bio-Logic SP-150) under illumination using a solar simulator (SOL3A, Oriel) equipped with a 450 W xenon lamp (91160, Oriel). EIS spectra were recorded over a frequency range of 100 mHz to 200 kHz at 298 K. The applied bias voltage was set at the V_{oc} of the DSSCs, with AC amplitude set at 10 mV. The electrical impedance spectra were fitted using Z-Fit software (Bio-Logic). The graphs obtained from EIS measurements are depicted in **Fig.3.14** and **3.15**.

3.2.4 Theoretical calculations

The DFT calculations were performed using Turbomole software package. For all the geometry optimizations, the default convergence criteria were maintained. Further, all the calculations were performed using def-TZVP basis set. Furthermore, time-dependent density functional theory (TDDFT) calculations were performed to predict spectroscopic properties of the chromophores. TDDFT offers a computationally inexpensive and reliable

tool to comprehend the electronic excitations of sensitizers in the presence of time-dependent perturbations. All the results obtained from the aforesaid calculations are discussed. The optimized geometries and electronic distribution in the HOMO-1, HOMO and LUMO levels are depicted in **Fig.3.10**.

3.2.5 DSSC fabrication

Fluorine-doped tin oxide (FTO) coated glasses (2.2 mm thickness, sheet resistance of 8 Ω cm^{-2}, TEC, Pilkington) were washed with detergent, water, acetone and ethanol, sequentially. After this, thoroughly cleaned plates were immersed into an aqueous solution containing 40 mM of $TiCl_4$, maintained at 70 °C for 30 minutes and subsequently washed with water and ethanol. A thin layer (8-12 μm) of TiO_2 (Solaronix, Ti-Nanoxide T/SP) was deposited (active area, 0.18 cm^2) on transparent conducting glass by squeegee printing followed by drying at 125 °C for 5 minutes, 350 °C for 5 minutes and curing at 500 °C for 30 minutes. Next, scattering layer of (5 μm) TiO_2 particles (Solaronix, Ti-Nanoxide R/SP,) was printed. Then, TiO_2 electrodes were heated under an air flow at 350 °C for 10 minutes, followed by heating at 500 °C for 30 minutes. After cooling to room temperature, the TiO_2 electrodes were treated with 40 mM aqueous solution of $TiCl_4$ at 70 °C for 30 minutes and then washed with water and ethanol. The electrodes were heated again at 500 °C for 30 minutes and then allowed to cool to 80 °C.

The dye solutions (0.5 mM) were prepared by dissolving the dye in 1:1 acetonitrile and *tert*-butyl alcohol. The co-adsorbate deoxycholic acid (CDCA) was added to the dye solution at a concentration of 1, 10 and 20 mM. The electrodes were immersed in the dye solutions and then kept at 25 °C for 20 hours to adsorb the dye onto the TiO_2 surface. For preparing the counter electrode, pre-cut TCO (Transparent Conducting Oxide) glasses were washed with water followed by 0.1M HCl in EtOH, and sonicated in acetone bath for 10 minutes. These washed TCO were then dried at 400 °C for 15 minutes. A thin layer of Pt-paste (Solaronix, Platisol T/SP) on TCO was printed and the printed electrodes were then cured at 450 °C for 10 minutes. The dye sensitized TiO_2 electrodes were sandwiched with Pt counter electrodes and the electrolyte (Solaronix, Iodolyte AN-50) was then injected

into the cell, while the two electrodes were held together with the clips. The fabricated cell was subjected to measurement of J_{sc}, V_{oc}, *ff*, η and IPCE. The results are tabulated in **Table 3.2**.

3.2.6 Synthetic methods

Synthesis of *1-hexyl-5-methoxy-1H-indole-3-carbaldehyde (3.1)*

A mixture of 1-bromohexane (0.565 g, 3.42 mmol), 5-methoxy-1H-indole-3-carbaldehyde (0.5 g, 2.85 mmol) and potassium carbonate (0.591 g, 4.28 mmol), in DMF (15 mL) was stirred at 30 C for 10 h. After completion of the reaction, the contents were neutralized with dil. HCl and the product was extracted using ethyl acetate (50 mL× 3). Organic phase was dried using sodium sulfate. Then, ethyl acetate was removed under reduced pressure. The crude oily product obtained was purified by column chromatography on silica gel using hexane as an eluent, to get a white solid. Yield: 83%. ^{1}H NMR (400 MHz DMSO-d_6, ppm): δ 9.93 (s,1H), 7.79 (s,1H), 7.64 (s, 1H), 7.24 (d, J = 9 Hz, 1H), 6.95 (s, J = 8.5 Hz, 1H), 4.10 (t, J = 7 Hz, 2H), 3.89 (s, 3H),1.85 (d, J = 6 Hz, 2H),1.30 (s, 6H), 0.87 (t, 3H). ESI-MS (+ve mode) m/z Calcd for $C_{16}H_{21}N_2O_2$: 259.16. Found: 260.16 $[M+H]^+$.

Synthesis of *3-(1-hexyl-5-methoxy-1H-indol-3-yl)-2-(thiophen-2-yl)acrylonitrile (3.2)*

To a freshly prepared solution of sodium methoxide (0.053 g, 2.31 mmol of sodium in 10 mL of methanol), thiophene-2- acetonitrile (0.285 g, 2.31 mmol) was added slowly while stirring. 1-Hexyl-5-methoxy-1H-indole-3-carbaldehyde (1, 0.5 g, 1.92 mmol) was then added to reaction mass. Stirring was continued for 6 h at 30 ^{o}C. The precipitated solid was collected by filtration, washed with methanol and finally recrystallized from chloroform. Yellow solid, yield 61%. ^{1}H NMR (400 MHz DMSO-d_6, ppm): δ 8.46 8.25 (s, 1H), 7.97 (s, 1H), 7.56 (s, 2H), 7.49 (d, J = 8.8 Hz, 1H), 7.40 (s, 1H), 7.14 (d, J = 2.0 Hz, 1H), 6.90 (d, J = 8.8 Hz, 1H), 4.26 (s, 2H), 3.84 (s, 3H), 1.76 (s, 2H), 1.25 (s, 6H), 0.83 (t, 3H). ESI-MS (+ve mode) m/z Calcd for $C_{22}H_{24}N_2OS$: 364.16. Found: 365.16 $[M+H]^+$.

Synthesis of *2-(5-formylthiophen-2-yl)-3-(1-hexyl-5-methoxy-1H-indol-3-yl)acrylonitrile* (*3.3*)

A two neck round bottomed flask was charged with freshly distilled DMF (1.0 mL, 5 eq) and $POCl_3$ was added to it drop-wise, with constant stirring (1.26 mL, 5 eq) at 0 ^oC under nitrogen. The reaction mixture was stirred for 30 minutes to obtain a glassy white solid and to this 3-(1-hexyl-5-methoxy-1*H*-indol-3-yl)-2- (thiophen-2-yl) acrylonitrile (2, 1 g, 2.74 mmol) dissolved in dichloroethane (10 mL) was added while stirring. The stirring was continued at 30 C for 12 h. The contents were then poured into crushed ice and subsequently basified using 5 M NaOH solution. The precipitated crude product was collected by filtration and it was purified by column chromatography to give brown colored solid. Silica gel was used as stationary phase and ethyl acetate/hexane (1:5) as mobile phase. Yield: 63%. ^{1}H NMR (500 MHz $CDCl_3$, ppm): δ 9.85 (s, 1H), 8.32 (s, 1H), 7.83 (s, 1H), 7.69 (d, J = 4 Hz, 1H), 7.28 (q, J = 6.8 Hz, 2H), 7.16 (d, J = 1.5 Hz 1H), 6.97 (q, J = 3.5 Hz, 1H), 4.16 (t, J = 7.5 Hz, 2H), 3.92 (s, 3H), 1.89 (t, J = 6.5 Hz, 2H), 1.32 (s, 6H), 0.88 (t, J = 6.5 Hz, 3H). ^{13}C (125 MHz, DMSO-d_6) δ (ppm): 182.38, 155.97, 150.11, 141.16, 137.43, 134.95, 131.38, 131.04, 128.84, 124.91, 118.39, 113.74, 111.46, 110.02, 99.96, 96.37, 55.92, 47.72, 31.28, 29.93, 26.50, 22.48, 13.97. ESI-MS (+ve mode) m/z Calcd for $C_{23}H_{24}N_2O_2S$: 392.16. Found: 393.16 $[M+H]^+$.

Synthesis of *2-cyano-3-(5-((Z)-1-cyano-2-(1-hexyl-5-methoxy-1H-indol-3-yl)vinyl)thiophen-2-yl)acrylic acid (E_1)*

A dried two neck round bottomed flask was charged with 2-(5-formylthiophen-2-yl)-3-(1-hexyl-5-methoxy-1H-indol-3-yl) acrylonitrile (**3.3**, 0.100 g, 0.254 mmol), cyano acetic acid (0.026 g, 0.305 mmol), and ammonium acetate (0.216 g, 2.80 mmol). The mixture was dissolved in glacial acetic acid (15 mL) under argon atmosphere. The contents were then refluxed for 12 h with continuous stirring. After completion of the reaction, the mass was cooled to ambient temperature and was poured into ice cold water. The precipitate was filtered. The crude product was purified by column chromatography using silica gel and $CHCl_3$:CH_3OH (10: 2) as mobile phase to obtain red color solid. Yield: 51%. 1H NMR (400MHz DMSO-d_6, ppm): δ 8.46 (s, 1H), 8.39 (s, 1H), 8.3 (s, 1H), 8.00 (d, *J* = 3.6 Hz, 1H), 7.72 (d, *J* = 4.0 Hz, 1H), 7.65 (s, 1H), 7.54 (d, *J* = 8.4 Hz, 1H), 6.94 (d, *J* = 8.8 Hz, 1H), 4.30 (t, *J* = 6.4 Hz, 2H), 3.85 (s, 3H), 1.78 (s, 2H), 1.26 (s, 6H), 0.83 (t, *J* =

6.4 Hz, 3H). ^{13}C (100MHz, DMSO-d$_6$) δ (ppm): 164.11, 156.00, 149.73, 146.54, 141.63, 136.91, 134.13, 132.53, 131.40, 128.93, 124.72, 119.14, 117.12, 113.68, 112.52, 110.42, 102.06, 98.95, 94.95, 56.12, 47.15, 31.15, 29.93, 26.19, 22.47, 14.30. Anal. Calcd. for $C_{26}H_{25}N_3O_3S$: C,67.95; H,5.48; N, 9.14 found: C, 67.77; H, 5.45; N, 9.21. ESI-MS (+ve mode) *m/z* Calcd for $C_{26}H_{25}N_3O_3S$:459.16. Found: 460.16 $[M+H]^+$.

Synthesis of *2-((Z)-5-((5-((Z)-1-cyano-2-(1-hexyl-5-methoxy-1H-indol-3-yl)vinyl) thiophen-2-yl)methylene)-4-oxo-2-thioxothiazolidin-3-yl)acetic acid* (*E_2*)

The compound **3.3** (0.150 g, 0.382 mmol), rhodanine-3-acetic acid (0.087 g, 0.458 mmol), ammonium acetate (0.324 g, 4.20 mmol), and glacial acetic acid (10 mL) were mixed together and refluxed for 12 h with continuous stirring. The clear reddish solution was cooled to room temperature and the obtained precipitate was filtered and washed with cooled acetic acid and water mixture. The obtained solid was further purified by column chromatography using silica gel and $CHCl_3$:CH_3OH (10: 1) as mobile phase to obtain a dark red solid. Yield: 49%. ^{1}H NMR (400MHz DMSO-d6, ppm): δ 8.37 (s, 1H), 8.23 (s, 1H), 8.14 (s, 1H), 7.82 (s, 1H), 7.68 (s, 1H), 7.62 (s, 1H), 7.54 (d, *J* = 9.2 Hz, 1H), 6.94 (d, *J* = 8.4 Hz, 1H), 4.71 (s, 2H), 4.30 (s, 2H), 3.86 (s, 3H), 1.78 (s, 2H), 1.27 (s, 6H), 0.83 (s, 3H). ^{13}C (100MHz, DMSO-d$_6$) δ (ppm): 192.12, 167.75, 166.40, 155.93, 149.11, 138.34, 135.97, 135.68, 132.18, 131.37, 128.88, 125.89, 119.03, 118.71, 113.57, 112.38, 110.44, 102.20, 95.41, 56.18, 47.11, 31.17, 29.93, 26.22, 22.48, 14.31. Anal. Calcd. for $C_{28}H_{27}N_3O_4S_3$: C, 59.45; H, 4.81; N, 7.43 found: C, 59.61; H, 4.75; N, 7.49. ESI-MS (+ve mode) *m/z* Calcd for $C_{28}H_{27}N_3O_4S_3$:565.12. Found: 566.12 $[M+H]^+$.

Synthesis of *4-((E)-(5-((Z)-1-cyano-2-(1-hexyl-5-methoxy-1H-indol-3-yl)vinyl)thiophen-2-yl)methyleneamino)benzoic acid* (*E_3*)

A mixture of 2-(5-formylthiophen-2-yl)-3-(1-hexyl-5-methoxy-1*H*-indol-3-yl)acrylonitrile (**3.3**, 0.100 g, 0.254 mmol) and 4-aminobenzoic acid (0.035 g, 0.254 mmol) was heated under reflux in absolute methanol for 3 h. The separated solid was filtered and recrystallized from methanol to obtain bright orange color solid. Yield 81%. ^{1}H NMR

(400MHz DMSO-d6, ppm): δ 12.89 (s, 1H), 8.81 (s, 1H), 8.35 (s, 1H), 7.98 (d, *J* = 5.6 Hz, 2H), 7.70 (d, *J* = 19.6 Hz, 2H), 7.52 (d, *J* = 7.2 Hz, 1H), 7.44 (s, 1H), 7.35 (s, 2H), 6.92 (d, *J* = 6.4 Hz, 1H), 4.29 (s, 2H), 3.86 (s, 3H), 1.77 (s, 2H), 1.26 (s, 6H), 0.83 (s, 3H). ^{13}C (100MHz, DMSO-d_6) δ (ppm): 167.43, 155.84, 155.41, 154.90, 145.39, 141.01, 135.96, 135.20, 131.52, 131.27, 131.13, 128.88, 128.55, 125.22, 121.69, 119.07, 113.76, 112.34, 110.22, 101.69, 96.21, 56.13, 47.03, 31.16, 29.96, 26.20, 22.47, 14.30. Anal. Calcd. for $C_{30}H_{29}N_3O_3S_3$: C, 70.43; H, 5.71; N, 8.21 found: C, 70.61; H, 5.75; N, 8.27. ESI-MS (+ve mode) *m/z* Calcd for $C_{30}H_{29}N_3O_3S$: 511.19. Found: 512.19 $[M+H]^+$.

3.3 RESULTS AND DISCUSSION

3.3.1 Structural characterization

The chemical structures of newly synthesized compounds were determined by ^{1}H NMR, ^{13}C NMR spectroscopy and elemental analysis. The compound **E_3**, in ^{1}H NMR spectrum showed unique resonance at δ 12.89 ppm for the protons corresponding to acid group. Appearance of a singlet at δ 8.81 ppm indicates the presence of an aromatic proton at the second position of indole ring. All the other aromatic protons depicted peaks between 8.36 and 6.91 ppm. Further, two protons of –NCH_2 of hexyl chain resonated as a singlet at δ 4.40 ppm, whereas, the appearance of a singlet at 3.83 ppm can be attributed to –OMe group on the indole moiety. Furthermore, signal due to primary and secondary protons of alkyl chain resonated in the range of δ 1.77-0.83 ppm in the ^{1}H NMR spectrum. This confirmed the presence of one hexyl chain. The ^{13}C NMR spectrum of **E_3** showed the characteristic signals obtained at higher frequency (downfield region). The carbonyl carbon atoms in acid group resonated at δ 167.43 ppm. The remaining signals appearing in the region of δ 155.84-96.21 ppm are due to other aromatic carbons. The first carbon in the hexyl chain attached directly to the aromatic nitrogen in the indole ring displayed a peak at 56.13 ppm. Further, the remaining aliphatic carbons appeared between 47.03-14.30 ppm. Furthermore, its mass spectrum exhibited the $[M+H]^+$ peak at 512.19, which is in agreement with the calculated molecular weight for the formula of $C_{30}H_{29}N_3O_3S$. **Fig.3.2-3.3** show ^{1}H NMR and ^{13}C NMR of **3.3**, while, **Fig.3.4-3.5** those of **E_3** respectively.

Spectrograms of selected target compounds

^{1}H NMR and ^{13}C NMR spectra of representative title compounds are given below.

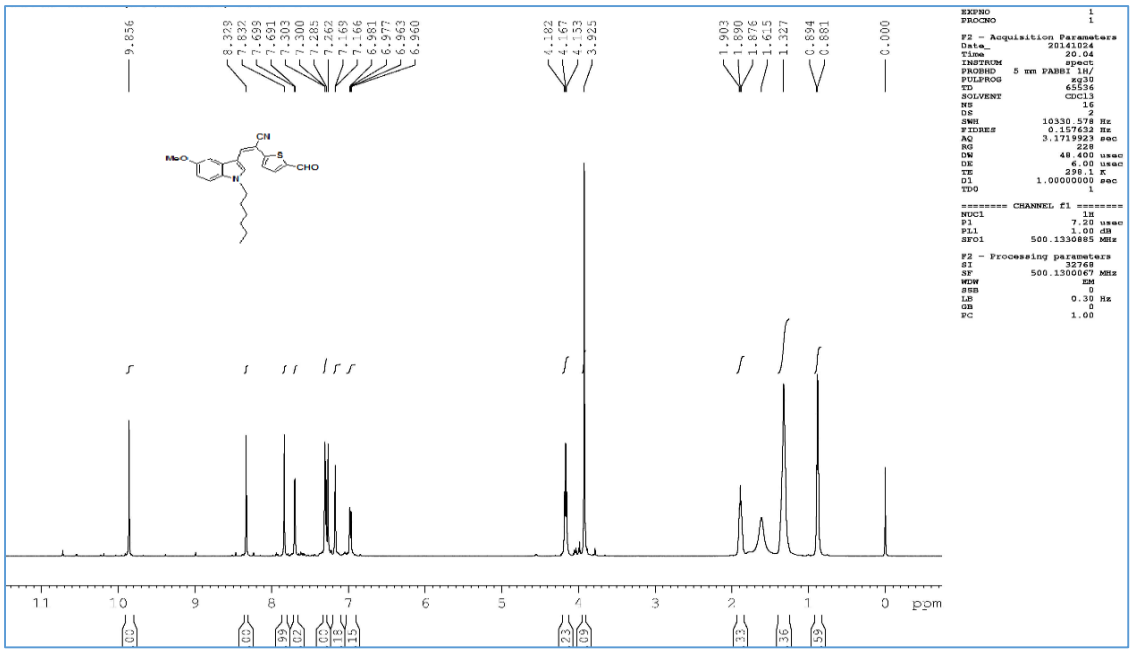

Fig.3.2 ^{1}H NMR spectrum of **3.3** in $CDCl_3$

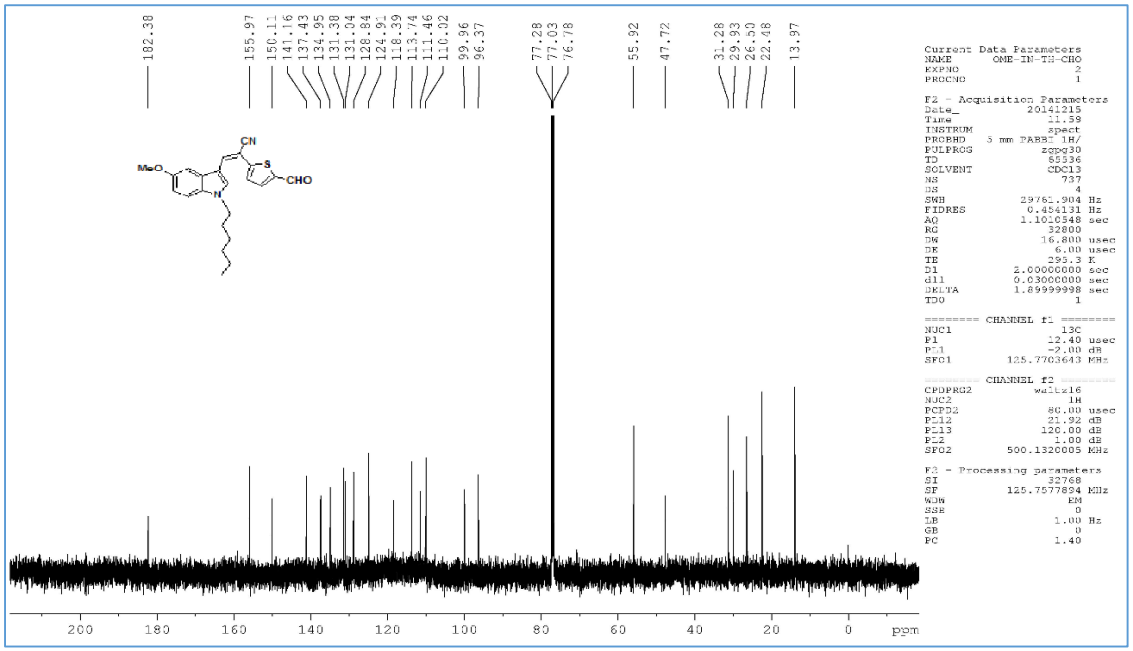

Fig.3.3 ^{13}C NMR spectrum of **3.3** in $CDCl_3$

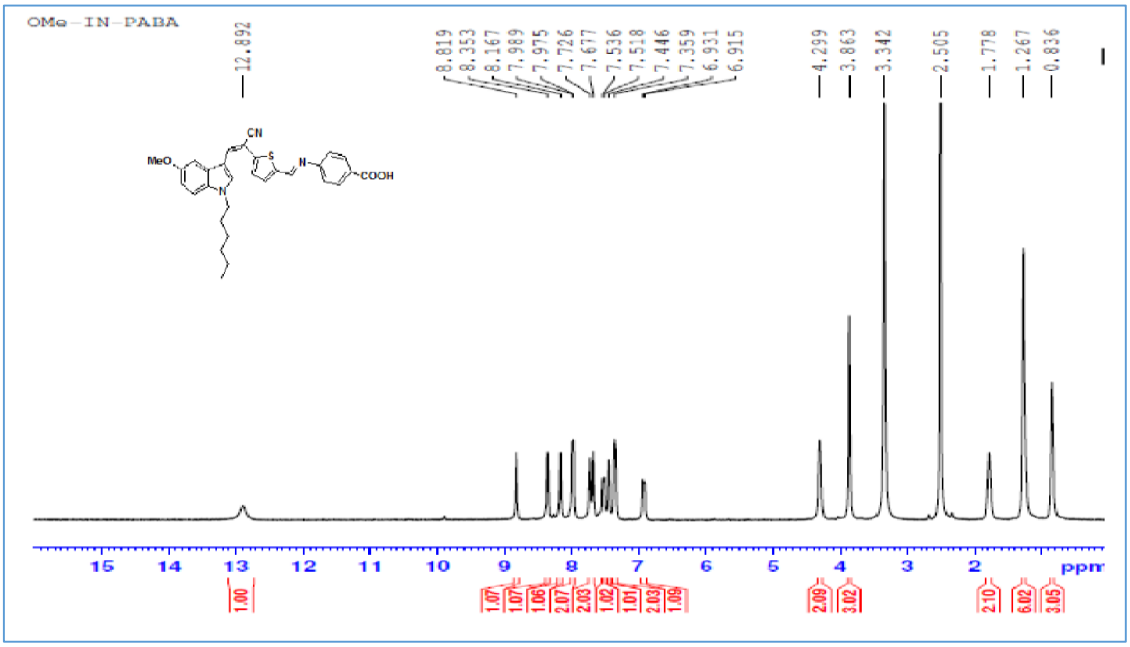

Fig.3.4 [1]H NMR spectrum of **E₃** in DMSO-d_6

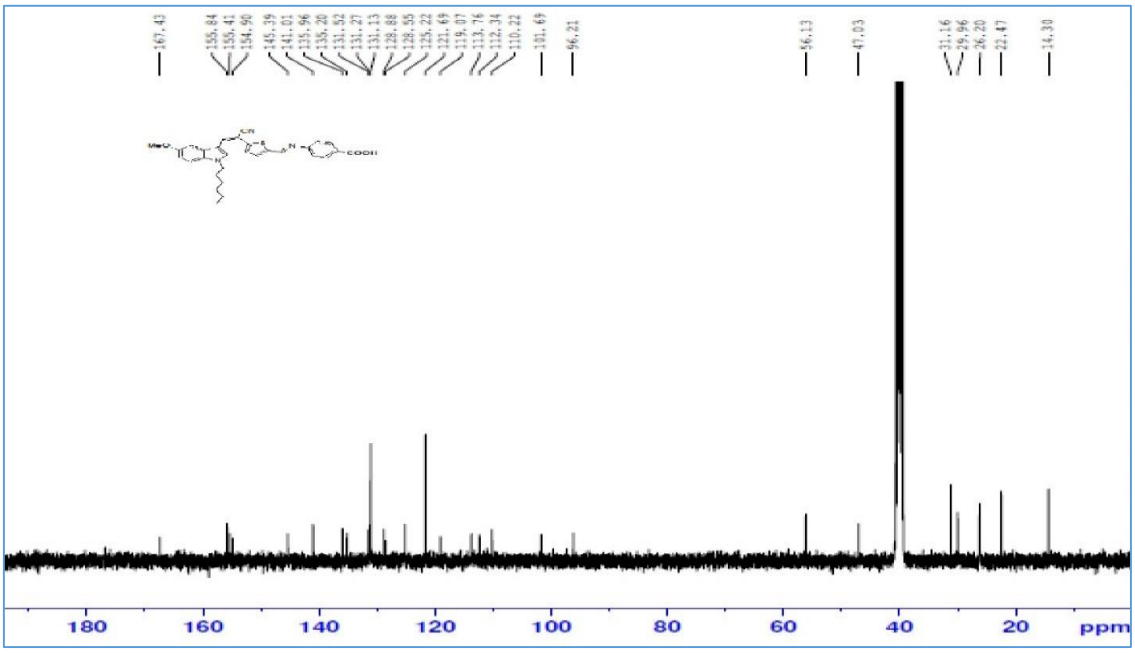

Fig.3.5 [13] C NMR spectrum of **E₃** in DMSO-d_6

3.3.2 Photophysical properties

All the dyes (**E$_{1-3}$**) exhibit two broad absorption peaks, the absorption bands in the shorter wavelength region (<400 nm) can be attributed to the π-π* electronic excitations localized within the indole and π-bridge segments, whereas the band in the longer wavelength region (462-517 nm) corresponds to the intramolecular charge transfer (ICT) transition from indole (donor) to the corresponding acceptor segment.

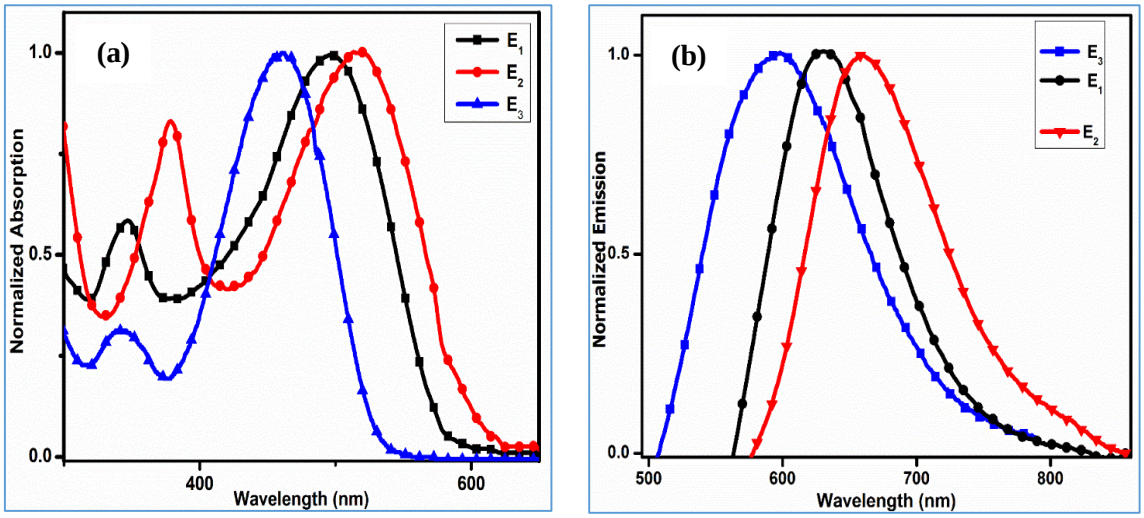

Fig.3.6 (a) UV-visible spectra of **E$_{1-3}$** in chloroform (10^{-5} M) **(b)** Fluorescence spectra of **E$_{1-3}$** in chloroform (10^{-5} M).

Usually, when organic dyes are adsorbed onto the TiO_2 films, the absorption spectra may show blue-shift or red-shift as compared to the spectra recorded in solutions state depending on the interaction between the sensitizer and the semiconductor surface. In fact, it is well known that, J-aggregation of the dye on titanium dioxide surface leads to red shift, whereas, H-aggregation results in blue shift of the absorption spectra. **Fig.3.7** depicts the absorption spectra of the dye loaded onto the TiO_2 films. Upon comparing the aforementioned spectra with the absorption spectra of the corresponding dyes in solution state, a clear red shift is observed in all the three sensitizers. This can be attributed to the J-aggregation occurred by an increased delocalization of the π* orbital of the conjugated system as a result of interaction between the carboxylate group of the corresponding sensitizer and Ti^{4+} ions that directly lowers the energy of the π* level and thereby resulting

in broadening of the absorption spectra. Thus, introducing an indole unit and incorporating D-D-A-π-A architecture can be an efficient way to lower the aggregation tendency.

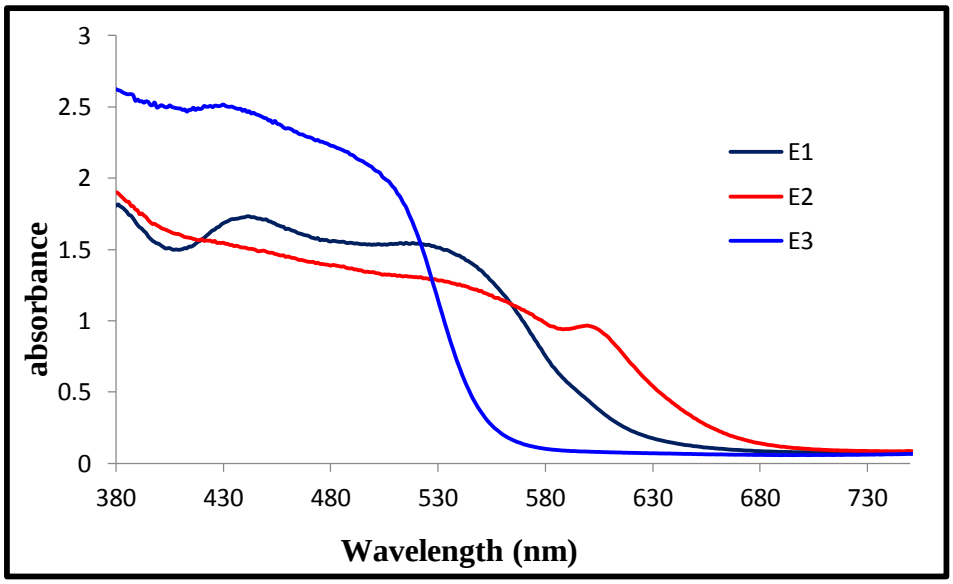

Fig.3.7 UV-visible spectra of $\mathbf{E_{1\text{-}3}}$ for solid films while attached to TiO_2

Further, the extent of charge transfer in these sensitizers is established by analyzing the absorption spectrum of the precursors **(Fig.3.8)**. The absorption spectra of compound **3.1** showed λ_{max} at 301nm, which can be attributed to weak charge transfer from indole to aldehyde group, on extending the conjugation by incorporation a cyanovinylene and thiophene unit (**3.2**) causes a nearly 100 nm red shift due to more effective delocalization of the electron density on indole into the π-conjugation. Moreover, this progression of donor-acceptor interaction is also apparent on comparing the absorption spectra of the aldehyde precursor **3.3** and that of the sensitizers. This progressive bathochromic shift in the absorption maxima exhibits the electron-withdrawing nature of aldehyde as well as all the respective acceptors units in $\mathbf{E_{1\text{-}3}}$. Further, the presence of acid-base equilibrium was confirmed by studying the change in absorption characteristics of the sensitizers on addition of trifluoroacetic acid (TFA) or triethylamine (TEA) to their chloroform solutions. The corresponding spectra of dyes $\mathbf{E_1}$ and $\mathbf{E_3}$ are shown in **Fig.3.9**.

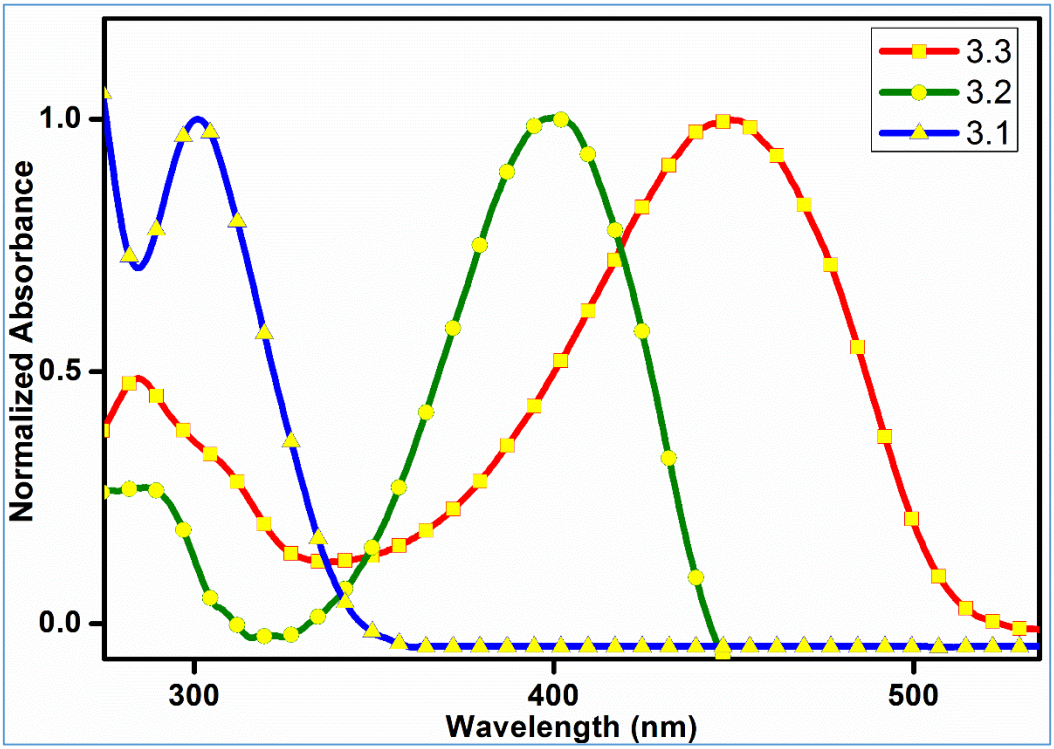

Fig.3.8 UV-visible spectra of compounds **3.1-3.3** in chloroform (10^{-5} M).

It was observed that, the addition of TEA to the dye solution resulted in blue shift of absorption spectra. Whereas, TFA addition manifested a red shift. This observation indicates that, in the chloroform solution the dye predominantly exists in the protonated form, but addition of TEA results in the deprotonation of the dye (carboxylic acid segment) reducing the acceptor strength and thus weakening the donor-acceptor interactions. On the other hand, addition of TFA to the dye solution will favor the amount of protonated form in the solution and thereby reversing the equilibrium Compared to dyes **E**$_1$ and **E**$_2$, absorption changes on interaction with TFA/TEA were predominant in **E**$_3$ which illustrates stronger donor–acceptor interactions in **E**$_3$.

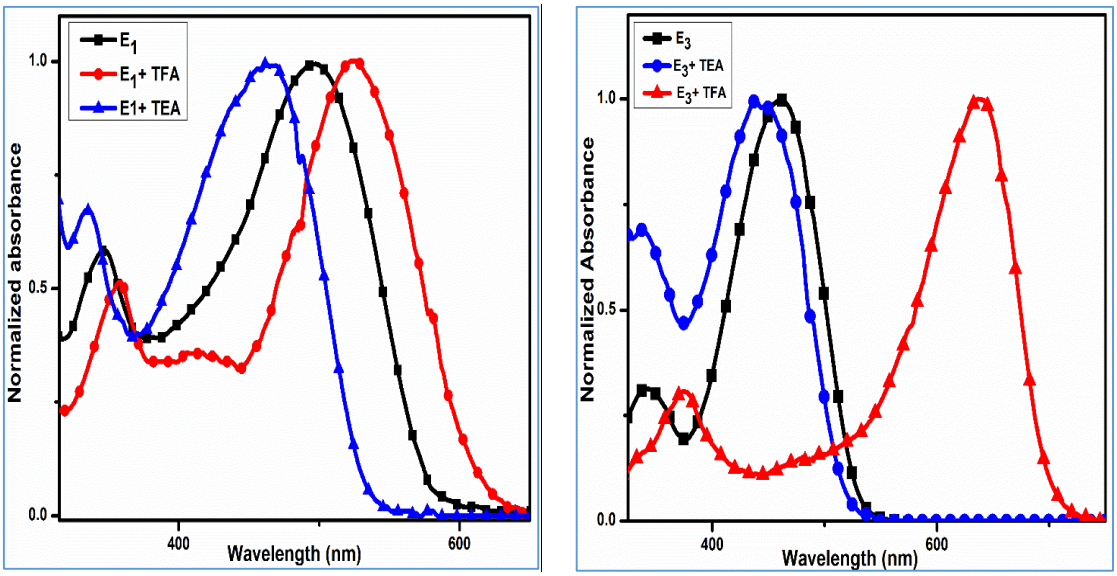

Fig.3.9 Absorption spectra of the dyes **E_1** and **E_3** recorded in DCM before and after addition of TFA and TEA

Table 3.1 Absorption and emission properties of **E_{1-3}** sensitizers.

Sensitizer	Absorption λ_{max} (nm)	Emission λ_{max} (nm)	Stokes Shift	ε ($M^{-1}cm^{-1}$)	E_{0-0}
E_1	503	633	130	30500	2.16
E_2	517	656	139	36000	2.08
E_3	462	601	169	33000	2.36

3.3.3. Molecular modeling

The optimized geometries as well as the electronic distribution in HOMO-1, HOMO and LUMO are displayed in **Fig.3.10**. The HOMO-1 is mainly localized on methoxy-indole unit, whereas in HOMO a delocalization is observed up to bridging thiophene unit. In the LUMO level a clear shift of electron density towards the acceptor segment is observed. This sort of charge separation between HOMO and LUMO is quite desirable as it favors the effective electron migration from donor to acceptor segment of

the dye and then to TiO_2 conduction band. The low performance of sensitizer **E_2** could be explained by taking a closer look at the electronic distribution in its LUMO level, the breakage of conjugation impairs the efficient injection of electron density into the conduction band of TiO_2. Another noteworthy outcome from the DFT studies is that extent of the electronic overlap between the HOMO and LUMO levels for **E_3** is less than that of the other sensitizers (**E_1** and **E_2**). This leads to a favorable charge separation and hence impending the electron–hole recombination in **E_3** and thereby resulting in a much better overall efficiency (Baheti et al. 2014).

Furthermore, time-dependent density functional theory (TDDFT) calculations were performed to predict spectroscopic properties of the chromophores. TDDFT offers a computationally inexpensive and reliable tool to comprehend the electronic excitations of sensitizers in the presence of time-dependent perturbations. The simulated absorption spectrum of **E_2** obtained at the BP86 functional and def-TZVPP basis set are shown in **Fig. 3.11**. The theoretically obtained spectrum depicted only one band. It was observed that on rescaling the standard deviation value (as given by the TurbomoleX) of 37.05 to 9 leads to an overall refinement of spectrum. The aforementioned spectrum clearly depicts two distinct bands and is well in agreement with experimental spectrum. The band at higher energy can be attributed to π-π^* transition, whereas the band at lower energy may be assigned to the charge transfer from the donor to the acceptor segment. Hence, the theoretically obtained UV spectrum is well in agreement with the experimentally obtained one.

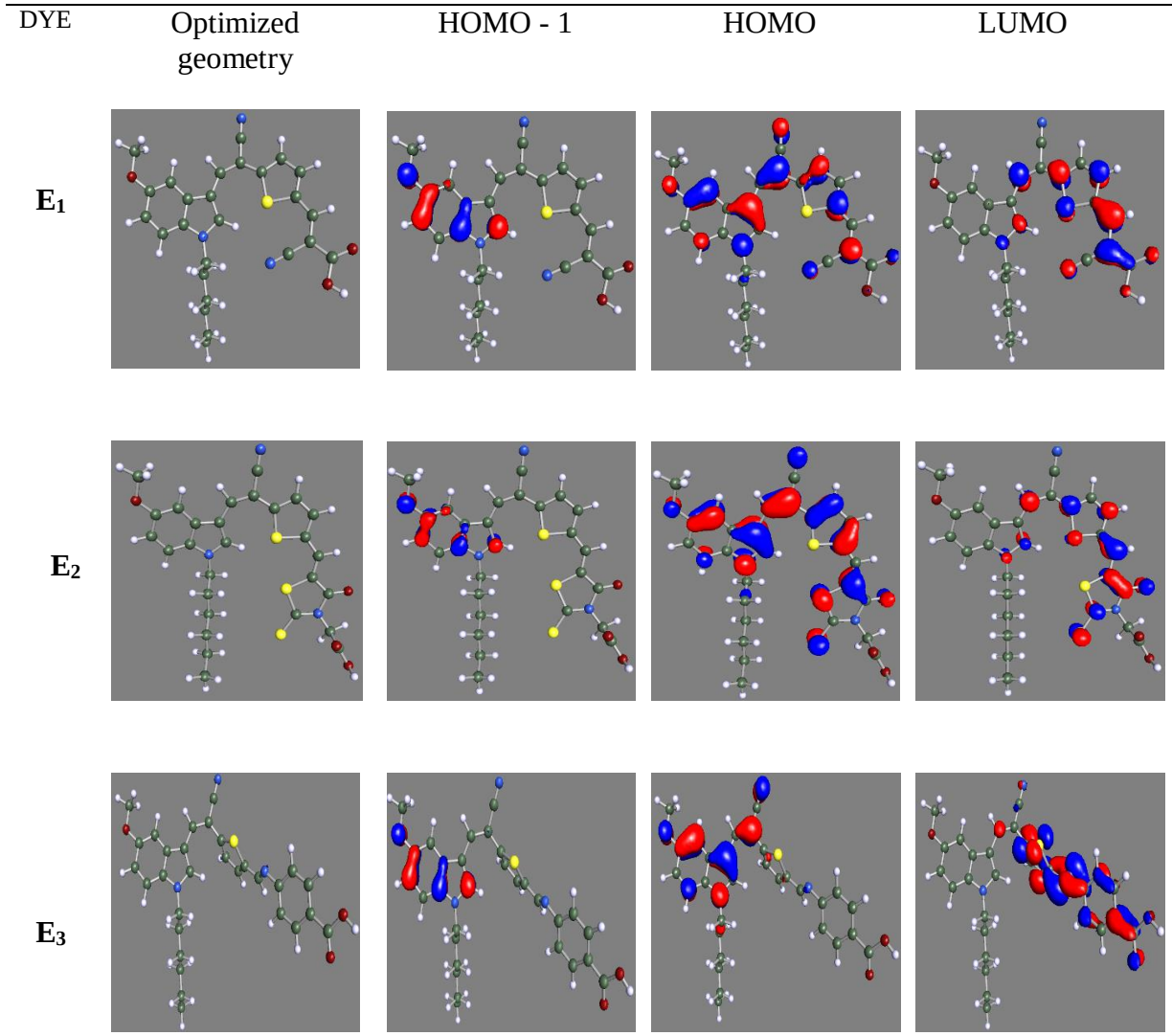

Fig.3.10 Optimized structure and frontier molecular orbitals (HOMO and LUMO) of **E_{1-3}**

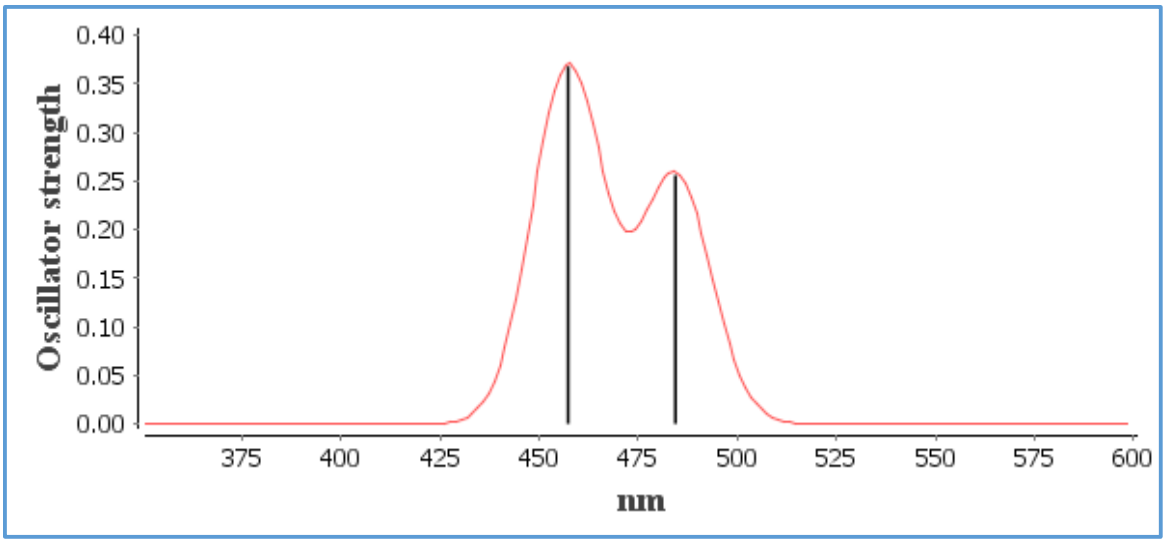

Fig.3.11 Simulated absorption spectra of **E_2**

3.3.4 Electrochemical properties

Cyclic voltammetry (CV) method was used to obtain ground state oxidation potential (GSOP) of the newly synthesized dyes in solution state. Cyclic voltammograms were used to calculate the oxidation onset (GSOP). Additionally, $E_{0\text{-}0}$ was calculated from absorption and corrected emission spectra of the compounds. $E_{0\text{-}0}$ and GSOP values were used to calculate the excited state oxidation potential (ESOP); the values in volts (V) against NHE were converted to electron volt (eV) according to the following equation.

$$\text{ESOP} = [(\text{GSOP (V)} + 4.7) - E_{0\text{-}0}]\ \text{eV}$$

The energy level diagram (**Fig.3.12**) depicts the GSOP and ESOP of **$E_{1\text{-}3}$** dyes. GSOP potential of **E_3** (-5.84 eV), **E_2** (-5.85 eV) and **E_1** (-5.87 eV) are lower in energy than that of I_3^-/I^- redox system (-5.2 eV) (Qu and Meyer 2001), thus providing ample driving force for effective dye regeneration. In addition, ESOP of **E_3** (-3.48 eV), **E_2** (-3.69 eV) and **E_1** (-3.79 eV) were higher in energy than the conduction band edge of nanocrystalline TiO_2 (-4.2 eV) (Oskam et al. 2001). This may result in efficient electron injection. Electron injection free

energy for dyes is in the order **E**$_3$>**E**$_2$>**E**$_1$, where dye regeneration free energy was almost similar for all the dyes, due to the fact that all of the dyes have similar electron donating group, thus similar HOMO delocalization (Babu et al. 2015).

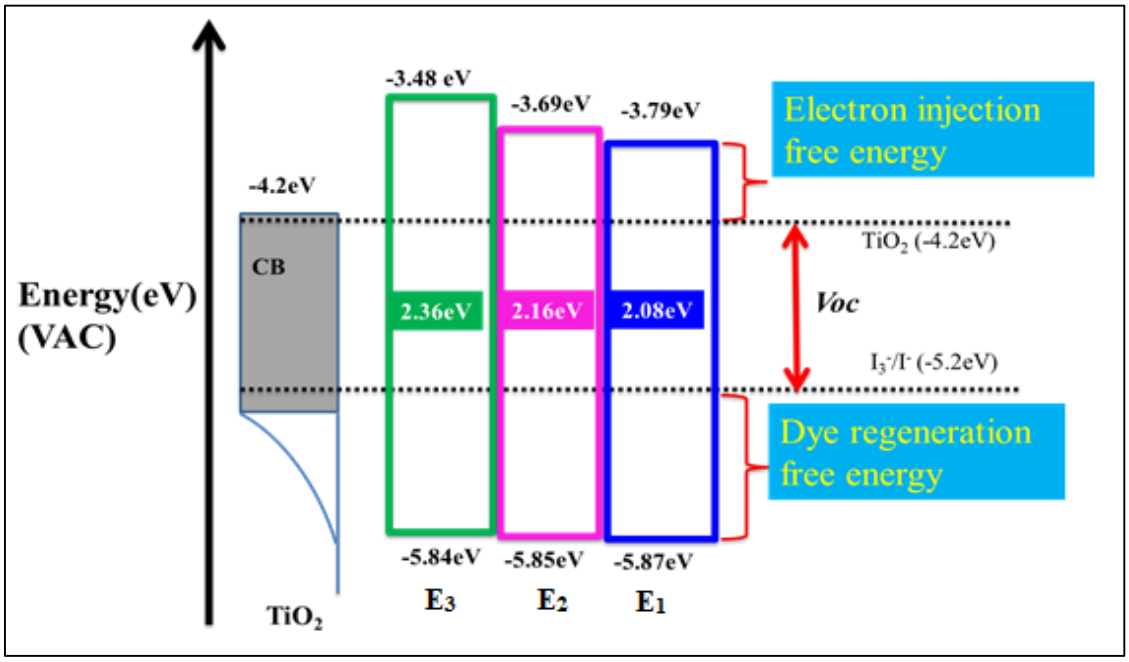

Fig.3.12 Energy level diagram of **E**$_{1\text{-}3}$ dyes.

Under optimized conditions, electron injection free energy greater than 150 meV should result in efficient electron injection (Koops et al. 2009) and dye regeneration free energy as low as 250 meV should lead to efficient dye regeneration as reported previously (Hardin et al. 2012, Hussain et al. 2014). All of the dyes meet these stringent thermodynamic requirements, as compared in energy level diagram of **Fig.3.12**.

3.3.5 Photovoltaic device characterizations

In order to establish the structure-performance relationship and determine the best anchoring group for indole based electron donating groups, photovoltaic characterizations were carried out. Photocurrent action spectra for dyes **E**$_{1\text{-}3}$ are depicted in **Fig.3.13**. Incident photon to current conversion efficiency (IPCE) response of higher than 55% from 375nm to 550nm was exhibited by **E**$_3$ reaching a maximum of 67% at 440 nm in the presence of

10 mM CDCA, whereas **E_1** and **E_2** showed comparatively lower IPCE response. It was found that, these dyes result in best IPCE response in the presence of 10 mM CDCA. CDCA was added as a co-adsorber to the dye solution to act as anti-aggregation reagent (Ito et al. 2008). The added co-adsorbers have shown to assist in favorable packing of the dye by covering the spaces between dye molecules. It has been also reported that co-adsorbers decrease the dye loading up to 60% (Neale et al. 2005), which can significantly lower the photocurrent density, such a decrease in dye loading in the presence of CDCA (20 mM) was observed for **E_{1-3}** dyes based on IPCE response. However, in the presence of 1 mM CDCA surface passivation was not optimum as can be incurred from IPCE response of solar devices.

Fig.3.14 shows the I-V characteristics of the solar devices prepared from dyes **E_{1-3}**, and the corresponding data is depicted in **Table 3.2**. It was observed that better IPCE response of **E_3** translated into higher J_{sc} of 9.35 mAcm^{-2} compared to 4.5 mAcm^{-2} of **E_1** and 0.28 mAcm^{-2} of **E_2** in the presence of 10 mM CDCA. Higher J_{sc} of **E_3** can be attributed to higher free energy of electron injection in TiO_2 conduction band compared to **E_2** and **E_1** (**Fig.3.12**, energy level diagram). Solar cells employing dyes **E_3**, **E_2** and **E_1** yielded overall power conversion efficiency ($\%\eta$) of 4.1 (V_{oc} = 0.62 V and *ff* = 0.71), ($\%\eta$) of 0.05 (V_{oc} = 0.3 V and *ff* = 0.53), ($\%\eta$) of 1.48 (V_{oc} = 0.52 V and *ff* = 0.63), respectively compared to ($\%\eta$) of 7.64 for **N719** (J_{sc} = 15.9 mAcm^{-2}, V_{oc} = 0.73 and *ff* = 0.66). Sensitizer **E_3** outperformed **E_1** and **E_2** in overall solar cell performance.

Table 3.2 Photovoltaic parameters of **E_{1-3}** sensitizers

Sensitizer	CDCA mM	*Adsorption solvent*	J_{sc} (mAcm^{-2})	V_{oc} (V)	*ff* (%)	η (%)
E_1	10	ACN:Tert. Butanol (1:1)	4.5	0.52	63	1.48
E_2	10	ACN:Tert. Butanol (1:1)	0.28	0.3	53	0.046
E_3	10	ACN:Tert. Butanol (1:1)	9.35	0.62	71	**4.12**
E_3	20	ACN:Tert. Butanol (1:1)	8.3	0.64	72	3.82

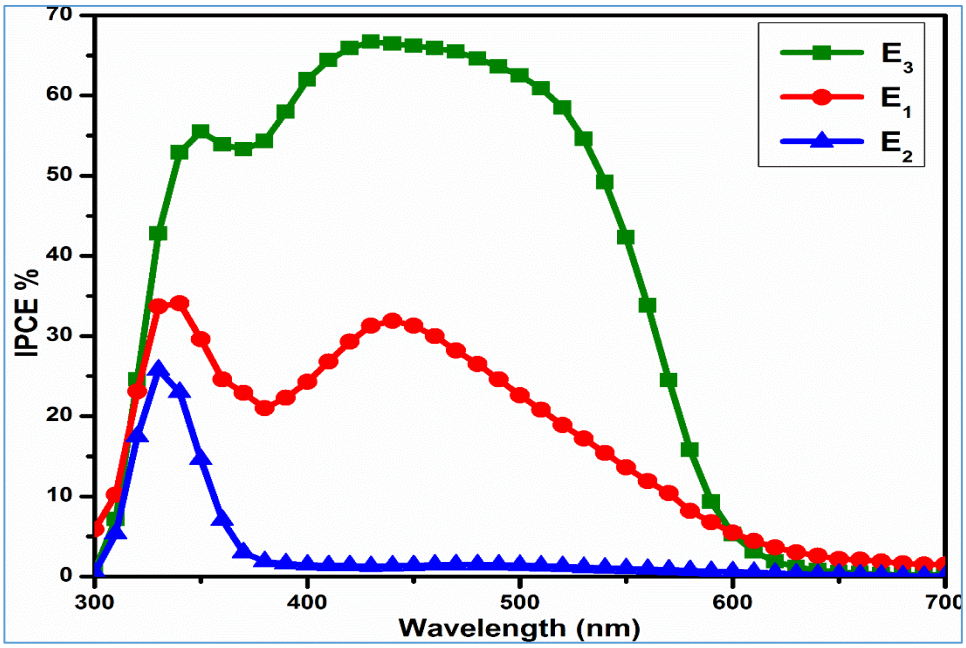

Fig.3.13 IPCE for $\mathbf{E_{1\text{-}3}}$ anchored on TiO_2 film in presence of 10 mM CDCA

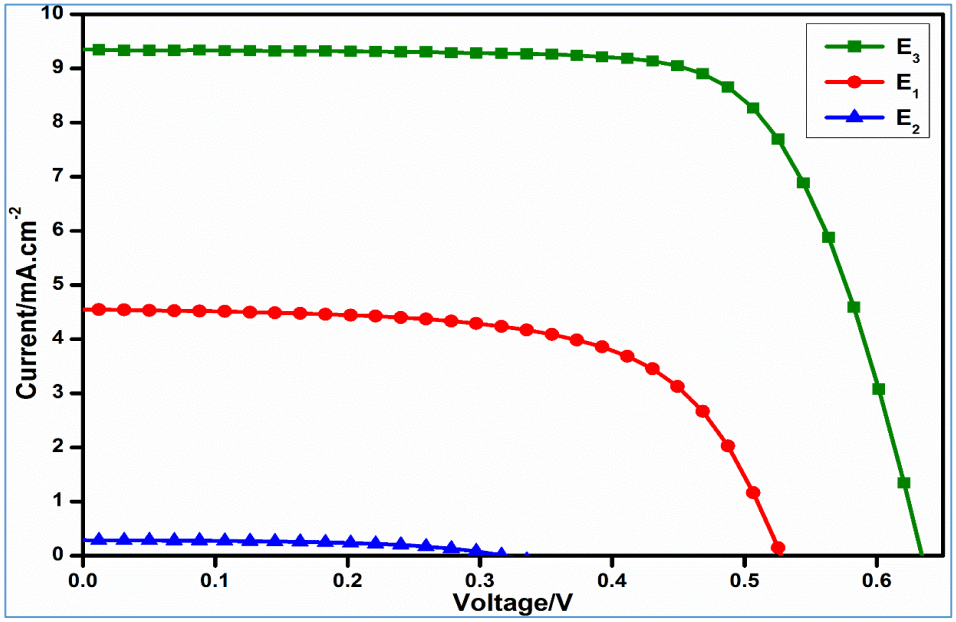

Fig.3.14 Photocurrent-voltage characteristics of DSSCs sensitized with $\mathbf{E_{1\text{-}3}}$

The better efficiency of **E_3** dye can be attributed to efficient electron withdrawing and injection to TiO_2 of 4-aminobenzoic acid as anchoring group, thus leading to efficient charge generation, transport and injection. The clear separation of the electronic overlap as found by modelling studies (**Fig.3.10**) between the HOMO and LUMO levels for **E_3** compared to the other sensitizers (**E_1** and **E_2**) leads to a favorable charge separation and thereby hindering for electron-hole recombination in **E_3**; this could explain the superior overall efficiency. Thus, the theoretical predictions are in accordance with the experimentally obtained results. To further probe the interface characteristics, electrochemical impedance measurements were performed.

3.3.6. Electrochemical impedance spectroscopy characterization

Electrochemical impedance spectroscopy (EIS) successfully models the charge transfer and chemical capacitance at the interface of TiO_2/dye/electrolyte and Pt/eletrolyte in DSSC under operational conditions (Kern et al. 2002, Wang et al. 2005, and Koide et al. 2006). Typical EIS measurements result in Nyquist and Bode plots. In Nyquist plot, intermediate frequecny semicirlce is related to electron transport through mesoporous TiO_2 and back electron transfer from TiO_2 to electrolyte. Bigger the radius of middle semicircle, higher is the charge recombination resistance (R_{ct}) from TiO_2 to electrolyte (Han et al. 2006, Cheema et al. 2014) corresponding to Nernst impedance, whereas radius of same semicircle corresponds to resistance to charge diffusion (R_d) under Gerischer impedance as discussed by Wang and co-workers (Wang et al. 2005).

In EIS Nyquist plots (**Fig.3.15 (a)**), for the best performing sensitizer **E_3**, semicircles of similar size were observed in the presence of different concentrations of CDCA, depicting low to minimum effect of CDCA on recombinaiton resistance (R_{ct}). However, Nyquist plot semicircles (**Fig.3.15 (b)**) for **E_2** based solar devices were biggest in radius followed by **E_1** based solar devices. For the same sensitizer, *e.g.* radius of semicircle of **E_2** increased with the concentration of CDCA, due to enhanced diffusion resistance (R_d). The difference in the impedance behavior of **E_3** versus **E_2** and **E_1** is due to the nature of impedance involved, which can be predicted as Nernst for **E_3** and Gerischer for **E_2** and **E_1**. The nature of the impedance for **E_2** and **E_1** based solar devices can be

attributed to Gerischer impedance, where $R_d >> R_{ct}$, such a condition is valid for solar devices with substantial charge generation and diffusion related losses (Han et al. 2006, Cheema et al. 2014, Bisquert 2001) as seen from photovoltaic results (**Table 3.2**).

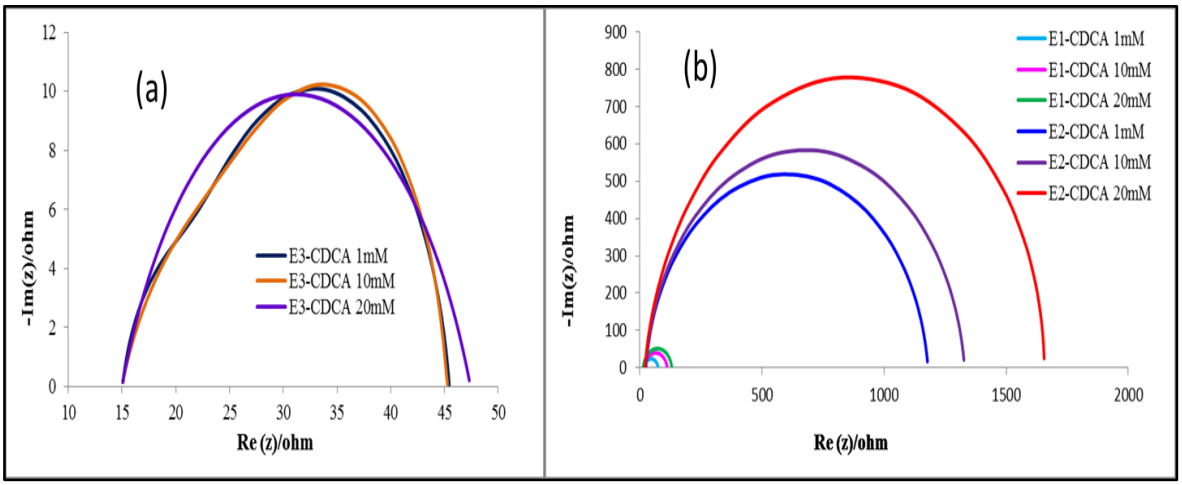

Fig.3.15 EIS Nyquist plots for DSSCs sensitized using **(a) E_3** and **(b) E_2** and **E_1** dyes

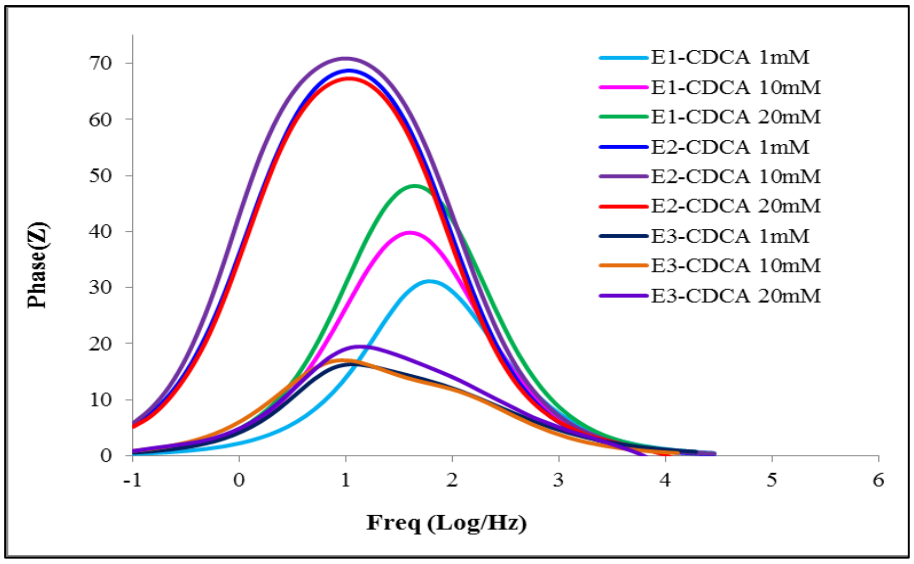

Fig.3.16 EIS Bode plots for DSSCs sensitized with **E_3**, **E_2** and **E_1** dyes

In Bode frequency plots (**Fig.3.16**), lifetime for injected electrons into TiO_2 conduction band can be determined by using the the relation ($\tau_{CB} = 1/2\pi f$), where τ is the lifetime of electrons in TiO_2 and *f* is the mid frequency peak in Bode plots. The frequency

peak of the DSSCs based on **E_3**, **E_2**, **E_1** and **N719** are at 7, 11, 35 and 29 Hz, respectively corresponding to lifetime time of 23, 14.5, 4.5 and 5.5 ms respectively. Though, generally higher lifetime time is related with improved V_{oc}, however that seems plausible for **E_3** and **N719** dyes, whereas the complex nature of results of **E_1** and **E_2** cannot be explained based on these findings only, since impedance for these two systems is much higher due to reasons discussed for Nyquist plot.

3.3.7. FT-IR analysis: anchoring studies of the dyes on TiO_2

FTIR spectroscopy is widely applied in order to gain an insight into the nature of anchoring groups and the mode of their interaction with the TiO_2 substrate. By implementing this technique one can elucidate the absorption states of the sensitizers and/or bonds formed upon adsorption on the TiO_2 nanoparticles using a set of rules developed by Deacon and Phillips (Deacon and Phillips 1980). According to these rules, there is a direct correlation between the difference ($\Delta\nu$) between symmetric and asymmetric bond stretching frequencies of a carbonyl group of carboxylic acid and its corresponding coordination type. Three possible scenarios exist; if ($\Delta\nu$) of the dye adsorbed onto TiO_2 ($\Delta\nu_{abs}$) is smaller than that of the free molecule ($\Delta\nu_{free}$), *i.e* ($\Delta\nu_{abs}$) < ($\Delta\nu_{free}$), the bidentate adsorption mode will be present; if ($\Delta\nu_{abs}$) << ($\Delta\nu_{free}$), in all probability the chelating mode is present. Whereas, if ($\Delta\nu_{abs}$) > ($\Delta\nu_{free}$), the dye molecule takes a monodentate binding mode (Deacon and Phillips 1980). Against this background, the infrared absorption spectra were measured for each of the dyes and the corresponding sensitized TiO_2 films. FT-IR spectrum of the solid **E_3** dye shows prominent bands at 1687 cm^{-1} and 2220 cm^{-1} corresponding to the >C=O and -C≡N stretching, respectively.

The FT-IR spectrum of the **E_3** anchored on TiO_2 film (**Fig.3.17**) clearly depicts bands at 1570 and 1400 cm^{-1} for the asymmetric and symmetric stretching modes of the >C=O group, indicating that the carboxylic acid group is deprotonated and is involved in the adsorption of the sensitizer on TiO_2. Further, the disappearance of $\nu_{C=O}$ and the appearance of new peaks of symmetric and asymmetric stretching reveal that the dye is chemisorbed, thereby ruling out physisorption. Furthermore, from vibrational frequency

analysis, the nature of the binding mode can be elucidated by implementing Deacon and Phillips rules. From the obtained data it can be inferred that the dye is anchored on TiO_2 through the carboxylate group by means of a bidentate chelation or a bridging of surface titanium ions rather than an ester type linkage.

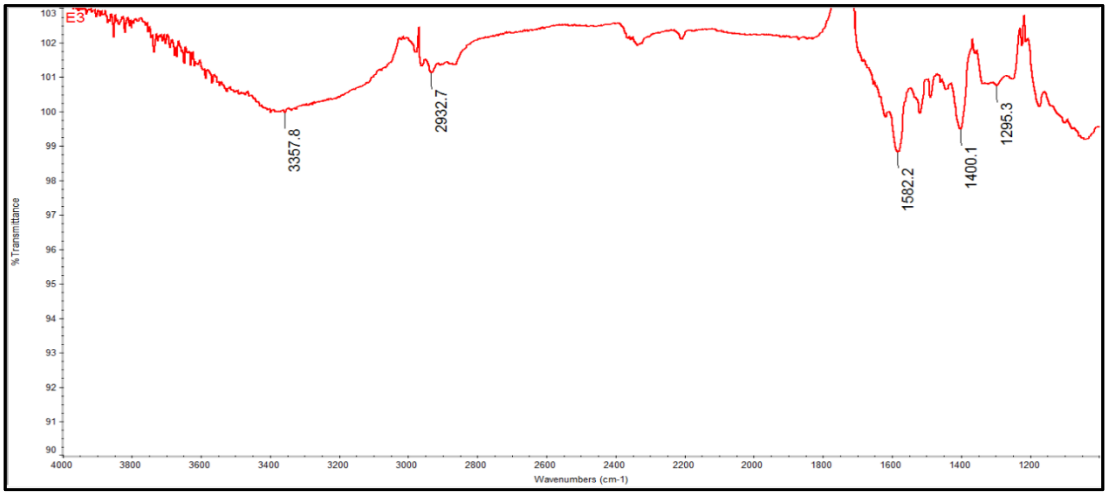

Fig.3.17 FT-IR spectrum of $\mathbf{E_3}$ on TiO_2

Similar trend was observed in the other two sensitizers ($\mathbf{E_1}$ and $\mathbf{E_2}$) as well. Further, in the all the three dyes the -C≡N band frequency remains unchanged, demonstrating that, the cyano group is not involved in dye-adsorption process.

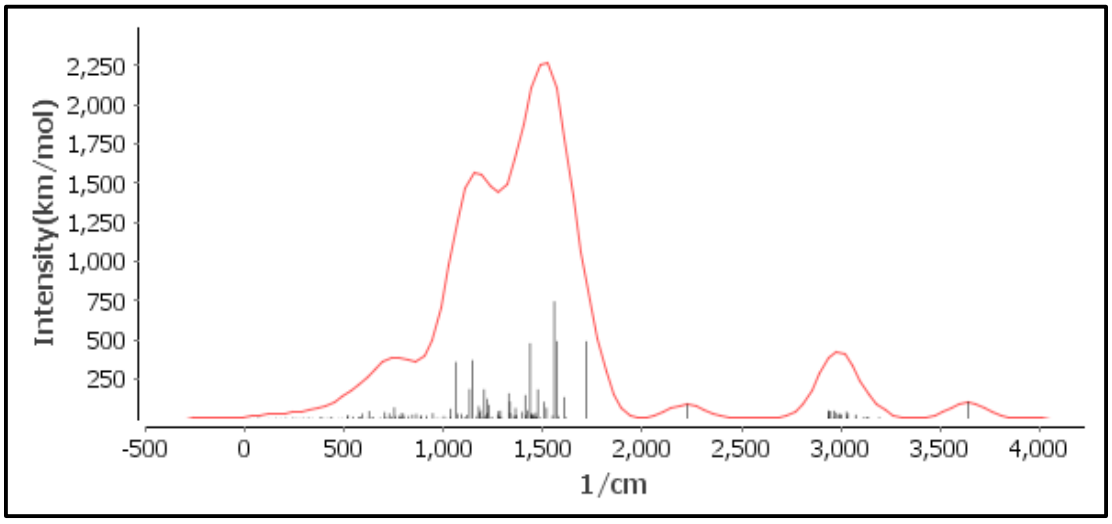

Fig.3.18 Theoretically obtained FT-IR spectrum of $\mathbf{E_3}$

Another peculiar feature observed in all the FT-IR spectra is the presence of a broad absorption band around 3400 cm^{-1}, which might be attributed to absorption of moisture from the dye solution, as the TiO_2 film was heated prior to staining. Further, the infrared absorption spectra of all the sensitizers were calculated using Turbomole software package and compared the aforementioned spectra with the experimentally obtained ones. **Fig.3.18** depicts the theoretically obtained FT-IR spectrum of **E_3**. It is evident that, the theoretically obtained spectrum is well in agreement with the experimentally acquired one.

3.4 CONCLUSIONS

Three new sensitizers (**E_{1-3}**) carrying D-D-A-π-A architecture have been successfully designed and synthesized. In the new design methoxy group acts as an auxiliary donor to the principal donor, *i.e.* indole moiety, cyanovinylene performs as an auxiliary acceptor, thiophene takes on the role of π-conjugation bridge and varying groups (2-cyanoacrylic acid, rhodanine-3-acetic acid and 4-aminobenzoic acid) function as principal acceptor/anchoring units. The effective conjugation in the new sensitizers leads to a broad absorption spectrum and a high molar extinction coefficient of the corresponding dyes, which in turn facilitates the dyes to harvest more photoelectrons. The DSSC fabricated using **E_3** showed the highest efficiency (4.12%), which is consistent with the fact that, sensitizer **E_3** has the widest IPCE response among the three sensitizers. Further, the higher efficiency of **E_3** can also be attributed to its longer electron lifetime ($eTiO_2$) and high lying LUMO which enhances the thermodynamic feasibility of electron injection into the conduction band of TiO_2. The DFT studies reveal a better charge separation between the HOMO and LUMO levels of the **E_3** sensitizer. The large difference in efficiency between **E_3** and the other two sensitizers indicates that, the acceptor/anchoring segment should be screened with caution as they are instrumental in governing the overall efficiency.

CHAPTER 4

5-NITROINDOLE BASED CHOMOPHORES WITH A-D-A-π-A CONFIGURATION: SYNTHESIS, CHARACTERIZATION AND PERFORMANCE EVALUATION

Abstract

This chapter covers the synthesis and structural characterization of three new organic co-sensitizers ***N*****$_{1-3}$***. *Further, it includes linear optical and electrochemical studies along with DFT calculations. Furthermore, fabrication results of devices with* ***N*****$_{1-3}$** *dyes have been incorporated. Finally, all the aforesaid results have been discussed.*

4.1 INTRODUCTION

Based on the comprehensive literature survey and by following the design strategy described in **chapter 1 (Section 1.11)**, three new dyes **N$_{1-3}$ (series 3)** with A-D-A-π-A (acceptor-donor-acceptor-π-bridge-acceptor) architecture carrying indole and thiophene units attached to different acceptors/anchoring groups, were synthesized starting from simple organic molecules, as promising co-sensitizers for DSSC application. Their synthetic protocols, optical and electrochemical characterizations as well as theoretical calculations have been described. Further, photovoltaic performance studies of the aforesaid co-sensitizers have been discussed. **Fig.4.1** depicts the chemical structures of the newly designed co-sensitizers (**N$_{1-3}$**) and ruthenium based sensitizer **HD-14**.

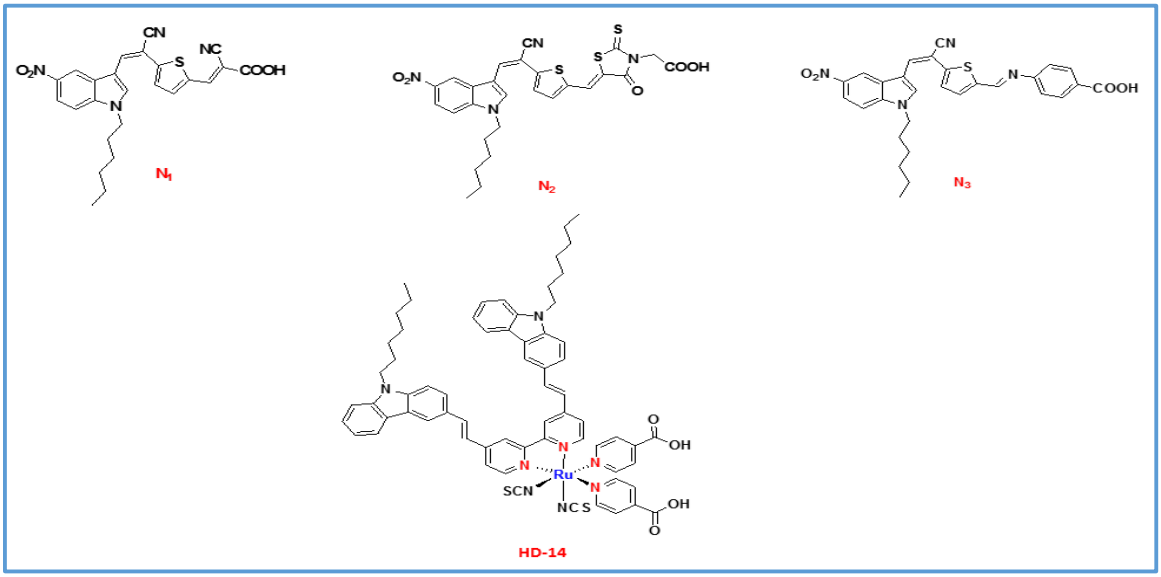

Fig.4.1 Chemical structures of co-sensitizers **N$_{1-3}$** and ruthenium based sensitizer **HD-14**

4.2 EXPERIMENTAL

4.2.1 Materials and methods

The starting materials 5-nitro-1*H*-indole, thiophene-2-acetonitrile, 1-bromohexane, cyanoacetic acid, rhodanine-3-acetic acid and 4-aminobenzoic acid were purchased from Sigma-Aldrich and were used without any further purification unless stated otherwise. Ruthenium based sensitizer **HD-14** was synthesized as per the literature. All the solvents were freshly distilled prior to use. All the reactions were performed under argon atmosphere and the progress of reaction was monitored by TLC technique. Chromatographic separations were carried out using silica gel (100–200 mesh).^{1}H NMR and ^{13}C NMR spectra were recorded using a Bruker avance 500 MHz and 400 MHz spectrometers, using DMSO-d_6 or $CDCl_3$ as solvents and TMS as an internal standard. Mass spectra were recorded on thermo scientific-EXACTIVE (ESI-MS), whereas the elemental analysis was carried out on a Flash EA1112 CHNS analyzer (Thermo Electron Corporation). The FTIR spectra were obtained using Nicolet Avatar 5700.

4.2.2 Synthesis of sensitizers N_{1-3}

The synthetic pathways of the three new sensitizers $\mathbf{N_{1-3}}$ are depicted in **Scheme 4.1**. N-alkylation of 5-nitro-1*H*-indole was done using 1-bromohexane to yield compound **4.1**. It was then subjected to Vilsmeier–Haack formylation to give compound **4.2**. The product was coupled with the active methylene compound thiophene-2-acetonitrile by Knoevenagel condensation to yield the product **4.3**. 2-(5-Formylthiophen-2-yl)-3-(1-hexyl-5-nitro-1*H*-indol-3-yl)-acrylonitrile (**4.4**) was obtained by formylation of compound **4.3** by Vilsmeier–Haack protocol. Finally, Knoevenagel condensation of this aldehyde **4.4** with cyanoacetic acid and rhodanine-3-acetic acid in the presence of ammonium acetate produced the desired dyes $\mathbf{N_1}$ and $\mathbf{N_2}$, respectively, whereas $\mathbf{N_3}$ was obtained by condensation of compound **4.4** with 4-aminobenzoic acid in methanol.

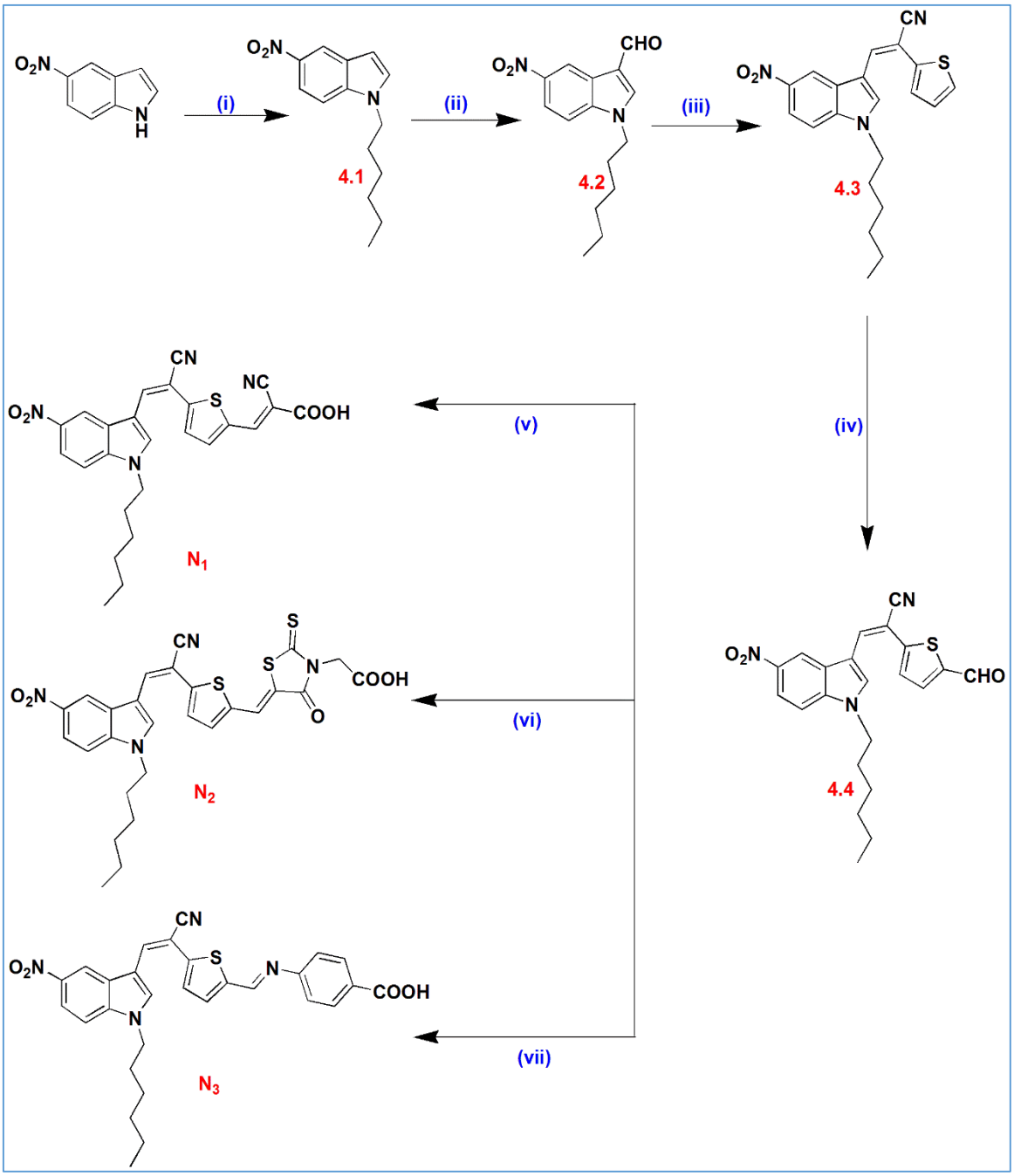

Scheme 4.1 Synthetic route of the sensitizers (i) 1-Bromohexane, K_2CO_3, DMF, 80 ^{0}C (ii) $POCl_3$, DMF, 60 ^{0}C (iii) 2-(thiophen-2-yl)-acetonitrile, NaOMe, CH_3OH, RT (iv) $POCl_3$, DMF, RT (v) Cyanoacetic acid, ammonium acetate, glacial CH_3COOH, 110 ^{0}C (vi) Rhodanine-3-acetic acid, ammonium acetate, glacial CH_3COOH, 110 ^{0}C (vii) 4-Aminobenzoic acid, CH_3OH, 80 ^{0}C

4.2.3 Optical, electrochemical and theoretical studies

The optical, electrochemical, EIS, photovoltaic and theoretical studies were carried out by following the procedures described in **section 3.2** of **chapter 3.**

4.2.4 DSSC fabrication

DSSC were fabricated as per the procedure described in **section 3.2** of **chapter 3.** In the experiment, the dye solution was prepared by mixing of ruthenium based sensitizer (**HD-14**) and the respective co-sensitizer (**N_{1-3}**) in 0.2 mM or 0.3 mM concentration, respectively with addition of CDCA at a concentration of 20 mM. The above solutions were used for DSSC device fabrication studies and their results are summarized in **Table 4.2**.

4.2.5 Synthetic methods

Synthesis of *1-hexyl-5-nitro-1H-indole (4.1)*

A mixture of 1-bromohexane (0.610 g, 3.70 mmol), 5-nitro-1*H*-indole (0.5 g, 3.08 mmol), potassium carbonate (0.639 g, 4.62 mmol), in DMF (15 mL) was stirred at 85 ^{0}C for 10 h. After that, water was added to the reaction mixture and neutralized with dil. HCl. The product was extracted using ethyl acetate/water (50 mL × 3). Organic phase was dried over sodium sulfate. The solvent was removed under reduced pressure and the crude oily product obtained was further purified by column chromatography on silica gel using hexane as an eluent to give off white solid. Yield: 87%. ^{1}H NMR (400MHz DMSO-d_6, ppm): δ 10.00 (s, 1H), 8.95 (s, 1H), 8.63 (s, 1H), 8.19 (d, J = 8.8 Hz, 1H), 7.90 (d, J = 8.4 Hz, 1H), 4.36 (s, 2H), 1.81 (s, 2H), 1.26 (s, 6H), 0.83 (s, 3H). Calcd. for $C_{14}H_{18}N_2O_2$: C, 68.27; H,7.37; N, 11.37 found: C, 68.41; H, 7.41; N, 11.25.ESI-MS (+ve mode) *m/z* Calcd for $C_{14}H_{18}N_2O_2$: 246.14. Found: 247.14 $[M+H]^+$.

Synthesis of *1-hexyl-5-nitro-1H-indole-3-carbaldehyde (4.2)*

A two neck round bottom flask was charged with freshly distilled DMF (1.48 mL, 5 eq) and $POCl_3$ (1.86 mL, 5 eq) was added to it drop-wise, with constant stirring at 0 ^{o}C under nitrogen to obtain a glassy white solid and to this 1-hexyl-5-nitro-1*H*-indole (**4.1**, 1

g, 4.06 mmol) dissolved in dichloroethane (10 mL) was added while stirring. The stirring was continued at 50 °C for 12 h. The reaction mass was then poured into crushed ice and subsequently basified using 5 M NaOH solution. The precipitated solid was collected by filtration and the crude product was purified by column chromatography on silica gel using ethyl acetate/hexane (1:5) as mobile phase. Brown solid, yield 73%. ^{1}H NMR (400MHz DMSO-d_6, ppm): δ 10.00 (s, 1H), 8.95 (s, 1H), 8.63 (s, 1H), 8.19 (d, J = 8.8 Hz, 1H), 7.90 (d, J = 8.4 Hz, 1H), 4.36 (s, 2H), 1.81 (s, 2H), 1.26 (s, 6H), 0.83 (s, 3H). Calcd. for $C_{15}H_{18}N_2O_3$: C, 65.68; H,6.61; N, 10.21 found: C, 65.41; H, 6.67; N, 10.15.ESI-MS (+ve mode) *m/z* Calcd for $C_{15}H_{18}N_2O_3$: 274.13. Found: 275.14 $[M+H]^+$.

Synthesis of *3*-(*1-hexyl-5-nitro-1H-indol-3-yl)-2-(thiophene-2-yl)acrylonitrile* (*4.3*)

To a freshly prepared solution of sodium methoxide (0.060 g, 2.62 mmol of sodium in 10 mL of methanol), thiophene-2-acetonitrile (0.323 g, 2.62 mmol) was added slowly while stirring. 1-hexyl-5-nitro-*1H*-indole-3-carbaldehyde (**4.2**, 0.600 g, 2.18 mmol) was then added to reaction mass. Stirring was continued for 9 h at room temperature. The precipitated yellow solid was collected by filtration, washed with methanol and finally recrystallized from chloroform. Yellow solid, yield 69%. ^{1}H NMR (400MHz DMSO-d_6, ppm): δ 9.14 (s, 1H), 8.48 (s, 1H), 8.17 (d, J = 24 Hz, 2H), 7.84 (s, 1H), 7.64 (s, 1H), 7.53 (s, 1H), 7.17 (d, 1H), 4.40 (s, 2H), 1.79 (s, 2H), 1.27 (s, 6H), 0.83 (t, 3H). Anal. Calcd. for $C_{21}H_{21}N_3O_2S$: C, 66.47; H,5.58; N, 11.07 found: C, 66.31; H, 5.61; N, 11.15. ESI-MS (+ve mode) *m/z* Calcd for $C_{21}H_{21}N_3O_2S$: 379.14. Found: 380.14 $[M+H]^+$.

Synthesis of 2-(5-formylthiophen-2-yl)-*3*-(*1-hexyl-5-nitro-1H-indol-3-yl)-acrylonitrile* (*4.4*)

A two neck round bottom flask was charged with freshly distilled DMF (0.48 mL, 5 eq) and $POCl_3$ was added to it drop-wise, with constant stirring (0.60 mL, 5 eq) at 0 °C under nitrogen. The mixture was stirred for 30 minutes to obtain a glassy white solid and to this 3-(1-hexyl-5-nitro-*1H*-indol-3-yl)-2-(thiophene-2-yl)acrylonitrile (**4.3**, 0.5 g, 1.31 mmol) dissolved in dichloroethane (10 mL) was added while stirring. The stirring was continued at 80 °C for 12 h. After cooling, the reaction mass was then poured into crushed

ice and subsequently basified using 5M NaOH solution. The precipitated solid was collected by filtration and the crude product was purified by column chromatography on silica gel using ethyl acetate/hexane (1:5) as mobile phase to give red colored solid. Yield: 63%. δ 9.90 (s, 1H), 8.73 (d, *J* = 1Hz, 1H), 8.49 (s, 1H), 8.24 (q, *J* = 8Hz, 1H), 7.85 (s, 1H), 7.73 (d, *J* = 3.5 Hz, 1H), 7.48 (d, *J* = 9 Hz, 1H), 7.40 (d, *J* = 4 Hz, 1H), 4.27 (t, *J* = 7 Hz, 2H), 1.92 (q, *J* = 7 Hz, 2H), 1.33 (s, 6H), 0.88 (t, *J* = 6.5 Hz, 3H). ESI-MS (+ve mode) *m/z* Calcd for $C_{22}H_{21}N_3O_3S$: 407.13. Found: 408.13 $[M+H]^+$.

Synthesis of *2-cyano-3-(5-(1-cyano-2-(1-hexyl-5-nitro-1H-indol-3-yl)vinyl)thiophen-2-yl)acrylic acid (N_1)*

A dried two neck round bottomed flask was charged with 2-(5-formylthiophen-2-yl)-3-(1-hexyl-5-nitro-1*H*-indol-3-yl)-acrylonitrile (**4.4**, 0.150 g, 0.368 mmol), cyano acetic acid (0.046 g, 0.552 mmol), and ammonium acetate (0.312 g, 4.05 mmol) and the mixture was dissolved in glacial acetic acid (15 mL) under argon atmosphere. This mixture was then refluxed for 12 h under continuous stirring. After completion of the reaction, the mass was cooled to room temperature and was poured onto crushed ice. The obtained solid was filtered. The crude product was purified by column chromatography using silica gel and $CHCl_3$:CH_3OH (10: 3) as mobile phase to obtain red color solid. Yield: 53%. ^{1}H NMR (400MHz DMSO-d_6, ppm): ^{1}H NMR (400MHz DMSO-d6, ppm): δ 9.21 (s, 1H), 8.66 (s, 1H), 8.49 (d, *J*= 13.2 Hz, 2H), 8.15 (d, *J*= 8.4 Hz, 1H), 8.01 (s, 1H), 7.85 (t, *J*= 9.2 Hz, 2H), 4.43 (s, 2H), 1.81 (s, 2H), 1.27 (s, 6H), 0.83 (s, 3H). ^{13}C (100MHz, DMSO-d_6) δ (ppm): 163.97, 148.47, 146.67, 142.91, 141.49, 139.22, 135.51, 135.11, 134.69, 127.39, 125.91, 118.77, 118.39, 117.33, 116.87, 112.47, 112.33, 98.68, 47.38, 31.14, 29.99, 26.15, 22.45, 14.29. Anal. Calcd. for $C_{25}H_{22}N_4O_4S$: C,63.28; H,4.67; N, 11.81 found: C, 63.45; H, 4.61; N, 11.87. ESI-MS (+ve mode) *m/z* Calcd for $C_{25}H_{22}N_4O_4S$:474.14. Found: 475.14 $[M+H]^+$.

Synthesis of *2-((Z)-5-((5-((Z)-1-cyano-2-(1-hexyl-5-nitro-1H-indol-3-yl)vinyl)thiophen-2-yl)methylene)-4-oxo-2-thioxothiazolidin-3-yl)acetic acid* (N_2)

The compound **4.4** (0.150 g, 0.368 mmol), rhodanine-3-acetic acid (0.084 g, 0.442 mmol), ammonium acetate (0.312 g, 4.05 mmol), and glacial acetic acid (10 mL) were mixed together and refluxed for 15 h with continuous stirring. The solution was cooled to room temperature and the obtained precipitate was filtered, and washed with acetic acid and water. The obtained solid was further purified by column chromatography using silica gel and $CHCl_3$:CH_3OH (10:2) as mobile phase to obtain a dark red solid. Yield: 53%. ^{1}H NMR (400MHz DMSO-d6, ppm): δ 9.23 (s, 1H), 8.56 (s,1H), 8.41 (s, 1H), 8.14 (d, *J* = 9.2 Hz, 1H), 8.08 (s, 1H), 7.83 (t, *J* = 9.2 Hz, 2H), 7.71 (s, 1H), 4.70 (s, 2H), 4.42 (s, 2H), 1.81 (s, 2H), 1.28 (s, 6H), 0.84 (s, 3H). ^{13}C (100MHz, DMSO-d_6) δ (ppm): ^{13}C (100MHz, DMSO-d_6) δ (ppm): 166.39, 142.86, 139.17, 137.09, 134.37, 112.59, 47.35, 45.74, 31.15, 30.01, 26.17, 22.47, 14.31. Anal. Calcd. for $C_{27}H_{24}N_4O_5S_3$: C, 55.84; H, 4.17; N, 9.65 found: C, 55.61; H, 4.25; N, 9.69. ESI-MS (+ve mode) *m/z* Calcd for $C_{27}H_{24}N_4O_5S_3$: 580.09. Found: 581.09 $[M+H]^+$.

Synthesis of 4-((E)-(5-((Z)-1-cyano-2-(1-hexyl-5-nitro-1H-indol-3-yl)vinyl)thiophen-2-yl)methyleneamino)benzoic acid (*N3*)

A mixture of 2-(5-formylthiophen-2-yl)-3-(1-hexyl-5-nitro-*1H*-indol-3-yl)-acrylonitrile (**4.4**, 0.150 g, 0.368 mmol) and 4-aminobenzoic acid (0.050 g, 0.368 mmol) was refluxed in 10 mL of absolute methanol for 4 h. The separated solid was filtered and recrystallized from methanol to obtain bright orange color solid. Yield 79%. ^{1}H NMR (400MHz DMSO-d_6, ppm): ^{1}H NMR (400MHz DMSO-d_6, ppm): δ 12.86 (s, 1H), 9.23 (s, 1H), 8.80 (s,1H), 8.54 (s, 1H), 8.35 (s, 1H), 8.12 (s, 1H), 7.98 (s, 2H), 7.83 (s, 1H), 7.71 (s, 1H), 7.53 (s, 1H), 7.34 (s, 2H), 4.40 (s, 2H), 1.80 (s, 2H), 1.27 (s, 6H), 0.83 (s, 3H). ^{13}C (100MHz, DMSO-d_6) δ (ppm): 184.15, 155.97, 155.84, 149.49, 141.35, 139.44, 136.78, 135.94, 132.13, 131.31, 131.12, 128.95, 128.88, 125.17, 121.67, 118.97, 113.77, 112.44, 110.18, 101.83, 95.29, 56.13, 47.10, 31.15, 29.92, 26.18, 22.46, 14.30. Anal. Calcd. for $C_{29}H_{26}N_4O_4S$: C, 66.14; H, 4.98; N, 10.64 found: C, 66.33; H, 4.91; N, 10.69. ESI-MS (+ve mode) *m/z* Calcd for $C_{29}H_{26}N_4O_4S$: 526.17. Found: 527.17 $[M+H]^+$.

4.3 RESULTS AND DISCUSSION

4.3.1 Structural characterization

The chemical structures of newly synthesized compounds were confirmed by ^{1}H NMR, ^{13}C NMR spectroscopy and elemental analysis. The compound **N_3**, in ^{1}H NMR spectrum showed unique resonance at δ 12.84 ppm for the protons corresponding to acid group. Appearance of a singlet at δ 9.23 ppm has confirmed the presence of an aromatic proton at the second position of indole ring. All the other aromatic protons depicted peaks between 8.80 and 7.34 ppm. Further, two protons of $–NCH_2$ of hexyl chain resonated as a singlet at δ 4.40 ppm, whereas the appearance of signal of primary and secondary protons in the range of δ 1.85-0.83 ppm in its ^{1}H NMR spectrum confirmed the presence of hexyl chain.

The ^{13}C NMR spectrum of **N_3** showed the characteristic signals which appeared at higher frequency (downfield region). The carbonyl carbon atoms in acid group resonated at δ 184.15 ppm. The remaining signals appearing in the region of δ 155.97-95.29 ppm are due to other aromatic carbons. The first carbon in the hexyl chain attached directly to the aromatic nitrogen in the indole ring displayed a peak at 47.10 ppm. Further, the remaining aliphatic carbons appeared between 31.15-14.30 ppm. Furthermore, its mass spectrum exhibited the $[M+H]^+$ peak at 527.17, which is in agreement with the calculated molecular weight for the formula of $C_{29}H_{26}N_4O_4S$. **Fig.4.2-4.3** show ^{1}H NMR and mass spectra of compound **4.4**, respectively, whereas, **Fig.4.4-4.6** depict the ^{1}H NMR, ^{13}C NMR and Mass spectra of sensitizer **N_3**, respectively.

Spectrograms of selected target compounds

^{1}H NMR, ^{13}C NMR and Mass spectra of representative compounds are given below.

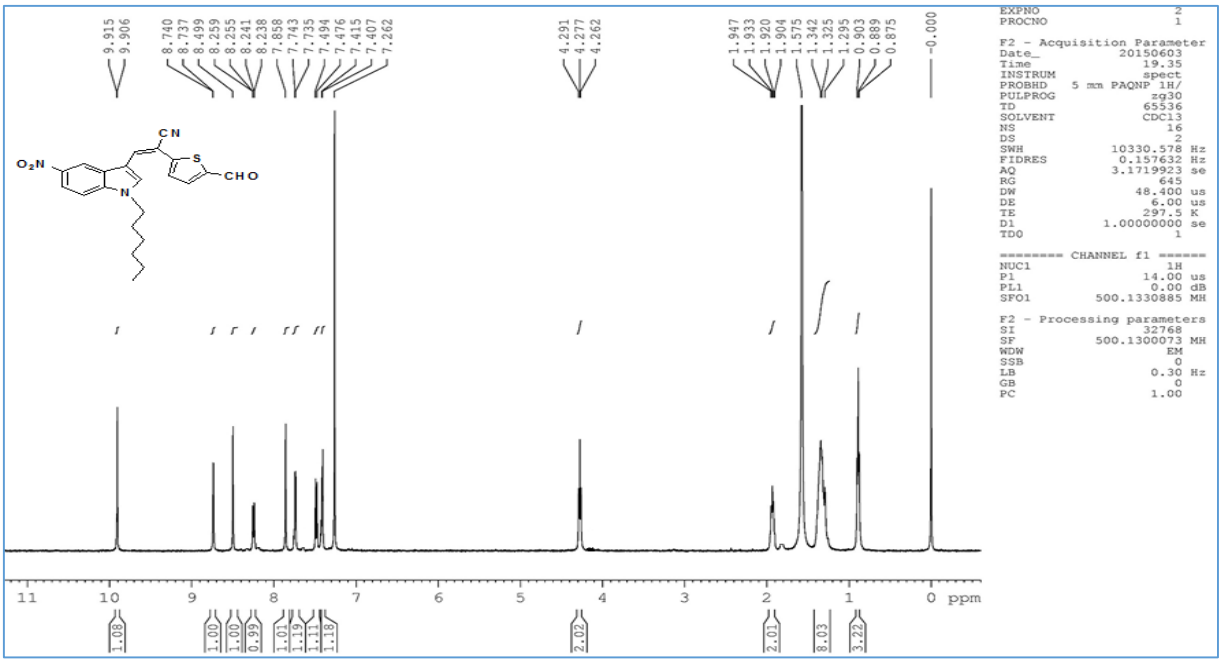

Fig.4.2 ^{1}H NMR spectrum of **4.4** in $CDCl_3$

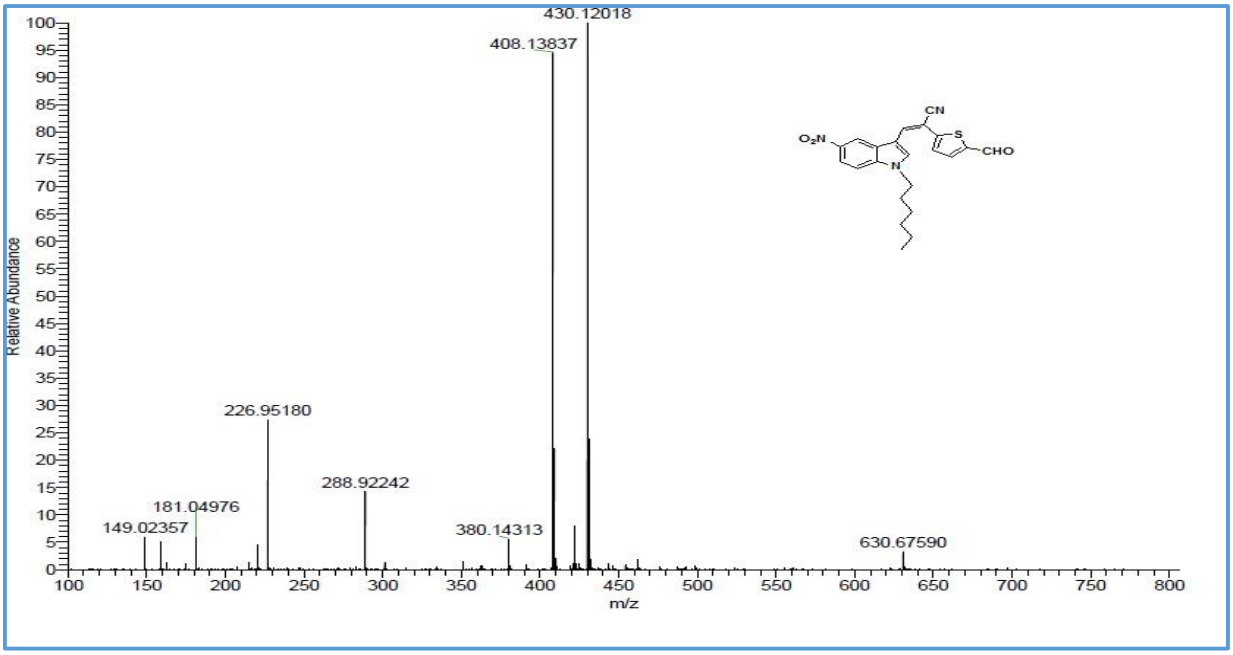

Fig.4.3 Mass spectrum of **4.4**

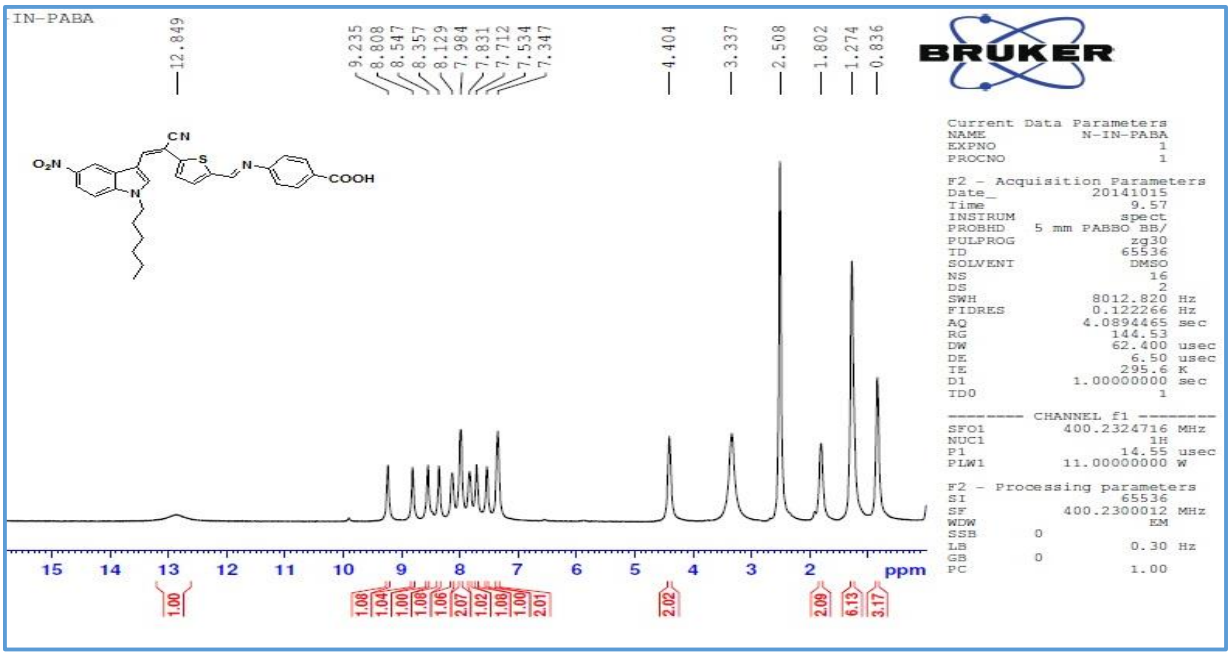

Fig.4.4 ^{1}H NMR spectrum of **N_3** in DMSO-d_6

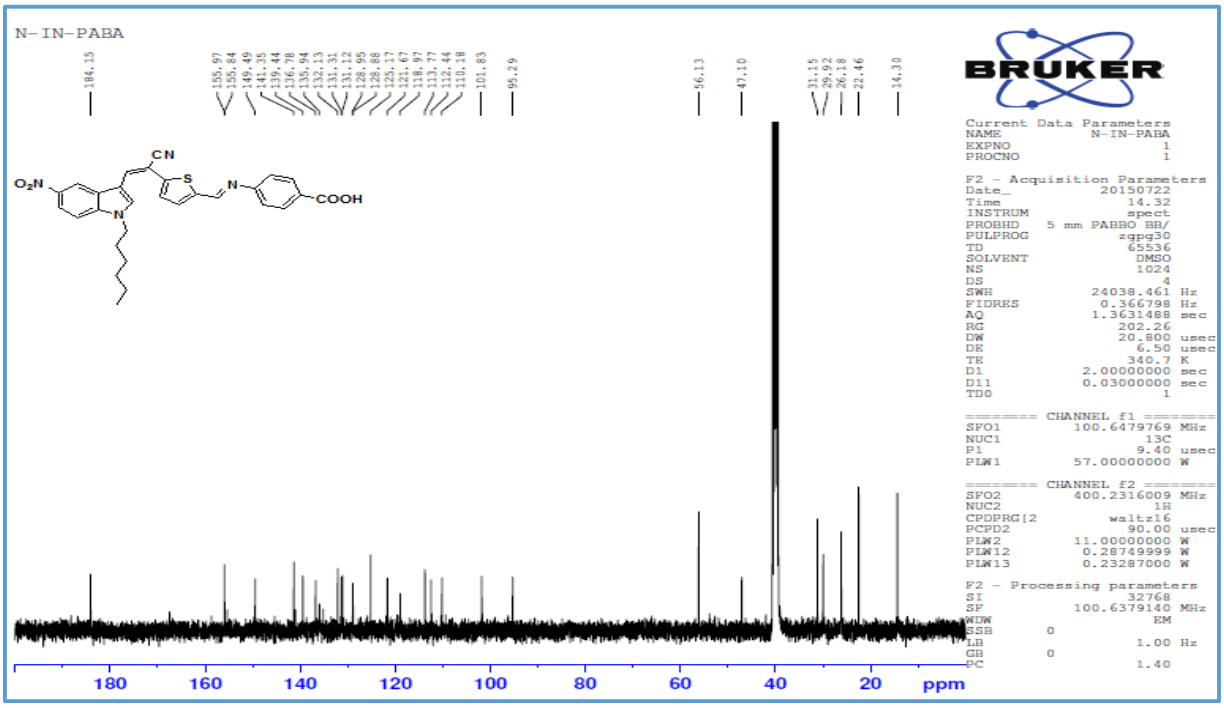

Fig.4.5 ^{13}C NMR spectrum of **N_3** in DMSO-d_6

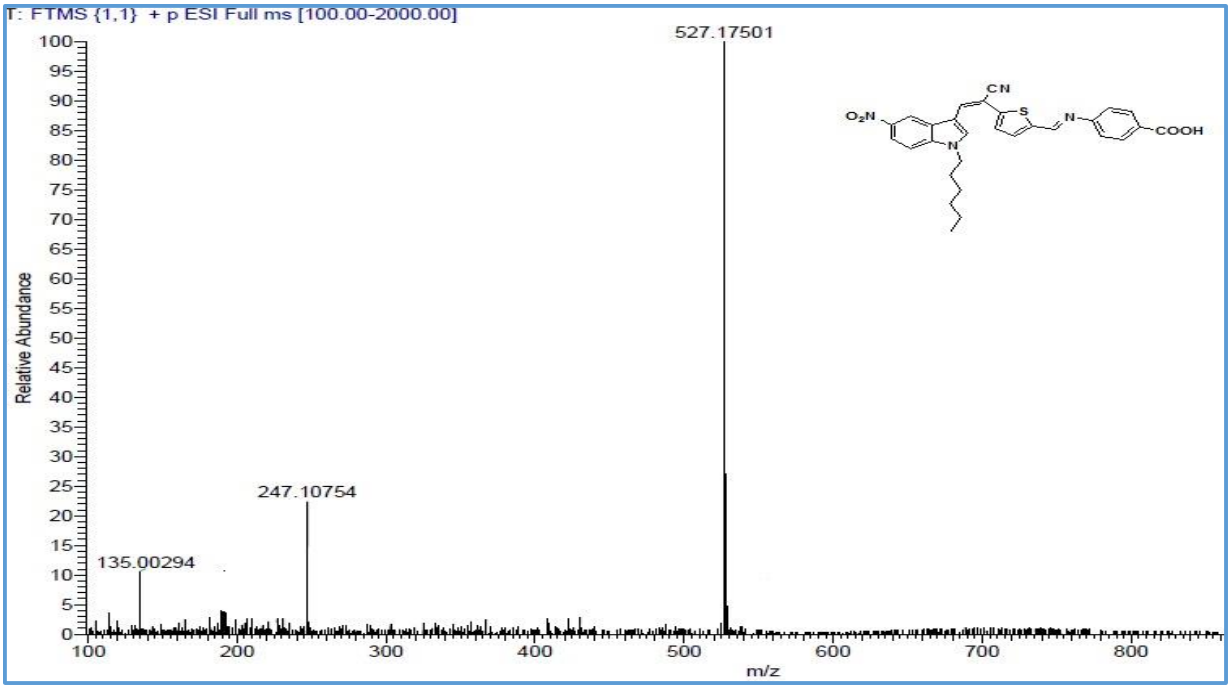

Fig.4.6 Mass spectrum of $\mathbf{N_3}$

4.3.2 Photophysical properties

The absorption and emission spectra of the co-sensitizers ($\mathbf{N_{1\text{-}3}}$) recorded in chloroform (3×10^{-5} M) solutions are shown in **Fig.4.7 (a)** and **(b)**, respectively; and the pertinent results are presented in **Table 4.1**. The dyes show two major absorption bands, the absorption bands in the shorter wavelength region (<400 nm) corresponding to π-π* electronic excitations localized within the indole and π-bridge segments, whereas the band in the longer wavelength region (451-497 nm) can be attributed to an intramolecular charge transfer (ICT) transition from indole (donor) to the corresponding acceptor segment. The high values of molar extinction coefficients in all the sensitizers (36.5×10^4- 48×10^4 $M^{-1}cm^{-1}$) confirm their good light-harvesting capability. These values are significantly higher than the ruthenium-based sensitizer (**HD-14**) in charge-transfer transitions. Further, **Fig.4.7 (c)** depicts the absorption spectrum of **HD-14** sensitizer. When adsorbed onto TiO_2 (**Fig.4.7 (d)**), all the sensitizers displayed a broadening as well as a red-shift in their absorption profile as compared to the corresponding spectra recorded in solution state.

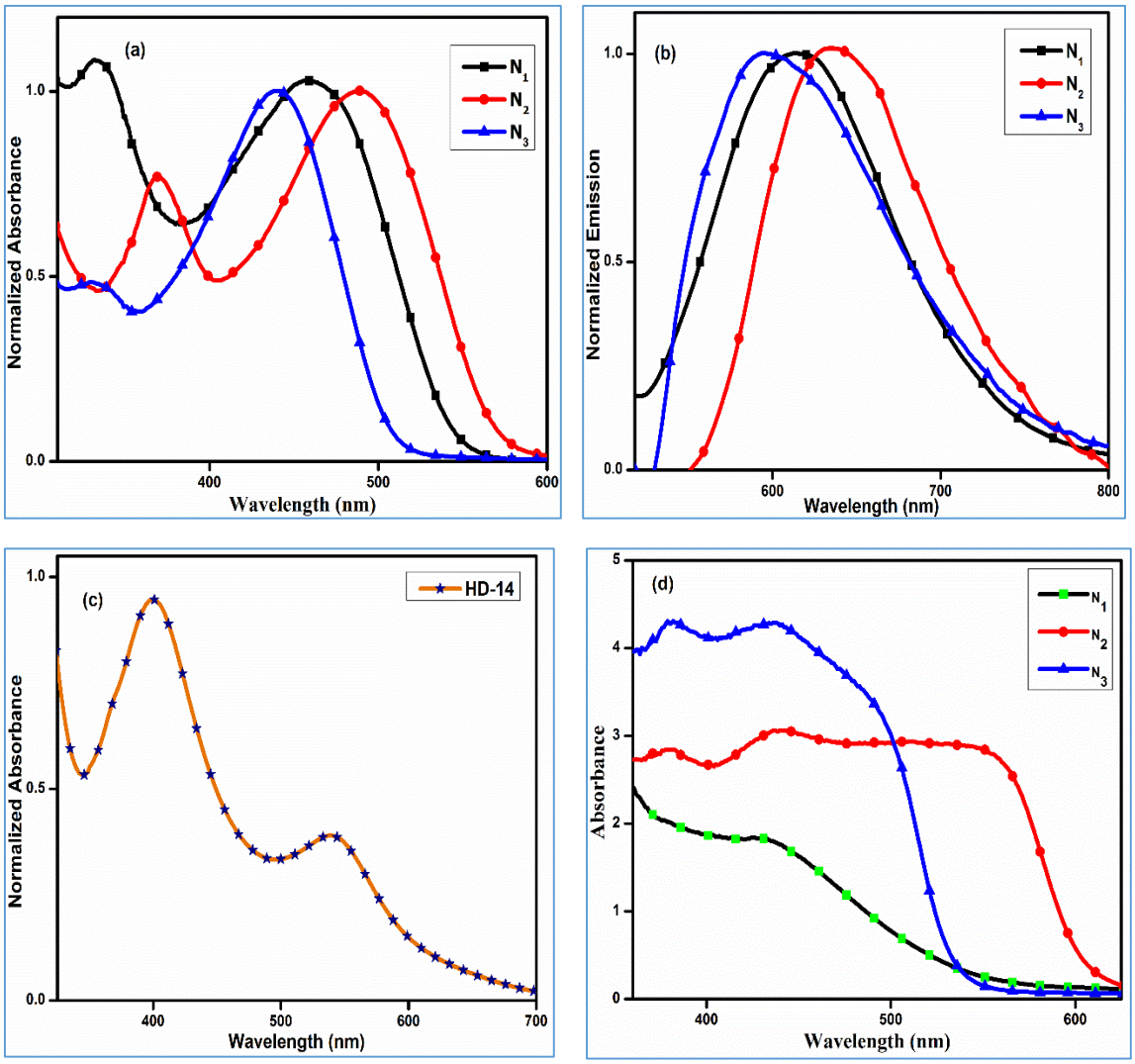

Fig.4.7 (a) UV-visible spectra of $\mathbf{N_{1\text{-}3}}$ in chloroform (10^{-5} M) **(b)** Fluorescence spectra of $\mathbf{N_{1\text{-}3}}$ in chloroform (10^{-5} M) **(c)** UV-visible spectrum of **HD-14** in chloroform (10^{-5} M) **(d)** Absorption spectra of $\mathbf{N_{1\text{-}3}}$ anchored on TiO_2.

The aforementioned red-shift is a stark contrast to the typically observed blue-shift for most of the organic dyes; it is caused by the deprotonation of the carboxylic acid unit of the sensitizer. The red-shift in the absorption can be attributed to the J-aggregation of the sensitizer molecules on the TiO_2 surface. The formation of J-aggregates can be attributed to the interaction between the carboxylate group of the sensitizer and Ti^{4+} ions of the semiconductor. This interaction results in the lowering of the π^* energy level of the

sensitizer molecule and thereby resulting in broadening of its absorption spectrum (Babu et al. 2015).

Further, an examination of the absorption spectra of the precursors (**Fig.4.8**) was done to investigate the magnitude of charge transfer in these sensitizers (**N_{1-3}**). The absorption spectrum of compound **4.2** showed λ_{max} at 317 nm, which can be attributed to weak charge-transfer from indole core to the nitro and aldehyde groups; by the incorporation of cyanovinylene and thiophene units (**4.3**) the π-conjugation was enhanced, causing a nearly 100 nm red shift due to more efficient delocalization of the electron density from indole to the π-conjugation bridge. Additionally, the enhancement of donor-acceptor interaction is further apparent on comparing the absorption spectrum of the aldehyde precursor **4.4** with that of the sensitizers.

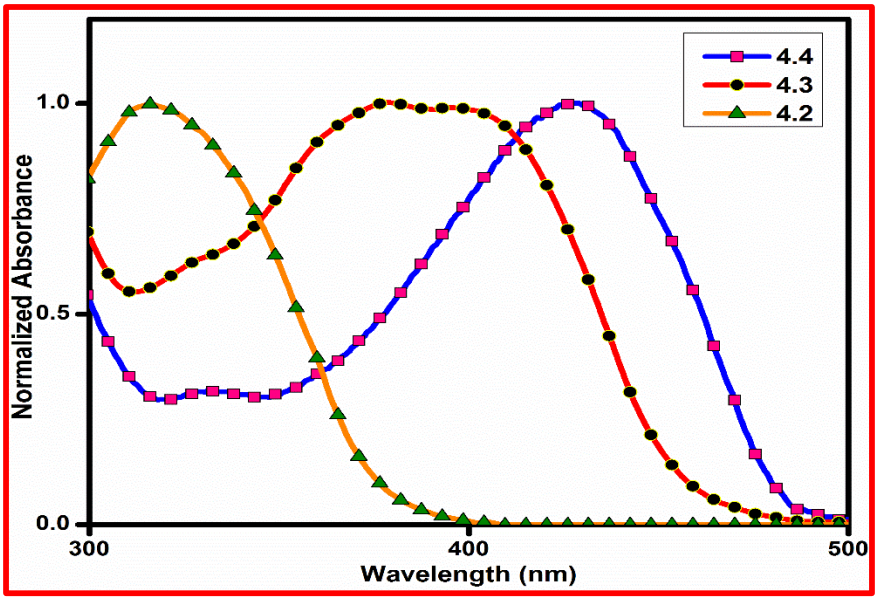

Fig.4.8 UV-visible spectra of compounds **4.2-4.4** in chloroform (10^{-5} M)

It is evident that, the variation in the values of λ_{max} exhibits the difference in electron-withdrawing nature of the respective acceptor units in **N_{1-3}**. Further, the charge-transfer nature of the absorption maxima at higher wavelength was established by observing the changes in absorption spectrum witnessed during the addition of the

trifluoroacetic acid (TFA) and triethylamine (TEA) to the solution of sensitizer in chloroform (Baheti et al. 2014).

Table 4.1 Absorption and emission properties of $\mathbf{N_{1\text{-}3}}$ and **HD-14**

Sensitizer	Absorption λ_{max} (nm)	Emission λ_{max} (nm)	Stokes Shift (cm^{-1})	ε ($M^{-1}cm^{-1}$)	$E_{0\text{-}0}$
N_1	460	614	5500	36500	2.37
N_2	497	635	4400	48000	2.22
N_3	451	595	5300	43300	2.37
HD-14	539	731	4900	19450	1.88

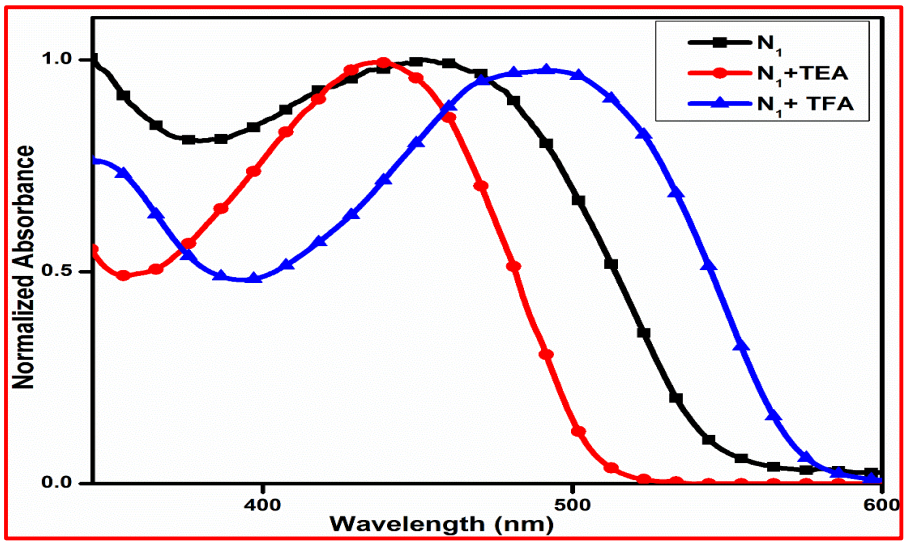

Fig.4.9 Absorption spectra of the dye $\mathbf{N_1}$ in $CHCl_3$ before and after addition of TFA and TEA

It is observed that, the addition of TFA or TEA to the dye solutions in chloroform resulted in bathochromic and hypsochromic shifts, respectively. From these observations the presence of a protonation-deprotonation equilibrium in the solution state of the dyes has been confirmed. **Fig.4.9** depicts the spectra of the aforementioned study conducted on sensitizer $\mathbf{N_1}$. From the spectral data it is evident that, in the chloroform solution the dye

predominantly exists in the protonated form, addition of TEA resulted in the hypsochromic shift of the absorption maxima. TEA deprotonates the carboxylic acid unit of the respective sensitizer and thereby, diminishes the acceptor strength and hence weakens the donor-acceptor interactions. In contrast, addition of TFA leads to bathochromic shift, which is attributed to the reversal of equilibrium and thus increasing the amount of protonated form in the solution. Further, all the sensitizers displayed large Stokes shift values, suggesting significant structural reorganization upon excitation.

4.3.3 Molecular modeling

All calculations were carried out using Turbomole software package. The optimized geometries and the corresponding electronic distribution in HOMO and LUMO levels are depicted in **Fig.4.10**. From the figure, it is evident that in the HOMO, the electron density is delocalized over the entire molecule, whereas in the LUMO, a clear shift of electron density towards the acceptor segment is evident. Such movement of electron density from HOMO to LUMO level is quite suitable and desirable for charge transfer and the effective interfacial injection of electrons from the excited state of the sensitizer into the conduction band edge of the semiconductor.

In addition, the hole localized on the indole core will be spatially favorable for the electron donors to approach, facilitating the dye regeneration process (Shi et al. 2008). The poor performance of $\mathbf{N_2}$, both as sensitizer and co-sensitizer can be attributed to the breakage of electronic conjugation in the LUMO level. The aforementioned breakage will in-turn impair the efficient electron injection into the conduction band of TiO_2, leading to a radical drop in the overall efficiency of the device. From DFT calculations, it was observed that the conjugation length for $\mathbf{N_1}$, $\mathbf{N_2}$ and $\mathbf{N_3}$ are 6.4, 5.4 and 10.8 Å, respectively (**Fig.4.11**). Noticeably, the co-adsorbent $\mathbf{N_3}$ has a relatively longer conjugated bridge than the other two ($\mathbf{N_1}$ and $\mathbf{N_2}$**)**. This ensures a better anchoring of $\mathbf{N_3}$ on TiO_2 surface by overcoming the barrier of alkyl chain created by **HD-14** sensitizer.

DYE	Optimized geometry	HOMO	LUMO
N_1	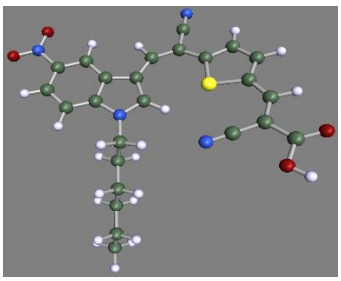	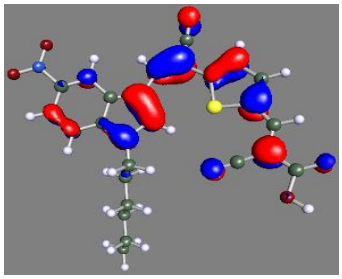	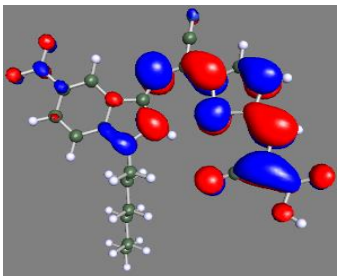
N_2	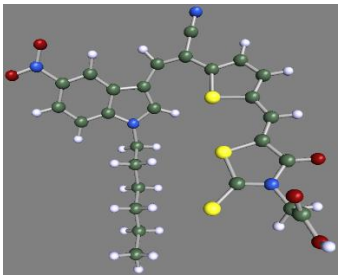	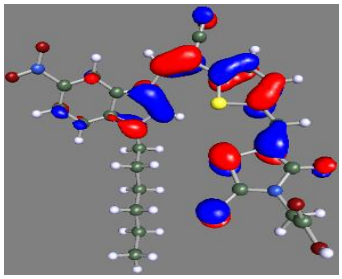	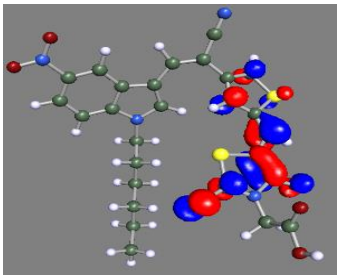
N_3	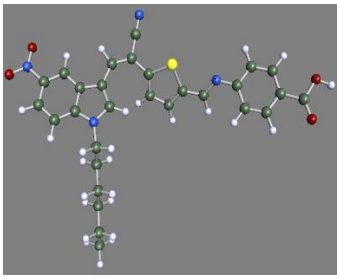	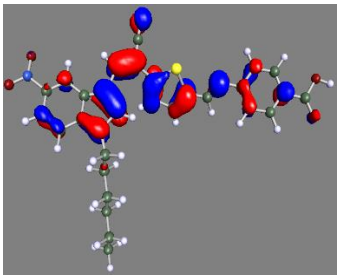	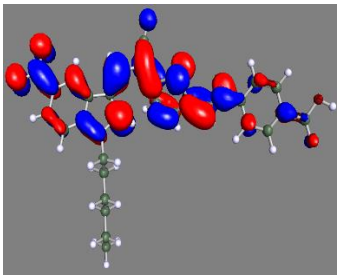

Fig.4.10 Optimized structure and Frontier molecular orbitals of **N_{1-3}**.

Further, the co-sensitization using **N_3** with an appropriate conjugation bridge can ensure the formation of a compact sensitization layer, and thereby preventing dye aggregation. Also, better packing and arrangement of the sensitizer molecules ensure the prevention of electronic recombination on the semiconductor surface and moderate dark

current. Whereas, $\mathbf{N_1}$ and $\mathbf{N_2}$ with their shorter length may have reduced prospects to pass through the barriers, and hence are less effective as co-sensitizers (Li et al. 2014).

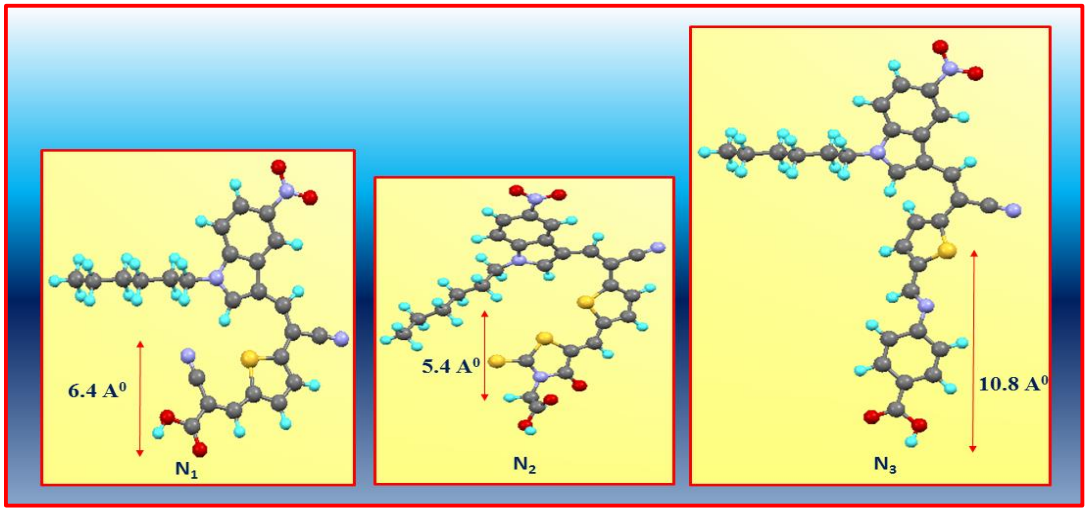

Fig. 4.11 Optimized molecular structures of $\mathbf{N_{1\text{-}3}}$ calculated from DFT

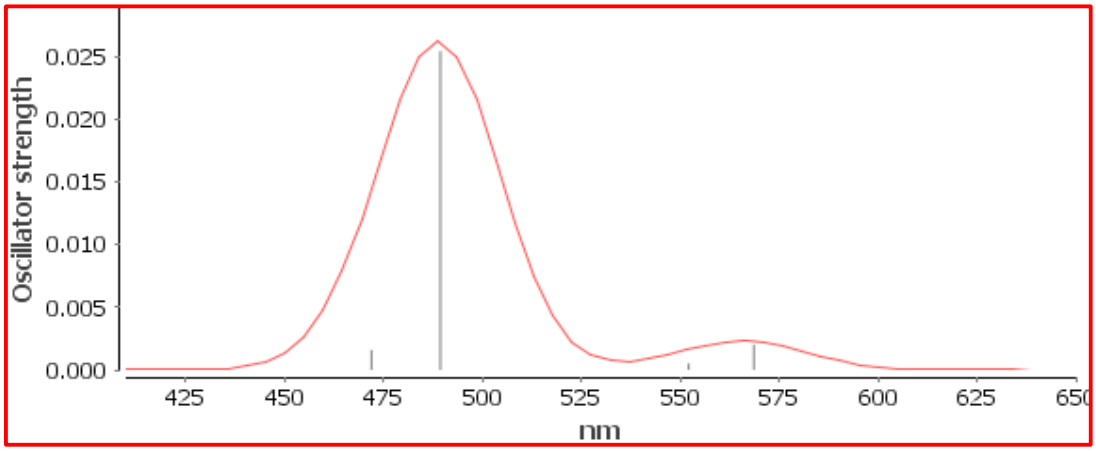

Fig.4.12 Simulated absorption spectrum of $\mathbf{N_1}$ using BP functional

Further, time-dependent density functional theory (TDDFT) studies were undertaken to simulate the electronic absorption spectra of the sensitizers using TurbomoleX. The calculated absorption spectrum of $\mathbf{N_1}$ obtained using def-TZVPP basis set at the BP86 functional is depicted in **Fig.4.12**. The calculated spectrum depicts two distinct bands. Although, the nature of simulated spectrum is well in agreement with the

experimentally obtained one, it still exhibits a slight underestimation of the excitation energy at λ_{max} and offers a red-shift compared to the experimental obtained values.

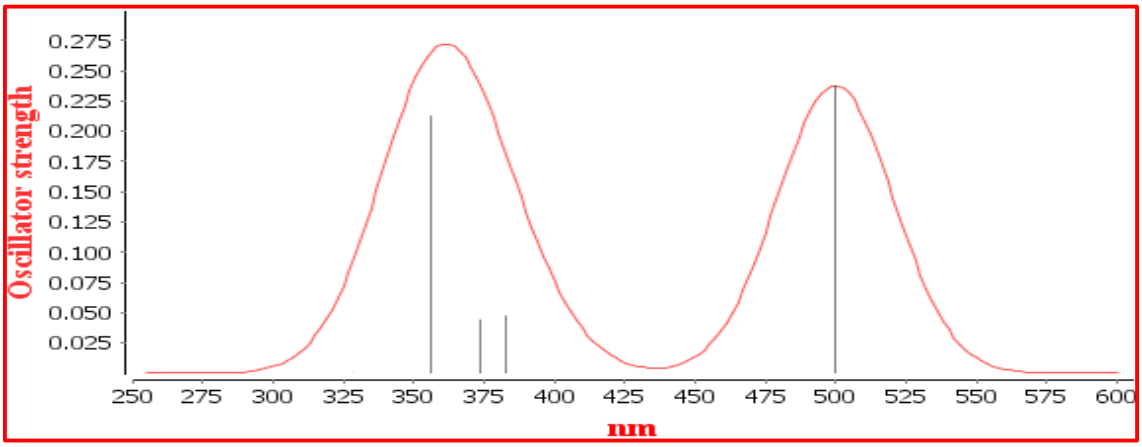

Fig.4.13 Simulated absorption spectrum of **N_1** using B3LYP functional

This anomaly can be attributed to the inadequacy of the conventional exchange–correlation functionals in suitably describing charge-transfer excitations. The above-mentioned problem can be alleviated by using hybrid functionals, such as B3LYP. The spectrum obtained using hybrid functional B3LYP (**Fig.4.13**) was found to be well in agreement with the experimental one. Although B3LYP does offer some improvement in defining the CT excitations, it is still not flawless with its 0.2 R^{-1} dependence instead of R^{-1} (Dev et al. 2013). The band at shorter wavelength can be assigned to π-π* transition, whereas the charge-transfer from the donor to the acceptor segment is responsible for peak at higher wavelength.

4.3.4 Electrochemical characterization

Cyclic voltammetry (CV) experiments were conducted to determine the ground and excited oxidation potentials of the newly synthesized co-absorbers/sensitizers (**N_{1-3}**) in order to estimate their GSOP and ESOP values. These values provide a deeper insight into the thermodynamic driving force of electron injection from the ESOP of dye molecule into the conduction band edge of TiO_2 and dye regeneration *via* replenishing the hole generated in the GSOP by the redox electrolyte. The obtained cyclic voltammogram of **N_2** is displayed

in **Fig.4.14 (a)** and the corresponding values are depicted in **Fig.4.14 (b)**. As evidenced from the **Fig.4.14 (b)**, all the three co-sensitizers have a more negative HOMO level (eV) than the Nernst potential of the I^-/I_3^- redox couple (-5.2 eV) (Qu and Meyer 2001), providing ample driving force for effective dye regeneration of the oxidized dyes by I^- species in the electrolyte. All the values in volts (V) against NHE were converted to electron volt (eV) by following equation.

$$\text{ESOP} = [(\text{GSOP (V)} + 4.7) - E_{0\text{-}0}]\ \text{eV}$$

Additionally, excited state oxidation potentials (ESOP) were obtained from the above-mentioned equation using ground state oxidation potential (GSOP) and $E_{0\text{-}0}$ (calculated from absorption and emission spectra of the compounds). It is quite evident that, the ESOP levels of the three dyes (-3.75 to -3.93 eV vs NHE) are much less negative than the conduction band edge of TiO_2 (-4.2 eV) (Oskam et al. 2001) providing sufficient driving force for efficient electron injection. The negative free energy for electron injection is in the order $\mathbf{N_3}$>$\mathbf{N_2}$>$\mathbf{N_1}$. From the aforementioned order, one could predict that, sensitizer $\mathbf{N_3}$ will be more efficient than the other two sensitizers ($\mathbf{N_1}$ and $\mathbf{N_2}$) in injecting electrons into the conduction band of TiO_2.

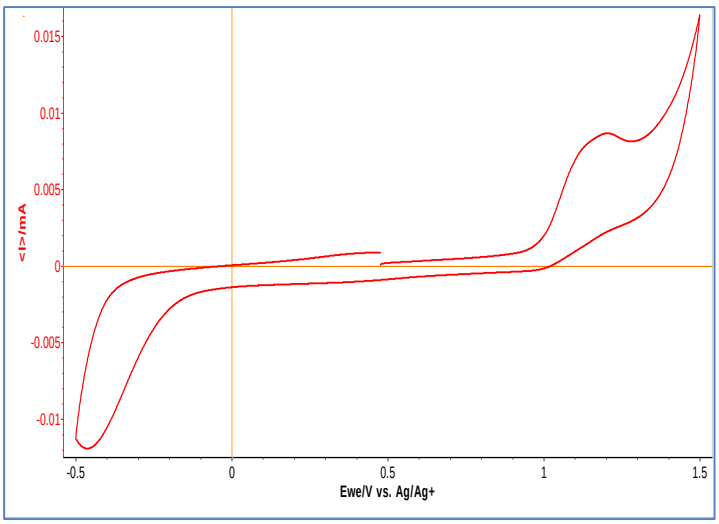

Fig.4.14 (a) Cyclic voltammogram of $\mathbf{N_2}$

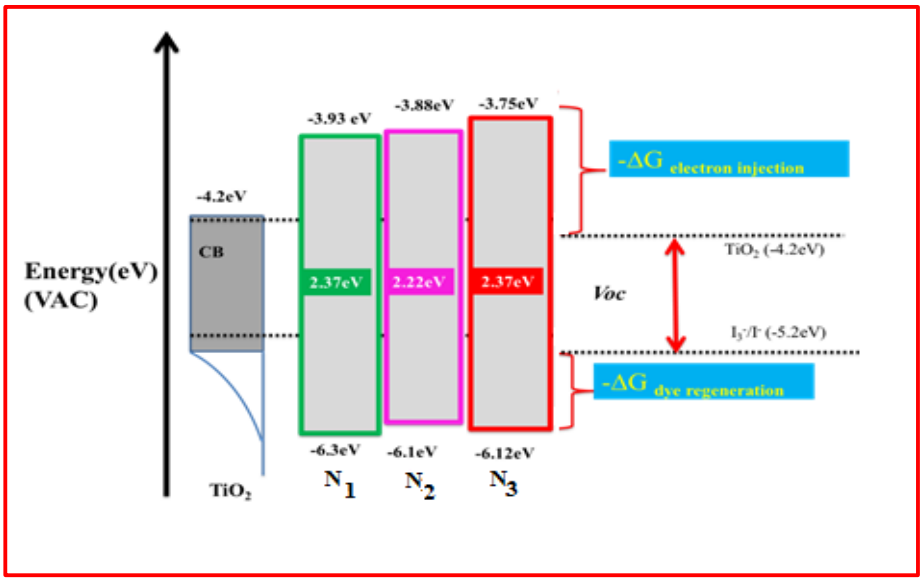

Fig.4.14 (b) Energy level diagram of $\mathbf{N_{1\text{-}3}}$ dyes

It is well know that, a prerequisite for efficient electron injection is a negative free energy value greater than 150 meV (Koops et al. 2009). Whereas, the minimum value of free energy required for effective dye regeneration is 250 meV (Hardin et al. 2012, Hussain et al. 2014). Clearly, all the sensitizers ($\mathbf{N_{1\text{-}3}}$) meet the prerequisite thermodynamic conditions and hence making them suitable to be employed as sensitizers in TiO_2-based DSSCs.

4.3.5 Photovoltaic device characterizations

The broadening of light absorption and photon harvesting range are indispensable approaches towards the enhancement of DSSC's performance. In this context, the three new organic dyes ($\mathbf{N_{1\text{-}3}}$) have been designed and synthesized to be deployed as co-sensitizers. These dyes were applied as co-sensitizers along with **HD-14** dye. The introduction of electron withdrawing substituent on the ethylene group in all dyes as π-spacers helps to improve the performance of the DSSCs. With only a difference of the electron acceptors, $\mathbf{N_{1\text{-}3}}$ dyes exhibit significantly different incident photon-to-current conversion performances and photovoltaic properties. The $\mathbf{N_3}$ with 4-aminobenzoic acid as

anchoring/acceptor group showed superior performance than cyanoacrylic acid terminated dye ($\mathbf{N_1}$) and the rhodanine dye ($\mathbf{N_2}$), which showed the lowest photovoltaic properties.

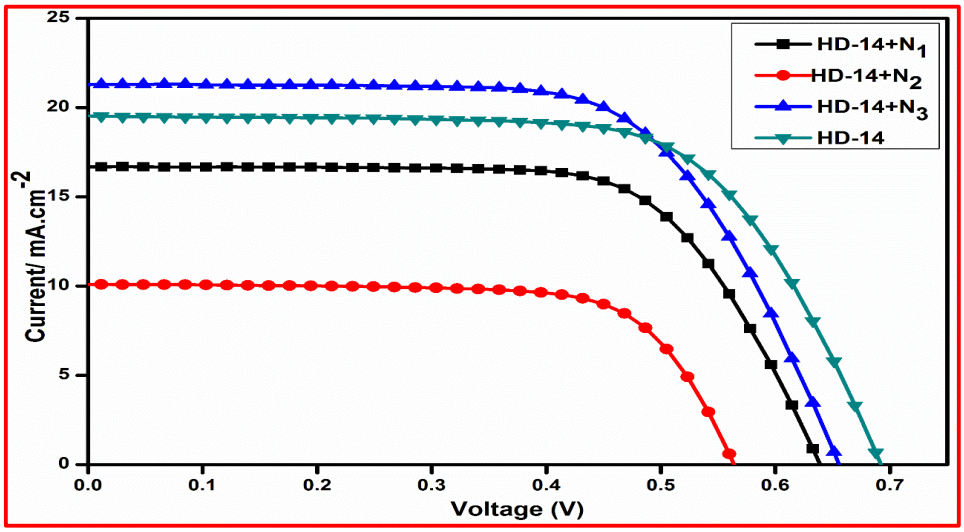

Fig.4.15 *J-V* characteristics of the DSSCs sensitized with different co-sensitizers.

Although, the sensitizer **HD-14** absorbs light in a wide range of wavelengths, the co-adsorbers are employed to see the potential of novel co-adsorbents for surface passivation and improvement in light harvesting efficiency in the range from 400 to 500 nm. The molar extinction coefficients of $\mathbf{N_{1\text{-}3}}$ are in the range from 3.65×10^4 to 4.8×10^4 $M^{-1}cm^{-1}$, which is much higher than that of I_3^- (2.5×10^4 $M^{-1}cm^{-1}$) at this wavelength. Hence, the use of the aforementioned co-adsorbers could help in reducing the competitive absorption of light by I_3^- and thereby resulting in an enhancement in IPCE efficiency. Further, organic co-adsorbers with their smaller size can cover the surface of the TiO_2 nanoparticles efficiently, where the large three-dimensional ruthenium based dye (**HD-14**) cannot get adsorbed, providing a better surface coverage. In addition, the presence of co-sensitizers also helps in suppressing the charge re-combinations caused by dye aggregation or close π-π stacking and thereby improving the device performance significantly. Current-voltage (*J-V*) characteristics of the cell based on **HD-14** and the corresponding co-sensitized solar cells using $\mathbf{N_{1\text{-}3}}$ are presented in **Fig.4.15**, while the corresponding photovoltaic parameters are given in **Table 4.2**. Interestingly, the co-sensitized solar cell

exhibited a wide range of PCE values (4.13-9.26%), depending upon the co-sensitizer used. The photovoltaic performances of the DSSCs co-sensitized using **N_1**, **N_2** and **N_3** are: J_{sc} =16.67, 10.09 and 21.29 mAcm^{-2}; V_{oc} = 0.65, 0.57 and 0.67 V; fill factor (*ff*) of 67.95, 71.11 and 65.09%; and the corresponding PCE (η) of 7.39, 4.13 and 9.26%, respectively.

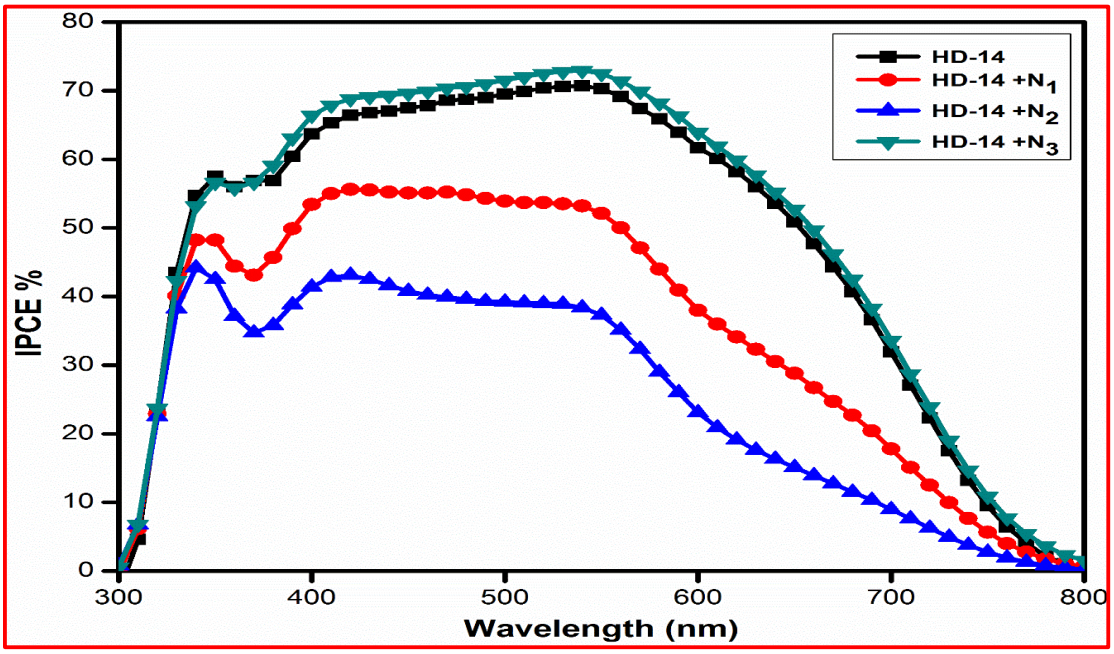

Fig.4.16 IPCE spectra of the DSSCs sensitized with different co-sensitizers.

In the quest to comprehend the reasons for this widespread difference in the photovoltaic performances, IPCE studies were performed (**Fig.4.16)**. The pivotal cause for the enhanced photovoltaic performance of the cell co-sensitized by **N_3** with respect to the cell sensitized using only **HD-14** is the improvement of J_{sc} (from 19.52 to 21.29 mAcm^{-2}).

The aforementioned enhancement in photocurrent can be attributed to the improved light harvesting efficiency of the co-sensitized solar cell. Whereas, in the case cells co-sensitized using **N_1** (η =7.39%) and **N_2** (η = 4.13%) a decrease in the overall photovoltaic efficiency was observed. Interestingly, both these cells displayed lowered J_{sc} as well as V_{oc} values as compared to the cell sensitized by **HD-14** alone. The lowering of J_{sc} can be attributed to the reduced light harvesting capability, as depicted in the IPCE graph. Further,

the drop in V_{oc} values suggests that the electron recombination rate has been increased as a result of co-sensitization, leading to the inferior performance of the cells co-sensitized by **N_1** and **N_2**. A closer examination of the absorption spectrum of the co-sensitizers on TiO_2 reveals the enhanced light harvesting capability of the sensitizer **N_3** as compared to the other two co-adsorbers, rendering it highly attractive for co-sensitization.

To further confirm the above-mentioned observations DSSCs are fabricated using only the co-sensitizer molecules (**N_{1-3}**). **Fig.4.17** shows the IPCE response of the co-sensitizers. The IPCE response of **N_1** was found to be 37% at 340 nm and 33% in the range from 410 to 430 nm. The onset wavelength of the IPCE spectrum of **N_1** is 620 nm. Although the photo responsive area of **N_2** was extended to about 620 nm, the IPCE values were extremely low, around 32% from 330 to 340 nm and 2% from 380 to 620 nm. This value for **N_3** is greater than that of **N_2**; **N_3** exhibited IPCE of 41% at 340 nm and decreased to around 23% from the region of 385 to 510 nm. The onset wavelength of the IPCE spectrum of **N_3** is close to 590 nm.

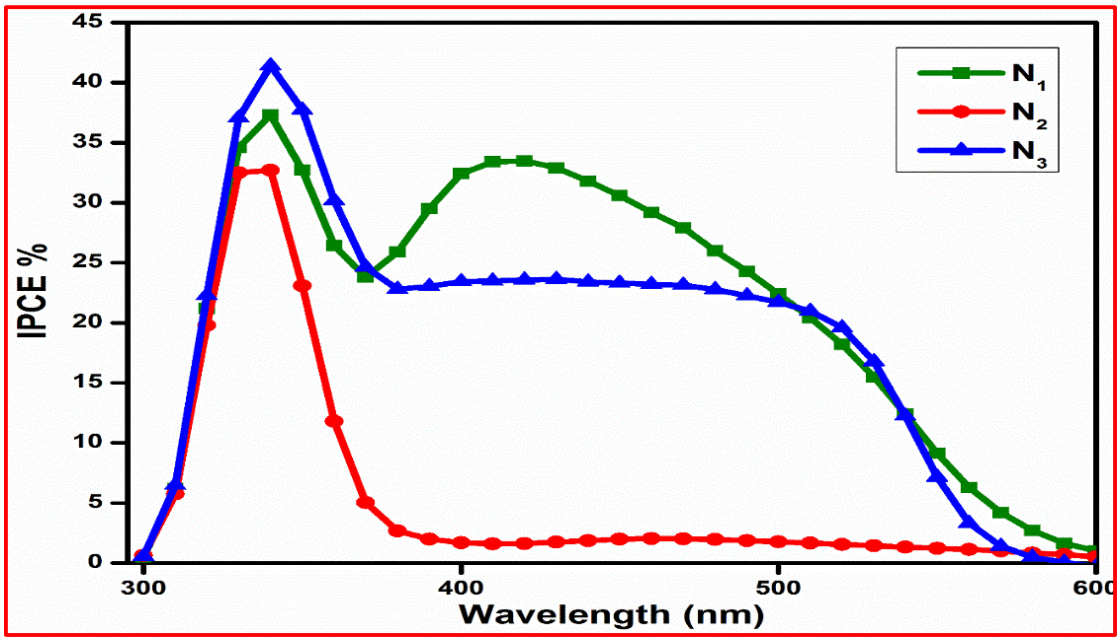

Fig.4.17 IPCE spectra of DSSCs sensitized with **N_{1-3}** dyes

Better IPCE response of **N_1** translated into higher J_{sc} of 3.66 $mAcm^{-2}$ compared to 3.30 $mAcm^{-2}$ of **N_3** and 0.42 $mAcm^{-2}$ of **N_2** in the presence of 10 mM CDCA. Although,

rhodanine-3-acetic acid as electron acceptor in the **N2** contributed to the bathochromic shift of the absorption spectra, it was found that, it exhibited extremely low efficiency (0.11%). These results may indicate that rhodanine-3-acetic acid is a poor anchoring group in comparison to cyanoacrylic acid (Tian et al. 2007, Liang et al. 2007). The J_{sc} of **N2** was measured to be 0.42 $mAcm^{-2}$. **Fig.4.18** depicts the *J-V* curves obtained by employing the co-sensitizers **N1-3**. The photovoltaic parameters and overall cell efficiencies are summarized in **Table 4. 2**. From all the aforementioned studies it is evident that, acceptor moieties play a profound role in influencing the photovoltaic properties of a dye molecule both as sensitizer and co-sensitizer.

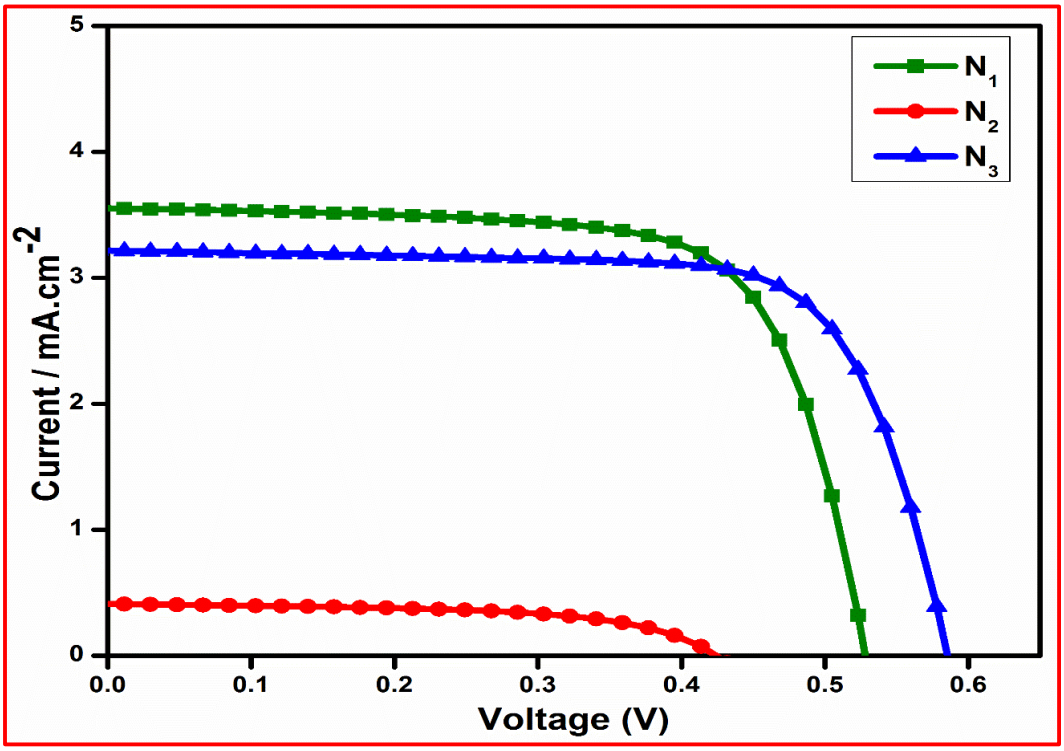

Fig.4.18 Photocurrent-voltage characteristics of DSSCs sensitized with **N1-3**

Table 4.2 Photovoltaic parameters of DSSCs based on **HD-14** with/without co-sensitization

Sensitizer	Adsorption solvent	J_{sc} ($mAcm^{-2}$)	V_{oc} (V)	*ff* (%)	η (%)
HD-14	ACN:*Tert*. Butanol (1:1)	19.52	0.70	66.76	9.20
HD-14 + N_1	ACN:*Tert*. Butanol (1:1)	16.67	0.65	67.95	7.39
HD-14 + N_2	ACN:*Tert*. Butanol (1:1)	10.09	0.57	71.11	4.13
HD-14 + N_3	ACN:*Tert*. Butanol (1:1)	21.29	0.67	65.09	**9.26**
N_1	ACN: Tert. Butanol (1:1)	3.66	0.54	70.81	1.39
N_2	ACN:*Tert*. Butanol (1:1)	0.42	0.43	58.48	0.11
N_3	ACN:*Tert*. Butanol (1:1)	3.30	0.59	73.15	1.44
N719	ACN:*Tert*. Butanol:DMSO (1:1:1)	15.90	0.73	66.00	7.64

4.3.6 Electrochemical impedance spectroscopy characterization

In DSSC studies, electrochemical impedance spectroscopy (EIS) can provide significant insights on the interfacial charge recombination dynamics and redox reaction process happening in the cells. **Fig.4.19** depicts the Nyquist plots of DSSC sensitized with only ruthenium based sensitizer **HD-14** as well as the devices co-sensitized using **N_{1-3}**. All the devices displayed two distinct semicircles, the peak in high frequency region is attributed to resistance at the counter electrode/electrolyte interface; whereas the middle frequency range (R_{ct}) is attributed to charge recombination resistance at TiO_2/dye/electrolyte interface. Further, the peak in the low frequency region can be attributed to Warburg diffusion process of I^-/I_3^- in the electrolyte (Wang et al. 2005). From the Nyquist plots it is evident that radius of semicircle in the middle-frequency range decreased in the order of **N_2>N_1>HD-14≈N_3**. The larger R_{ct} value for **N_2** in comparision to other devices suggests that the rate of charge recombination is the slowest for this device. But, as evidenced from the I-V curves, device co-sensitized using **N_2** showed the lowest power conversion efficiency.

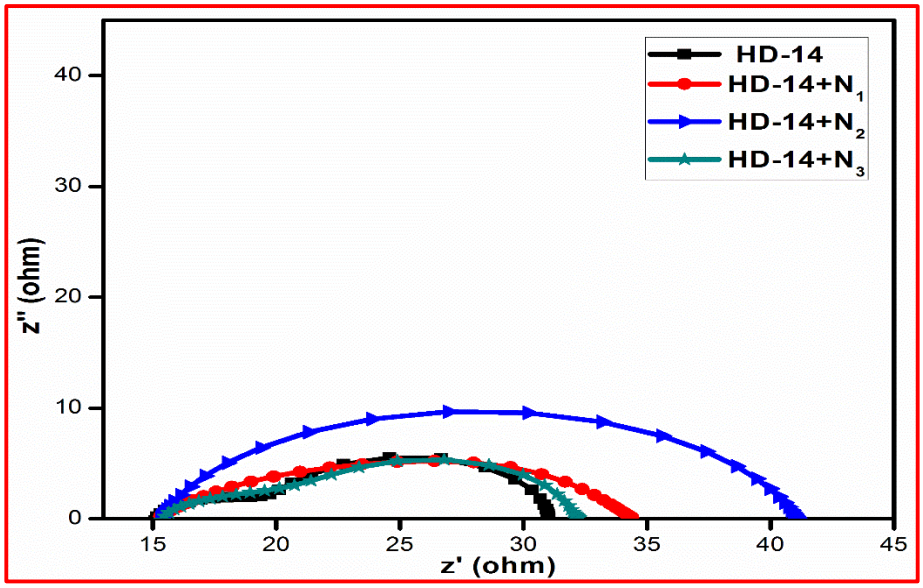

Fig.4.19 Nyquist plots for DSSCs based on **HD-14** and co-sensitized with **N_{1-3}**

The difference in the impedance response of **HD-14** and **N_3** versus **N_2** and **N_1** can be attributed to the difference in nature of impedance involved. The type of impedance

observed in the case of **N_1** and **N_2** based cells can be ascribed to Gerischer impedance, wherein $R_d >> R_{ct}$. The aforementioned condition is applicable for devices associated with substantial losses in charge generation as well as diffusion related losses (Bisquert et al. 2001) Additionally, it is interesting to note that, the device sensitized by only **HD-14** and the one co-sensitized using **N_3** display similar charaterstics. This observation suggests that, the rate of charge recombination is almost unchanged in the device sensitized using only **HD-14** as well as the one co-sensitized using **N_3**. Further, Bode phase plots (**Fig.4.20**) were utilized to calculate the electron lifetime by following the relation: $\tau_{CB} = 1/2\pi f$, where τ is the lifetime of electrons in TiO_2 and f is the intermediate frequency peak from Bode plot. The electron lifetimes for the DSSCs co-sensitized using **N_1**, **N_2** and **N_3** were found to be 1.2, 0.3 and 2.1 ms, respectively. These results suggest that, the charge recombination is suppressed in **N_3** when compared to the other two co-sensitizers **$N_{1\text{-}2}$**. The calculated electron lifetime values are well in agreement with the V_{oc} values of these devices (**Table 4.2**).

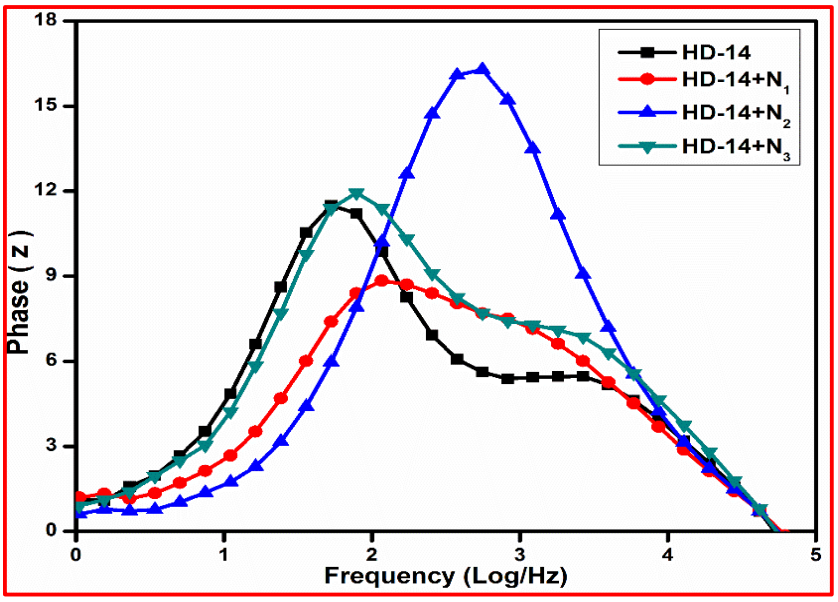

Fig.4.20 Bode plots for DSSCs based on **HD-14** and co-sensitized with **$N_{1\text{-}3}$**

Interestingly, the cell fabricated without co-adsorbents displayed higher V_{oc} (3-13 mV) as compared to the ones fabricated in the presence of the co-adsorbents **$N_{1\text{-}3}$**. It is well

known that the bonding between iodine and electron-rich segments of the sensitizer molecules could result in an enhancement of charge recombination at the TiO_2/electrolyte interface. It is evident that, all the co-absorbers in the present study possess a thiophene unit and the sulfur atom of this thiophene unit leads to the formation of dye-iodine complexes, resulting in a lower V_{oc} for the co-sensitized solar cells (Li et al. 2013). These results showcase the profound influence of acceptor groups on the electron recombination processes between the the electrolyte species and electrons injected into TiO_2 film.

4.3.7 FT-IR analysis: anchoring studies of the dyes on TiO_2

FT-IR spectroscopic studies were performed to examine the anchoring mechanism of the sensitizers on the TiO_2 electrodes. Deacon and Phillips formulated a set of rules to elucidate the binding modes of the sensitizers upon adsorption onto the TiO_2 nanoparticles (Deacon and Phillips 1980). Keeping the aforesaid rules in view, FT-IR spectra of all the dyes both in free form and adsorbed on the titanium dioxide film, were recorded.

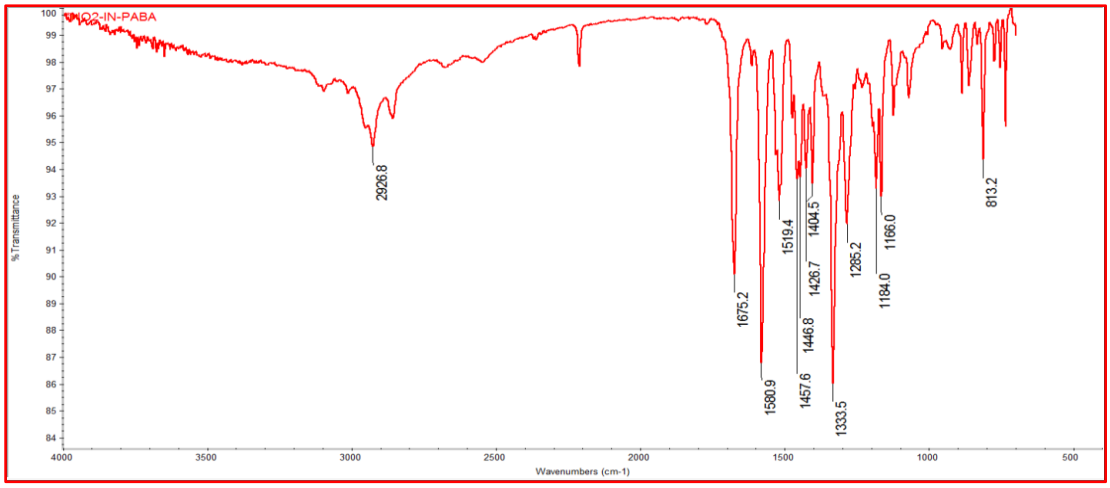

Fig.4.21 FT-IR spectrum of **N_3**

FT-IR spectrum of the free **N_3** dye (**Fig.4.21**) depicts noticeable bands at 2220 cm^{-1} and 1675 cm^{-1} corresponding to the –C≡N and >C=O stretching, respectively. Whereas, the spectrum of sensitizer **N_3** anchored onto the semiconductor **(Fig.4.22)** clearly depicts bands at 1586 and 1528 cm^{-1} corresponding to asymmetric and symmetric stretching modes of the carbonyl group. This observation clearly indicates the deprotonation as well as the

involvement of carboxylic acid group in the adsorption of the sensitizer onto the semiconductor.

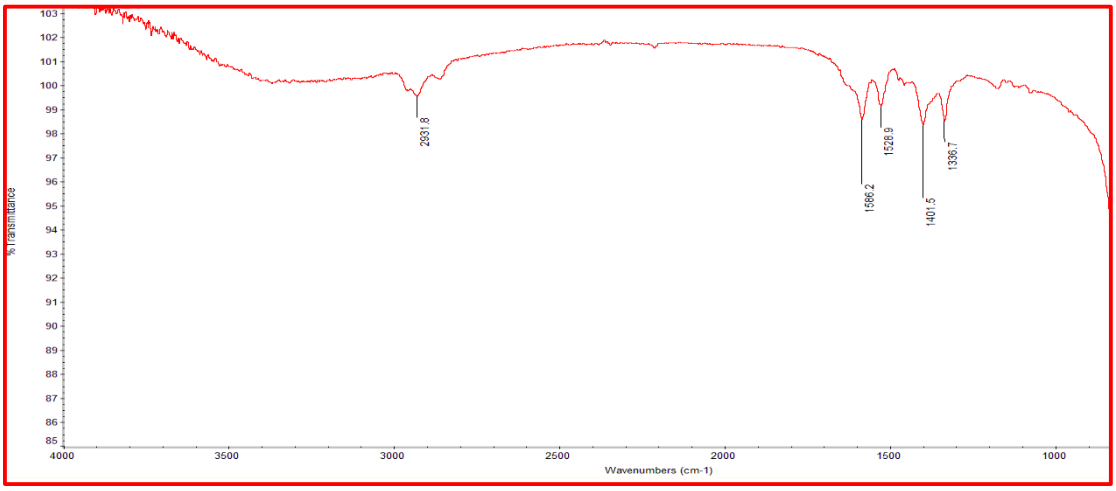

Fig.4.22 FT-IR spectrum of $\mathbf{N_3}$ on TiO_2

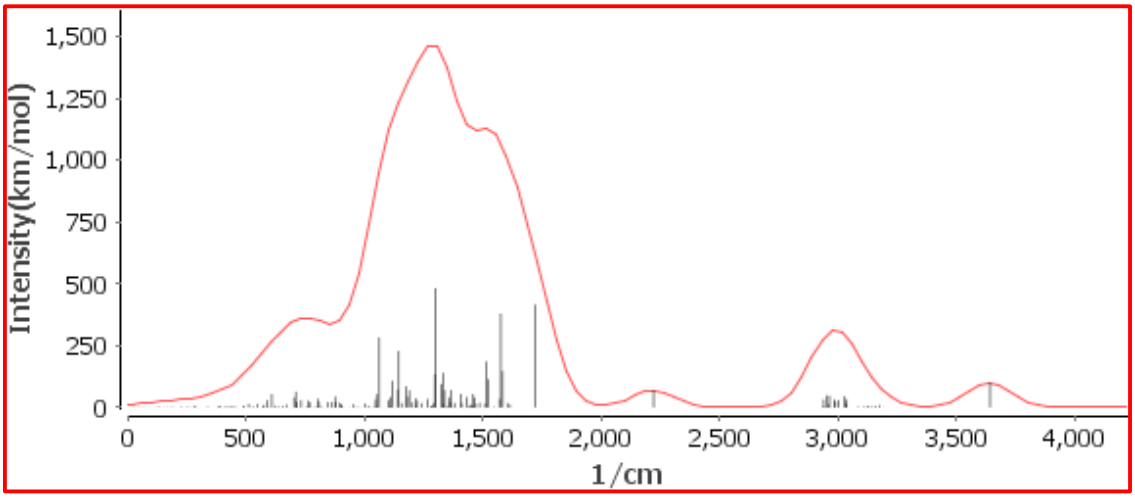

Fig.4.23 Theoretically obtained FT-IR spectrum of $\mathbf{N_3}$

Further, the disappearance of band corresponding to >C=O stretching and the appearance of two new peaks corresponding to the symmetric and asymmetric stretching vibrations confirm that, the dye is chemisorbed, and hence, physisorption can be ruled out. Furthermore, by applying the Deacon and Phillips rule, one can confirm that the dye is anchored onto the semiconductor surface by means of bidentate chelation or a bridging

rather than an ester type linkage. Another crucial inference which can be drawn from the FTIR analysis is that, the cyano group is not involved in dye-adsorption process, as the peak corresponding to it remains unchanged in both free and adsorbed states. Additionally, the FT-IR spectra of **N_1** and **N_2** depicted similar trends as well. Furthermore, the IR-absorption spectra of all the sensitizers have been simulated using Turbomole software. **Fig.4.23** portrays the simulated FT-IR spectrum of **N_3**. As expected, the experimentally obtained spectrum is well in agreement with the theoretically acquired one.

4.4 CONCLUSIONS

In conclusion, three novel organic dyes (**N_{1-3}**) have been engineered with varying acceptor/anchoring units as alternative co-adsorbents to CDCA, have been successfully synthesized. The cell co-sensitized with **N_3** and ruthenium based sensitizer **HD-14** exhibited the highest efficiency (9.26%) among all the cells sensitized either with individual dyes or co-sensitized using **HD-14** and **N_1** or **N_2**. This can be attributed to the enhanced light harvesting capability throughout the visible and near IR wavelengths. The reduced dye aggregation and superior coverage of the semiconductor surface by the small sized organic dye **N_3** also play crucial roles in influencing the overall efficiency. However, the cells co-sensitized using **N_1** or **N_2** along with **HD-14** exhibited a drastic reduction in the overall efficiency (7.39% for **N_1** and 4.13% for **N_2**), as compared to the cell sensitized using only **HD-14**. Further, it was observed that, the degree of molecular matching between the principle dye as well as the co-sensitizer is pivotal in surface blocking of the dye layer. The EIS analysis revealed that, in cells co-sensitized using **N_3** the kinetics of electron recombination and regeneration remained constant, whereas cells co-sensitized with **N_1** and **N_2** displayed enhanced rate of electron recombination. These results showcase the profound effect of acceptor units on the overall performance of the co-sensitizers. Therefore, it suggests that, strategic structural modifications of co-sensitizers should focus not only on the bulky-donor and robust π-conjugation units but also on the acceptor units. Thus, this structure-performance relationship study will bring forth a better molecular design strategy for the co-sensitizers and it will provide insight on selection of proper acceptors for further amelioration of DSSC performance.

CHAPTER 5

INDOLE BASED SENSITIZERS CARRYING TRIPHENYL AMINE MOIETY: SYNTHESIS, CHARACTERIZATION AND PERFORMANCE EVALUATION

Abstract

*In this chapter, synthetic methods and structural characterization, of two new organic co-sensitizers **DBA-1** and **DBA-2** have been incorporated. Further, it includes linear optical and electrochemical studies along with theoretical calculations. Furthermore, fabrication results of devices co-sensitized with the aforesaid dyes have been included. Finally, a detailed discussion on obtained results has been incorporated.*

5.1 INTRODUCTION

Two novel organic co-sensitizers **DBA-1** and **DBA-2** (**series 4**) with D-D-A (donor-donor-acceptor) architecture have been designed. The new design consists of a strong electron donating triphenylamine group with indole moiety attached to different acceptors/anchoring groups. They have been synthesized from simple indole derivatives following well-known synthetic protocols and structures have been confirmed by various spectral and elemental analyses. Further, they are subjected to photophysical, electrochemical, theoretical and device fabrication studies. The pertaining results have been discussed in detail. **Fig.5.1** depicts the chemical structures of both the co-sensitizers and ruthenium based sensitizer **HD-2**.

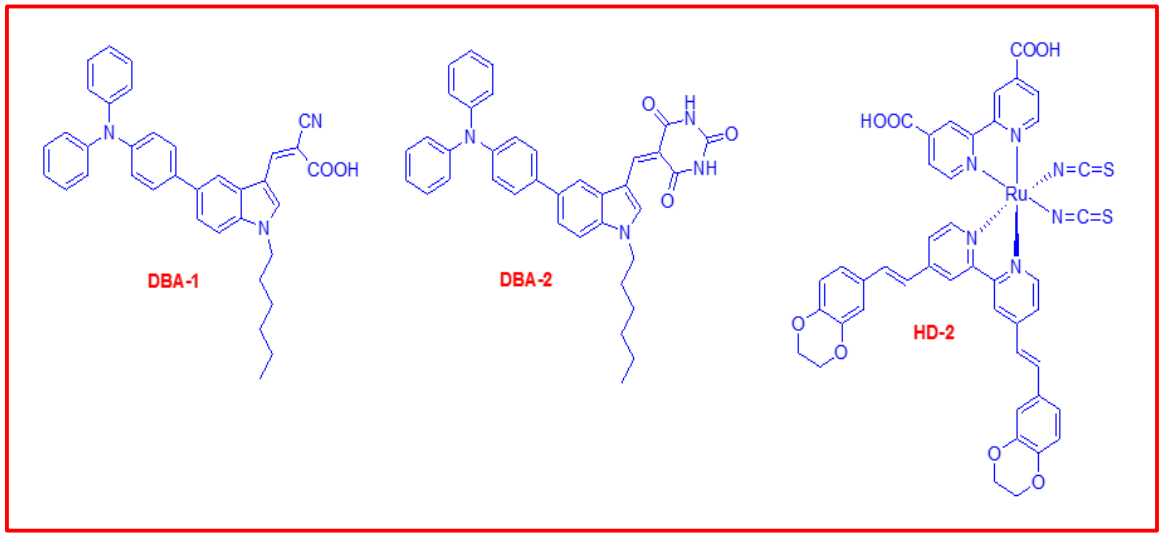

Fig.5.1 Chemical structures of **DBA-1**, **DBA-2** and ruthenium sensitizer **HD-2**

5.2 EXPERIMENTAL

5.2.1 Materials and methods

The starting materials 5-bromo-1*H*-indole, sodium hydride, 1-bromohexane, 4-(diphenylamino) phenylboronic acid, tetrakis(triphenylphosphine)palladium(0) [$Pd(PPh_3)_4$] and cyanoacetic acid, were obtained from Sigma-Aldrich. The solvents were dried following standard protocols prior to use. All the reactions were carried out under argon atmosphere and the reaction completion was monitored by TLC technique. Chromatographic separations were carried out using silica gel (100–200 and 230-400 mesh). ^{1}H NMR and ^{13}C NMR spectra were recorded using a Bruker avance 500 MHz and 400 MHz spectrometers, in DMSO-d_6 or $CDCl_3$ and tetramethylsilane as internal standard. Mass spectra were obtained from thermo scientific-EXACTIVE (ESI-MS), while the elemental analysis was acquired from a Flash EA1112CHNS analyzer (Thermo Electron Corporation).

5.2.2 Synthesis of co-sensitizers

The synthetic pathway of the two new sensitizers **DBA-1** and **DBA-2** is depicted in **Scheme 5.1**. N-alkylation of 5-bromo-1*H*-indole was done using 1-bromohexane to yield **5.1**. It was then subjected to Vilsmeier–Haack formylation to give compound **5.2**. The product was coupled with 4-(diphenylamino)phenylboronic acid *via* Suzuki coupling to yield compound **5.3**. Finally, Knoevenagel condensation of this aldehyde **5.3** with cyanoacetic acid in the presence of ammonium acetate produced the co-sensitizer **DBA-1**, whereas, **DBA-2** was obtained by condensation of compound **5.3** with barbituric acid in methanol.

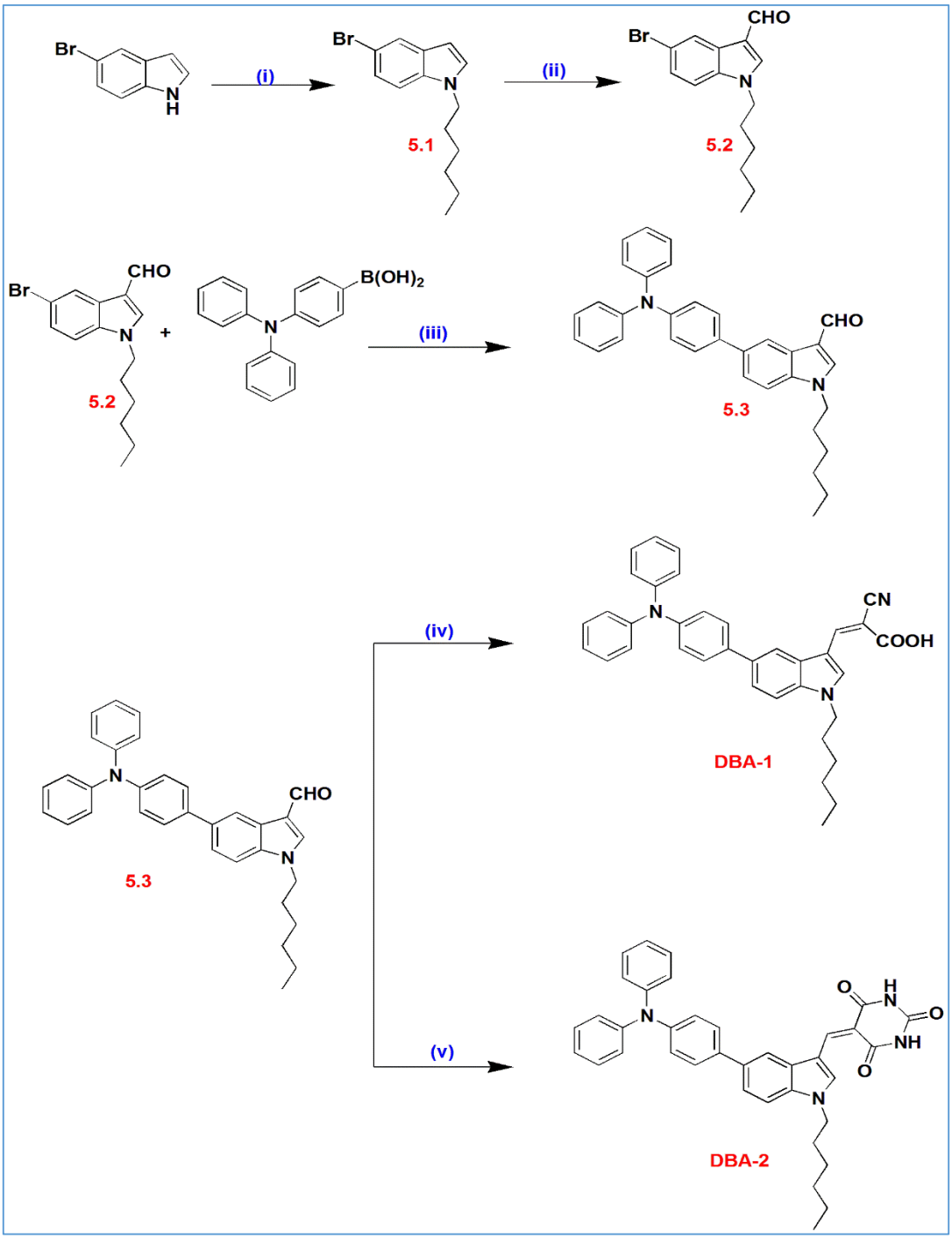

Scheme 5.1 Synthetic route of the co-sensitizers (i) 1-Bromohexane,NaH, DMF, RT (ii) $POCl_3$, DMF, RT (iii) Pd $(PPh_3)_4$, K_2CO_3, THF, ethanol, water (iv) Cyanoacetic acid, ammonium acetate, glacial CH_3COOH, 110 ^0C (v) Barbituric acid, CH_3OH, 80 ^0C

5.2.3 Optical, electrochemical and theoretical studies

The optical, electrochemical, EIS, photovoltaic and theoretical studies were carried out by following the procedures described in **section 3.2** of **chapter 3.**

5.2.4 DSSC fabrication

DSSC fabrications and characterizations were performed by following the procedures described in **section 3.2** of **chapter 3**.The dye solution used was a mixture of **HD-2** and the respective co-sensitizer (**DBA-1** and **DBA-2**) in 0.2 mM or 0.3 mM concentration, with addition of CDCA at a concentration of 20 mM.

5.2.5 Synthetic methods

Synthesis of *5-bromo-1-hexyl-1H-indole (5.1)*

A solution of 5-bromo-1*H*-indole (1 g, 5.1 mmol), NaH (0.244 g, 0.01 mmol) in DMF (10 mL) was stirred at room temperature for 0.5 h under argon. Then 1-bromohexane (0.925 g, 5.6 mmol) was added into the mixture and stirred at room temperature for 12 h. After the completion of reaction, water was added and neutralization was done using 2N HCl. The product was extracted with DCM. Further, organic phase was dried over sodium sulfate and the solvent was removed under reduced pressure. The residue was purified by column chromatography on silica gel using hexane as an eluent to give **5.1** as a colorless liquid. Yield: 83%. ^{1}H NMR (500MHz, $CDCl_3$, ppm): δ 8.46 (d, *J* = 1.5 Hz, 1H), 7.69 (s, 1H), 7.42-7.40 (m, 1H), 7.24 (t, *J* = 9 Hz, 1H), 4.14 (t, *J* = 7 Hz, 2H), 1.90-1.84 (m, 2H), 1.31-1.29 (m, 6H), 0.87 (t, *J* = 7 Hz, 3H). Calcd. for $C_{14}H_{18}$BrN: C, 60.01; H,6.47; N, 5.00 found: C, 60.21; H, 6.41; N, 5.05. ESI-MS (+ve mode) *m/z* Calcd for $C_{14}H_{18}$BrN: 279.06. Found: 280.06 $[M+H]^+$.

Synthesis of *5-bromo-1-hexyl-1H-indole-3-carbaldehyde (5.2)*

A two neck round bottom flask was charged with freshly distilled DMF (1.56 mL, 5 eq) and $POCl_3$ (1.96 mL, 5 eq) was added to it drop-wise, with constant stirring at 0 ^{o}C under argon to obtain a glassy white solid and to this 5-bromo-1-hexyl-1*H*-indole (**5.1**, 1.2

g, 4.28 mmol) dissolved in dichloroethane (10 mL) was added while stirring. The stirring was continued at ambient temperature for 15 h. After completion of reaction, the reaction mass was poured into crushed ice and subsequently basified using 5M NaOH solution. The precipitated solid was filtered and the crude product was purified by column chromatography on silica gel using ethyl acetate/hexane (1:10) as mobile phase to give **5.2**. Light brown solid. Yield 77%. ^{1}H NMR (500MHz, $CDCl_3$, ppm): δ 9.95 (s, 1H), 8.46 (d, *J* = 1.5 Hz, 1H), 7.69 (s, 1H), 7.42-7.40 (m, 1H), 7.24 (t, *J* = 8.5 Hz, 1H), 4.14 (t, *J* = 7 Hz, 2H), 1.90-1.84 (m, 2H), 1.31-1.29 (m, 6H), 0.87 (t, *J* = 7 Hz, 3H). ^{13}C (125 MHz, $CDCl_3$, ppm): δ 184.19, 138.59, 135.87, 126.92, 124.80, 117.42, 116.51, 111.49, 47.50, 31.25, 29.69, 26.47, 22.44, 13.94. Anal. Calcd. for $C_{15}H_{18}$BrNO: C, 58.45; H,5.89; N, 4.54 found: C, 58.23; H, 5.81; N, 4.55. ESI-MS (+ve mode) *m/z* Calcd for $C_{15}H_{18}$ BrNO: 307.06. Found: 308.06 $[M+H]^+$.

Synthesis of *5-(4-(diphenylamino)phenyl)-1-hexyl-1H-indole-3-carbaldehyde (5.3)*

A 15 mL THF solution of compound **5.2** (0.5 g, 1.6 mmol), 4-(diphenylamino) phenylboronic acid (0.562 g, 1.94 mmol), Pd $(PPh_3)_4$ (0.187 g, 0.16 mmol), and 2M K_2CO_3 (5 mL) was refluxed under argon atmosphere for 24 h. After cooling to room temperature, water was added to quench the reaction. The product was extracted with dichloromethane (25 mL × 3). The organic layer was dried over anhydrous Na_2SO_4, and the solvent was removed under vacuum. The crude product was purified by column chromatography on silica with hexane/ethyl acetate mixture (20: 1). Product **5.3** was obtained as a white solid. Yield 73%.^{1}H NMR (500 MHz, $CDCl_3$, ppm): δ 10.02 (s, 1H), 8.50 (d, *J* = 1.5 Hz, 1H), 7.73 (s, 1H), 7.57-7.55 (m, 3H), 7.41 (d, *J* = 8.5 Hz, 1H), 7.28-7.25 (m, 4H), 7.16-7.13 (m, 6H), 7.01 (*t*, *J* = 1.0 Hz, 2H), 4.18 (*t*, *J* = 7.0 Hz, 2H), 1.92 (*t*, *J* = 7.0 Hz, 2H), 1.37-1.30 (m, 6H), 0.88 (*t*, *J* = 4.5 Hz, 3H). ^{13}C (125 MHz, $CDCl_3$, ppm): 184.40, 147.78, 146.80, 145.39, 138.71, 136.47, 136.08, 135.87, 129.24, 128.20, 126.06, 124.27, 124.17, 123.28, 122.76, 120.12, 118.22, 110.29, 47.46, 31.30, 29.78, 26.54, 22.48, 13.96. Anal. Calcd. for $C_{33}H_{32}N_2O$: C, 83.86; H,6.82; N, 5.93 found: C, 83.75; H,6.85; N, 5.87. ESI-MS (+ve mode) *m/z* Calcd for $C_{33}H_{32}N_2O$: 472.25 Found: 473.25 $[M+H]^+$.

Synthesis of *(Z)-2-cyano-3-(5-(4-(cyclohexa-1,5-dien-3-ynyl(phenyl)amino)phenyl)-1-hexyl-1H-indol-3-yl)acrylic acid (DBA-1)*

A mixture of *5*-(4-(diphenylamino)phenyl)-1-hexyl-1*H*-indole-3-carbaldehyde (**5.3**, 500 mg, 1.05 mmol) with cyanoacetic acid (269 mg, 3.17 mmol) in glacial acetic acid (15 mL) was refluxed in the presence of ammonium acetate (400 mg) for 15 h under argon atmosphere. After completion of the reaction, the mass was cooled to ambient temperature and was poured into ice cold water. The precipitate was filtered. The crude product was purified by column chromatography using silica gel and $CHCl_3$:CH_3OH (10: 3) as mobile phase to obtain yellow color solid. Yield: 71%. ^{1}H NMR (500 MHz, $CDCl_3$, ppm): δ 8.67 (s, 1H), 8.59 (s, 1H), 7.98 (s, *J* = 1.0 Hz, 1H), 7.58 (*d*, *J* = 1.5 Hz, 1H), 7.56-7.52 (m, 2H), 7.45 (d, *J* = 8.5 Hz, 1H), 7.28-7.25 (m, 4H), 7.18-7.14 (m, 6H), 7.03 (*t*, *J* = 7.5 Hz, 2H), 4.23 (*t*, *J* = 7.5 Hz, 2H), 1.93 (*t*, *J* = 7.5 Hz, 2H), 1.34-1.32 (m, 6H), 0.89 (*t*, *J* = 7.0 Hz, 3H). ^{13}C (125 MHz, $CDCl_3$, ppm): 207.07, 147.69, 147.10, 136.10, 135.49, 135.38, 134.69, 129.29, 129.08, 128.11, 124.38, 124.08, 123.37, 122.93, 116.57, 110.99, 110.37, 100.00, 47.99, 31.27, 30.94, 29.87, 29.70, 26.51, 22.47, 13.96. Anal. Calcd. for $C_{36}H_{33}N_3O_2$: C, 80.12; H,6.16; N, 7.79 found: C, 80.25; H,6.21; N, 7.73. ESI-MS (+ve mode) *m/z* Calcd for $C_{36}H_{33}N_3O_2$: 539.26. Found: 540.26 $[M+H]^+$.

Synthesis of *5-((5-(4-(diphenylamino)phenyl)-1-hexyl-1H-indol-3-yl)methylene)-pyrimidine-2,4,6(1H,3H,5H)-trione* (*DBA-2*)

A mixture of 5-(4-(diphenylamino)phenyl)-1-hexyl-1*H*-indole-3-carbaldehyde (**5.3**, 500 mg, 1.05 mmol) and barbituric acid (135 mg, 1.05 mmol) was refluxed in absolute methanol for 5 h. The precipitate was filtered and recrystallized from methanol to obtain bright orange color solid. Yield 85%. ^{1}H NMR (400 MHz DMSO-d_6, ppm): δ 11.14 (s, 1H), 11.06 (s, 1H), 9.55 (s, 1H), 8.74 (s, 1H), 8.06 (s, 1H), 7.78-7.65 (m, 4H), 7.33 (s, 4H), 7.08 (s, 8H), 4.42 (s, 2H), 1.85 (s, 2H), 1.29 (s, 6H), 0.83 (s, 3H). ^{13}C (100 MHz, DMSO-d_6) δ (ppm): 164.99, 163.70, 150.87, 147.59, 146.90, 143.44, 142.78, 136.25, 135.60, 135.36, 130.84, 130.06, 128.58, 124.47, 124.11, 123.59, 112.77, 111.32, 109.04, 47.57, 31.15, 29.70, 26.19, 22.42, 14.32. Anal. Calcd. for $C_{37}H_{34}N_4O_3$: C, 76.27; H, 5.88; N,

9.62 found: C, 76.31; H, 5.85; N, 9.67. ESI-MS (+ve mode) *m/z* Calcd for $C_{37}H_{34}N_4O_3$: 582.27. Found: 583.27 $[M+H]^+$.

5.3 RESULTS AND DISCUSSION

5.3.1 Structural characterization

The chemical structures of newly synthesized compounds were confirmed by ^1H NMR, ^{13}C NMR spectroscopy and elemental analysis. The compound **DBA-2**, in ^1H NMR spectrum showed unique resonances at δ 11.14, 11.06 ppm for the protons of aromatic amines in the barbituric acid segment. Appearance of a singlet at δ 9.55 ppm has confirmed the presence of aromatic proton at the second position of indole ring. All the other aromatic protons depicted peaks between 8.74 and 7.08 ppm. Also, two protons of $–NCH_2$ of hexyl chain resonated as a singlet at δ 4.4 ppm, whereas the appearance of signal of primary and secondary protons in the range of δ 1.85-0.83 ppm confirmed the presence of one hexyl chain. The ^{13}C NMR spectrum of **DBA-2** showed the characteristic signals at higher frequency (downfield region). The three keto carbon atoms resonate at δ 164.99, 163.70 and 150.87 ppm. The remaining signals appearing in the region of δ 147.59-109.04 ppm are due to other aromatic carbons. The first carbon in the hexyl chain attached directly to the aromatic nitrogen in the indole ring displayed a peak at 47.57 ppm. Further, the remaining aliphatic carbons appeared between 31.15-14.32 ppm. Furthermore, its mass spectrum showed a $[M+H]^+$ peak at 583.27, which is in agreement with the calculated molecular weight for the formula of $C_{37}H_{34}N_4O_3$. **Fig.5.2** shows the ^1H NMR of compound **5.3. Fig.5.3-5.8** display, ^1H NMR, ^{13}C NMR and Mass spectra of compounds **DBA-1** and **DBA-2**.

Spectrograms of selected target compounds

^1H NMR, ^{13}C NMR and Mass spectra of representative compounds are given below.

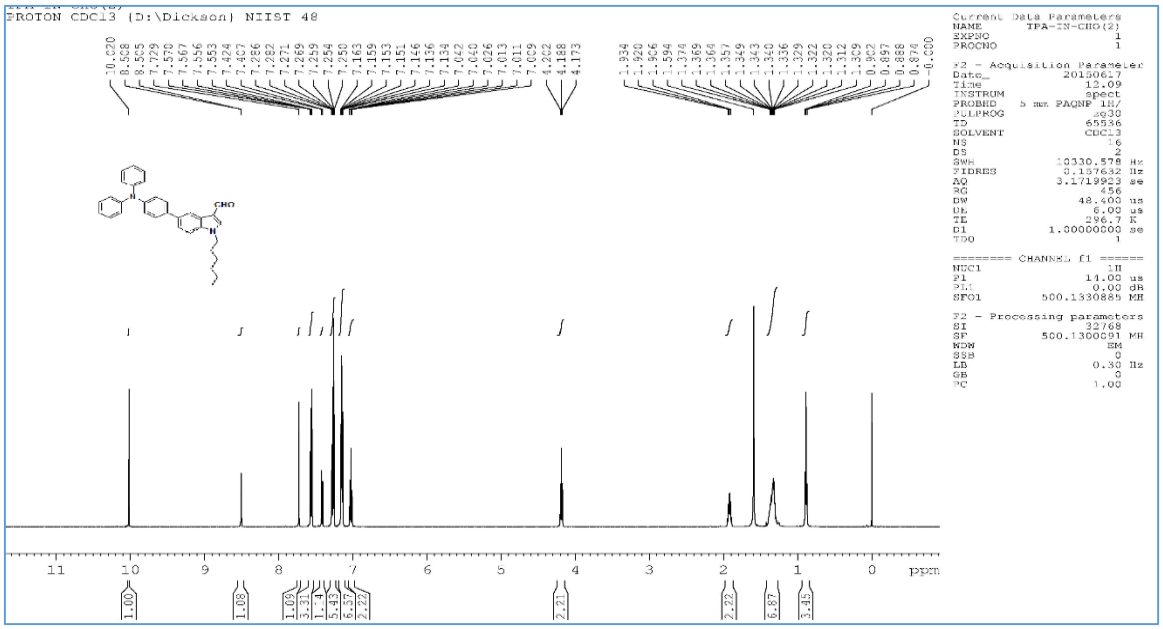

Fig.5.2 ^{1}H NMR spectrum of **5.3** in $CDCl_3$

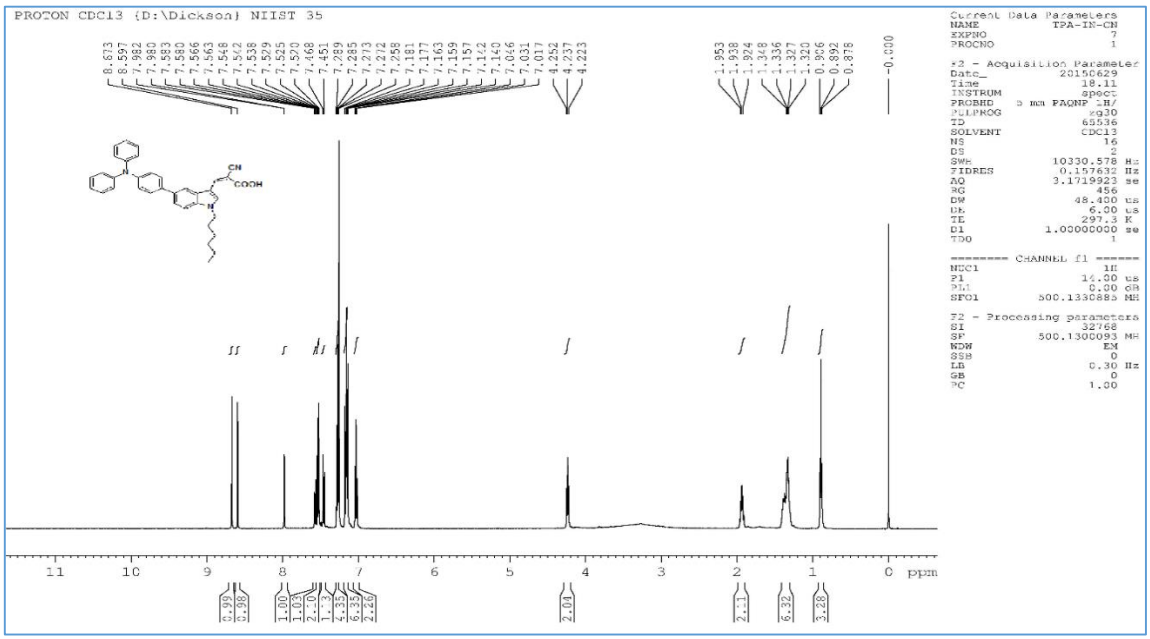

Fig.5.3 ^{1}H NMR spectrum of **DBA-1** in $CDCl_3$

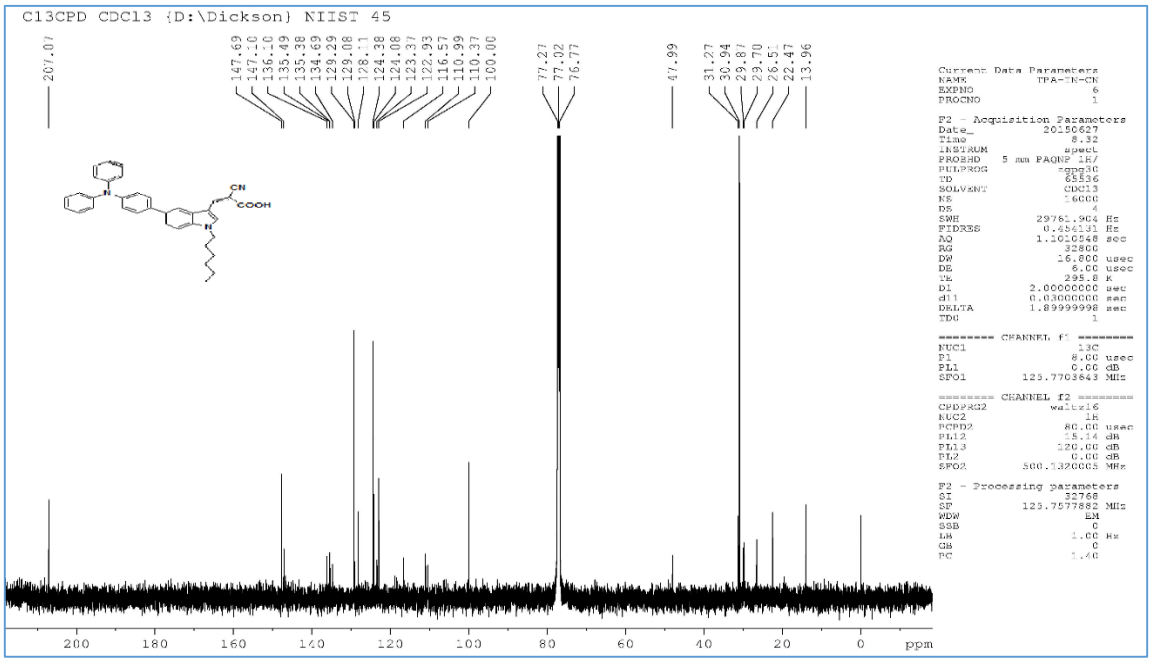

Fig.5.4 ^{13}C NMR spectrum of **DBA-1** in $CDCl_3$

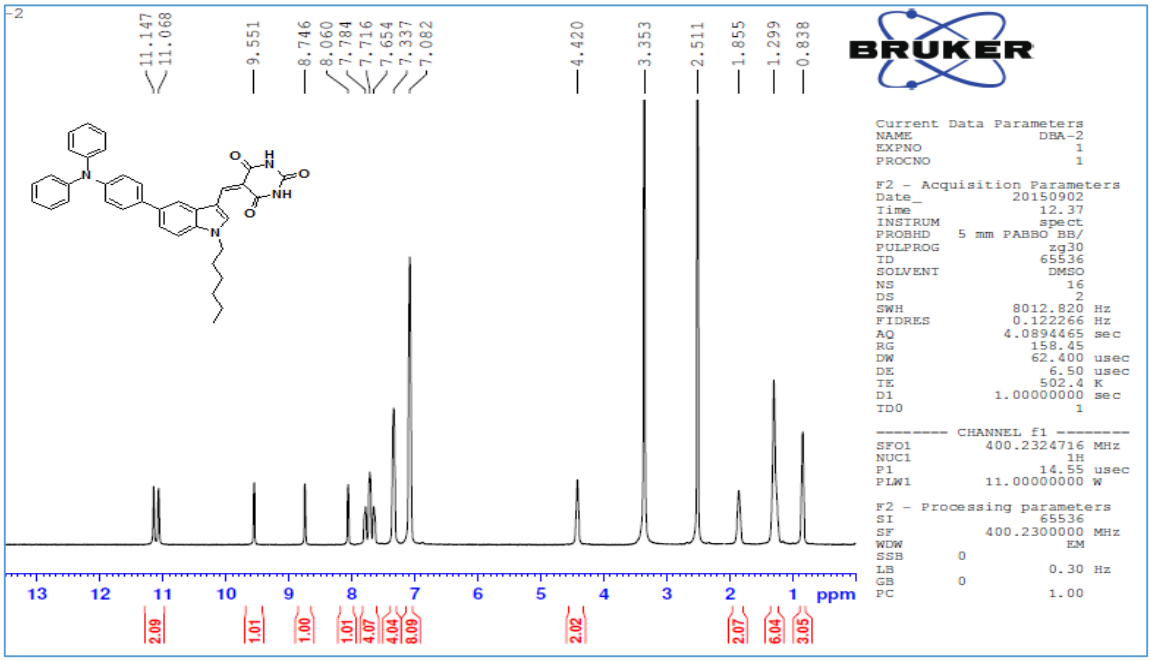

Fig.5.5 ^{1}H NMR spectrum of **DBA-2** in DMSO-d_6

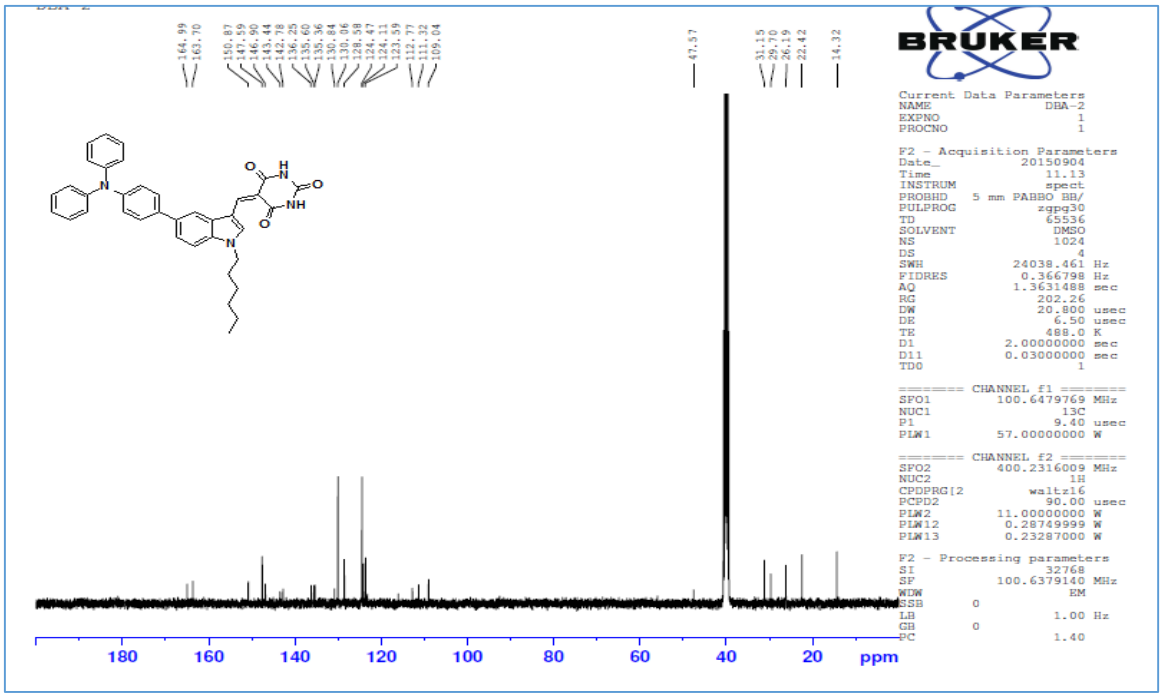

Fig.5.6 ^{13}C NMR spectrum of **DBA-2** in DMSO-d_6

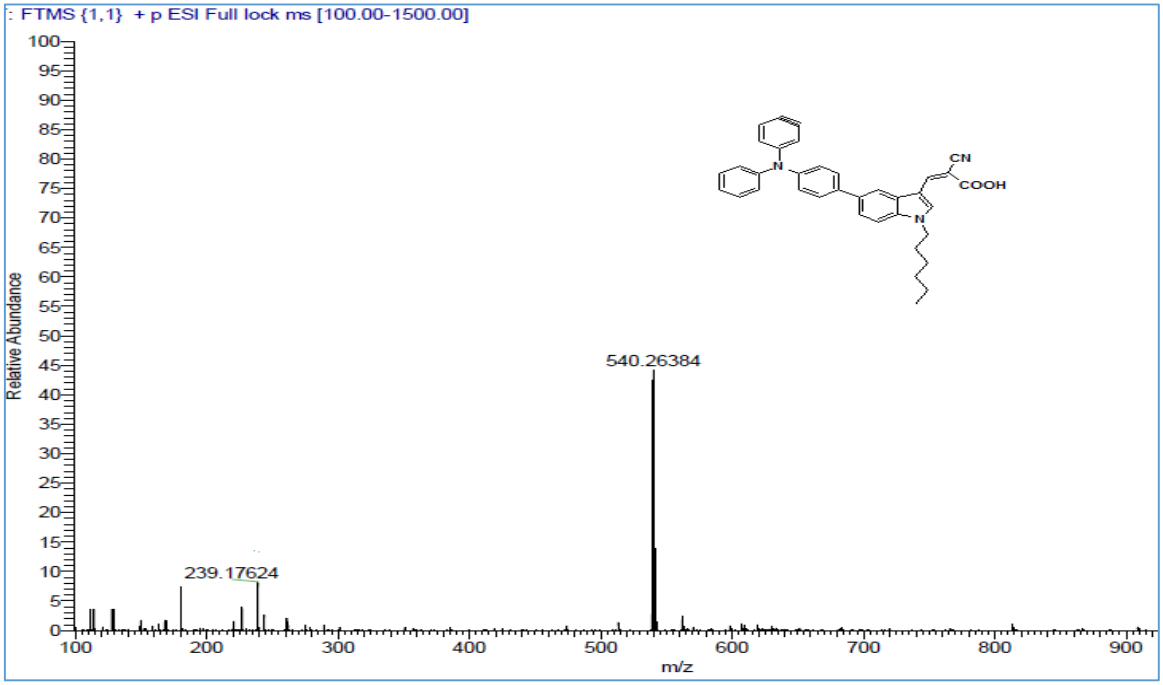

Fig.5.7 Mass spectrum of **DBA-1**

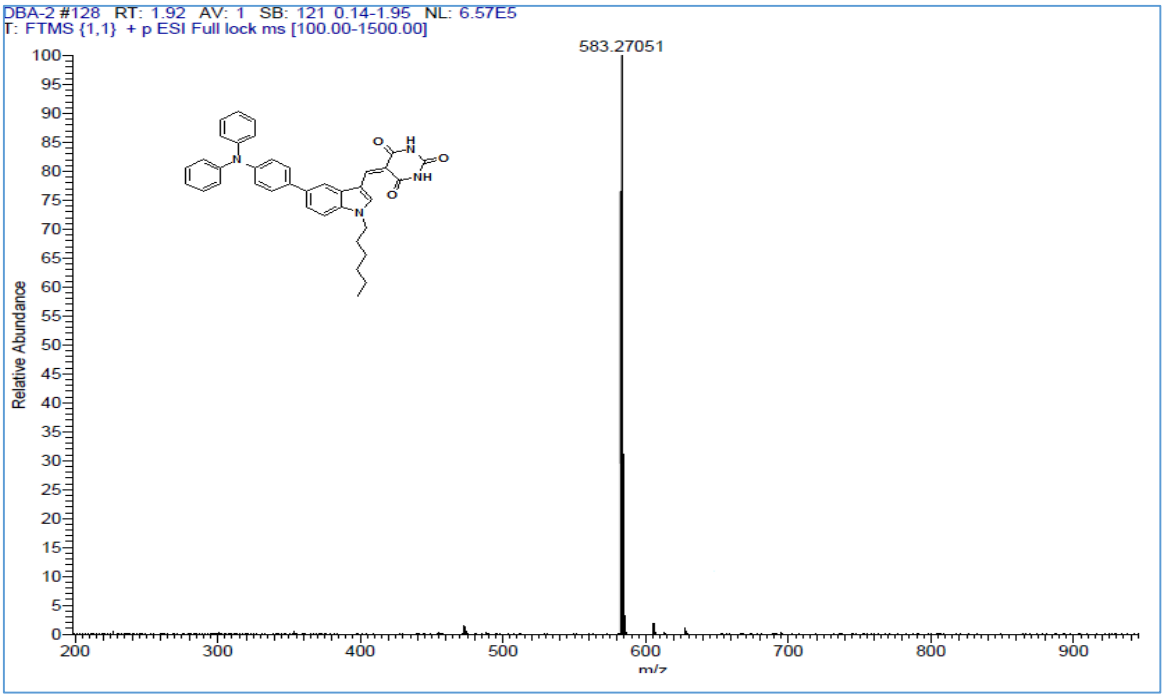

Fig.5.8 Mass spectrum of **DBA-2**

5.3.2 Crystal structure analysis

A suitable sized crystal of intermediate compound **2** was obtained by slow evaporation of chloroform-methanol solution and crystal data collection was performed on a Bruker Apex II instrument with micro-focus Mo Kα radiation (λ = 0.71073) at room temperature. The crystal structure was solved by using the SHELXTL package. The ORTEP diagram was created using Mercury 3.0 software and the corresponding data is presented in **Table 5.1**. Further, compound **5.2** crystallizes in the monoclinic crystal system with the P21/c space group and cell parameters are: a = 9.4128 (2) Å, b = 9.3806 (2) Å, c = 16.1820 (3) Å, V = 1428.80(5) $Å^3$ with Z = 4. The molecular structure of compound **5.2** with atom labeling is shown in **Fig.5.9**.

Table 5.1 Crystal and structure refinement data for compound **5.2**

Compound	**5.2**
Formula	$C_{15}H_{18}BrNO$
Formula weight	308.21
CCDC number	1426320
Temperature (K)	296(2)
Crystal form Color	Brown
Crystal system	Monoclinic
Space group	P 21/c
a (Å)	9.4128(2)
b (Å)	9.3806(2)
c (Å)	16.1820(3)
α (^{0})	90
β (^{0})	90.3890(10)
γ (^{0})	90
Volume (Å^3)	1428.80(5)
Z	4
Density (g cm^{-3})	1.433
μ (mm^{-1})	2.866
F (000)	632
$h_{min, max}$	-11,11
$k_{min, max}$	-11, 11
$l_{min, max}$	-19, 19
Reflections collected	2815
R_all, R_obs	0.0334, 0.0272
wR2_all, wR2_obs	0.1020, 0.0915
GOOF	0.764

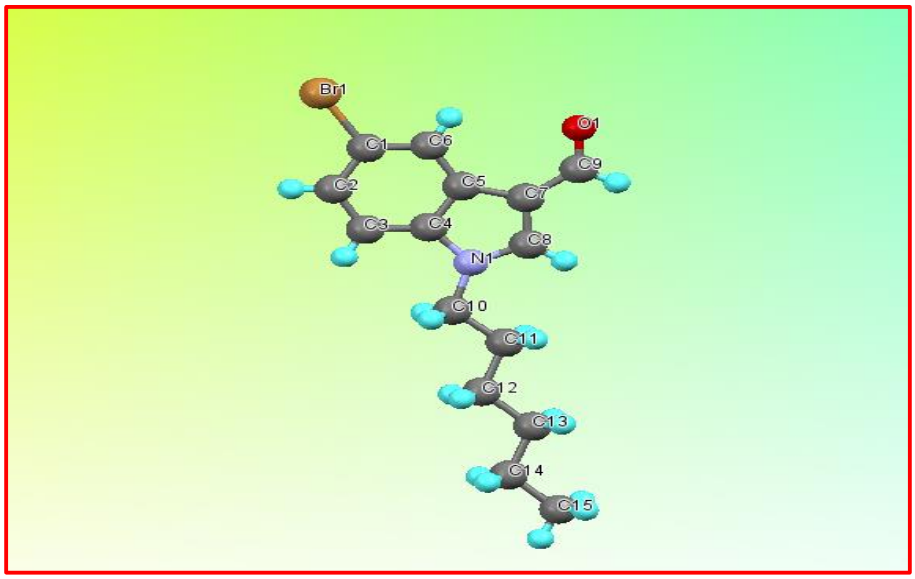

Fig.5.9 ORTEP (50% probability) diagram of compound ***5.2***

5.3.3 Photophysical properties

The absorption and emission spectra of the dyes recorded in chloroform are depicted in **Fig.5.10 (a)** and **(b)**, respectively; while the corresponding data is summarized in **Table 5.2**. Both the dyes exhibit two distinctive bands in the absorption spectra. The band in the longer wavelength region of 400-450 nm can be ascribed to the charge transfer (CT) from triphenylamine donor to corresponding acceptor moiety, whereas the band, in the region of 300-350 nm, can be attributed to the π-π* electronic excitations localized within the triphenylamine donor and indole π-bridge segments. It is important to note that, the molar extinction coefficients for the charge transfer transition in these dyes are considerably higher than the ruthenium based sensitizers. Further, absorption maxima of **DBA-2** is slightly red-shifted when compared to the **DBA-1**. This bathochromic shift is probably due to the elongation of conjugation in **DBA-2** and stronger electron withdrawing capability of barbituric acid. The aforementioned shift is quite desirable as it enhances the light harvesting capability of the sensitizer (Babu et al. 2015).

When adsorbed onto TiO_2 (**Fig.5.10 (c)**), both the sensitizers displayed a broadening in their absorption profile as compared to the corresponding spectra recorded

in solution state. The aforementioned red-shift is a stark contrast to the typically observed blue-shift for most of the organic dyes; it is caused by the deprotonation of the carboxylic acid unit of the sensitizer. The red-shift in the absorption profile can be attributed to the J-aggregation of the sensitizer molecules on the TiO_2 surface. The formation of aforesaid J-aggregates can be accredited to the interaction between the carboxylate group of the sensitizer and Ti^{4+} ions of the semiconductor. This interaction results in the lowering of the π^* energy level of the sensitizer molecule and thereby resulting in broadening of its absorption spectrum. Such broadening of the absorption profile is quite desirable for the fabrication of light harvesting devices as it may lead to improvement in photocurrent.

Another interesting observation which can be made from **Fig.5.10 (c)** is the higher absorbance values exhibited by sensitizer **DBA-1** as compared to **DBA-2** and hence it can be inferred that, **DBA-1** has better light harvesting capability than **DBA-2**. The aforesaid statement is evidenced by the superior photocurrent values exhibited by the sensitizer **DBA-1** over **DBA-2**. Further, the high values of molar extinction coefficients in both the sensitizers (38.5×10^4- 45.2×10^4 $M^{-1}cm^{-1}$) confirm their good light-harvesting capability. These values are significantly higher than the ruthenium based sensitizer **HD-2** in charge-transfer transitions. Further, **Fig.5.10 (a)** depicts the absorption spectrum of **HD-2** sensitizer. Furthermore, the degree of charge transfer in these sensitizers is confirmed by investigating the absorption spectrum of the precursors (**Fig.5.11**). The absorption spectrum of compound **5.2** displays λ_{max} of 300 nm, attributed to the weak charge transfer from indole core to bromo and aldehyde groups; on extending the conjugation by the incorporation of triphenylamine unit displays a clear red shift in the absorption spectrum of the precursor **5.3**, due to a better delocalization of the electron density in triphenylamine and indole moieties. Another peculiar feature of the absorption spectrum of the precursor **5.3** is the appearance of charge transfer peak. Although, due to the weak charge transfer from the triphenylamine amine and indole segments into the aldehyde group in **5.3**, this peak is not as prominent as the one observed for the sensitizers.

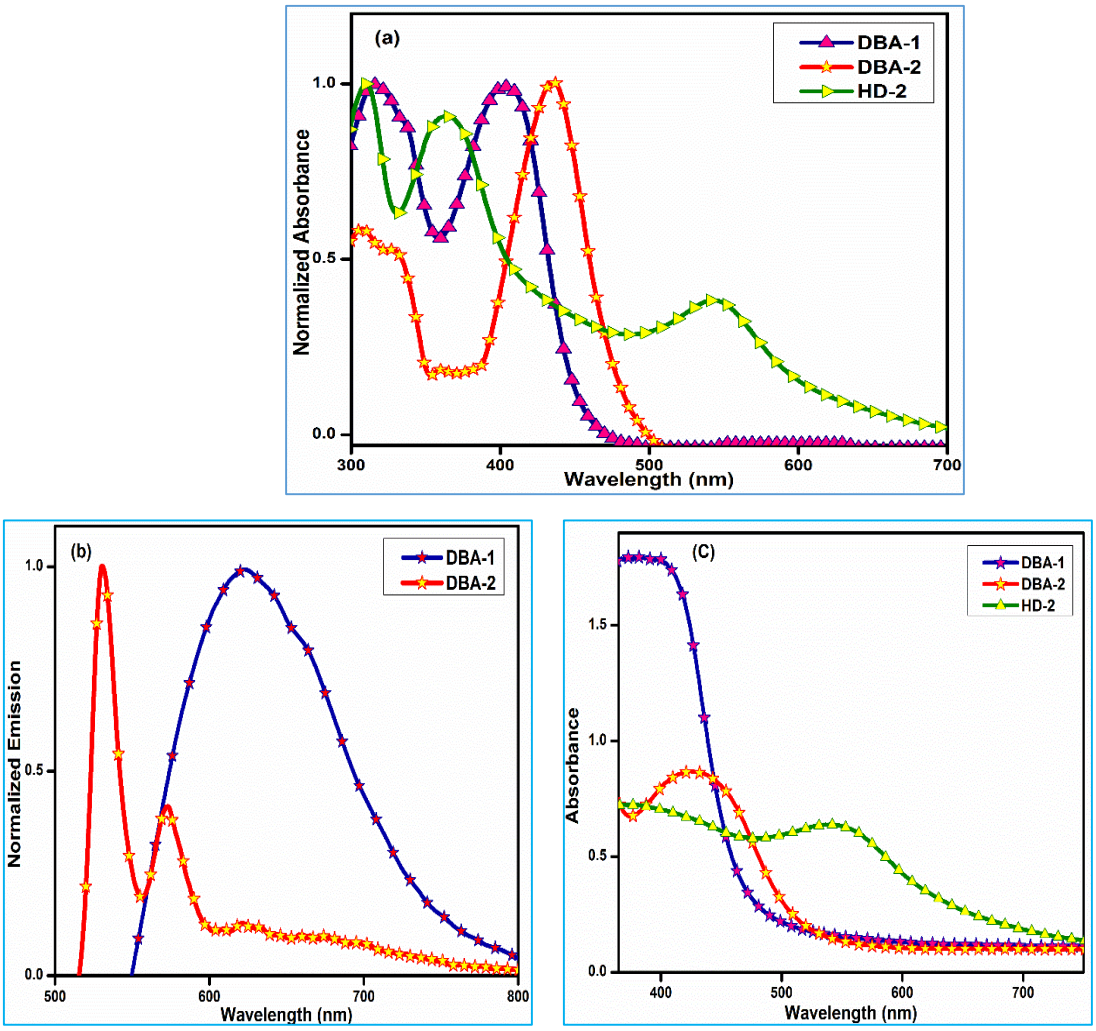

Fig.5.10 (a) UV-visible spectra of **DBA-1**, **DBA-2** and **HD-2** in chloroform (10^{-5} M) **(b)** Fluorescence spectra of **DBA-1** and **DBA-2** in chloroform (10^{-5} M) **(c)** UV-Vis spectra of **DBA-1**, **DBA-2** and **HD-2** for solid films while attached to TiO_2

The charge-transfer nature of the peak observed at higher wavelength was further established by studying the change in absorption spectrum of the sensitizers upon addition of trifluoroacetic acid (TFA) or triethylamine (TEA) to the chloroform solutions of the respective dyes (Babu et al. 2015). As evidenced from **Fig.5.12**, addition of TFA to the dye solution manifested a red shift, whereas the addition of TEA resulted in blue shift of absorption spectra. It is worth noting that, the addition of TEA to the dye solution not only resulted in a massive blue shift of the absorption maxima, it also lead to the disappearance

of the charge transfer band. This observation can be attributed to the deprotonation of the dye molecule (carboxylic acid segment) as a result of TEA addition.

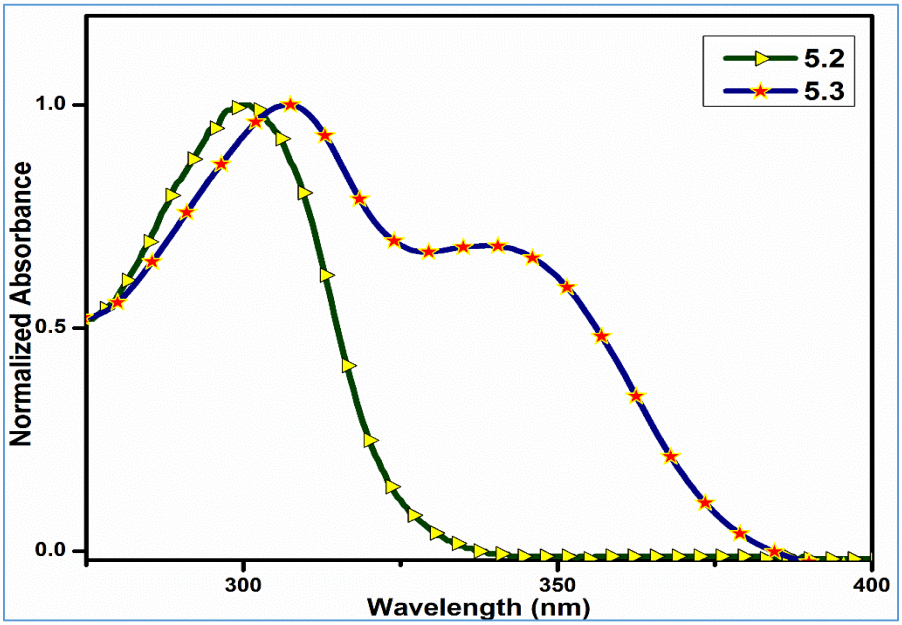

Fig.5.11 UV-visible spectra of compounds **5.2** and **5.3** in chloroform (10^{-5} M)

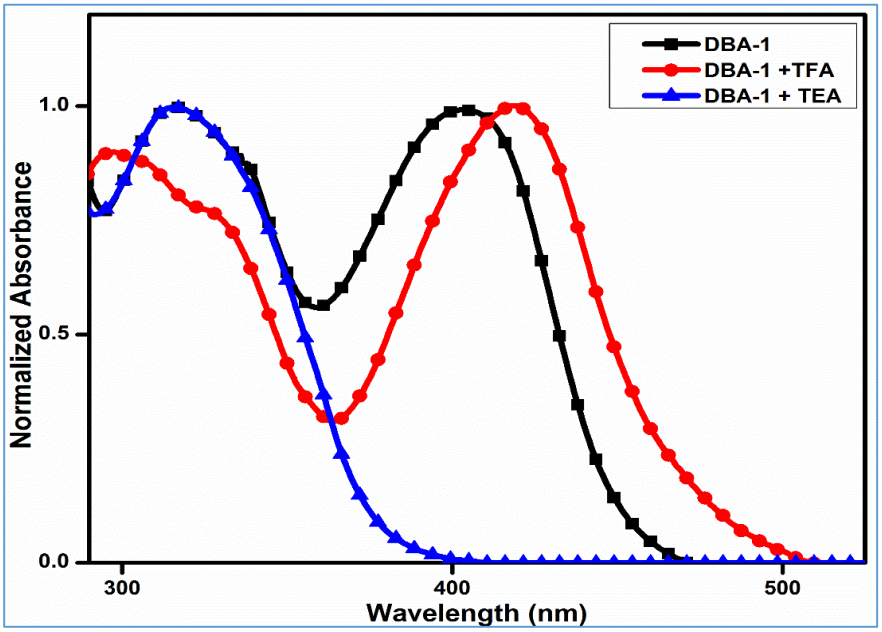

Fig.5.12 Absorption spectra of the dye **DBA-1** in $CHCl_3$ before and after addition of TFA and TEA

Table 5.2 Absorption and emission properties for **DBA-1**, **DBA-2** and **HD-2**

Sensitizer	Absorption λ_{max} (nm)	Emission λ_{max} (nm)	Stokes shift (cm^{-1})	ε ($M^{-1}cm^{-1}$)	E_{0-0}
DBA-1	404	627	8800	36500	2.59
DBA-2	440	530	3853	45200	2.40
HD-14	543	740	4910	19100	1.86

Further, the fluorescence emission spectra of both the sensitizers were recorded upon their excitation wavelengths and the pertaining results are summarized in **Table 5.2**, while the corresponding spectra are shown in **Fig.5.10 (b)**. Furthermore, the large Stokes shift obtained in these sensitizers can be attributed to the efficient charge transfer from the arylamine donor moiety to the respective acceptor groups.

5.3.4 Molecular modeling

All DFT calculations were executed using Turbomole software package. The ground state geometries were first optimized with semi empirical AM1 basis with MOPAC in Tmolex. Further optimization of the aforementioned geometries were done using C_1 point group symmetry at DFT level *via* the Becke's three-parameter hybrid functional and Lee-Yang-Parr's gradient-corrected correlation functional (B3LYP) .

For all the geometry optimizations, the default convergence criteria were maintained. Further, all the calculations were performed using def-TZVP basis set. The optimized geometries and electron density distributions in the HOMOs and LUMOs of the two dyes are depicted in **Fig.5.13**. As evidenced from the figure, in the HOMO level, the electron density is mainly located on the triphenylamine segment, whereas in the corresponding LUMOs, a clear shift of density towards π-bridge and acceptor parts is observed. This seamless shift in electron density from HOMO to LUMO level is desirable for superior charge transfer and the efficient interfacial injection of electrons from the

excited state of the sensitizer molecule into the conduction band of the semiconductor. Further, time-dependent density functional theory (TD-DFT) studies were also carried out. TD-DFT offers a computationally economical means to probe the electronic excitations of material in presence of time-dependent perturbations. In TD-DFT, time-dependent Schrödinger equations are solved to elucidate the excited-state properties. Further, TD-DFT depends on adiabatic approximation. In the aforementioned approximation, temporal nonlocality is neglected and an assumption is made that, at any particular moment, the exchange-correlation functional (xc) depends purely on the instantaneous density (Peach et al. 2008).

DYE	Optimized geometry	HOMO	LUMO
DBA-1	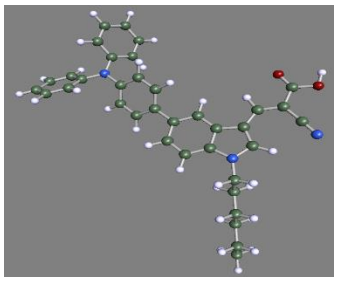	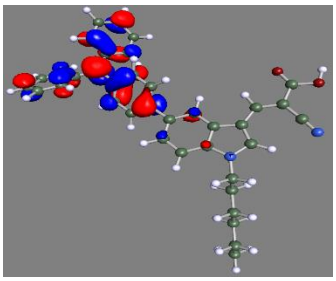	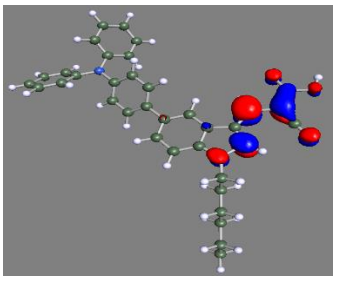
DBA-2	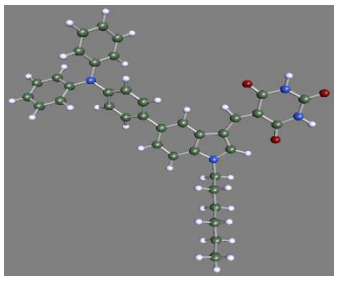	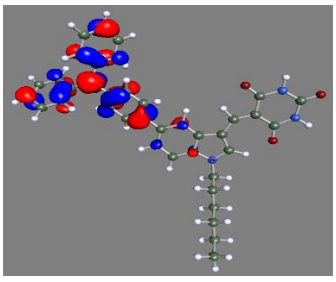	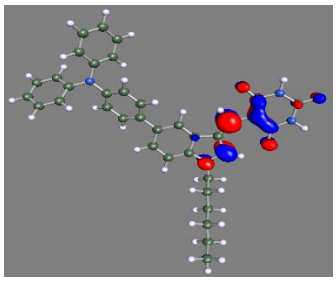

Fig.5.13 Optimized structure and Frontier molecular orbitals of **DBA-1** and **DBA-2**

Due to the aforesaid approximation, traditional approximations (time-independent) can be applied to the xc-functional derived for ground state DFT, *i.e.* BP (Beck-Perdew)

and hybrid functionals (B3LYP) (Becke 1993, Lee et al. 1988). Typically, the accuracy of the results obtained using TD-DFT depends on the functional and basis set employed for the calculations. **Fig.5.14** depicts the simulated absorption spectrum of **DBA-1** obtained at the BP86 functional and def-TZVPP basis set. Although, it is well documented that TD-DFT can substantially under estimate the energies associated with long-range charge transfer states. The aforementioned anomaly is not observed in the current study, as the molecules **DBA-1** and **DBA-2** under investigation are not sufficiently large enough to exhibit a long-range intramolecular charge transfer.

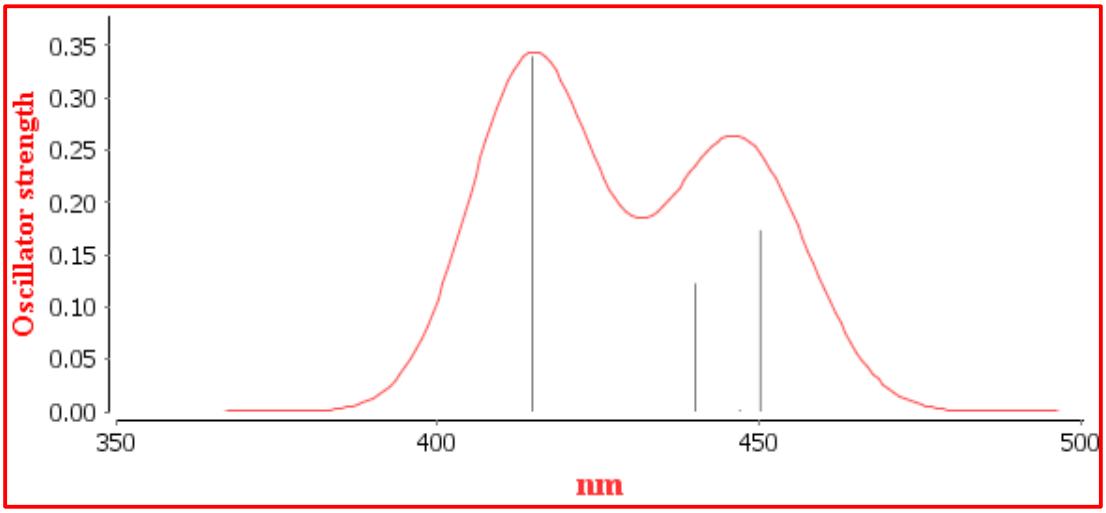

Fig. 5.14 Simulated absorption spectrum of **DBA-1**

As evidenced from the simulated spectrum of **DBA-1(**reported at the default standard deviation value of 37.05), the molecule exhibits two distinct bands, corresponding to π-π* and charge transfer phenomenon. These precise and reliable predictions made by TD-DFT studies indicate that, the functional and basis set chosen for TD-DFT studies are quite appropriate.

5.3.5 Electrochemical characterization

In order to forecast the prospects of electron injection from the excited state of the sensitizers into the conduction band (CB) of the TiO_2 film and effective dye regeneration by avoiding the geminate charge recombinations between oxidized dye molecules and

photo-injected electrons in the conduction band of the semiconductor, the ground and excited oxidation potentials of the newly synthesized co-absorbers/sensitizers were determined by Cyclic voltammetry (CV). The results of the aforementioned study is presented in **Fig.5.15**. From the figure, it is evident that, both sensitizers have a more negative GSOP (ground state oxidation potentials) (eV) than the Nernst potential of the I^-/I_3^- redox couple (-5.2 eV) (Qu et al. 2001), indicating that, the oxidized dyes can be reduced and regenerated by I^- species in the electrolyte and thereby, circumventing the charge recombination between oxidized dye molecules and photo-injected electrons in the conduction band of the semiconductor. All the values in volts (V) against NHE were converted to electron volt (eV) using the following equation.

$$ESOP = [(GSOP\ (V) + 4.7) - E_{0\text{-}0}]\ eV$$

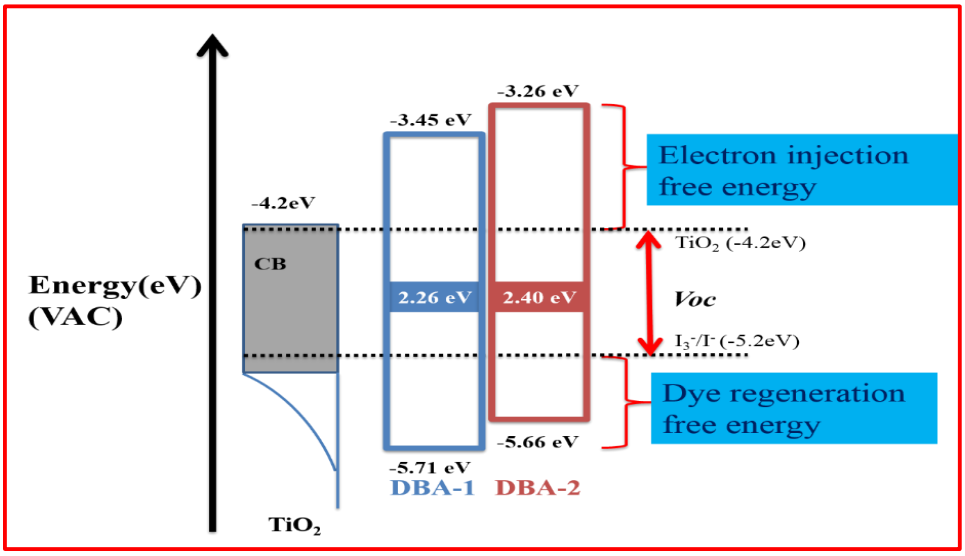

Fig.5.15 Energy level diagram of **DBA-1** and **DBA-2**

Further, the ESOP (excited state oxidation potentials) of dyes can be calculated by using GSOP energy level and zeroth-zeroth energy (E_{0-0}) of the dyes, by using the aforementioned equation. It is evident that, the excited state oxidation potentials of both the sensitizers are much more positive than the conduction band edge of TiO_2 which is

located at -4.2 eV and hence, providing sufficient thermodynamic driving force for efficient electron injection. The negative free energy for electron injection is in the order: **DBA-2** > **DBA-1**. From the aforementioned order, one could predict that, sensitizer **DBA-2** will be more efficient than **DBA-1** in injecting electrons into the conduction band of TiO_2. Thus, the electronic structures of these two sensitizers appear to confirm a favorable flow of charges throughout the photo-electronic conversion cycle.

5.3.6 Photovoltaic device characterization

The photovoltaic characteristics of the co-sensitized devices were measured so as to comprehend the effect of anchoring groups on the co-sensitization properties and thereby, establishing a link between the structure of the co-sensitizer and their corresponding performance in the cell. Current-voltage (*J-V*) characteristics of the cell based on **HD-2** and the corresponding co-sensitized solar cells using **DBA-1** and **DBA-2** are displayed in **Fig.5.16**, while the pertaining photovoltaic parameters are given in **Table 5.3**. It is evident that, all the co-sensitized devices yielded enhanced efficiency, except the one co-sensitized using 0.3 mM concentration of **DBA-1**. The solar cells employing 0.2 mM of **DBA-1** and **DBA-2** as the co-sensitizers yielded η % of 7.82 (J_{sc} = 16.12 $mAcm^{-2}$, V_{oc} = 0.729 V, *ff* = 0.665) and 7.97 (J_{sc} = 17.10 $mAcm^{-2}$, V_{oc} = 0.726 V, *ff* = 0.641), respectively, compared to η % of 7.61 for pure **HD-2** (J_{sc} = 16.81 $mAcm^{-2}$, V_{oc} = 0.723 V, *ff* = 0.626).

It was noticed that, as a result of co-sensitization, all the V_{oc} values were increased; this suggests that the charge recombination caused by ruthenium dye aggregation is suppressed by the co-sensitizers, resulting in better performance of solar devices co-sensitized with **DBA-1** and **DBA-2**. Besides, all the fill factor values were also found to be enhanced except the one co-sensitized with 0.3 mM **DBA-1**, which indicates that, smaller sized organic co-sensitizers provide more sufficient TiO_2 surface coverage compared to the bulky ruthenium dye that leaves large nanoparticle area unadsorbed. The aforementioned dip in J_{sc} for the device co-sensitized with 0.3 mM **DBA-1**, can be attributed to intense competitive adsorption between co-sensitizer and sensitizer and thereby, resulting in

decrease in the adsorption of **HD-2** sensitizer onto TiO_2 surface. This has resulted in reduced light harvesting proficiency.

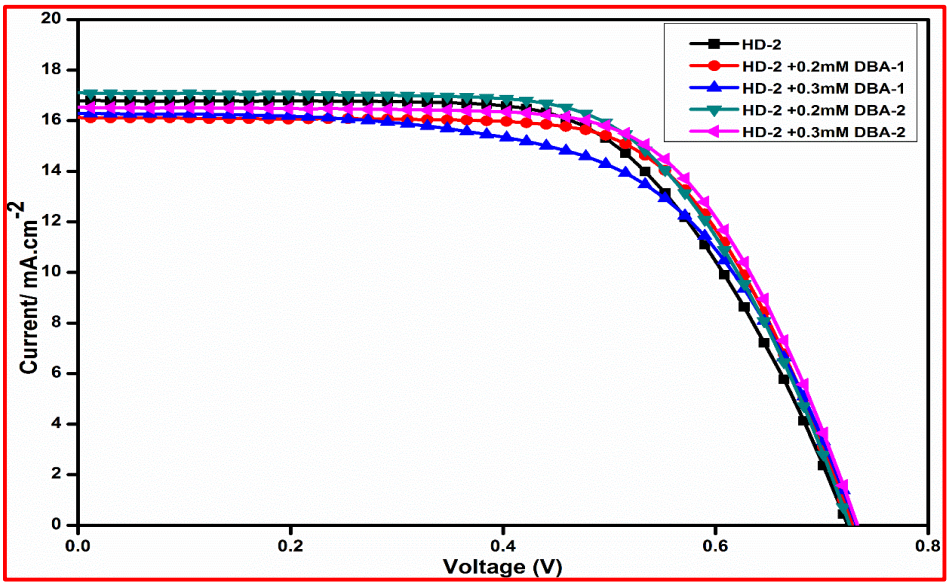

Fig.5.16 *J-V* characteristics of DSSCs based on **HD-2** and co-sensitized with **DBA-1** and **DBA-2**

To further examine the photovoltaic performances of co-sensitized solar devices, the incident photon to current efficiency (IPCE) was carried out and the corresponding plot is depicted in **Fig.5.17**. In comparison with solar cell purely sensitized by **HD-2**, the J_{sc} of the one co-sensitized with 0.2 mM **DBA-2** increased (from 16.81 to 17.10 $mAcm^{-2}$), which translated into the best IPCE response. The IPCE of 0.2 mM **DBA-2** co-sensitized solar cell was found to be 68% at 540 nm and higher than 60% in the range of 450 nm and 580 nm. Further, it is interesting to note that, even though the cells co-sensitized by 0.2 mM **DBA-1** and 0.3 mM **DBA-2** offered better efficiency compared to the one sensitized by **HD-2** alone, but their J_{sc} values were found to be lowered. The lowering of J_{sc} can be attributed to the reduced light harvesting capability, as depicted in the IPCE graph. The aforesaid can be attributed to competitive adsorption between co-sensitizer and sensitizer molecules and thereby, resulting in decrease in the adsorption of **HD-2** sensitizer onto TiO_2 surface. Further, the reduced concentration of the sensitizer **HD-2** on the semiconductor

surface negatively affects the light harvesting capability of the cell in the longer wavelength region of the electro-magnetic spectrum. On the other hand, the presence of co-sensitizer on the semiconductor surface has resulted in enhanced V_{oc} values. The aforementioned observation vindicates the efficient role played by co-sensitizers in diminishing undesirable charge recombinations within the cell. The presence of co-sensitizers also helps in suppressing the charge re-combinations caused by dye aggregation or close π–π stacking and thereby improving the device performance significantly. Another interesting inference which can be drawn from these results is that, the concentration of co-sensitizer used substantially affects the overall efficiency of the cell and therefore, one has to strike a balance between the sensitizer and co-sensitizer concertation to obtain maximum efficiency from the cell.

Table 5.3 Photovoltaic parameters of DSSCs based on **HD-2** with/without co-sensitization

Sensitizer	Concentration of co-sensitizer (mM)	J_{sc} ($mAcm^{-2}$)	V_{oc} (V)	*ff* (%)	η (%)
HD-2	_	16.81 ± 0.02	0.723 ± 0.003	62.60 ± 0.9	**7.61 ± 0.05**
HD-2 + DBA-1	0.2	16.12 ± 0.03	0.729 ± 0.003	66.50 ± 0.3	7.82 ± 0.03
HD-2 + DBA-1	0.3	16.26 ± 0.04	0.731 ± 0.001	60.60 ± 0.5	7.20 ± 0.06
HD-2 + DBA-2	0.2	17.10 ± 0.02	0.726 ± 0.002	64.10 ± 0.8	7.97 ± 0.06
HD-2 + DBA-2	0.3	16.54 ± 0.04	0.732 ± 0.003	66.50 ± 0.4	**8.06 ± 0.03**
DBA-1	_	4.86± 0.05	0.660± 0.001	72.37± 0.2	2.32± 0.02
DBA-2	_	2.23 ± 0.07	0.661 ± 0.001	68.30 ± 0.3	1.01 ± 0.03
N719	_	15.90± 0.04	0.730± 0.003	66.00± 0.4	7.64± 0.03

Overall, the cell co-sensitized by 0.2 mM **DBA-2** provides both of enhanced light harvesting capability and reduced electron recombination, which makes it more attractive for co-sensitization. The enhancement in efficiency of the co-sensitized devices can be attributed to the optimized packing of the sensitizer (**HD-2**) molecules on the TiO_2 surface due to the presence of co-adsorbent molecules, which occupy the vacant spaces between **HD-2** dye molecules. The co-adsorbent molecules situated between the sensitizer molecules on the TiO_2 surface impedes the rate of interfacial back electron transfer from the conduction band of the TiO_2 film to the I_3^- ions and thereby, leading to higher photovoltage. This has been highlighted in **Fig.5.18**.

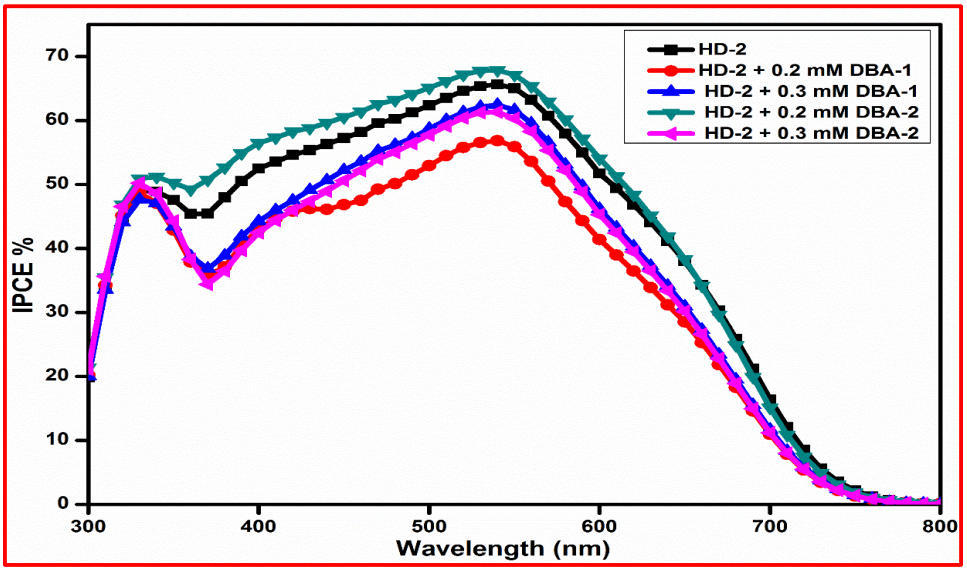

Fig.5.17. IPCE spectra of the DSSCs based on **HD-2** and co-sensitized with **DBA-1** and **DBA-2**

On the other hand, co-adsorbers are known to decrease the dye loading up to 60%, and hence, leading to lower photocurrent density. The aforesaid can be attributed for the lower J_{sc} values observed in most of the co-sensitized devices in the present study. However, in the presence of 0.2 mM **DBA-2** surface passivation was found to be optimum as can be incurred from IPCE spectrum of the corresponding device. Further, cells using only the co-sensitizer molecules (**DBA-1** and **DBA-2**) have been fabricated so as to further

ascertain the above-mentioned observations. **Fig.5.19** shows the IPCE spectra of the co-sensitizer molecules. The IPCE response of **DBA-1** was found to be 42% at 330 nm and 44% in the range from 385 to 415 nm. The onset wavelength of the aforesaid IPCE spectrum was observed to be 550 nm. Although, the photo responsive span of **DBA-1** based devices co-sensitized using CDCA remained unaffected, the IPCE response dipped to 36% and 21% in devices co-sensitized using 10 mM and 20 mM CDCA, respectively. On the other hand, the devices based on **DBA-2** displayed an extended photo responsive area as compared to their **DBA-1** based counter-parts.

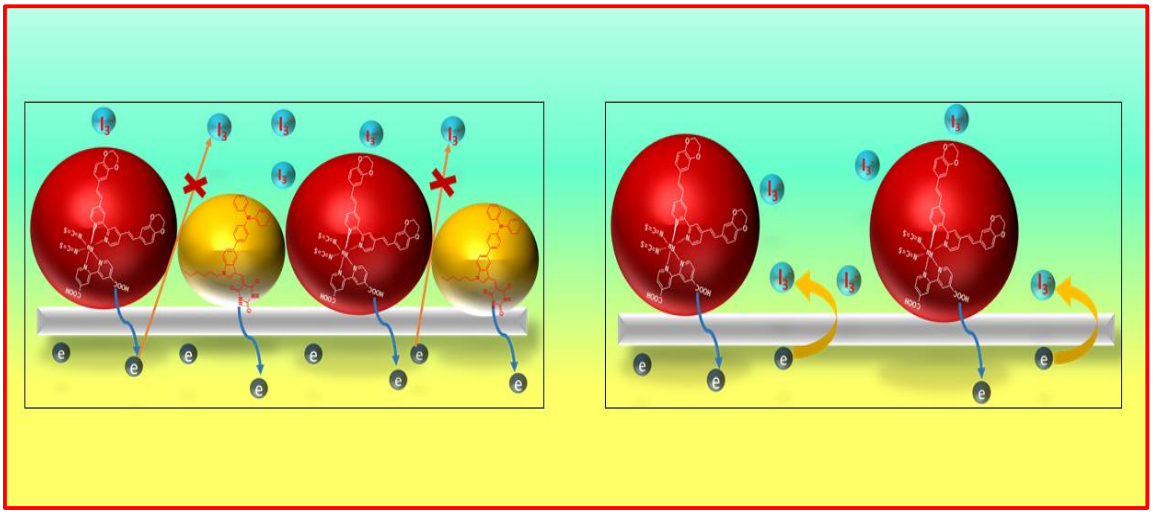

Fig.5.18 Simple sketch map of the devices sensitized by **HD-2+ DBA-2** and **HD-2** on the TiO_2 surface.

In fact, **DBA-2** based devices displayed superior IPCE values in the 330 nm region, but the IPCE values were extremely low (6-16%) from 415 to 450 nm and 1-9% from 480 to 550 nm region. Superior IPCE response for **DBA-1** rendered into higher J_{sc} of 4.86 $mAcm^{-2}$ compared to 2.23 $mAcm^{-2}$ for **DBA-2**. Although, barbituric acid as an electron acceptor in the **DBA-2** contributed to the bathochromic shift of the absorption spectrum, it was found that, it exhibited lower efficiency (1.01%). These results may indicate that, barbituric acid is a poor anchoring group in comparison to cyanoacrylic acid for a sensitizer. **Fig.5.20** depicts the *J-V* curves obtained by employing **DBA-1** and **DBA-2** as sensitizers.

The overall cell efficiencies and the corresponding photovoltaic parameters are summarized in **Table 5.3**. All the aforementioned observations and results vindicate the profound role played by the acceptor moieties in influencing the photovoltaic properties of a dye molecule both as sensitizer and co-sensitizer.

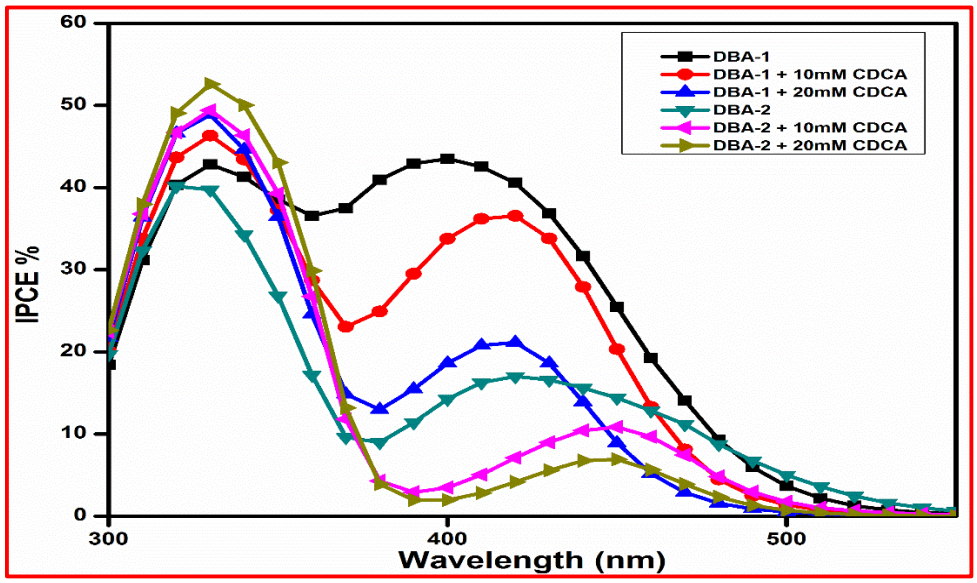

Fig.5.19. IPCE spectra of DSSCs sensitized with **DBA-1** and **DBA-2**

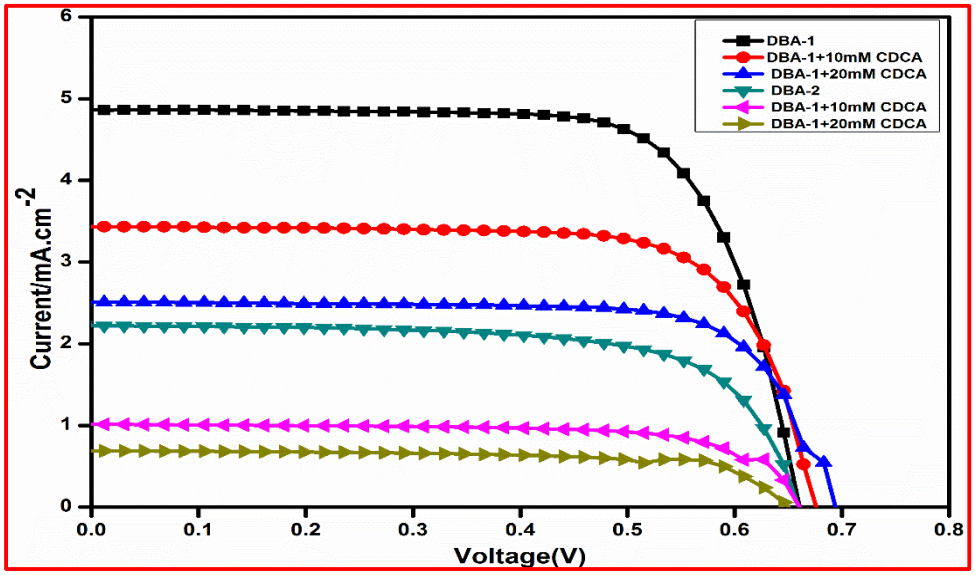

Fig.5.20 Photocurrent-voltage characteristics of DSSCs sensitized with **DBA-1** and **DBA-2**

5.3.7 Electrochemical impedance spectroscopy characterization

To further probe the interface characteristics between the dyes and TiO_2, electrochemical impedance spectroscopy (EIS) was employed, which is a useful tool to analyze the charge transfer and chemical capacitance at the interfaces of TiO_2/dye/electrolyte and Pt/eletrolyte in DSSCs. Typical EIS measurements result in Nyquist and Bode plots. **Fig.5.21** compares EIS plots for sensitized cells based on **DBA-1** and **DBA-2**. All the devices presented two distinct semicircles. Small semicircle at lower frequency models the cathode charge transfer resistance which is directly related with *ff*, whereas the large semicircle at middle frequency models the charge recombination resistance (R_{ct}) from TiO_2 to electrolyte that is directly related to V_{oc}. In Nyquist plots, the radius of the large semicircle of the cells co-sensitized by **DBA-1** and **DBA-2** were all larger than that sensitized by **HD-2** only. This clearly indicates that the co-sensitizers are helpful in the suppression of dark current. The aforesaid is consistent with the V_{oc} values in **Table 5.3**. Therefore, Nyquist plots also prove that, the co-sensitization contributes to the suppression of charge recombination at TiO_2/dye/electrolyte interface.

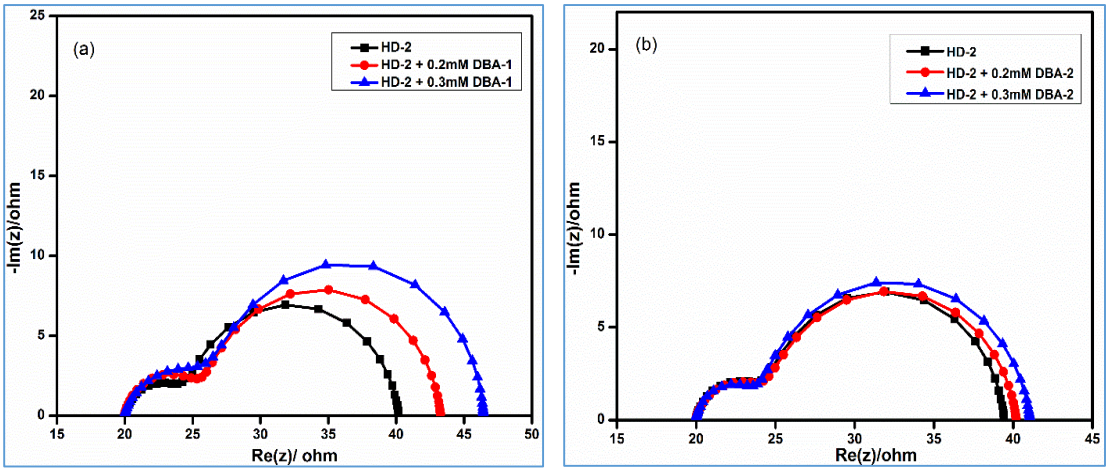

Fig.5.21 EIS Nyquist plots for DSSCs based on **HD-2** and co-sensitized with **a) DBA-1** b**) DBA-2**

In Bode frequecy plots, lifetime for injected electrons into TiO_2 conduction band can be calculated using the equation: $\tau_{CB} = 1 / (2\pi f)$, where τ is the lifetime of electrons in TiO_2 and f is the mid frequency peak in Bode plots. The electron lifetime depends on the

density of charge traps, which is ultimately related to V_{oc}. The electron lifetimes for the DSSCs sensitized using only **HD-2** and the ones co-sensitized using **DBA-1** and **DBA-2** were determined using Bode frequency plots (**Fig.5.22**). The mid frequency peaks of the Bode plots displayed the order: **DBA-2** (0.3mM) > **DBA-1** (0.3mM) > **DBA-1** (0.2mM) > **DBA-2** (0.2mM) > **HD-2**. The corresponding to electron lifetimes were found to be 4.8, 4.6, 4.4, 3.1 and 2.9 ms, respectively. These results suggest that, in all the cases the addition of co-adsorbent effectively suppressed the undesirable charge recombinations. Further, the calculated electron lifetime values are well in agreement with the V_{oc} values of these devices (**Table 5.3**). These results showcase the profound influence of acceptor groups on the electron recombination processes between the electrolyte species and elcetrons injected into TiO_2 film.

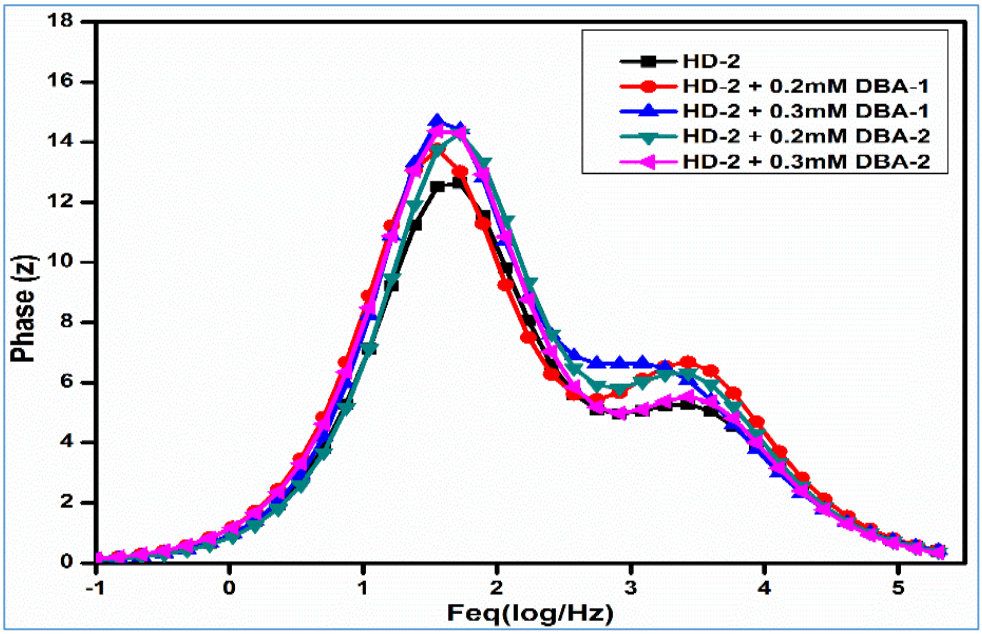

Fig.5.22 Bode plots for DSSCs based on **HD-2** and co-sensitized with **DBA-1** and **DBA-2**

5.3.8 FT-IR analysis: anchoring studies of the dyes on TiO_2

To elucidate the binding states of the sensitizers **DBA-1** and **DBA-2** on TiO_2 nanoparticles, FT-IR spectra of the dye in free form as well as the dyes adsorbed on TiO_2 nanoparticles were recorded. It is well documented that, a carboxylic acid group can bind

to the TiO_2 in several modes such as physisorption (due to the H-bonding interaction between the acidic proton on the carboxylic acid group and oxygen atom of TiO_2) or chemisorption (monodentate, bidentate bridging or bidentate chelating). In the case of **DBA-1** and **DBA-2**, because of the disappearance of peak due to $\nu_{C=O}$ and the presence of new peaks of ν_{sym} and ν_{asym}, one can discount the possibility of physisorption.

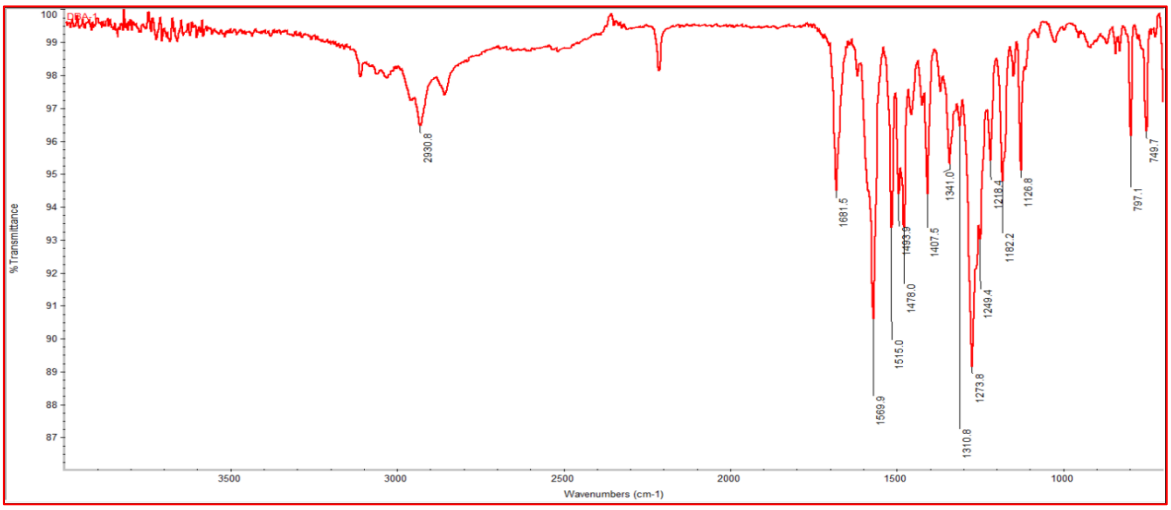

Fig.5.23 FT-IR spectrum of **DBA-1**

Deacon and Phillips stated a set of rules to determine the nature of the binding of the sensitizer on the semiconductor surface from vibrational frequency analysis (Deacon and Phillips 1980). From the aforesaid rules in view, the nature of the binding modes can be correlated to the difference between symmetric and asymmetric bond stretching frequencies of the >C=O of carboxylic acid group of the anchoring unit. FT-IR spectrum of the free **DBA-1** dye (**Fig.5.23**) depicts noticeable bands at 1681 cm^{-1} and 2220 cm^{-1} corresponding to the >C=O and –C≡N stretching, respectively. Whereas, the spectrum of sensitizer **DBA-1** anchored onto the semiconductor (**Fig.5.24**) clearly portrays bands at 1516 and 1596 cm^{-1} corresponding to symmetric and asymmetric stretching modes of the carbonyl group, respectively. These observations evidently indicate the deprotonation as well as the involvement of carboxylic acid group in the adsorption of the sensitizer onto the semiconductor surface. Further, the disappearance of band corresponding to >C=O

stretching and the appearance of two new peaks corresponding to the symmetric and asymmetric stretching vibrations confirm that, the dye is chemisorbed, and thereby ruling out the possibility of physisorption.

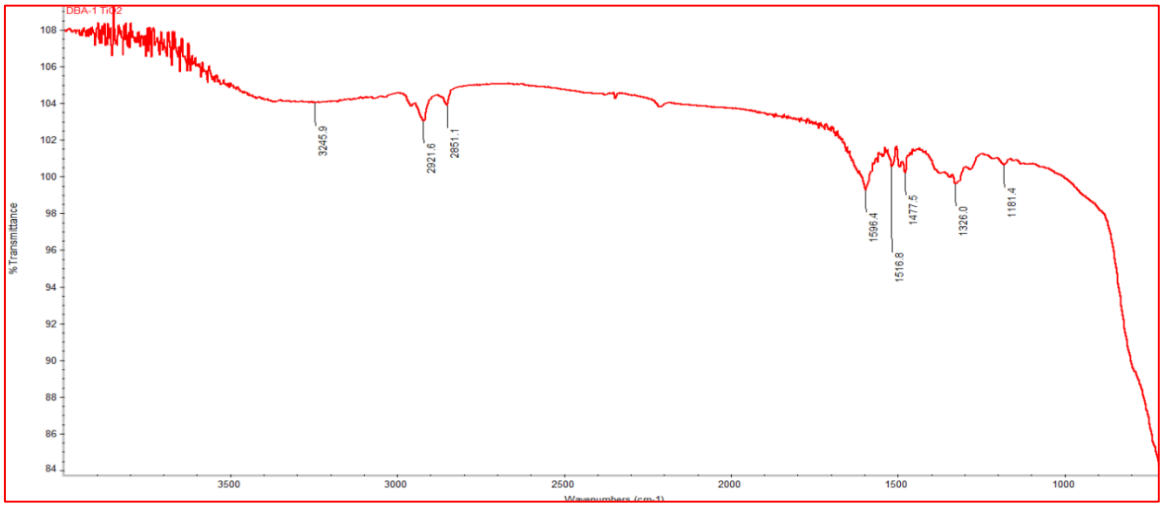

Fig. 5.24 FT-IR spectrum of **DBA-1** on TiO_2.

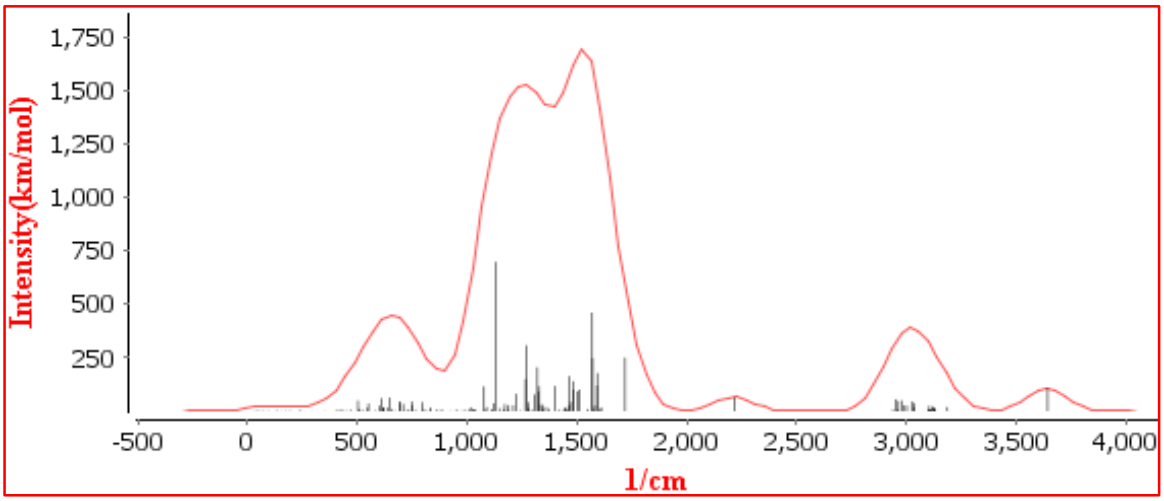

Fig.5.25 Theoretically obtained FT-IR spectrum of **DBA-1**

Further, by following the Deacon and Phillips rules, one can explain the adsorption states as well as the nature of bonds formed upon adsorption of the sensitizers on the TiO_2 nanoparticles. In the present study, it is evident that, the dye is anchored onto the semiconductor surface by means of bidentate chelation or a bridging rather than an ester type linkage. Another decisive piece of information which can be drawn from the FT-IR

analysis is that the cyano group is not involved in dye-adsorption process, as the peak corresponding to it remains unchanged in both free and adsorbed states. Likewise, the FT-IR spectrum of **DBA-2** depicted similar trends as well. Further, the IR-absorption spectra of both the sensitizers have been simulated using Turbomole software. **Fig.5.25** depicts the simulated FT-IR spectrum of **DBA-1**. As anticipated, the theoretically acquired spectrum is well in agreement with the experimentally obtained one.

5.4 CONCLUSIONS

In the present work, two donor-acceptor type dyes have been successfully designed and synthesized as alternative co-adsorbents to CDCA. A systematic investigation on the structure-photovoltaic performance relationship of the co-sensitizers has been carried out. Although, both the co-sensitizers were found to be successful in enhancing the overall efficiency of the co-sensitized devices, the device co-sensitized using **DBA-2** displayed the higher efficiency as compared to the one co-sensitized using **DBA-1**. Further, it is interesting to note that, both the co-sensitizers have been successful in lowering the dye aggregation and impeding the unfavorable electron recombinations, as witnessed from the enhanced V_{oc} values of the co-sensitized devices. All the results highlight the significance of the strategy, which integrates multiple functionalities into one co-sensitizer and thereby, enhancing the overall performance of the device. The results also showcase the profound effect of acceptor units on the overall performance of the co-sensitizers. Further, it is believed that, the aforementioned structure-performance relationships will facilitate in augmenting the efficiency of DSSCs by providing insights into the selection of proper acceptor moieties to further ameliorate DSSC performance.

CHAPTER 6

INDOLE BASED CO-SENSITIZERS WITH D-D-A CONFIGURATION: SYNTHESIS, CHARACTERIZATION AND PERFORMANCE STUDIES

Abstract

*In this chapter, synthetic protocols, optical and electrochemical studies of three new organic co-sensitizers **DBA-3**, **DBA-4** and **DBA-5** have been incorporated. Further, it includes the theoretical calculations as well as fabrication studies of devices co-sensitized with the aforesaid dyes. Finally, a detailed discussion on obtained results has been incorporated.*

6.1. INTRODUCTION

Based on the comprehensive literature survey and by following the design strategy described in **chapter 1 (Section 1.11)**, three new co-sensitizers **DBA-3**, **DBA-4**, and **DBA-5** (**series 5)**, where the indole moiety forms the core and barbituric acid acts as an acceptor/anchoring group, have been synthesized. A detailed account of synthetic procedures, photophysical, electrochemical, theoretical and device fabrication studies has been described. Further, results pertaining to the aforementioned studies have been described.**Fig.6.1** depicts the chemical structures of the co-sensitizers and ruthenium based sensitizer **NCSU-10**.

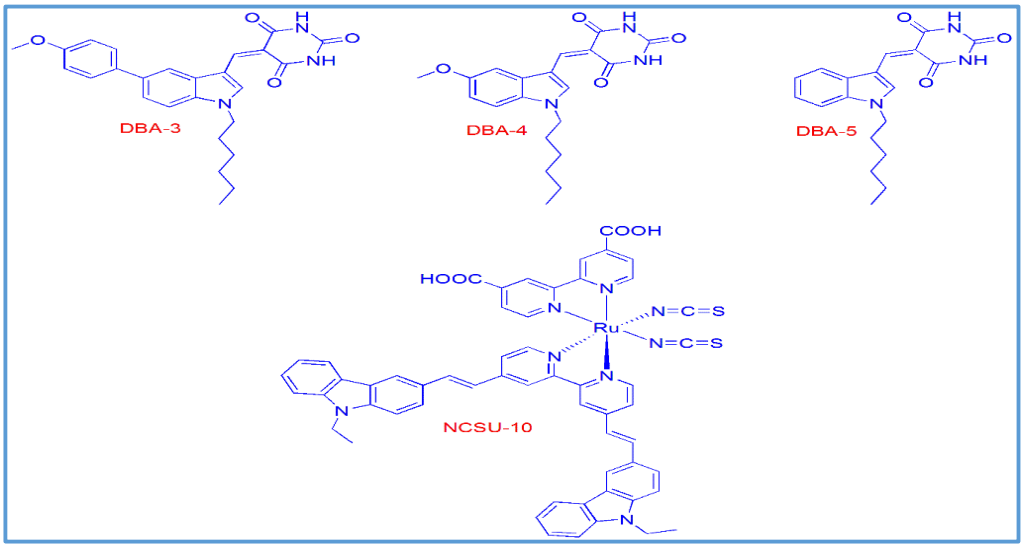

Fig.6.1 Chemical structures of co-sensitizers and **NCSU-10**

6.2 EXPERIMENTAL

6.2.1 Materials and methods

The starting materials 5-bromo-1*H*-indole, 5-methoxy-1*H*-indole-3-carbaldehyde, indole-3-carbaldehyde, 1-bromohexane, sodium hydride, 4-methoxyphenylboronic acid, tetrakis(triphenylphosphine)palladium(0) [$Pd(PPh_3)_4$] and barbituric acid, were obtained from Sigma-Aldrich. All the solvents were dried prior to use by following standard protocols. All the reactions were conducted under argon atmosphere and the reaction progression was monitored by TLC technique. Chromatographic separations were performed using silica gel (230-400 mesh). ^{1}H NMR and ^{13}C NMR spectra were recorded using Bruker avance 500 MHz and 400 MHz spectrometers, in $CDCl_3$ or DMSO-d_6 and tetramethylsilane as internal standard. Mass spectra were acquired from thermo scientific-EXACTIVE (ESI-MS), while the elemental analysis was attained from a Flash EA1112CHNS analyzer (Thermo Electron Corporation).

6.2.2 Synthesis of co-sensitizers

The synthetic pathways of the three new co-sensitizers **DBA-3, DBA-4** and **DBA-5** are depicted in **Scheme 6.1** and **6.2**. N-alkylation of 5-bromo-1*H*-indole was done using 1-bromohexane to yield compound **6.1**. Compound **6.1** was then subjected to Vilsmeier-Haack formylation to give compound **6.2**. The product was coupled with 4-methoxyphenylboronic acid *via* Suzuki coupling to yield compound **6.3**. Further, Knoevenagel condensation of this aldehyde with barbituric acid in methanol was carried out to obtain **DBA-3**. Compounds **5a** and **5b** are obtained by *N*-alkylation of the corresponding indole derivatives **4a** and **4b**, respectively. Finally, Knoevenagel condensation of the corresponding aldehydes with barbituric acid in methanol was carried out to obtain **DBA-4** and **DBA-5**.

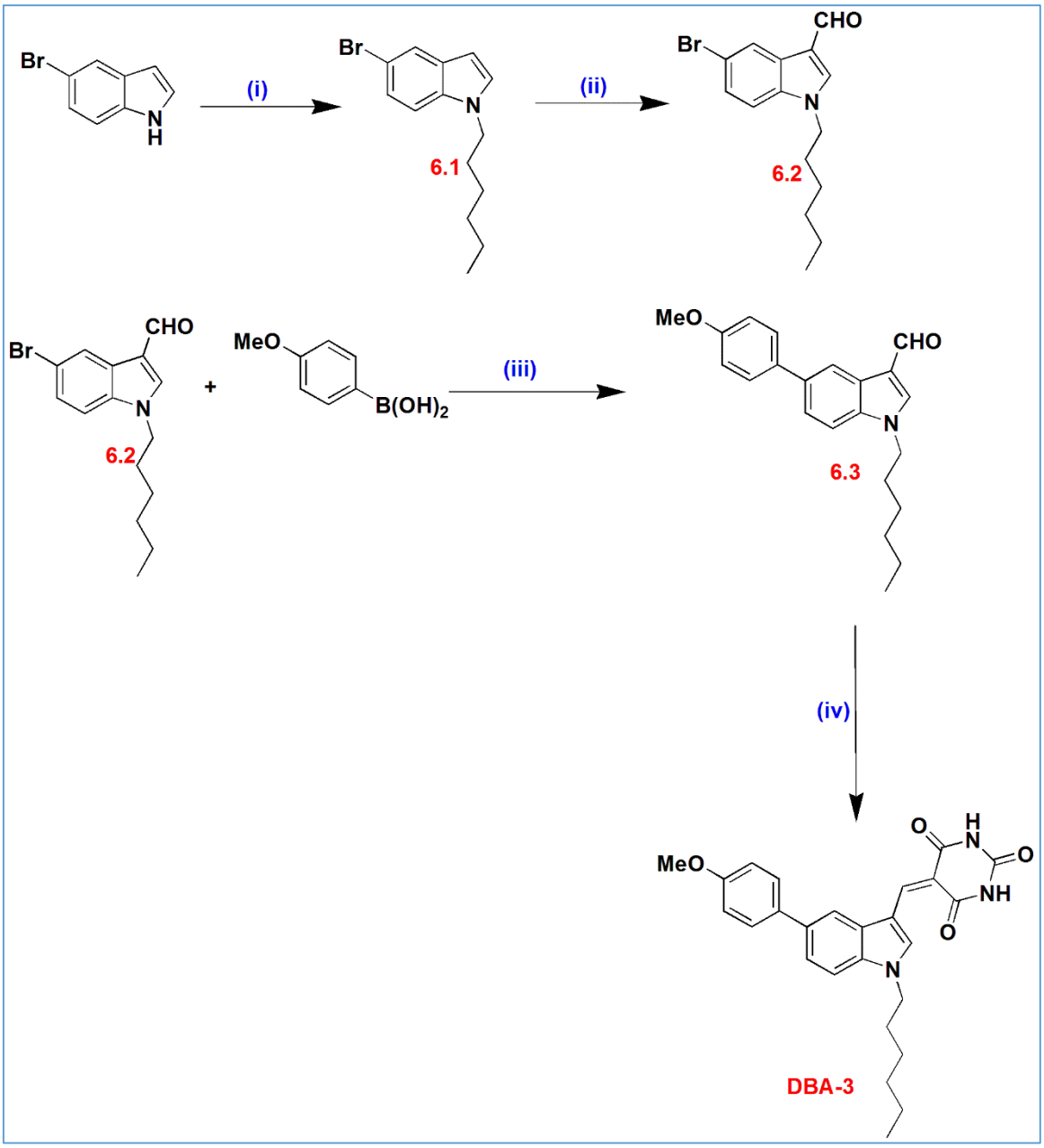

Scheme 6.1 Synthetic route of the co-sensitizer (i) 1-Bromohexane, NaH, DMF, RT (ii) $POCl_3$, DMF, RT (iii) Pd $(PPh_3)_4$, K_2CO_3, THF, ethanol, water (iv) Barbituric acid, CH_3OH, 80 ^0C

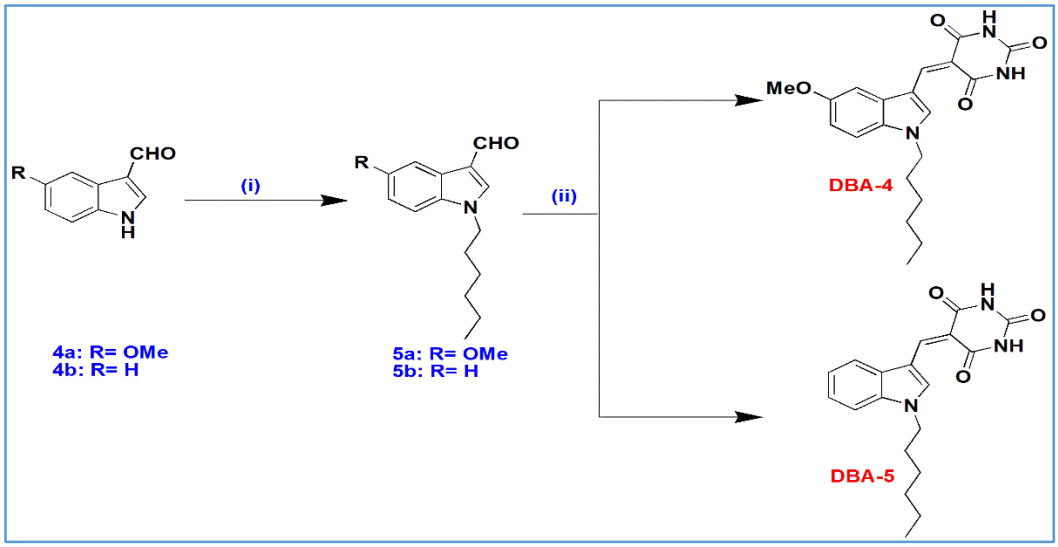

Scheme 6.2 Synthetic route of the co-sensitizers (i) 1-Bromohexane, K_2CO_3, DMF, RT (ii) Barbituric acid, CH_3OH, 80 ^0C

6.2.3 Optical, electrochemical and theoretical studies

The optical, electrochemical, EIS, photovoltaic and theoretical studies were carried out by following the procedures described in **section 3.2** of **chapter 3**.

6.2.4 DSSC fabrication

DSSCs were fabricated as per the procedure described in **section 3.2** of **chapter 3**. In the experiment, the dye solution was prepared by mixing of ruthenium based sensitizer (**NCSU-10**) and the respective co-sensitizer in 0.2 mM or 0.3 mM concentration, respectively with addition of CDCA at a concentration of 20 mM. The above solutions were used for DSSC device fabrication studies and their results are summarized in **Table 6.2**.

6.2.5 Synthetic methods

Synthesis of *5-bromo-1-hexyl-1H-indole (6.1)*

A solution of 5-bromo-1*H*-indole (1 g, 5.1 mmol), NaH (0.244 g, 0.01 mmol) in DMF (10 mL) was stirred at room temperature for 0.5 h under argon. Then 1-bromohexane (0.925 g, 5.6 mmol) was added into the mixture and stirred at room temperature for 12 h.

After the completion of reaction, water was added and neutralization was done using 2N HCl. The product was extracted with DCM. Further, organic phase was dried over sodium sulfate and the solvent was evaporated under reduced pressure. The residue was purified by column chromatography on silica gel using hexane as an eluent to give **6.1** as a colorless liquid. Yield: 83%. ^{1}H NMR (500 MHz, $CDCl_3$, ppm): δ 8.46 (d, *J* = 1.5 Hz, 1H), 7.69 (s, 1H), 7.42-7.40 (m, 1H), 7.24 (t, *J* = 9 Hz, 1H), 4.14 (t, *J* = 7 Hz, 2H), 1.90-1.84 (m, 2H), 1.31-1.29 (m, 6H), 0.87 (t, *J* = 7 Hz, 3H). Calcd. for $C_{14}H_{18}BrN$: C, 60.01; H,6.47; N, 5.00 found: C, 60.21; H, 6.41; N, 5.05. ESI-MS (+ve mode) *m/z* Calcd for $C_{14}H_{18}BrN$: 279.06. Found: 280.06 $[M+H]^+$.

Synthesis of *5-bromo-1-hexyl-1H-indole-3-carbaldehyde (6.2)*

A two neck round bottom flask was charged with freshly distilled DMF (1.56 mL, 5 eq) and $POCl_3$ (1.96 mL, 5 eq) was added to it drop-wise, with constant stirring at 0 ^{o}C under argon to obtain a glassy white solid and to this 5-bromo-1-hexyl-1*H*-indole (**6.1**, 1.2 g, 4.28 mmol) dissolved in dichloroethane (10 mL) was added while stirring. The stirring was continued at ambient temperature for 15 h. After completion of reaction, the reaction mass was poured into crushed ice and subsequently basified using 5M NaOH solution. The precipitated solid was filtered and the crude product was purified by column chromatography on silica gel using ethyl acetate/hexane (1:10) as mobile phase to give **6.2**. Light brown solid, yield 77%. ^{1}H NMR (500 MHz, $CDCl_3$, ppm): δ 9.95 (s, 1H), 8.46 (d, *J* = 1.5 Hz, 1H), 7.69 (s, 1H), 7.42-7.40 (m, 1H), 7.24 (t, *J* = 8.5 Hz, 1H), 4.14 (t, *J* = 7 Hz, 2H), 1.90-1.84 (m, 2H), 1.31-1.29 (m, 6H), 0.87 (t, *J* = 7 Hz, 3H). ^{13}C (125 MHz, $CDCl_3$, ppm): δ 184.19, 138.59, 135.87, 126.92, 124.80, 117.42, 116.51, 111.49, 47.50, 31.25, 29.69, 26.47, 22.44, 13.94. Anal. Calcd. for $C_{15}H_{18}BrNO$: C, 58.45; H,5.89; N, 4.54 found: C, 58.23; H, 5.81; N, 4.55. ESI-MS (+ve mode) *m/z* Calcd for $C_{15}H_{18}BrNO$: 307.06. Found: 308.06 $[M+H]^+$.

Synthesis of *1-hexyl-5-(4-methoxyphenyl)-1H-indole-3-carbaldehyde (6.3)*

A 15mL THF solution of compound **6.2** (0.5 g, 1.6 mmol), 4-methoxyphenylboronic acid (0.371 g, 2.44 mmol), Pd $(PPh3)_4$ (0.187 g, 0.16 mmol), and

2M K_2CO_3 (5 mL) was refluxed under argon atmosphere for 15 h. After cooling to room temperature, water was added to quench the reaction and extraction was done with dichloromethane (25 mL×3). The organic layer was dried over anhydrous sodium sulphate, and the solvent was removed under reduced pressure. The crude product was purified by column chromatography on silica with hexane / ethyl acetate mixture (15:1). Product **6.3** was obtained as off-white solid. Yield 79%.^{1}H NMR (500 MHz, $CDCl_3$, ppm): δ 10.02 (s, 1H), 8.49 (d, *J* = 1 Hz, 1H), 7.73 (s, 1H), 7.61 (d, *J* = 8.5 Hz, 2H), 7.55-7.53 (m, 1H), 7.41 (d, *J* = 8.5Hz, 1H), 6.99 (d, *J* = 8.5Hz, 1H), 4.19 (*t*, *J* = 7.5 Hz, 2H), 3.86 (s, 1H), 1.94-1.89 (*m*, 2H), 1.35-1.25 (m, 6H), 0.88 (*t*, *J* = 7Hz, 3H). Anal. Calcd. for $C_{22}H_{25}NO_2$: C, 78.77; H,7.51; N, 4.18 found: C, 78.61; H,7.49; N, 4.17. ESI-MS (+ve mode) *m/z* Calcd for $C_{20}H_{21}NO_2S$: 335.19 Found: 336.19 $[M+H]^+$.

Synthesis of *1-hexyl-5-methoxy-1H-indole-3-carbaldehyde* (5a)

A mixture of 1-bromohexane (0.565 g, 3.42 mmol), 5-methoxy-1*H*-indole-3-carbaldehyde (0.5 g, 2.85 mmol) and potassium carbonate (0.591 g, 4.28 mmol), in DMF (15 mL) was stirred at 30 ^{0}C for 10 h. After completion of the reaction, the contents were neutralized with 2N HCl and the product was extracted using ethylacetate (50 mL×3). Organic phase was dried using sodium sulfate. Then, ethyl acetate was removed under reduced pressure. The crude oily product obtained was purified by column chromatography on silica gel using hexane as an eluent, to get a white solid. Yield: 83%. 1H NMR (400 MHz DMSO-d_6, ppm):d 9.93 (s,1H), 7.79 (s,1H), 7.64 (s, 1H), 7.24 (d, J = 9 Hz, 1H), 6.95 (s, J = 8.5 Hz, 1H), 4.10 (t, J = 7 Hz, 2H), 3.89 (s, 3H),1.85 (d, J = 6 Hz, 2H),1.30 (s, 6H), 0.87 (t, 3H). ESI-MS (+ve mode) m/z Calcd for $C_{16}H_{21}N_2O_2$: 259.16. Found: 260.16 $[M+H]^+$.

Synthesis of *1-hexyl-1H-indole-3-carbaldehyde (5b)*

A mixture of 1-bromohexane (0.682 g, 4.13 mmol), indole-3-carbaldehyde (0.5 g, 3.44 mol), potassium carbonate (0.571 g, 4.13 mmol), in DMF (15 mL) was stirred at room temperature for 10 h. The reaction was then neutralized with 2N HCl and the product was extracted using ethyl acetate/water (50 mL×3). Organic phase was dried using sodium

sulfate. The solvent was removed under reduced pressure and the crude oily product obtained was further purified by column chromatography on silica gel using hexane as an eluent. The product was a light brown colored liquid. Yield: 85%. ^{1}H NMR (400 MHz, DMSO-d_6): δ (ppm) 9.92 (s, 1H), 8.32 (s, 1H), 8.13 (d, J = 7.6 Hz, 1H), 7.61 (d, J = 8.4 Hz, 1H), 7.33-7.23 (m, 2H), 4.26 (t, *J* = 6.8 Hz, 2H), 1.78 (t, J = 6.5 Hz, 2H), 1.24 (s, 6H), 0.83 (t, J = 6.8 Hz, 3H). Anal. Calcd for $C_{15}H_{19}NO$: C, 78.56; H, 8.35; N, 6.11 found: C 78.66; H, 8.43; N, 6.19.

Synthesis of *5-((1-hexyl-5-(4-methoxyphenyl)-1H-indol-3-yl)methylene)pyrimidine-2,4,6(1H,3H,5H)-trione (*DBA-3*)*

A mixture of 1-hexyl-5-(4-methoxyphenyl)-1*H*-indole-3-carbaldehyde (**6.3**, 0.5g, 1.49 mmol) and barbituric acid (0.210 mg, 1.63 mmol) was refluxed in absolute methanol for 5 h. The obtained precipitate was filtered and recrystallized from methanol to obtain bright yellow color solid. Yield 83%. ^{1}H NMR (400 MHz DMSO-d_6, ppm): δ 11.14 (s, 1H), 11.06 (s, 1H), 9.55 (s, 1H), 8.75 (s, 1H), 8.03 (s, 1H), 7.78-7.72 (m, 3H), 7.06 (s, 2H), 4.42 (s, 2H), 3.82 (s, 3H), 1.85 (s, 2H), 1.29 (s, 6H), 0.84 (s, 3H). ^{13}C (100 MHz, DMSO-d_6) δ (ppm): 165.02, 163.71, 150.89, 142.78, 135.85, 133.62, 130.84, 128.68, 123.26, 115.93, 114.86, 112.74, 111.28, 108.96, 55.65, 47.57, 31.15, 29.70, 26.18, 22.42, 14.32. Anal. Calcd. for $C_{26}H_{27}N_3O_4$: C, 70.09; H, 6.11; N, 9.43 found: C, 70.09; H, 6.11; N, 9.41 ESI-MS (+ve mode) *m/z* Calcd for $C_{26}H_{27}N_3O_4$: 445.20 Found: 446.20 $[M+H]^+$.

Synthesis of *5-((1-hexyl-5-methoxy-1H-indol-3-yl)methylene)pyrimidine-2,4,6(1H,3H,5H)-trione (*DBA-4*)*

The compound **DBA-4** was synthesized by refluxing **5a** (0.5 g, 1.92 mmol) with barbituric acid (0.271 mg, 2.12 mmol) in absolute methanol for 6 h. The obtained product was filtered and recrystallized from methanol to obtain yellow solid. Yield: 85%. ^{1}H NMR (400 MHz DMSO-d_6, ppm): δ 11.11 (s, 1H), 11.01 (s, 1H), 9.48 (s, 1H), 8.62 (s, 1H), 7.61 (d, *J* = 6.5 Hz, 1H), 7.34 (s, 1H), 6.98 (d, *J* = 7 Hz, 1H), 4.34 (s, 2H), 3.88 (s, 3H), 1.81 (s, 2H), 1.27 (s, 6H), 0.82 (d, *J* = 5 Hz, 3H). ^{13}C (100 MHz, DMSO-d_6) δ (ppm): 168.24, 165.10, 163.72, 156.95, 152.12, 150.90, 143.58, 142.46, 131.72, 131.42, 113.78, 113.30,

111.10, 108.07, 100.72, 56.05, 47.62, 31.11, 29.60, 26.14, 22.40, 14.29. Anal. Calcd. for $C_{20}H_{23}N_3O_4$: C, 65.03; H, 6.28; N, 11.37 found: C, 65.17; H, 6.31; N, 11.43 ESI-MS (+ve mode) *m/z* Calcd for $C_{20}H_{23}N_3O_4$: 369.17 Found: 370.17 $[M+H]^+$.

Synthesis of *5-((1-hexyl-1H-indol-3-yl)methylene)pyrimidine-2,4,6(1H,3H,5H)-trione (*DBA-5*)*

The compound **DBA-5** was synthesized by refluxing **5b** (0.5 g, 2.18 mmol) with barbituric acid (0.307 mg, 2.40 mmol) in absolute methanol for 5 h. The obtained precipitate was filtered and recrystallized from methanol to obtain yellow solid. Yield: 87%. ^{1}H NMR (400 MHz DMSO-d_6, ppm): δ 11.05 (s, 2H), 9.53 (s, 1H), 8.67 (s, 1H), 7.91 (s, 1H), 7.72(s, 1H), 7.38 (s, 1H), 4.39 (s, 2H), 1.83 (s, 2H), 1.28 (s, 6H), 0.83 (d, J = 5 Hz, 3H). ^{13}C (100 MHz, DMSO-d_6) δ (ppm): 168.23, 164.99, 163.69, 152.12, 150.90, 143.40, 142.33, 136.97, 130.24, 124.27, 123.53, 118.41, 112.32, 110.98, 108.96, 47.45, 31.13, 29.64, 26.17, 22.41, 14.31. Anal. Calcd. for $C_{19}H_{21}N_3O_3$: C, 67.24; H, 6.24; N, 12.38 found: C, 67.44; H, 6.29; N, 12.31 ESI-MS (+ve mode) *m/z* Calcd for $C_{19}H_{21}N_3O_3$: 339.16 Found: 340.16 $[M+H]^+$.

6.3 RESULTS AND DISCUSSION

6.3.1 Structural characterization

The chemical structures of newly synthesized compounds were confirmed by ^{1}H NMR, ^{13}C NMR spectroscopy and elemental analysis. The compound **DBA-3**, in its ^{1}H NMR spectrum showed unique resonances at δ 11.14 and 11.06 ppm for the protons of aromatic amines in the barbituric acid segment. Appearance of a singlet at δ 9.55 ppm confirmed the presence of a proton at the second position of the indole ring. All the other aromatic protons depicted peaks between 8.75 and 7.06 ppm. Also, two protons of $–NCH_2$ of hexyl chain resonated as a singlet at δ 4.42 ppm, whereas the protons corresponding to $–OCH_3$ group resonate at 3.82 ppm. Further, the appearance of signals due to primary and secondary protons in the range of δ 1.85-0.84 ppm in ^{1}H NMR spectrum confirmed the presence of hexyl chain. The ^{13}C NMR spectrum of **DBA-3** showed the characteristic signals at higher frequency (downfield region). The three keto carbon atoms resonate at δ

165.02, 163.71 and 159.18 ppm. The remaining signals appearing in the region of δ 150.89-108.96 ppm are due to other aromatic carbons. The first carbon in the hexyl chain attached directly to the aromatic nitrogen in the indole ring displayed a peak at 47.57 ppm. Further, the remaining aliphatic carbons appeared between 31.15-14.32 ppm. Furthermore, its mass spectrum showed the $[M+H]^+$ peak at 445.20, which is in agreement with the calculated molecular weight for the formula of $C_{26}H_{27}N_3O_4$. Similar observations were made for other two sensitizers (**DBA-4** and **DBA-5**) as well. The ^{1}H NMR spectrum of **DBA-4** depicted unique resonances at δ 11.13 and 11.01 ppm for the protons of aromatic amines in the barbituric acid segment. Appearance of a singlet at δ 9.48 ppm vindicated the presence of an aromatic proton at the second position of the indole ring. All the other aromatic protons resonated at the appropriate frequencies and similar trends were observed for aliphatic protons as well. **Fig.6.2-6.4** show ^{1}H NMR, ^{13}C NMR and Mass spectra of compound **DBA-3** respectively, whereas **Fig.6.5** depicts ^{1}H NMR spectrum of compound **DBA-4.**

Spectrograms of selected target compounds

^{1}H NMR, ^{13}C NMR and Mass spectra of representative title compounds are given below:

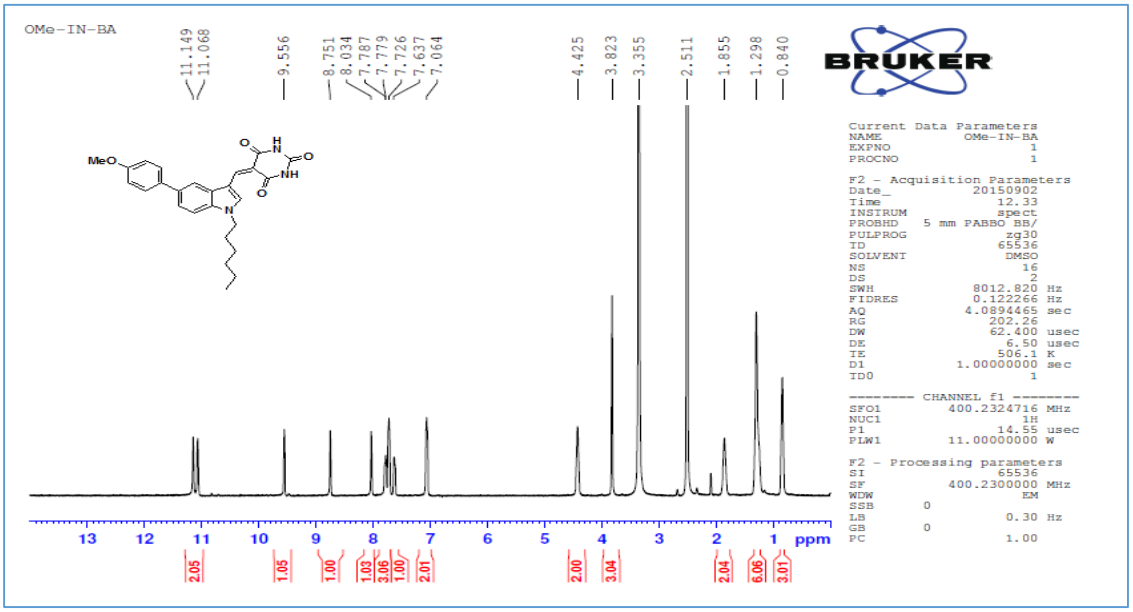

Fig.6.2 ^{1}H NMR spectrum of **DBA-3** in DMSO-d_6

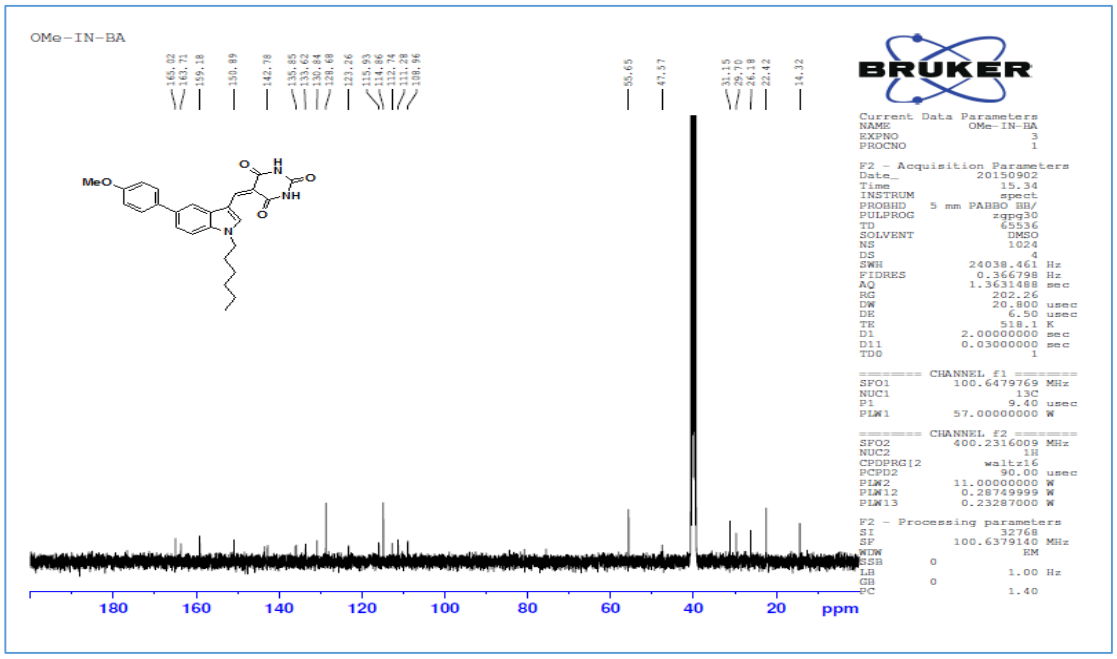

Fig.6.3 ^{13}C NMR spectrum of **DBA-3** in DMSO-d_6

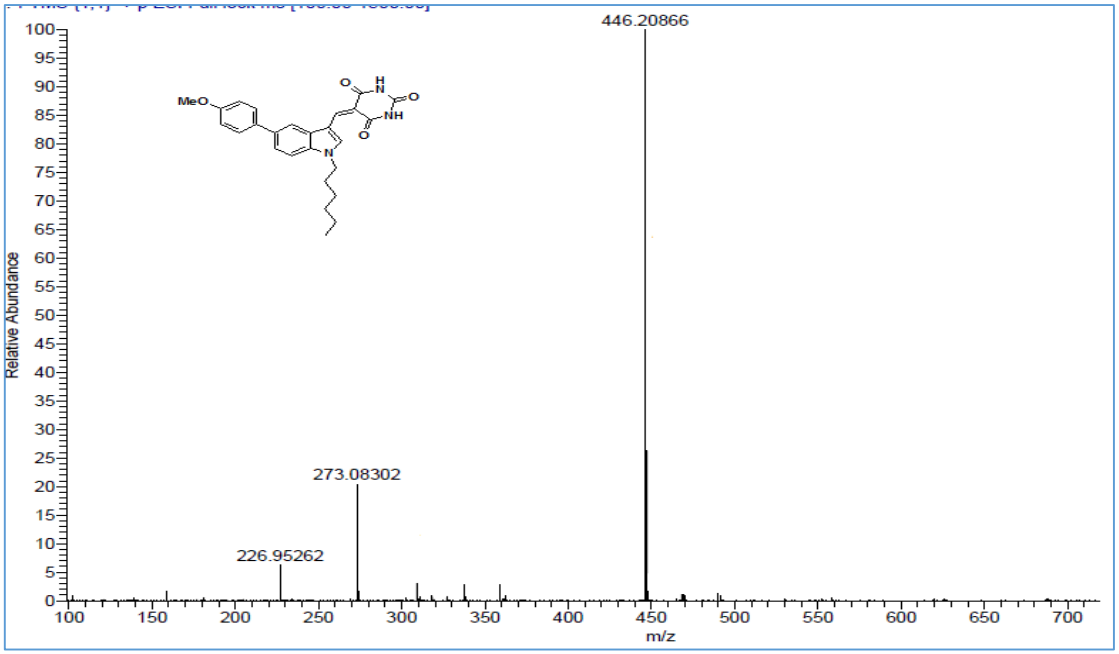

Fig.6.4 Mass spectrum of **DBA-3**

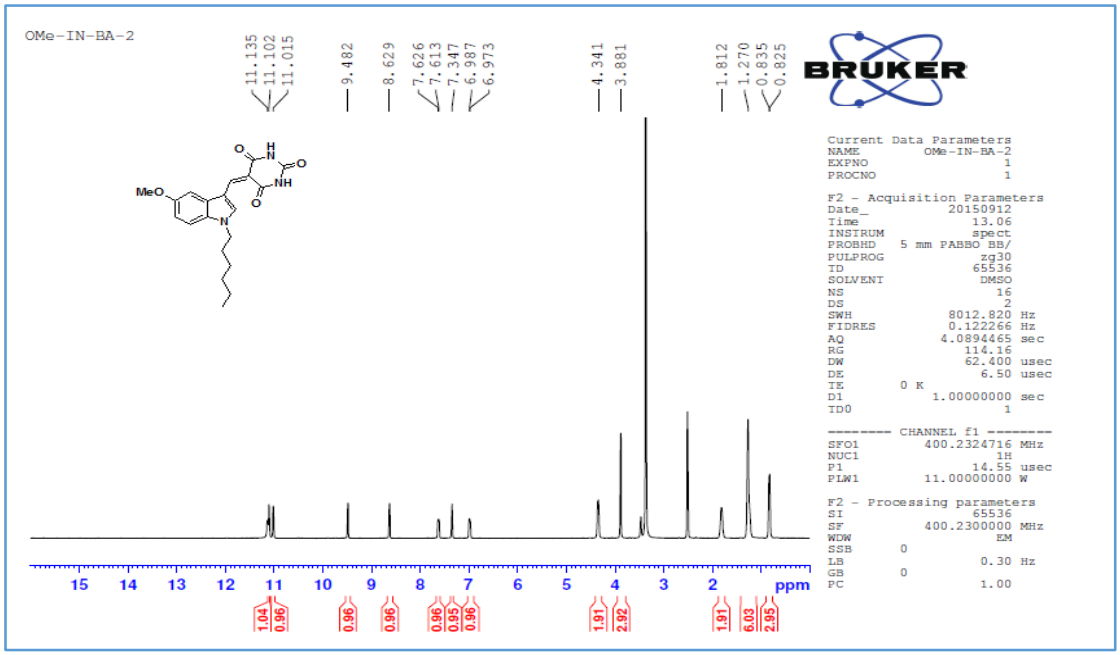

Fig.6.5 ^{1}H NMR spectrum of **DBA-4** in DMSO-d_6

6.3.2 Photophysical properties

The absorption and emission spectra of the co-sensitizers were recorded in $CHCl_3$ and are depicted in **Fig.6.6 (a)** and **(b)**, respectively; whereas the corresponding data are depicted in **Table 6.1**. From the absorption spectrum, it is evident that the dyes exhibit two distinct bands. The band, in the lower wavelength region is ascribed to the π-π* electronic excitations localized within the auxiliary donor and indole π-conjugated segment, while the band centered around 430 nm can be attributed to the charge transfer (CT) from indole donor to the barbituric acid acceptor moiety. Further, the fluorescence emission spectra of the co-sensitizers were recorded upon their excitation wavelengths and the relating results are tabulated in **Table 6.1**, whereas the corresponding spectra are shown in **Fig.6.6 (b)**. Furthermore, the large values of Stokes shift obtained in these co-sensitizers can be ascribed to the efficient charge transfer from the indole donor moiety to the two barbituric acid acceptor groups. **Fig.6.6 (c)** depicts the UV-visible spectrum of **NCSU-10**. It is

important to note that, the molar extinction coefficients for the charge transfer transition in these dyes are considerably higher than the ruthenium-based sensitizers.

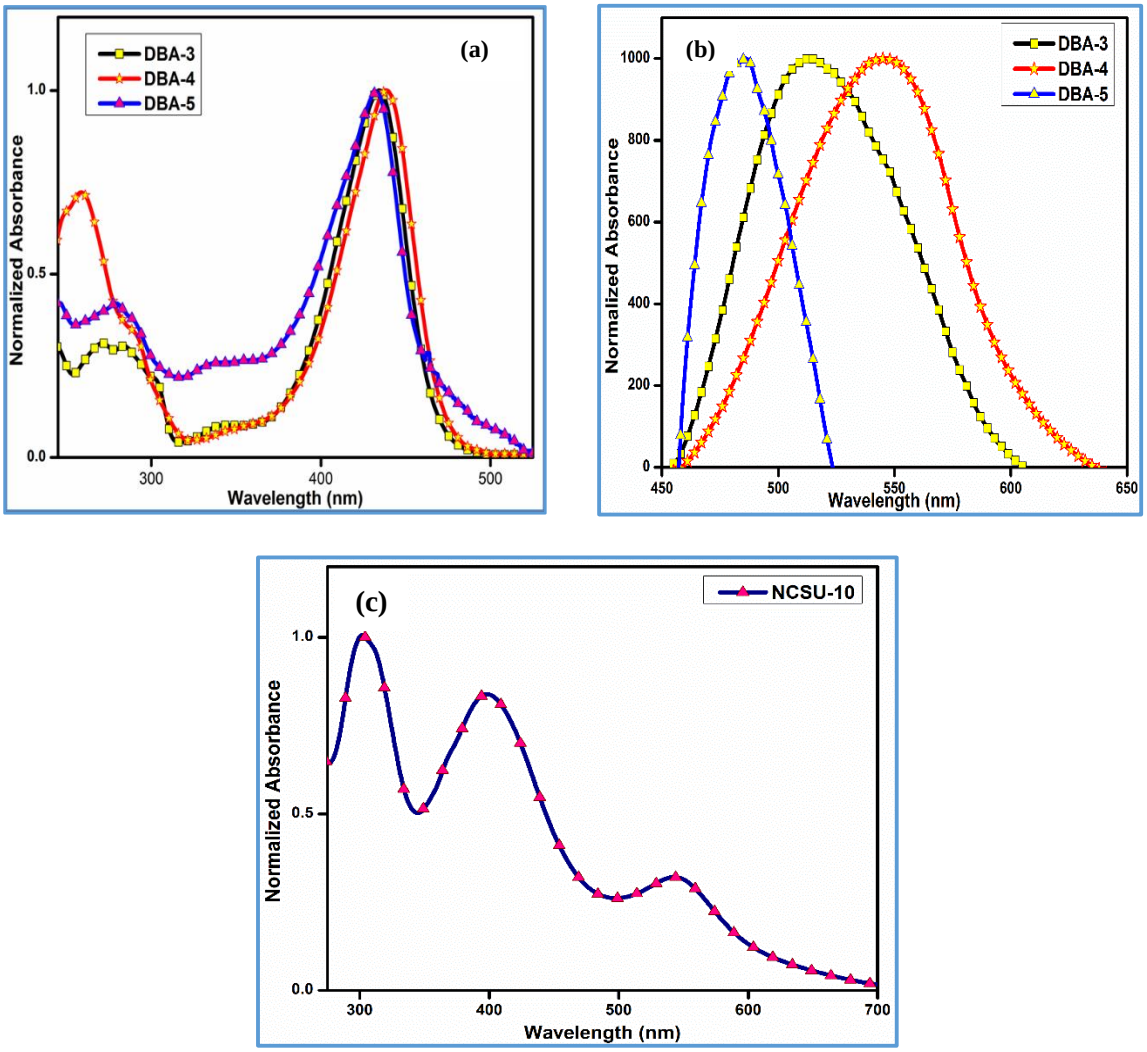

Fig.6.6 (a) UV-visible spectra of co-sensitizers in $CHCl_3$ (10^{-5} M) **(b)** Fluorescence spectra of co-sensitizers in $CHCl_3$ (10^{-5} M) **(c)** UV-visible spectrum of **NCSU-10**

These high values of molar extinction coefficients exhibited by the organic dyes can minimize the amount of the dye required to yield appropriate optical density, this can provide enough space on the TiO_2 for the attachment of other sensitizer molecules.

Table 6.1 Absorption and emission properties for **DBA-3**, **DBA-4**, **DBA-5** and **NCSU-10**

Sensitizer	Absorption λ_{max} (nm)	Emission λ_{max} (nm)	Stokes shift (cm^{-1})	ε ($M^{-1}cm^{-1}$)	$E_{0\text{-}0}$
DBA-3	435	514	3530	29990	2.65
DBA-4	438	546	4520	42540	2.69
DBA-5	434	486	2520	32310	2.75
NCSU-10	545	758	4900	20650	1.88

6.3.3 Molecular modeling

To gain a deeper understanding into the electronic and optical properties of the newly synthesized co-sensitizers, DFT calculations were performed using Turbomole software package. Initially all the geometry were optimized by means of semi empirical AM1 basis with MOPAC in TmoleX. Further optimization of the aforementioned geometries were carried out using C_1 point group symmetry at DFT level *via* the Becke's three-parameter hybrid functional and Lee-Yang-Parr's gradient-corrected correlation functional (B3LYP). Further, in all the calculations, default convergence criteria were maintained for the optimizations. Furthermore, all the calculations were performed using def-TZVPP basis set. **Fig.6.7 (a)** portrays the optimized geometries and electron density distributions in the HOMOs and LUMOs of the co-sensitizers. From the **Fig.6.7 (a)**, it is apparent that in the HOMO levels of all the sensitizers, the electron density is mainly located on the corresponding donor segment, whereas in the LUMO levels, a distinct shift of the electron density towards π-bridge and acceptor group can be observed. Additionally, the close proximity of the LUMO levels to the anchoring group would facilitate better orbital overlap between the *3d* orbitals of titanium and hence, excited electrons can be efficiently injected into conduction band of TiO_2.

DYE	Optimized geometry	HOMO	LUMO
DBA-3	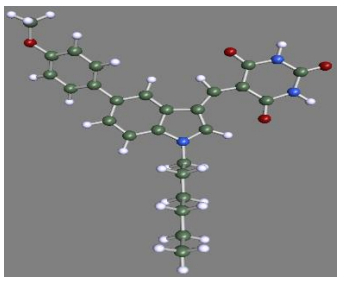	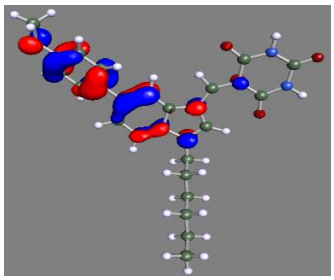	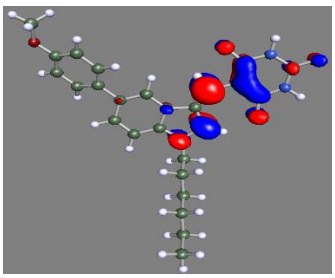
DBA-4	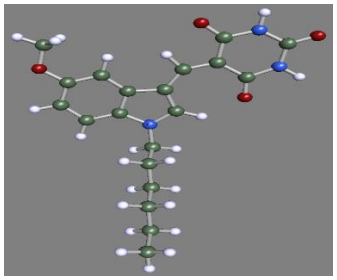	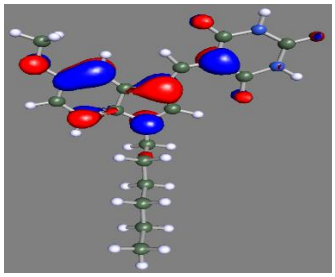	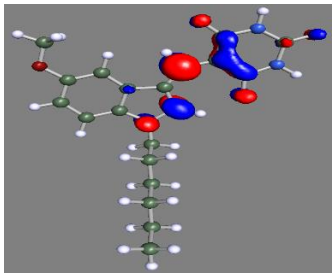
DBA-5	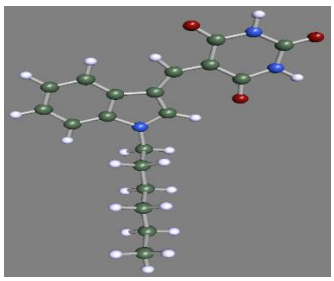	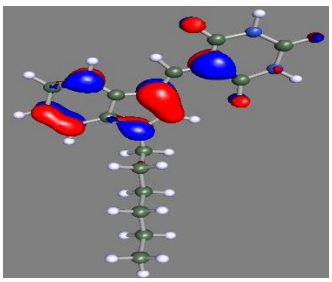	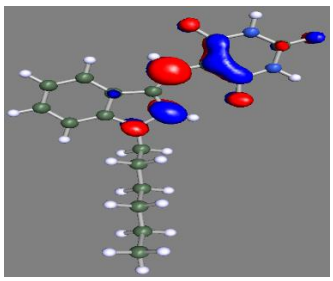

Fig.6.7 (a) Optimized structure and Frontier molecular orbitals of **DBA-3**, **DBA-4** and **DBA-5**

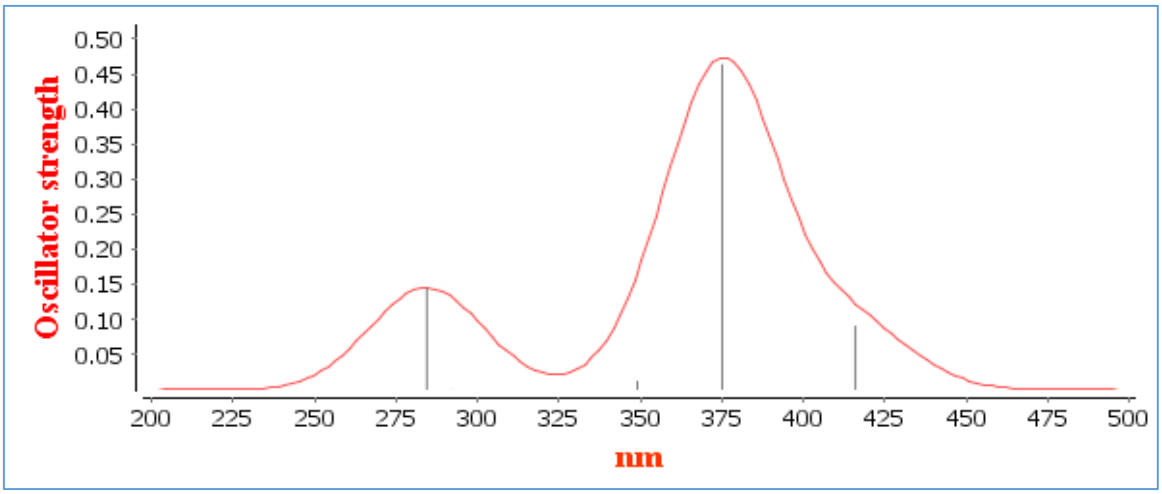

Fig.6.7 (b) Simulated absorption spectrum of **DBA-4**

Moreover, time-dependent density functional theory (TD-DFT) studies were conducted to examine the electronic excitations of co-sensitizers in presence of time-dependent perturbations. Typically, in TD-DFT, a time-dependent Schrödinger equation is solved to obtain the excited-state properties of the material. In TD-DFT an adiabatic approximation is made and following which temporal nonlocality is neglected. According to the aforementioned approximation, at any point of time, the exchange-correlation (xc) functional depends only on the instantaneous density.

Typically, the precision of the results acquired using TD-DFT profoundly depends on the functional and basis set employed for the calculations. The simulated absorption spectrum of **DBA-4** obtained at the B3LYP functional and def-TZVPP basis set is portrayed in **Fig.6.7 (b)**. Although, TD-DFT is known for its inabilities in precisely predicting energies related with long-range charge transfer states due to the self-interaction error in TD-DFT, which is owing to the electron transfer in the extended charge-transfer state. The above-mentioned variance is not observed in the present study, as the molecules under investigation are not large enough to display a long-range intramolecular charge transfer. From **Fig.6.7 (b)** it is evident that the simulated spectrum of **DBA-4** exhibits two distinct bands, corresponding to π-π* and charge transfer process. Further, the simulated

spectrum is well in accordance with the experimentally obtained one. The accuracy of TD-DFT studies demonstrate the validity of the basis set and functional used for the calculation.

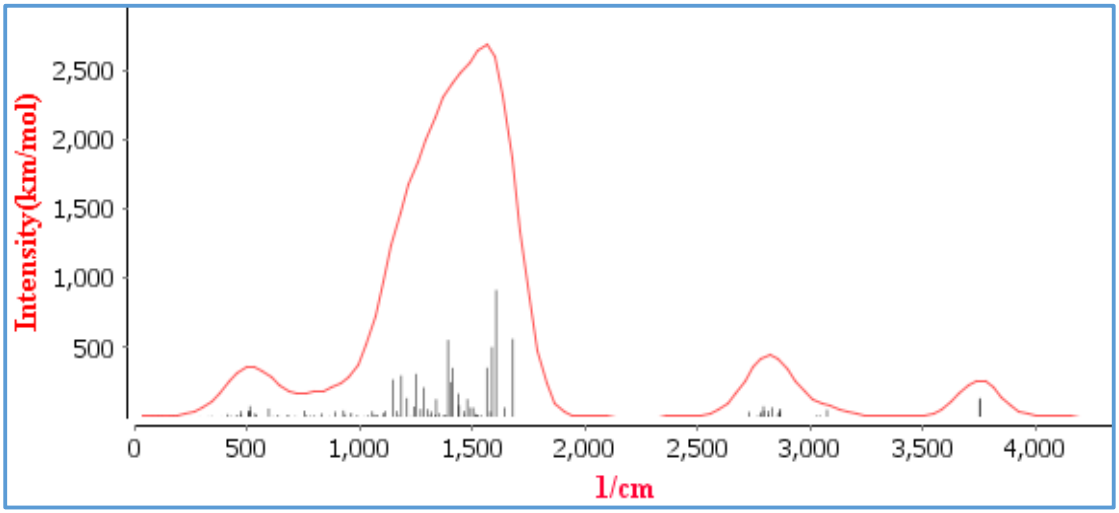

Fig.6.8 Theoretically obtained FT-IR spectrum of **DBA-4**

Further, the IR-absorption spectrum of the co-sensitizer has been simulated using Turbomole software. **Fig.6.8** portrays the simulated FT-IR spectrum of **DBA-4**. As anticipated, the theoretically obtained spectrum is well in agreement with the experimentally acquired one.

6.3.4 Electrochemical characterization

Cyclic voltammetry (CV) was employed to investigate the electrochemical behavior and to evaluate the position of the lowest unoccupied molecular orbital (LUMO and the highest occupied molecular orbital (HOMO) energy levels of the co-sensitizers. It is well established that, the efficient functioning of DSSCs necessitates that the LUMO level of the dye should be more negative than the conduction band edge of TiO_2 to ensure an effective electron injection from the dye molecules to the TiO_2 film and also, the HOMO level of the sensitizer is more positive than the redox potential of I_3^-/I^- to ensure the effective regeneration of dye molecules. **Fig.6.9** presents the energy band diagram of the indole based co-sensitizers. From the **Fig.6.9**, it is apparent that all the three co-sensitizers have a more negative GSOP (ground state oxidation potentials) (eV) than the Nernst

potential of the I^-/I_3^- redox couple (-5.2 eV) (Qu and Meyer 2001), indicating that the I^- species in the electrolyte can reduce and regenerate the oxidized dyes molecules and thereby preventing the charge recombinations between oxidized dye molecules and photo-injected electrons in the conduction band of the TiO_2. All the values in volts (V) against NHE were converted to electron volt (eV) using the equation:

$$ESOP = [(GSOP\ (V) + 4.7) - E_{0\text{-}0}]\ eV$$

The aforementioned equation was employed to calculate the ESOP (excited state oxidation potentials) levels of all the co-sensitizers by using GSOP values and zeroth–zeroth energy (E_{0-0}) of the corresponding co-sensitizer. It is evident that, the LUMO levels of all the co-sensitizers are sufficiently more negative than the conduction band edge of TiO_2 and hence, providing ample thermodynamic driving force for efficient electron injection. The negative free energy for electron injection is in the order: **DBA-4** > **DBA-5** > **DBA-3**. From the aforementioned data, it can be envisaged that, co-sensitizer **DBA-4** would be more efficient in injecting electrons into the conduction band of TiO_2 than the other two co-sensitizers.

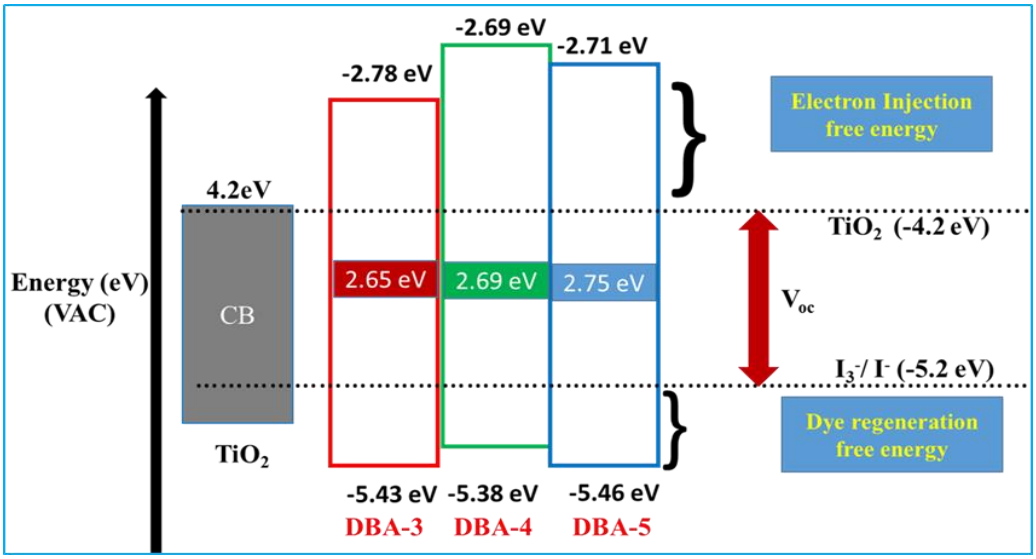

Fig.6.9 Energy level diagram of **DBA-3, DBA-4** and **DBA-5** co-sensitizers.

Thus, although all the three co-sensitizers fulfill the necessary criteria required for a molecule to act as a sensitizer, there is a stark contrast between the thermodynamic feasibility of electron injection. This difference might prove to be crucial in determining overall efficiency of the co-sensitized devices.

6.3.5 Photovoltaic device characterization

The photovoltaic performance of devices sensitized using **NCSU-10** alone and co-sensitized using **DBA-3**, **DBA-4** and **DBA-5** on a nanocrystalline TiO_2 electrode have been investigated under standard AM 1.5 irradiation (100 $mWcm^{-2}$). The photovoltaic properties of the co-sensitized devices were studied in order to comprehend the ramifications of axillary donor's architecture in the co-sensitizers and to establish a relationship between the structure of the co-sensitizers and their performance in the cell. The introduction of varying electron donating substituent on the principal donor group in all co-sensitizers have had profound influence on the incident photon-to-current conversion efficiency and photovoltaic properties of the co-sensitized devices. The device co-sensitized using **DBA-4** with methoxy group as axillary donor showed superior performance than the device co-sensitized using **DBA-5** and the one co-sensitized using **DBA-3**, which showed the lowest photovoltaic properties. Although, the ruthenium sensitizer **NCSU-10** absorbs light in a wide range of wavelengths, the co-sensitizers are employed to perceive the potential of novel co-sensitizers for improving the light harvesting efficiency in the range from 400 to 500 nm and to try and suppress the dark current due to back electron transfer between injected electrons in the conduction band of TiO_2 and triiodide species present in the electrolyte.

The molar extinction coefficients of the co-sensitizers are in the range from 2.9×10^4 to 4.2×10^4 $M^{-1}cm^{-1}$, which is much higher than that of I_3^- (2.5×10^4 $M^{-1}cm^{-1}$) at this wavelength. Therefore, the aforementioned co-sensitizers should be effective in reducing the competitive absorption of light by I_3^- and thereby resulting in an enhancement in IPCE efficiency. Moreover, owing to their small size the organic co-sensitizers can cover the surface of the TiO_2 nanoparticles more efficiently, where the large sized three-dimensional ruthenium based dye (**NCSU-10**) molecules cannot get adsorbed, and hence providing a

better surface coverage. Further, the presence of co-sensitizers also helps in suppressing the charge recombinations caused by dye aggregation or close π-π stacking and thereby considerably improving the V_{oc} values. Current-voltage (*J-V*) characteristics of the cell based on **NCSU-10** and the corresponding co-sensitized solar cells are presented in **Fig.6.10**, while the corresponding photovoltaic parameters are summarized in **Table 6.2**. The photovoltaic performances (η %) of the DSSCs co-sensitized using 0.2 mM of **DBA-3**, 0.3 mM of **DBA-3, DBA-4** and **DBA-5** are 8.61, 8.60, 10.12, and 9.20 %, respectively. In the quest to understand the reasons for this prevalent difference in the photovoltaic performances, IPCE studies were performed (**Fig.6.11)**. The pivotal cause for the enhanced photovoltaic performance of the cell co-sensitized by **DBA-4** and **DBA-5** with respect to the cell sensitized using only **NCSU-10** is the enhancement in photocurrent values. It was also proposed that, acidic co-adsorbents, such as CDCA, may act as a proton buffer for the dye, thus 'regulating' the dye proton content and assisting dye adsorption onto the semiconductor surface.

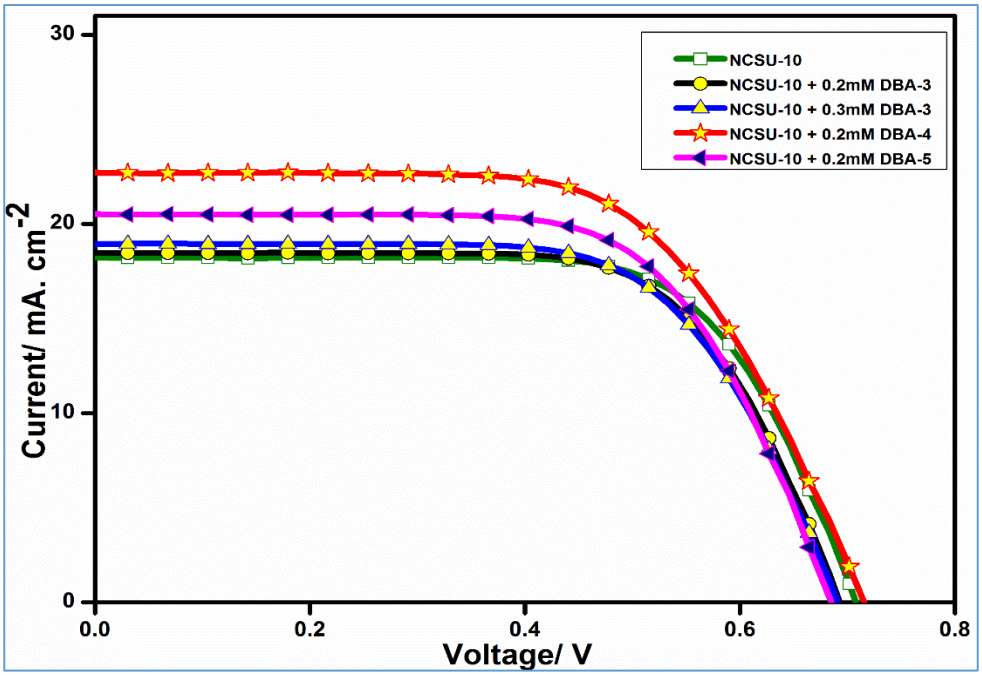

Fig.6.10 *J-V* characteristics of DSSCs based on **NCSU-10** and co-sensitized with **DBA-3**, **DBA-4** and **DBA-5**

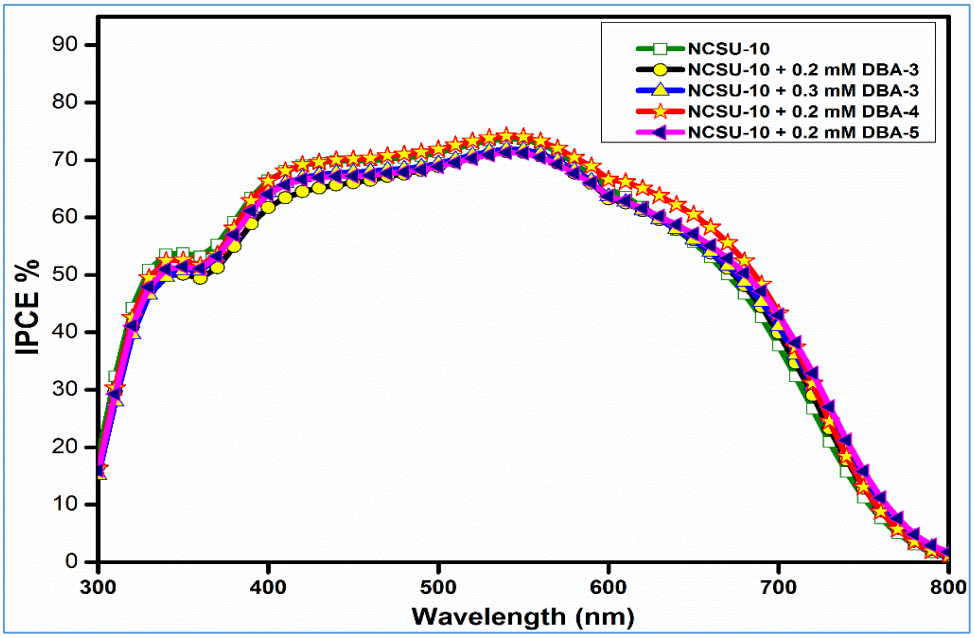

Fig. 6.11 IPCE spectra of the DSSCs based on **NCSU-10** and co-sensitized with **DBA-3**, **DBA-4** and **DBA-5**

Table 6.2 Photovoltaic parameters of DSSCs based on **NCSU-10** with/without co-sensitization

Sensitizer		CDCA (mM)	J_{SC} (mAcm^{-2})	V_{OC} (V)	*ff* (%)	η (%)
NCSU-10 (mM)	Co-sensitizers					
0.2	--	20	18.23 ± 0.04	0.706 ± 0.003	68.7 ± 0.2	8.84 ± 0.02
0.2	**DBA-3** 0.2 mM	20	18.47 ± 0.03	0.693 ± 0.002	67.3 ± 0.1	8.61 ± 0.01
0.2	**DBA-3** 0.3 mM	20	18.97 ± 0.04	0.690 ± 0.003	65.7 ± 0.2	8.60 ± 0.01
0.2	**DBA-4** 0.2 mM	20	22.69 ± 0.04	0.715 ± 0.003	62.4 ± 0.3	**10.12 ± 0.03**
0.2	**DBA-6** 0.2 mM	20	20.49 ± 0.04	0.687 ± 0.004	65.4 ± 0.3	9.20 ± 0.01

The aforementioned enhancement in photocurrent can be attributed to the improved light harvesting efficiency of the co-sensitized solar cell. Although, the devices co-sensitized using **DBA-3** also displayed improved light harvesting capabilities with a corresponding enhancement in J_{sc} values, but were dammed by lowered V_{oc} values as

compared to the cell sensitized by **NCSU-10** sensitizer alone. The drop in V_{oc} values suggests that the electron recombination rate has amplified as a result of co-sensitization, thereby leading to the inferior performance of the co-sensitized devices. All these observations were further established by performing electrochemical impedance spectroscopy analysis.

6.3.6 Electrochemical impedance spectroscopy characterization

Electrochemical impedance spectroscopy (EIS) provides rational insights into the charge dynamics of an operating solar cell and is powerful technique for evaluating the interfacial charge recombination dynamics and redox reaction process taking place at photoanode/electrolyte interface. **Fig.6.12** depicts the Nyquist plots of DSSC sensitized with only ruthenium based sensitizer **NCSU-10** as well as the devices co-sensitized using various co-sensitizers.

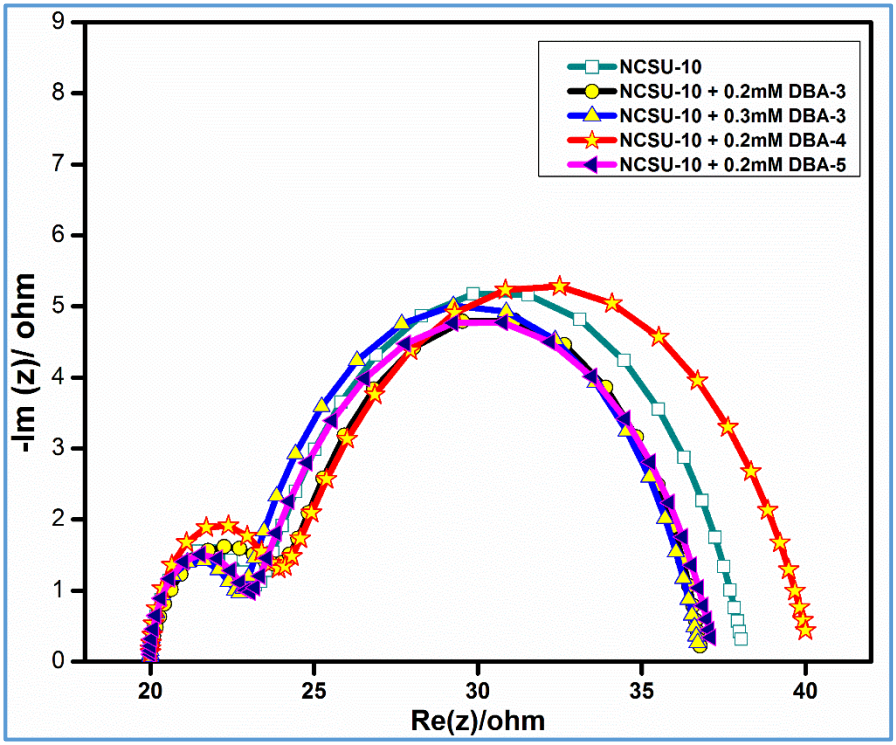

Fig.6.12 EIS Nyquist plots for DSSCs based on **NCSU-10** and co-sensitized with **DBA-3**, **DBA-4 and DBA-5**

As evidenced from the figure, all the devices depicted two distinct semicircles, the peak in high frequency region can be attributed to resistance at the counter electrode/electrolyte interface, whereas the peak in the middle frequency range is accredited to charge recombination resistance (R_{ct}) at TiO_2/dye/electrolyte interface. From the Nyquist plots it is evident that, radius of semicircle in the middle-frequency range decreased in the order: 0.2 mM **DBA-4**> **NCSU-10** > 0.2 mM **DBA-3** > 0.3 mM **DBA-3** > 0.2 mM **DBA-5**. The higher electron recombination resistance observed for the device co-sensitized using **DBA-4** relative to other devices indicates more effective suppression of the back reaction of the injected electrons with triiodide species in the electrolyte. The aforementioned is reflected in the improvements observed in the J_{sc} or V_{oc} value, yielding substantially enhanced device efficiency for the device co-sensitized using **DBA-4**.

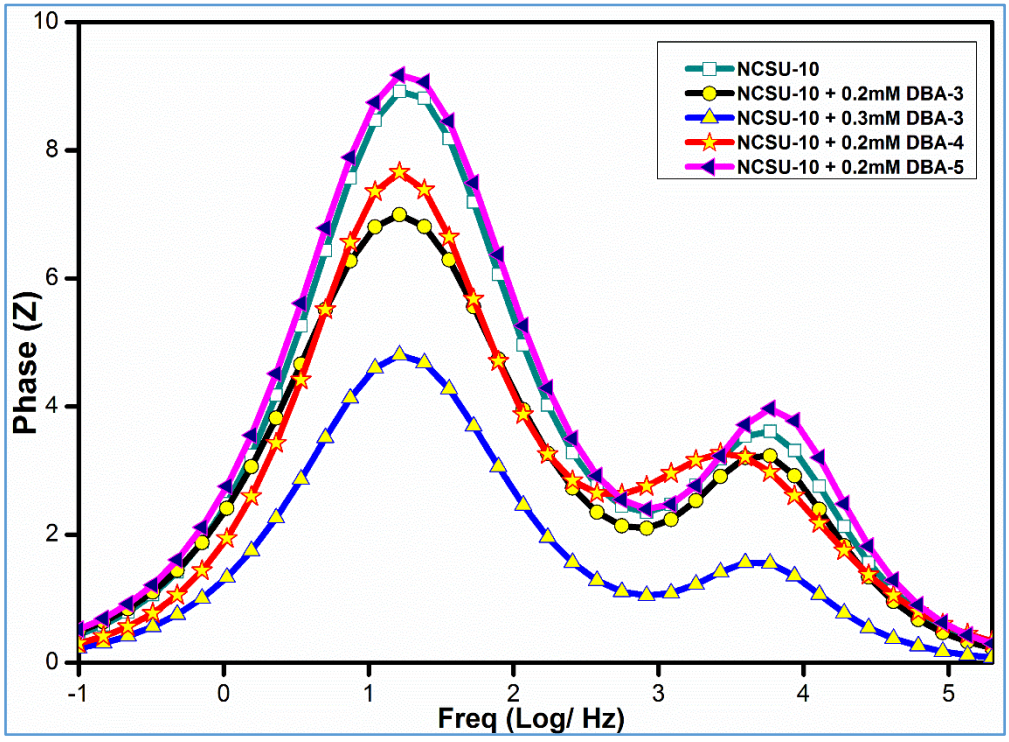

Fig. 6.13 Bode plots for DSSCs based on **NCSU-10** and co-sensitized with **DBA-3**, **DBA-4** and **DBA-5**

Further, the Bode plots (**Fig.6.13)** for all the dvices also exhibit two distinct peaks: one at lower frequency and another one at higher frequency. From the literature, it is well established that, the characteristic frequency at the lower frequency peak in the Bode plot is related to the charge recombination rate, and is associated with the electron lifetime according to the relation: $\tau_{CB} = 1 / (2\pi f)$, where τ is the lifetime of electrons in TiO_2 and f is the intermediate frequency peak from Bode plot. The electron lifetimes for the DSSCs co-sensitized using 0.2mM **DBA-3**, 0.3mM **DBA-3**, 0.2mM **DBA-4** and 0.2mM **DBA-5** were found to be 9.3, 8.7, 10.5 and 8.5 ms, respectively. Whereas, the electron lifetime in the device sensitized using only **NCSU-10** was found to be 9.8 ms. These results suggest that the charge recombination is suppressed in the device co-sensitized using **DBA-4**, when compared to the other two co-sensitizers (**DBA-3** and **DBA-5**). The calculated electron lifetime values are well in agreement with the V_{oc} values of these devices (**Table 6.2**).

6.4 Conclusions

In conclusion, three metal-free organic molecules (**DBA-3**, **DBA-4** and **DBA-5**) have been successfully designed and synthesized as effective co-sensitizers for application in DSSCs. A systematic exploration between the structure and photovoltaic performance of the co-sensitizers has been carried out. Further, based on the IPCE and photovoltaic studies, it is evident that, all the three co-sensitizers were successful in enhancing light harvesting efficiency and thereby increasing the photocurrent in the co-sensitized devices. The EIS studies revealed that, only the device co-sensitized using **DBA-4** was capable in effectively suppressing the undesirable charge recombinations occurring in the cell and longer electron lifetime, resulting in the highest PCE of **10.12 %** among the studied DSSCs. In addition, the profound role of axillary donor groups on the co-sensitization properties has been demonstrated. Finally, it is believed that, the aforementioned structure-performance relationships will facilitate in enhancing the overall efficiency of DSSCs.

CHAPTER 7

AN INDOLE BASED CO-SENSITIZER CARRYING DUAL ANCHORING GROUPS: SYNTHESIS, CHARACTERIZATION AND PHOTOVOLTAIC EVALUATION

Abstract

*This chapter covers synthetic methods and structural characterization of a newly designed organic co-sensitizer **DBA-8**. Further, it includes the photophysical, electrochemical, DFT and device fabrication studies of the co-sensitizer. Furthermore, a detailed account of discussion of the results pertaining to all the above studies have been incorporated.*

7.1 INTRODUCTION

A new unsymmetrical di-anchoring co-sensitizer **DBA-8**, having one donor and two acceptor/anchoring groups has been designed and synthesized as a potential co-sensitizer to be employed with ruthenium based dye **NCSU-10**. It has been synthesized from simple indole derivatives following well-known synthetic protocols and structures have been confirmed by various spectral and elemental analyses. Its optical, electrochemical, DFT and fabrication studies have been carried out. Further, results pertaining to all the aforesaid studies have been discussed. **Fig.7.1** depicts the chemical structures of the co-sensitizer **DBA-8** and ruthenium sensitizer **NCSU-10**.

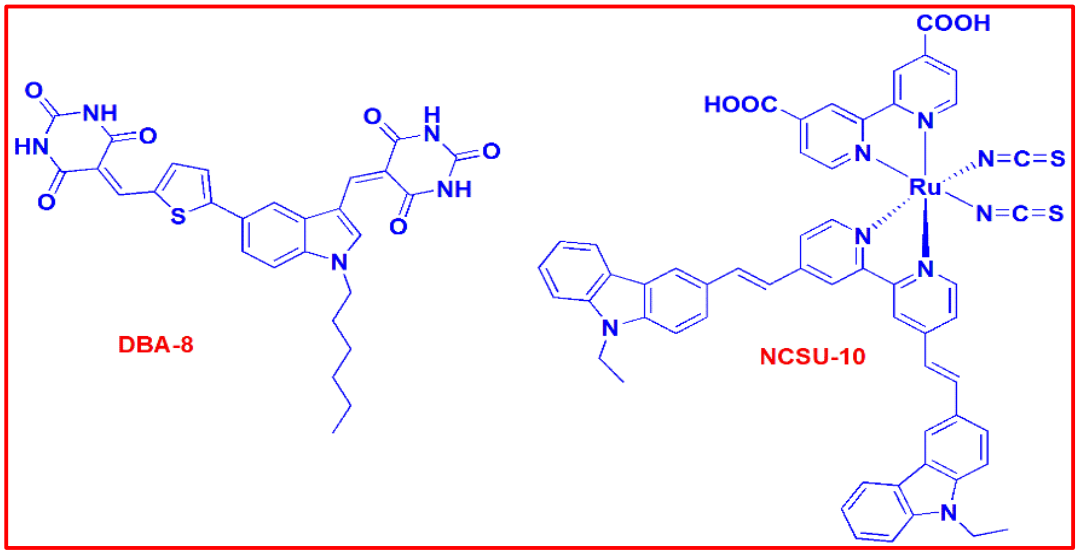

Fig.7.1 Chemical structures of co-sensitizer **DBA-8** and ruthenium sensitizer **NCSU-10**

7.2 EXPERIMENTAL

7.2.1 Materials and methods

The starting materials 5-bromo-1*H*-indole, 1-bromohexane, sodium hydride, 5-formylthiophen-2-ylboronic acid, tetrakis(triphenylphosphine)palladium(0) [$Pd(PPh_3)_4$] and barbituric acid, were obtained from Sigma-Aldrich. The solvents were dried prior to use following standard protocols. All the reactions were conducted under argon atmosphere and the reaction progression was monitored by TLC technique. Chromatographic separations were performed using silica gel (100-200 or 230-400 mesh). ^{1}H NMR and ^{13}C NMR spectra were recorded using Bruker avance 500 MHz and 400 MHz spectrometers, in $CDCl_3$ or DMSO-d_6 and tetramethylsilane as internal standard. Mass spectra were acquired from thermo scientific-EXACTIVE (ESI-MS), while the elemental analysis was attained from a Flash EA1112CHNS analyzer (Thermo Electron Corporation).

7.2.2 Synthesis of co-sensitizer (**DBA-8**)

The synthetic pathway of the new co-sensitizer **DBA-8** is depicted in **scheme 7.1**. N-alkylation of 5-bromo-1*H*-indole was done using 1-bromohexane to yield compound **7.1**. It was then subjected to Vilsmeier-Haack formylation to give **7.2**. The product was coupled with 5-formylthiophen-2-ylboronic acid *via* Suzuki coupling to yield **7.3**. Finally, Knoevenagel condensation of this aldehyde **7.3** with barbituric acid in methanol produced the co-sensitizer **DBA-8**.

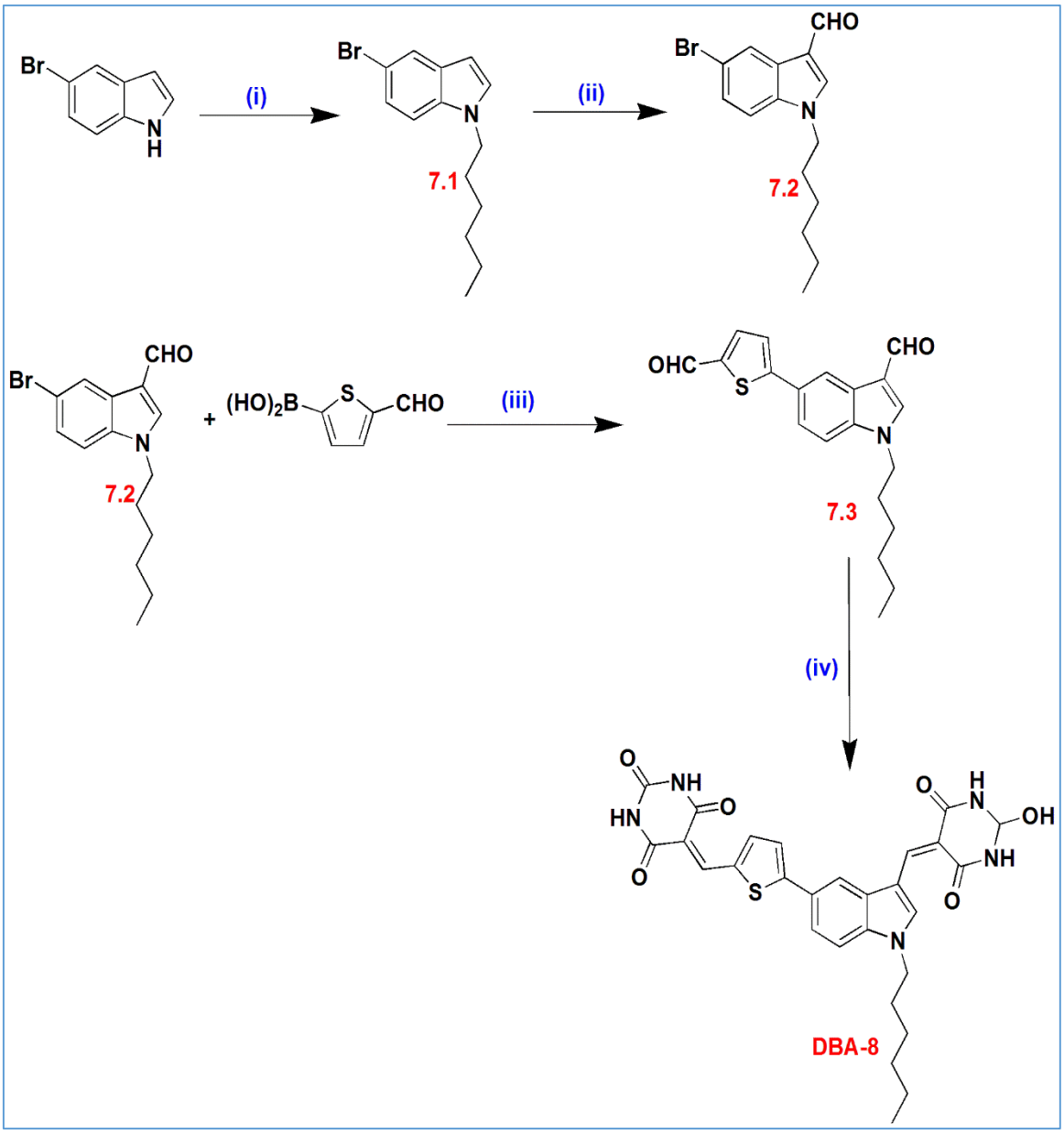

Scheme 7.1 Synthetic route of the co-sensitizer (i) 1-Bromohexane,NaH, DMF, RT (ii) $POCl_3$, DMF, RT (iii) Pd $(PPh_3)_4$, K_2CO_3, THF, ethanol, water (iv) Barbituric acid, CH_3OH, 80 ^0C

7.2.3 Optical, electrochemical and theoretical studies

The optical, electrochemical, EIS, photovoltaic and theoretical studies were carried out by following the procedures described in **section 3.2** of **chapter 3**.

7.2.4 DSSC fabrication

DSSC fabrications and characterizations were performed by following the procedures described in **section 3.2** of **chapter 3**.The dye solution used was a mixture of **NCSU-10** and the co-sensitizer **DBA-8** in 0.2 mM or 0.3 mM concentration, with addition of CDCA at a concentration of 20 mM.

7.2.5 Synthetic methods

Synthesis of *5-bromo-1-hexyl-1H-indole* (*7.1*)

A solution of 5-bromo-1*H*-indole (1 g, 5.1 mmol), NaH (0.244 g, 0.01 mmol) in DMF (10 mL) was stirred at room temperature for 0.5 h under argon. Then 1-bromohexane (0.925 g, 5.6 mmol) was added into the mixture and stirred at room temperature for 12 h. After the completion of reaction, water was added and neutralization was done using 2N HCl. The product was extracted with DCM (25 mL×2). Further, organic phase was dried over sodium sulfate and the solvent was evaporated under reduced pressure. The residue was purified by column chromatography on silica gel using hexane as an eluent to give **7.1** as a colorless liquid. Yield: 83%. ^{1}H NMR (500 MHz, $CDCl_3$, ppm): δ 8.46 (d, *J* = 1.5 Hz, 1H), 7.69 (s, 1H), 7.42-7.40 (m, 1H), 7.24 (t, *J* = 9 Hz, 1H), 4.14 (t, *J* = 7 Hz, 2H), 1.90-1.84 (m, 2H), 1.31-1.29 (m, 6H), 0.87 (t, *J* = 7 Hz, 3H). Calcd. for $C_{14}H_{18}$ BrN: C, 60.01; H,6.47; N, 5.00 found: C, 60.21; H, 6.41; N, 5.05. ESI-MS (+ve mode) *m/z* Calcd for $C_{14}H_{18}$ BrN: 279.06. Found: 280.06 $[M+H]^+$.

Synthesis of *5-bromo-1-hexyl-1H-indole-3-carbaldehyde* (*7.2*)

A two neck round bottom flask was charged with freshly distilled DMF (1.56 mL, 5 eq) and $POCl_3$ (1.96 mL, 5 eq) was added to it drop-wise, with constant stirring at 0 °C under argon to obtain a glassy white solid and to this 5-bromo-1-hexyl-1*H*-indole (**7.1**, 1.2 g, 4.28 mmol) dissolved in dichloroethane (10 mL) was added while stirring. The stirring was continued at ambient temperature for 15 h. After completion of reaction, the reaction mass was poured into crushed ice and subsequently basified using 5M NaOH solution. The precipitated solid was filtered and the crude product was purified by column

chromatography on silica gel using ethyl acetate/hexane (1:10) as mobile phase to give **7.2**. Light brown solid.Yield 77%. ^{1}H NMR (500 MHz, $CDCl_3$, ppm): δ 9.95 (s, 1H), 8.46 (d, *J* = 1.5 Hz, 1H), 7.69 (s, 1H), 7.42-7.40 (m, 1H), 7.24 (t, *J* = 8.5 Hz, 1H), 4.14 (t, *J* = 7 Hz, 2H), 1.90-1.84 (m, 2H), 1.31-1.29 (m, 6H), 0.87 (t, *J* = 7 Hz, 3H). ^{13}C (125 MHz, $CDCl_3$, ppm): δ 184.19, 138.59, 135.87, 126.92, 124.80, 117.42, 116.51, 111.49, 47.50, 31.25, 29.69, 26.47, 22.44, 13.94. Anal. Calcd. for $C_{15}H_{18}$BrNO: C, 58.45; H,5.89; N, 4.54 found: C, 58.23; H, 5.81; N, 4.55. ESI-MS (+ve mode) *m/z* Calcd for $C_{15}H_{18}$BrNO: 307.06. Found: 308.06 $[M+H]^+$.

Synthesis of *5-(5-formylthiophen-2-yl)-1-hexyl-1H-indole-3-carbaldehyde* (*7.3*)

A 15 mL THF solution of compound **7.2** (0.5 g, 1.6 mmol), 5-formylthiophen-2-ylboronic acid (0.279 g, 1.79 mmol), Pd $(PPh_3)_4$ (0.187 g, 0.16 mmol), and 2M K_2CO_3 (5 mL) was refluxed under argon atmosphere for 24 h. After cooling to room temperature, water was added to quench the reaction. The product was extracted with dichloromethane (25 mL×3). The organic layers was dried over sodium sulphate, and the solvent was removed under vacuum. The crude product was purified by column chromatography on silica with hexane/ethyl acetate mixture (20:1). Product **7.3** was obtained as a light orange solid. Yield 73%.^{1}H NMR (500 MHz, $CDCl_3$, ppm): δ 10.02 (s, 1H), 9.88 (s, 1H), 8.67 (d, *J* = 1.5 Hz, 1H), 7.76 (d, *J* = 4 Hz, 2H), 7.65-7.63 (m, 1H), 7.50 (d, *J* = 4 Hz, 1H), 7.42 (d, *J* = 8.5Hz, 1H), 4.19 (*t*, *J* = 7.0 Hz, 2H), 1.91 (*t*, *J* = 7.0 Hz, 2H), 1.37-1.30 (m, 6H), 0.88 (*t*, *J* = 7Hz, 3H). ^{13}C (125 MHz, $CDCl_3$, ppm): 184.40, 182.75, 168.70, 155.27, 144.53, 142.02, 139.21, 137.67, 128.20, 125.96, 123.98, 122.93, 120.31, 118.38, 110.86, 99.99, 94.04, 93.08, 47.53, 31.26, 29.78, 29.68, 29.35, 26.49, 22.45, 13.94. Anal. Calcd. for $C_{20}H_{21}NO_2S$: C, 70.77; H,6.24; N, 4.13 found: C, 70.61; H,6.29; N, 4.17. ESI-MS (+ve mode) *m/z* Calcd for $C_{20}H_{21}NO_2S$: 339.13 Found: 340.13 $[M+H]^+$.

Synthesis of *5-((5-(1-hexyl-3-((2,4,6(1H,3H,5H)-trione-tetrahydropyrimidin-5(6H)-ylidene)methyl)-1H-indol-5-yl)thiophen-2-yl)methylene)pyrimidine-2,4,6(1H,3H,5H)-trione* (DBA-8)

A mixture of 5-(5-formylthiophen-2-yl)-1-hexyl-1*H*-indole-3-carbaldehyde (**7.3**, 500 mg, 1.05 mmol) and barbituric acid (135 mg, 1.05 mmol) was refluxed in absolute methanol for 5 h. The precipitate was filtered and recrystallized from methanol to obtain dark green solid. Yield 85%. ^{1}H NMR (400 MHz DMSO-d_6, ppm): δ 11.29 (s, 2H), 11.20 (s, 1H), 11.12 (s, 1H), 9.55 (s, 1H), 8.72 (s, 1H), 8.51 (s, 1H), 8.32 (s, 1H), 8.22 (s, 1H), 7.95 (s, 1H), 7.86 (s, 2H), 4.43 (s, 2H), 1.84 (s, 2H), 1.29 (s, 6H), 0.82 (s, 3H). ^{13}C (100 MHz, DMSO-d_6) δ (ppm): 164.89, 164.03, 163.73, 159.30, 150.85, 150.77, 148.06, 143.16, 137.63, 135.64, 135.36, 130.81, 128.34, 111.33, 110.83, 110.02, 47.59, 31.13, 29.74, 26.15, 22.41, 14.31. Anal. Calcd. for $C_{28}H_{25}N_5O_6S$: C, 60.10; H, 4.50; N, 12.52 found: C, 60.21; H, 4.55; N, 12.47 ESI-MS (+ve mode) *m/z* Calcd for $C_{28}H_{25}N_5O_6S$: 559.15 Found: 560.15 $[M+H]^+$.

7.3 RESULTS AND DISCUSSION

7.3.1 Structural characterization

The chemical structures of newly synthesized compounds were confirmed by different spectroscopic and elemental analyses. The ^{1}H NMR spectrum of compound **7.3** (**Fig.4.2**) clearly depicts two singlets at 10.02 and 9.88 ppm, corresponding to the two aldehyde protons present in the molecule. Further, the compound **DBA-8**, in its ^{1}H NMR spectrum displayed unique resonances between δ 11.29-11.12 ppm accounting for the four protons of aromatic amines in the barbituric acid segments. Appearance of a singlet at δ 9.55 ppm confirmed the presence of an aromatic proton at the second position of indole ring. All the other aromatic protons depicted peaks between 8.72 and 7.86 ppm. Also, two protons of $-NCH_2$ of hexyl chain resonated as a singlet at δ 4.4 ppm, whereas the appearance of primary and secondary proton signals in the range of δ 1.84-0.82 ppm spectrum confirmed the presence of hexyl chain. The ^{13}C NMR spectrum of **DBA-8** showed the characteristic signals at higher frequency (downfield region). The keto carbon atoms resonated at δ 164.99, 163.70 and 150.87 ppm. The remaining signals appearing in the region of δ 147.59-109.04 ppm are due to other aromatic carbons. The first carbon in the hexyl chain attached directly to the aromatic nitrogen in the indole ring displayed a

peak at 47.57 ppm. Further, the remaining aliphatic carbons appeared between 31.15-14.32 ppm. Furthermore, its mass spectrum showed the $[M+H]^+$ peak at 559.15, which is in agreement with the calculated molecular weight for the formula of $C_{28}H_{25}N_5O_6S$. **Fig.7.2-7.5** show ^1H NMR, ^{13}C NMR and Mass spectra of the intermediate **7.3** and compound **DBA-8**.

Spectrograms of selected compounds

^1H NMR, ^{13}C NMR and Mass spectra of representative compounds are given below:

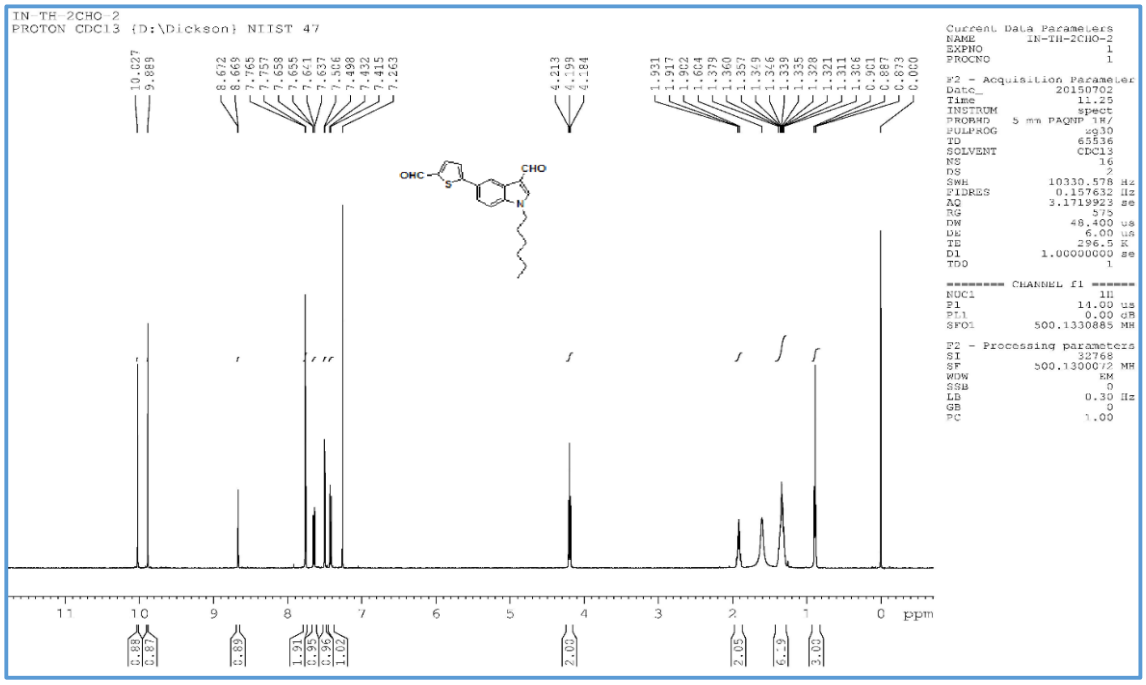

Fig.7.2 ^1H NMR spectrum of **7.3** in $CDCl_3$

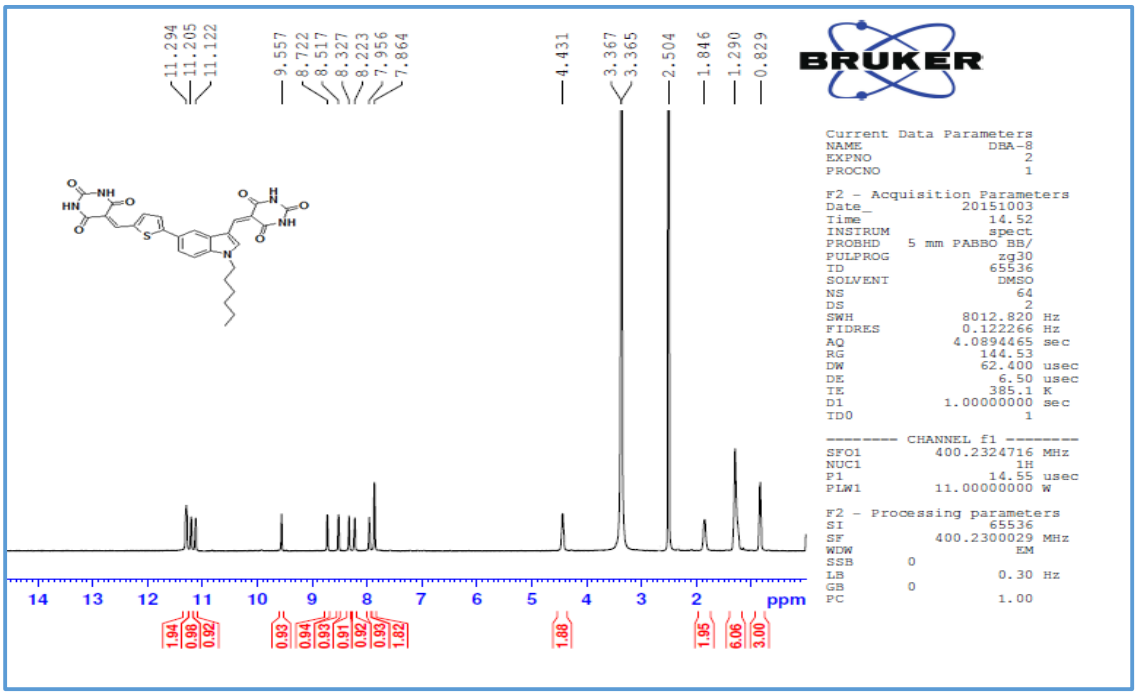

Fig.7.3 ^{1}H NMR spectrum of **DBA-8** in DMSO-d_6

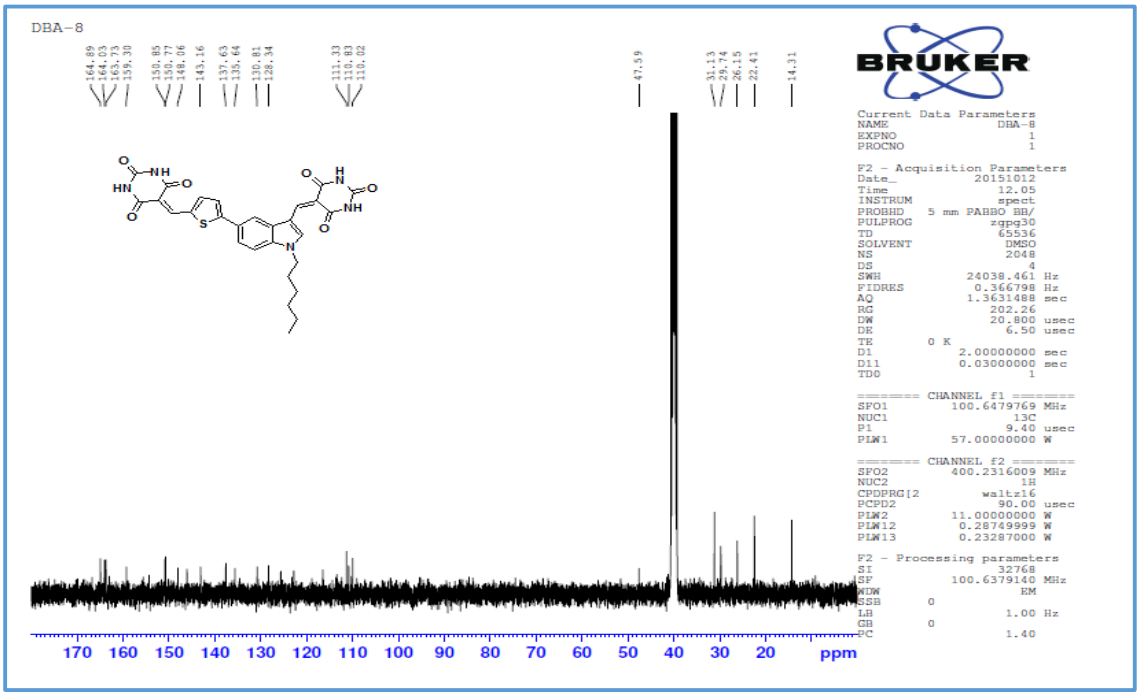

Fig.7.4 ^{13}C NMR spectrum of **DBA-8** in DMSO-d_6

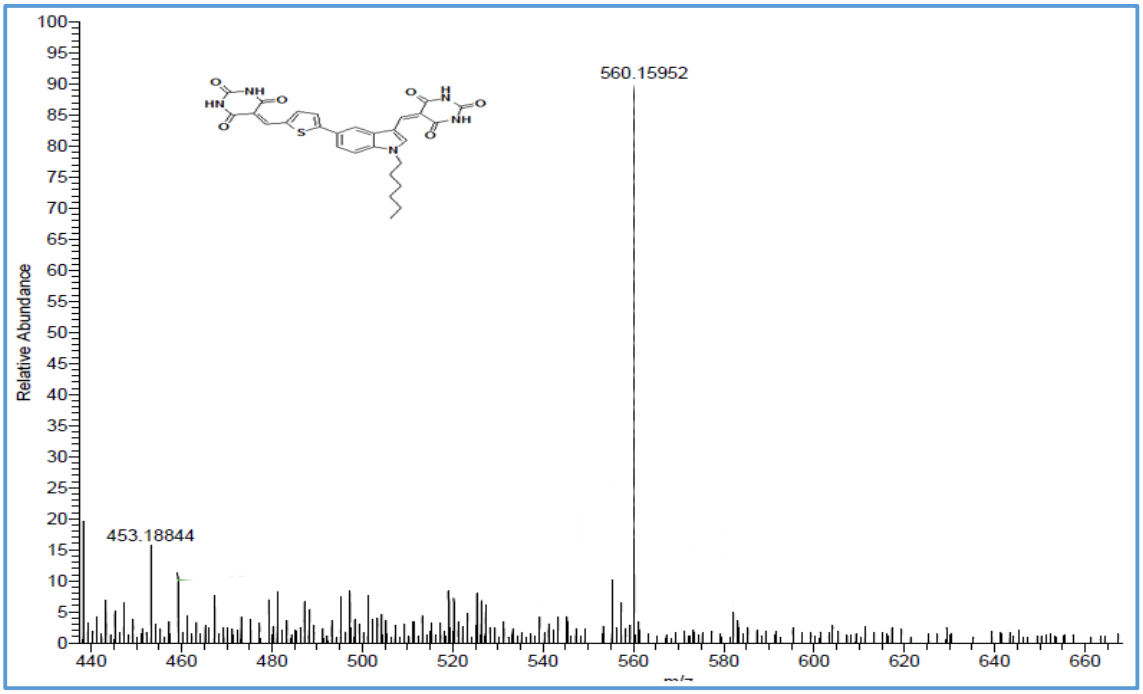

Fig.7.5 Mass spectrum of **DBA-8**

7.3.2 Photophysical properties

The absorption and emission spectra of the co-sensitizer were recorded in DMSO and are depicted in **Fig.7.6 (a)** and **(b)**, respectively; whereas the corresponding data is summarized in **Table 7.1**. From the absorption spectrum, it is evident that, the dye exhibits two distinct bands. The band, in the region of 400 nm, can be ascribed to the π-π* electronic excitations localized within the indole donor and thiophene π-conjugated segment, while the band centered on 460 nm can be attributed to the charge transfer (CT) from indole donor to the two acceptor moieties. Further, the fluorescence emission spectrum of **DBA-8** was recorded upon its excitation wavelengths and the pertaining results are tabulated in **Table 1**, whereas the corresponding spectrum is shown in **Fig.7.6 (b)**. Furthermore, the large values of Stokes shift obtained in this sensitizer can be ascribed to the efficient charge transfer from the indole donor moiety to the two barbituric acid acceptor groups. In addition, **Fig.7.6 (c)** depicts the UV-visible spectrum of **NCSU-10**.

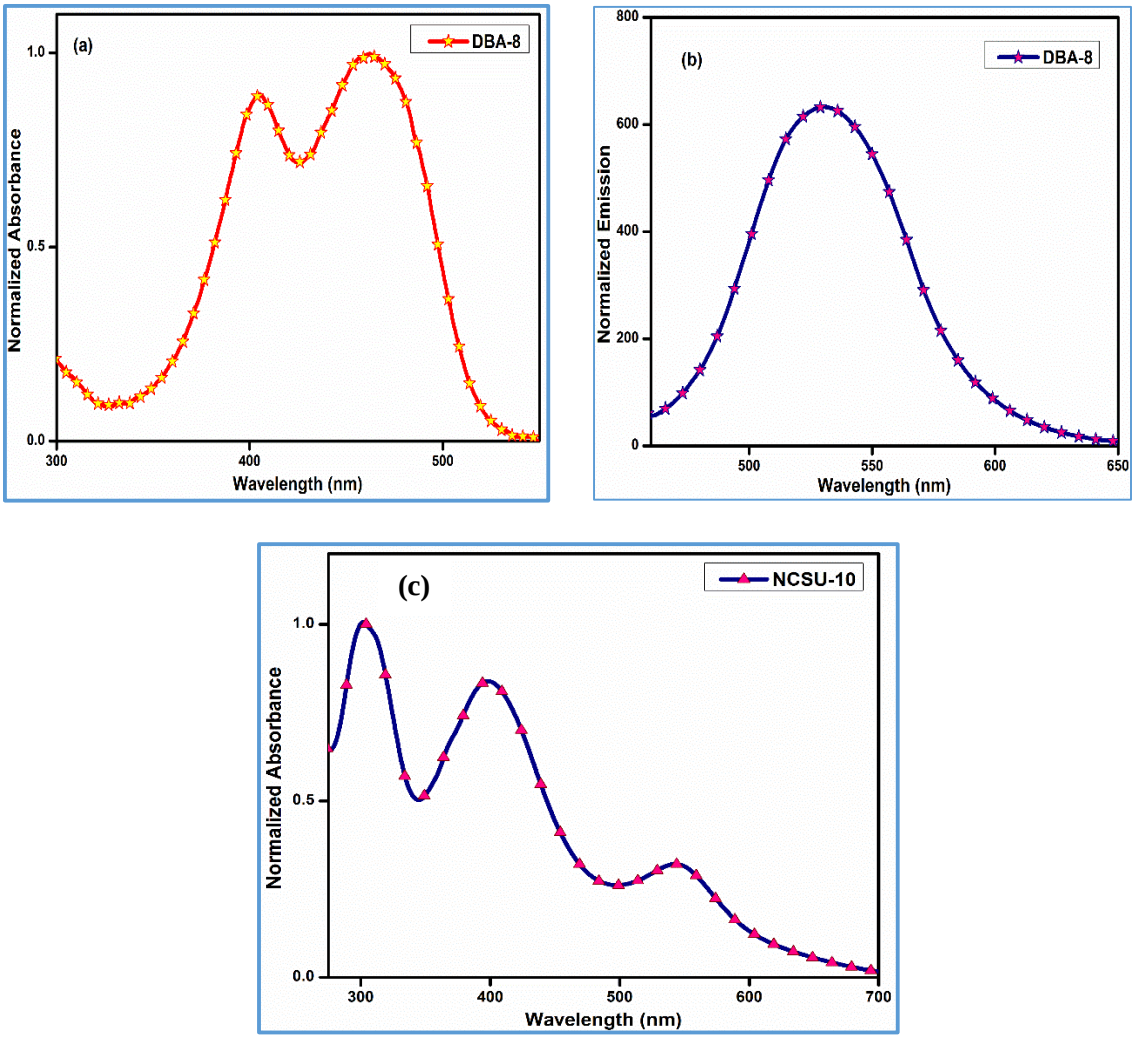

Fig.7.6 (a) UV-visible spectrum of **DBA-8** in DMSO (10^{-5} M) **b)** Fluorescence spectrum of **DBA-8** in DMSO (10^{-5} M) **(c)** UV-visible spectrum of **NCSU-10**

Further, the origin of the charge transfer transition is also confirmed by comparing the absorption spectrum of the sensitizer **DBA-8** with its precursors. From **Fig.7.7**, it is evident that, the peak corresponding to π-π* transition is retained in all the precursors, whereas the peak at longer wavelength appears only after the introduction of aldehyde or barbituric acid units on the indole core. The aforesaid red shift in the absorption profile reflects the electron withdrawing nature of aldehyde groups as well as barbituric acid segments.

Table 7.1 Absorption and emission properties for **DBA-8** and **NCSU-10**

Sensitizer	Absorption λ_{max} (nm)	Emission λ_{max} (nm)	Stokes shift (cm^{-1})	ε ($M^{-1}cm^{-1}$)	E_{0-0}
DBA-8	464	632	5750	48500	2.50
NCSU-10	545	758	4900	20650	1.88

Further, the charge-transfer nature of the absorption peak observed at higher wavelength can be further comprehended by studying the change in absorption characteristics on the addition of trifluoroacetic acid (TFA) or triethylamine (TEA) to the dye solution. Addition of TEA lead to a hypsochromic shift in the absorption maxima, whereas the addition of TFA resulted in a slight bathochromic shift as shown in **Fig.7.8**. The addition of TEA resulted in the deprotonation of the amine unit in barbituric acid and thereby, reducing its acceptor strength. As a result of the aforementioned blue shift in CT band of the absorption spectra, the band corresponding to π-π^* transition as well as CT transition merged together and gave rise to a single band in the intermediate wavelength.

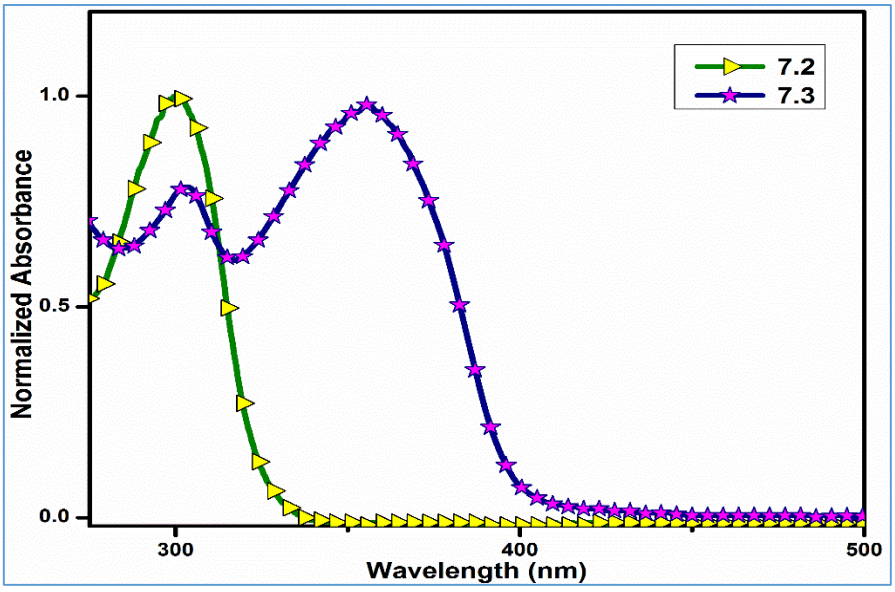

Fig.7.7 UV-visible spectra of compounds **7.2** and **7.3** in $CHCl_3$ (10^{-5} M)

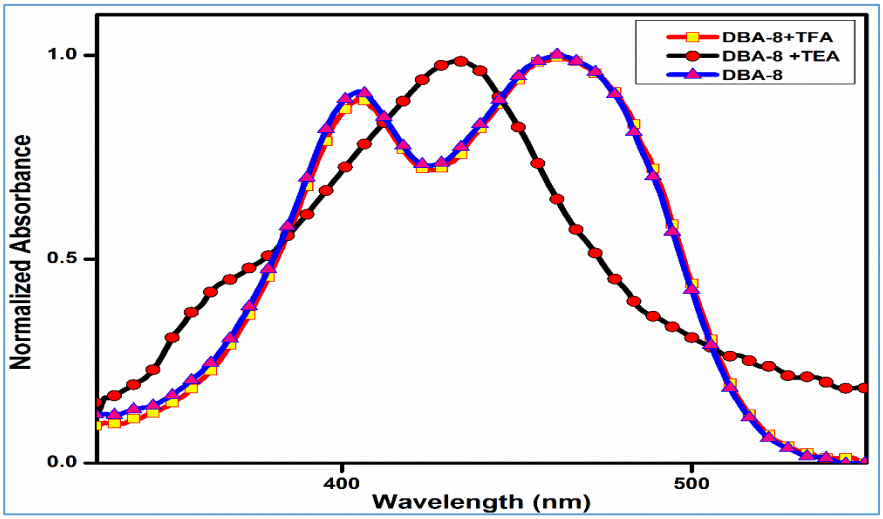

Fig.7.8 Absorption spectra of **DBA-8** in $CHCl_3$ before and after addition of TFA and TEA

7.3.3 Molecular modeling

Density functional theory (DFT) calculations were performed using Turbomole software package. At the outset, the geometry was optimized by means of semi empirical AM1 basis with MOPAC in TmoleX. Further optimization of the aforementioned geometry was done using C_1 point group symmetry at DFT level *via* the Becke's three-parameter hybrid functional and Lee-Yang-Parr's gradient-corrected correlation functional (B3LYP). The default convergence criteria were maintained for the geometry optimizations. Further, all the calculations were performed using def-TZVPP basis set. **Fig.7.9** depicts the optimized geometries and electron density distributions in the HOMO and LUMO of the sensitizer **DBA-8.** From the **Fig.7.9**, it is evident that in the HOMO level the electron density is mainly located on the indole donor segment as well as on the thiophene π-conjugation bridge, whereas in the LUMO level, a clear shift of density towards π-bridge and acceptor group can be observed. Interestingly, there seems to be a preferential flow of electron density towards acceptor group connected to the donor moiety *via* the π-conjugation bridge. The aforementioned observation can be attributed to the better electron-richness in the π-conjugation segment, which facilitates and enhances the donor-acceptor interactions. Further, the close proximity of the LUMO level to the anchoring

group would facilitate better orbital overlap with the *3d* orbitals of titanium and hence, excited electrons can be proficiently injected into conduction band of TiO_2.

DYE	Optimized geometry	HOMO	LUMO
DBA-8	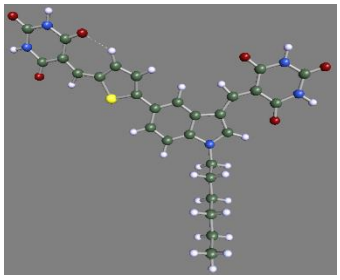	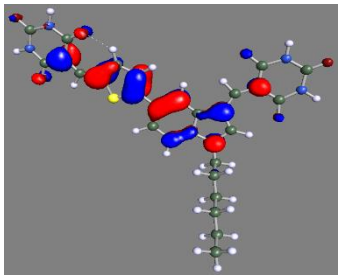	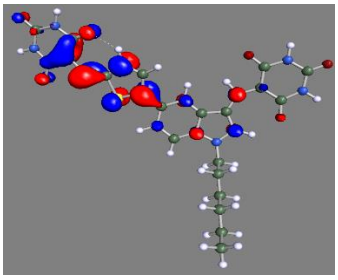

Fig.7.9 Optimized structure and Frontier molecular orbitals of **DBA-8**

Additionally, time-dependent density functional theory (TD-DFT) studies were carried out to probe the electronic excitations of sensitizer in presence of time-dependent perturbations. Typically, in TD-DFT, a time-dependent Schrödinger equation is solved to obtain the excited-state properties of the material. In TD-DFT an adiabatic approximation is made and following which temporal nonlocality is neglected. According to the aforesaid approximation, at any point of time, the exchange-correlation (xc) functional depends only on the instantaneous density. As a result of the aforementioned approximation, traditional approximations (time-independent) can be applied to the xc-functional derived for ground state DFT, *i.e*. BP (Beck-Perdew) and hybrid functionals (B3LYP). Typically, the precision of the results acquired using TD-DFT profoundly depends on the functional and basis set employed for the calculations. The simulated absorption spectrum of **DBA-8** obtained at the BP86 functional and def-TZVPP basis set is portrayed in **Fig.7.10**. Even though, TD-DFT is known to possess inabilities in precisely predicting energies related with long-range charge transfer states due to the self-interaction error in TD-DFT, which is owing to the

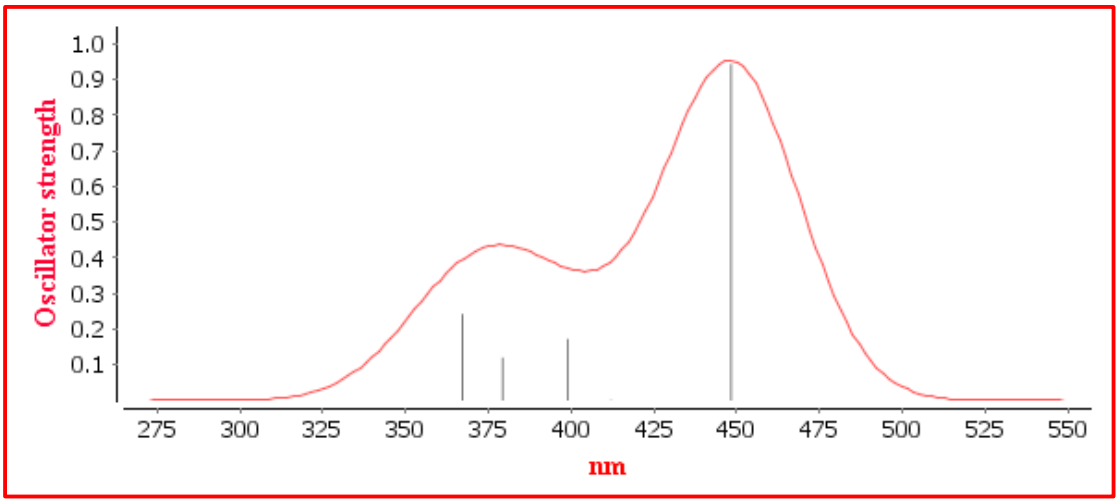

Fig.7.10 Simulated absorption spectrum of **DBA-8**

electron transfer in the extended charge-transfer state (Dreuw and Head-Gordon 2004).The aforementioned variance is not witnessed in the present study, as the molecule **DBA-8** under investigation is not large enough to display a long-range intramolecular charge transfer. From **Fig.7.10** it is evident that, the simulated spectrum of **DBA-8** exhibits two distinct bands, corresponding to π-π* and charge transfer process. Furthermore, the simulated spectrum is well in accordance with the experimentally obtained one. The accuracy of TD-DFT studies substantiate the validity of the basis set and functional used for the calculation.

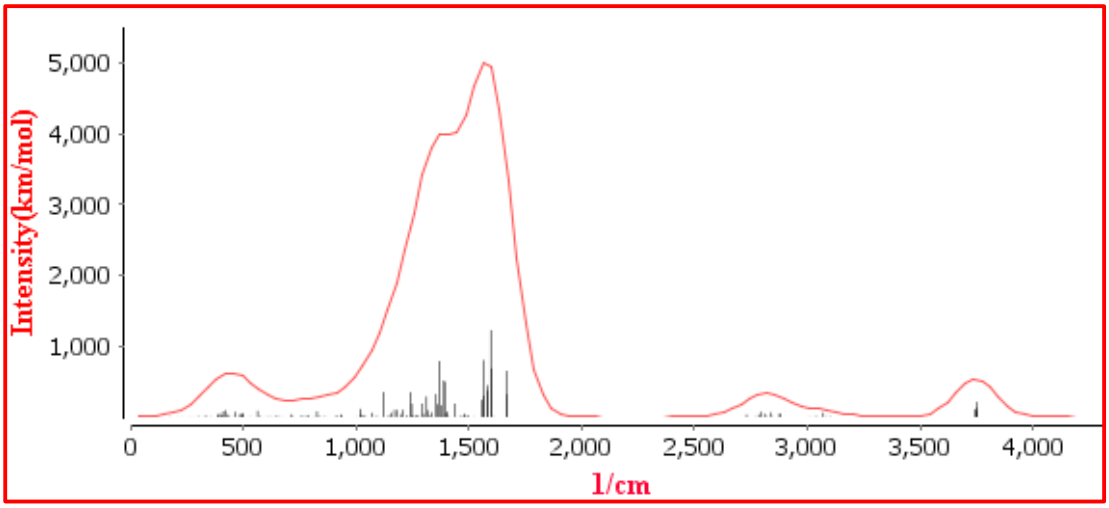

Fig.7.11 Theoretically obtained FT-IR spectrum of **DBA-8**

Further, the IR-absorption spectrum of the co-sensitizer has been simulated using Turbomole software. **Fig.7.11** portrays the simulated FT-IR spectrum of **DBA-8**. As expected, the experimentally obtained spectrum is well in agreement with the theoretically acquired one.

7.3.4 Electrochemical measurements

In order to estimate the prospects of electron injection from the excited state of the sensitizer into the conduction band (CB) of the TiO_2 as well as effective dye regeneration by avoiding undesirable charge recombinations between oxidized dye molecules and photo-injected electrons in the conduction band (CB) of the semiconductor, the ground and excited oxidation potentials of **DBA-8** was determined by Cyclic voltammetry (CV). The results of the aforementioned study is presented in **Fig.7.12**. From the **Fig.7.12**, it is apparent that, the sensitizer has a more negative GSOP (ground state oxidation potential) (eV) than the Nernst potential of the I^-/I_3^- redox couple (-5.2 eV) (Qu et al. 2001), indicating that the oxidized dyes can be reduced and regenerated by I^- species in the electrolyte effectively and thereby avoiding the charge recombination between oxidized sensitizer molecules and photo-injected electrons in the conduction band of the semiconductor. The following equation was utilized to convert all the values in volts (V) against NHE to electron volt (eV).

$$\text{ESOP} = [(\text{GSOP (V)} + 4.7) - E_{0\text{-}0}]\ \text{eV}$$

Further, the ESOP (excited state oxidation potential) of the dye was calculated using zeroth–zeroth energy ($E_{0\text{-}0}$) of the dyes and GSOP energy level, by employing the aforementioned equation. It was observed that, the excited state oxidation potential of the sensitizer was more negative than the conduction band edge of semiconductor, which is located at -4.2 eV and thus, providing adequate thermodynamic driving force for proficient electron injection. Therefore, the sensitizer **DBA-8** follows all the stringent requirements necessary for favorable flow of charges throughout the photo-electronic conversion cycle.

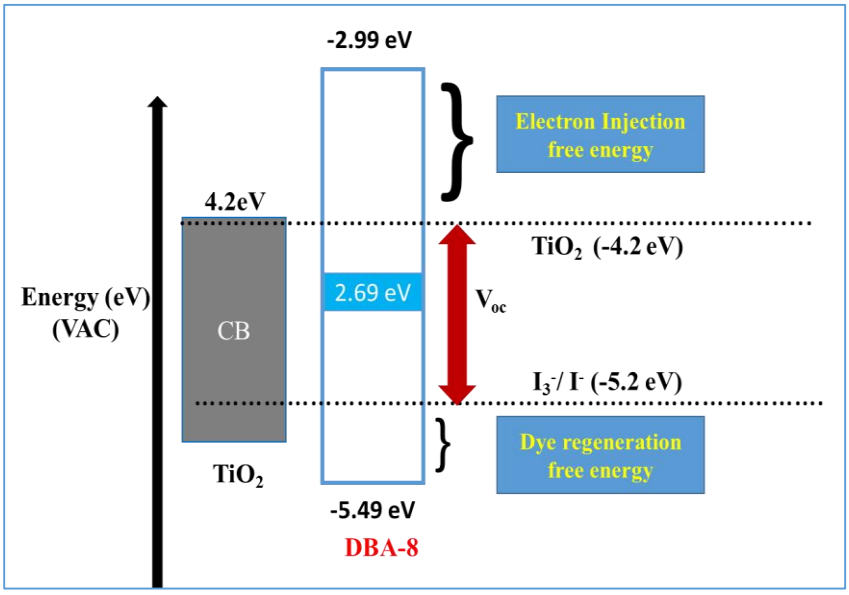

Fig.7.12 Energy level diagram of **DBA-8**

7.3.5 Photovoltaic device characterization

The photovoltaic properties of the devices sensitized using the ruthenium based sensitizer (**NCSU-10**) and co-sensitized devices were measured to ascertain the effect of co-sensitization on the device performance. Current-voltage (*J-V*) plots of the cell based on **NCSU-10** and the corresponding co-sensitized devices using 0.2 and 0.3 mM **DBA-8** are displayed in **Fig.7.13**, while the pertaining photovoltaic data are summarized in **Table 7.3**. It is apparent that, the device co-sensitized using 0.2 mM **DBA-8** yielded enhanced efficiency, while the one co-sensitized using 0.3 mM concentration of **DBA-8** resulted in reduced overall efficiency. The solar cells employing 0.2 and 0.3 mM **DBA-8** as the co-sensitizer yielded η of 10.68 and 9.72 % respectively, compared to η of 10.26 % for pure **NCSU-10**.

From the aforesaid values, it is evident that, the J_{SC} figures were improved as a result of co-sensitization, which suggests that the light harvesting capability of the cell is ameliorated in the co-sensitized device resulting in better performance of solar device co-sensitized with 0.2 mM of **DBA-8**. It has been also reported that, co-sensitizers may decrease the dye loading by up to 60%, which can considerably diminish the photocurrent

density. The aforesaid reduction in dye loading is witnessed in the presence of 0.3 mM **DBA-8** for **NCSU-10** dye resulting in reduced light harvesting proficiency. Besides, all the fill factor values were also enhanced for the co-sensitized devices, which indicates that smaller sized organic co-sensitizers provide more sufficient TiO_2 surface coverage compared to the bulky ruthenium dye, which leaves large nanoparticle area unadsorbed. Broadening the light absorption and photon harvesting range are indispensable approaches towards the enhancement of DSSCs performance.

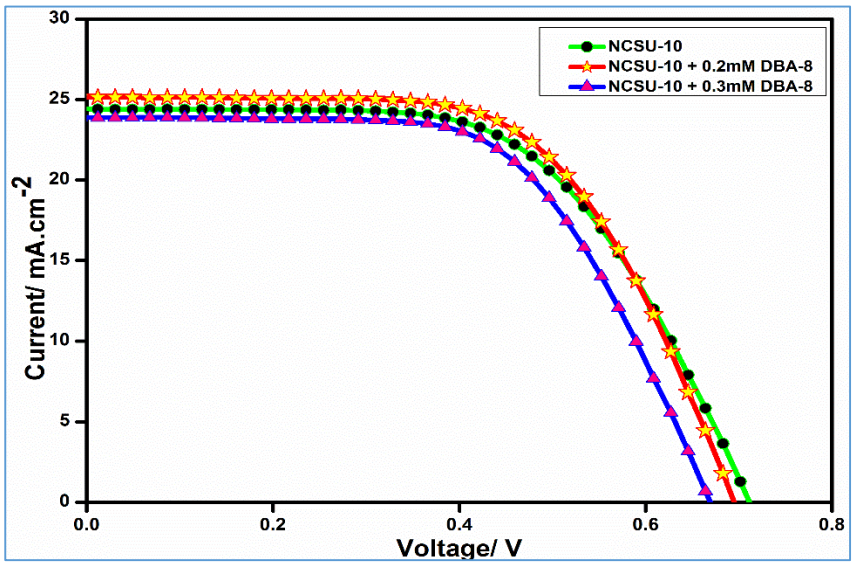

Fig.7.13. *J–V* characteristics of DSSCs based on **NCSU-10** and co-sensitized with **DBA-8**

To further scrutinize the photovoltaic performances of co-sensitized devices, the incident photon to current efficiency (IPCE) studies were undertaken and the corresponding plot is depicted in **Fig.7.14**. In comparison with solar cell sensitized only by **NCSU-10**, the one co-sensitized with 0.2 mM **DBA-8** depicted superior IPCE response, which translated into enhancement in J_{sc} of the one co-sensitized with 0.2 mM **DBA-8** (increased from 24.40 to 25.14 $mAcm^{-2}$). The IPCE of 0.2 mM **DBA-8** co-sensitized solar cell was found to be 75% at 550 nm and higher than 60% in the range of 395 nm and 655 nm. Further, it is interesting to note that, even though the cells co-sensitized by 0.2 and 0.3 mM **DBA-8** offered better efficiency compared to the one sensitized by **NCSU-10** alone, but their V_{oc} values were found to be lowered. The lowering of V_{oc} can be attributed to the

enhanced charge recombinations in the co-sensitized cells. The aforesaid inference can be corroborated by electrochemical impedance spectroscopy (EIS) studies.

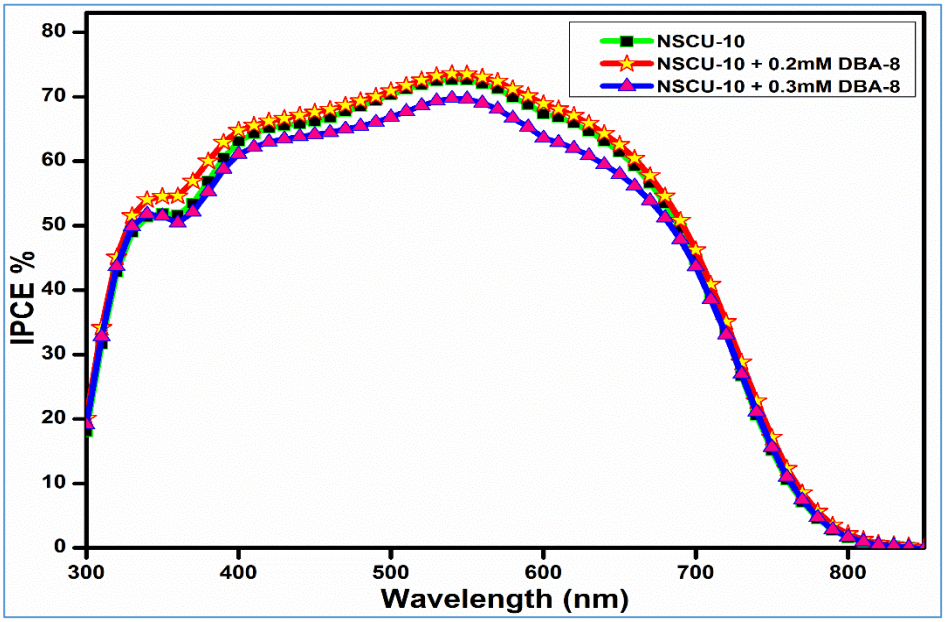

Fig.7.14 IPCE spectra of the DSSCs based on **NCSU-10** and co-sensitized with **DBA-8**

Table 7.3 Photovoltaic parameters of DSSCs based on **NCSU-10** with/without co-sensitization

Sensitizer		CDCA (mM)	J_{SC} (mAcm^{-2})	V_{OC} (V)	*ff* (%)	η (%)
NCSU-10 (mM)	**DBA-8** (mM)					
0.2	--	20	24.40 ± 0.05	0.711 ± 0.002	59.2 ± 0.4	10.26 ± 0.06
0.2	0.2	20	25.14 ± 0.04	0.695 ± 0.003	61.2 ± 0.3	**10.68 ± 0.01**
0.2	0.3	20	23.86 ± 0.05	0.672 ± 0.004	60.5 ± 0.5	9.72 ± 0.01

Another remarkable inference which can be drawn from these results is that, the concentration of co-sensitizer used substantially affects the overall efficiency of the cell and therefore, one has to strike a balance between the sensitizer and co-sensitizer concentration to obtain maximum efficiency from the cell. Overall, the cell co-sensitized by **DBA-8** provides enhanced light harvesting capability, *i.e*. **DBA-8** acts as a co- sensitizer

rather than a co-adsorber. Overall, the optimum concentration of the co-sensitizer **DBA-8**, which provides better light harvesting capability than the cell sensitized using only **NCSU-10** is 0.2 mM of **DBA-8**. The cell efficiencies and the corresponding photovoltaic parameters are summarized in **Table 7.3**. All the aforesaid results vindicate the pivotal role played by the concentration of the co-sensitizer in influencing the photovoltaic properties of the cell.

7.3.6 Electrochemical impedance spectroscopy characterization

Electrochemical impedance spectroscopy characterization (EIS) is an efficient tool to corroborate the charge transfer and chemical capacitance at the interface of dye/ TiO_2/electrolyte and Pt/electrolyte in DSSC under operational conditions. **Fig.7.16** compares EIS Nyquist plots for devices sensitized using **NCSU-10** and the ones co-sensitized using **DBA-8**. As evidenced from the aforesaid figure, all the devices presented two distinct semicircles. The smaller semicircle at lower frequency models the cathode charge transfer resistance, which is directly related with fill factor, whereas the larger semicircle in middle frequency region models the charge recombination resistance (R_{ct}) from TiO_2 to electrolyte, which is directly proportional to V_{oc} values exhibited by the cell. Further, from the Nyquist plots, it is evident that, the radius of the larger semicircles were in the order of **NCSU-10** > **DBA-8** (0.2 mM) > **DBA-8** (0.3 mM).

Keeping the aforementioned observation in view, it can be concluded that in the co-sensitized devices charge recombination has enhanced as compared to the cell sensitized using only the ruthenium based sensitizer. The aforesaid is consistent with the V_{oc} values in **Table 7.3**. From the Bode frequecy plots, lifetime for injected electrons into the conduction band of TiO_2 can be obtained by employing the equation: $\tau_{CB} = 1 / (2\pi f)$, where τ is the lifetime of electrons in TiO_2 and f is the mid frequency peak in Bode plots. Further, it is well know that, the electron lifetime depends on the density of charge traps, which is ultimately related to V_{oc}. The electron lifetimes for the DSSCs sensitized using only **NCSU-10** and the ones co-sensitized using 0.2 and 0.3 mM of **DBA-8** were assimilated using Bode frequency plots (**Fig.7.17**). The mid frequency peaks of the Bode plots displayed the order: **NCSU-10** > **DBA-8** (0.2mM) > **DBA-8** (0.3mM). The corresponding electron lifetimes

were found to be 6.6, 4.5 and 4.1 ms, respectively. These results suggest that, the addition of co-sensitizer is ineffective in suppressing the undesirable charge recombinations. Further, the calculated electron lifetime values are well in agreement with the V_{oc} values of these devices (**Table 7.3**). Interestingly, the cell fabricated without co-sensitizer displayed higher V_{OC}) than the one fabricated in the presence of the co-sensitizer (**DBA-8)**.

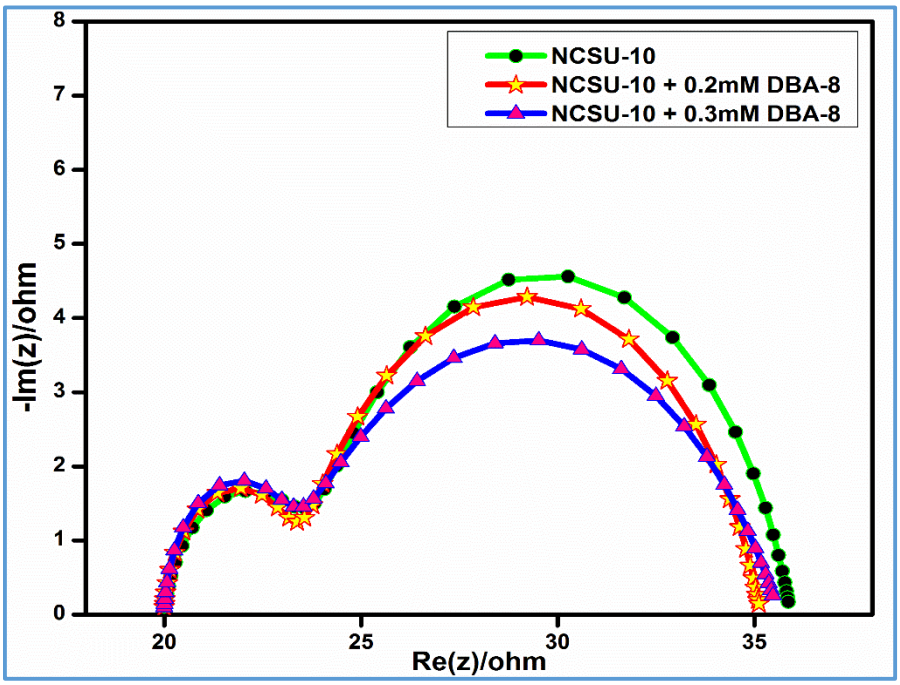

Fig.7.16 EIS Nyquist plots for DSSCs based on **NCSU-10** and cosensitized with **DBA-8**

Li et al. in 2013 proposed that, the interaction between iodine species present in the electrolyte and electron-rich segments of the dye molecules can lead to enhancement in charge recombinations at the TiO_2/electrolyte interface. In the present work, the co-sensitizer molecule encompasses a thiophene unit and the sulfur atom of this thiophene unit leads to the formation of dye-iodine complexes, which ultimately results in a lowering of V_{oc} for the co-sensitized solar cells.

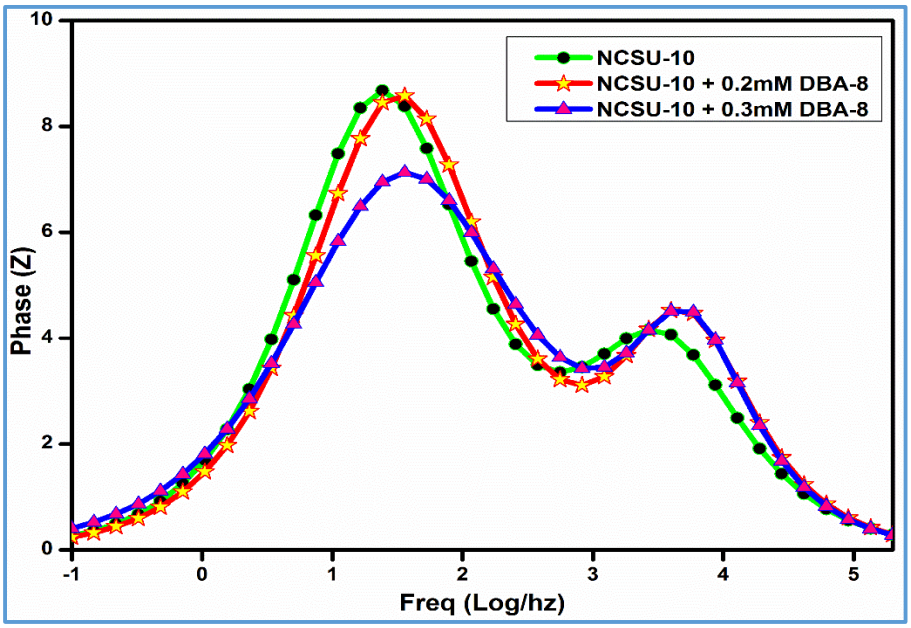

Fig.7.17 Bode plots for DSSCs based on **NCSU-10** and co-sensitized with **DBA-8**

7.4 CONCLUSIONS

A new di-anchoring co-sensitizer (**DBA-8**) having A-D-π-A architecture has been successfully designed and synthesized as alternative co-adsorbent to CDCA, wherein indole moiety acts as donor group, thiophene takes on the role of π-conjugation bridge and two barbituric acid moieties play the role of acceptor units. The newly synthesized co-sensitizer has been thoroughly characterized using various spectroscopic techniques. The photophysical and theoretical studies of the aforementioned sensitizer reveal that, it fulfills the essential criteria required by a molecule to act a good co-sensitizer in DSSC. The photovoltaic studies revealed that, the co-sensitizer **DBA-8** at 0.2 mM concentration enhances the light harvesting capability of the cells. The aforesaid is corroborated by the enhancement in J_{sc} values of the co-sensitized device as compared to the one sensitized using only the ruthenium based sensitizer. Further, the best performing co-sensitized device exhibited an overall efficiency of **10.68%**. Furthermore, all these observations showcase the vast potential of bi-anchoring molecules in enhancing the overall performance of the solar cells.

CHAPTER 8

SUMMARY AND CONCLUSIONS

Abstract

This chapter includes summary of the entire work and important conclusions drawn from the present research work. It also comprises a brief account on scope for the future work.

8.1 SUMMARY

Solar energy has emerged as a bright spot amidst the efforts to find clean and abundant source of renewable energy in order to meet the requirements and developments of contemporary society. In the field of solar-energy conversion into electricity, dye-sensitized solar cells (DSSCs) have engrossed remarkable attention due to their low cost to efficiency ratio and relative ease of fabrication. Although, there are many components which make-up a typical DSSC, the improvement in conversion efficiency of the cell (η) hinges on the development of new photosensitizers. In the recent years, many strategies have been employed by the researchers to develop efficient sensitizers having enhanced conversion efficiency and improved photo-stability. In this context, the metal-free organic sensitizers are of great interest owing to their facile synthesis, low cost and high molecular extinction coefficients. However, the performance of the DSSCs based on pure organic sensitizers is hampered due to the lack of metal-ligand charge transfer (MLCT) bands and their narrow absorption profiles. Taking all these points into consideration, co-sensitization strategy is employed, wherein, a DSSC based on ruthenium sensitizer is co-sensitized using an organic dye with complementary absorption spectra and thereby enabling the cell to harvest maximum number of photons.

Based on thorough literature review, it has been aimed at designing and synthesizing new series of D-π-A type metal-free sensitizers for application in DSSCs. Accordingly, six new series of sensitizers/co-sensitizers with varying configuration of donor-π-conjugation-acceptor species carrying methoxy, triphenylamine, anisole and thiophene as electron donors and nitro, cyanoacetic acid, rhodamine-3-acetic acid, 4-amino benzoic acid and barbituric acid as electron acceptor moieties have been designed. The newly designed molecules have been successfully prepared using appropriate synthetic

procedures from simple molecules and their synthetic protocols have been established. Structures of new intermediates and target compounds have been evidenced using FTIR, ^{1}H NMR, ^{13}C NMR, Mass spectral analyses, followed by elemental analysis. Further, their photophysical, electrochemical, theoretical and DSSC fabrication studies were carried out in detail.

The following important points can effectively summarize the present work:

- In **series 1**, three new Donor-π-Acceptor (**D-π-A**) type dyes **(D_{1-3})** with three different acceptor units were designed and synthesized. The new dyes were characterized using various spectroscopic techniques. Their optical and electrochemical properties were examined, while their photovoltaic performance was evaluated by device fabrication studies.
- In **series 2**, three new metal-free sensitizers **(E_{1-3})** with **D-π-A-π-A** (donor-π-conjugation-acceptor-π-conjugation-acceptor) were designed and synthesized starting from simple organic molecules as promising sensitizers for DSSC application. The new dyes were thoroughly characterized using various spectral and elemental analyses. Further, the device fabrication studies were carried out to evaluate their photovoltaic performance.

- In **series 3**, three new dyes **(N_{1-3})** with **A-D-A-π-A** (acceptor-donor-acceptor-π-bridge-acceptor) architecture carrying indole and thiophene units attached to different acceptors/anchoring groups, were synthesized starting from simple organic molecules. The photovoltaic performance studies of the aforesaid co-sensitizers was taken up to comprehend the role of anchoring moieties on co-sensitization properties.
- In **series 4**, two novel organic co-sensitizers **DBA-1** and **DBA-2** with **D-D-A** (donor-donor-acceptor) architecture have been synthesized and their structures have been confirmed by various spectral and elemental analyses. Further, the

aforesaid molecules were employed as co-sensitizers along with a ruthenium based dye (**HD-2**) and their photovoltaic performance has been evaluated.

- In **series 5**, three new co-sensitizers (**DBA-3**, **DBA-4**, and **DBA-5**) with **D-D-A** (donor-donor-acceptor) architecture were successfully designed and synthesized. Further, the molecules were thoroughly characterized by implementing various spectral techniques. Their photophysical and electrochemical studies were carried out and co-sensitization studies were performed using device fabrication.
- In **series 6**, an unsymmetrical di-anchoring co-sensitizers (**DBA-8**) having **A-π-D-A** configuration has been designed and synthesized. Further, the optical and electrochemical studies were conducted. Also, the aforesaid molecule has been employed as a co-sensitizer along with ruthenium based sensitizer **NCSU-10**. Further, the photovoltaic studies were performed to evaluate the effectiveness of the aforesaid co-sensitizer.
- For the first time, the effect of acceptor groups on co-sensitization performance has been studied.

8.2 CONCLUSIONS

- In **series 1**, the device sensitized by **D_3** with 4-aminobenzoic acid as an acceptor displayed the highest efficiency, which is mainly attributed to the longest electron lifetime. It also indicates that **D_3** is capable of reducing the electron recombination rates in the TiO_2 more effectively and hence leading to a higher efficiency than the dyes **D_1** and **D_2**. The device sensitized by **D_3** displayed the efficiency of **1.18%**.

- In **series 2**, the DSSC fabricated using **E_3** showed the highest J_{SC} (9.35 mA cm^{-2}), which is consistent with the fact that sensitizer **E_3** has the widest IPCE response among the three sensitizers. Further, the higher efficiency of **E_3** can also be attributed to its longer electron lifetime ($eTiO_2$) and high lying LUMO, which enhances the thermodynamic feasibility of electron injection into the conduction band of TiO_2. All this translated into an overall efficiency of **4.12%**.

- In **series 3**, amongst the three novel organic dyes (**N_{1-3}**) with varying acceptor/anchoring units as alternative co-adsorbents to chenodeoxycholic acid (CDCA), co-adsorbent **N_3** containing 4-aminobenzoic acid unit as the acceptor/anchoring group showed promising co-sensitization results and exhibited an enhanced efficiency of **9.26%**.

- In **series 4**, although both the co-sensitizers were found to be successful in enhancing the overall efficiency of the co-sensitized devices, the device co-sensitized using **DBA-2** displayed the higher efficiency as compared to the one co-sensitized using **DBA-1**. The cells co-sensitized by 0.3 mM **DBA-2** exhibited an enhanced efficiency of **8.06%** compared to the one sensitized by **HD-2** alone.

- In **series 5**, barbituric acid has been employed as the acceptor/anchoring group. The EIS studies revealed that, only the device co-sensitized using **DBA-4** was capable in effectively suppressing the undesirable charge recombinations happening in the cell and longer electron lifetime, resulting in highest PCE of **10.12%** among the studied DSSCs.

- In **series 6**, a newly designed dual anchoring unsymmetrical co-sensitizer **DBA-8**, carrying barbituric acid as the acceptor/anchoring group, showed an outstanding efficiency of **10.68%** in the co-sensitized device.

Conclusively, in the present research work new indole based sensitizers and co-sensitizers have been designed and synthesized. Further, various configurations of dye design, *viz.* **D-π-A-π-A**, **D-D-π-A-π-A**, **A- D-π-A-π-A**, **D-π-A**, **D-D-A** and **A-π-D-A** have been explored. Furthermore, the role of acceptor moieties on the overall performance of a sensitizer as well as co-sensitizer has also been studied in detail. It has been observed that, acceptor/anchoring groups play a pivotal role in determining the overall efficiency of the cell.

8.3 SCOPE FOR FUTURE WORK

In all the newly synthesized sensitizers having 4-aminobenzoic acid as acceptor/anchoring moiety exhibited good photovoltaic efficiency. The aforesaid acceptor can be incorporated into the high performing sensitizers in order to further ameliorate their performance. Further, sensitizer **E_3** displayed good photovoltaic characteristics and structural modification to its backbone by the incorporation of strong donor and rigid π-bridge segments can help to further improve the overall efficiency of the cell. In the present work, for the first time role of acceptor species in performance of co-sensitizers has been explored. The aforesaid can be explored for the best performing co-sensitizers in the future.

References

Abbotto, A., Leandri, V., Manfredi, N., Angelis, F. De, Pastore, M., Yum, J.-H., Nazeeruddin, M.K. and Grätzel, M. (2011). "Bis-Donor-Bis-Acceptor Tribranched Organic Sensitizers for Dye-Sensitized Solar Cells." *Eur. J. Org. Chem., 2011* (31), 6195–6205.

Ahlrichs, R., Bär, M., Häser, M., Horn, H. and Kölmel, C. (1989). "Electronic structure calculations on workstation computers: The program system turbomole." *Chem. Phys. Lett., 162* (3), 165–169.

Babu, D.D., Cheema, H., Elsherbiny, D., El-Shafei, A. and Adhikari, A.V. (2015). "Molecular Engineering and Theoretical Investigation of Novel Metal-Free Organic Chromophores for Dye-Sensitized Solar Cells." *Electrochim. Acta, 176* 868–879.

Babu, D.D., Gachumale, S.R., Anandan, S. and Adhikari, A.V. (2015). "New D-π-A type indole based chromogens for DSSC: Design, synthesis and performance studies." *Dyes Pigments, 112* 183–191.

Baheti, A., Thomas, K.R.J., Lee, C.-P., Li, C.-T. and Ho, K.-C. (2014). "Organic dyes containing fluoren-9-ylidene chromophores for efficient dye-sensitized solar cells." *J. Mater. Chem. A, 2* (16), 5766–5779.

Bai, Y., Zhang, J., Zhou, D., Wang, Y., Zhang, M. and Wang, P. (2011). "Engineering Organic Sensitizers for Iodine-Free Dye-Sensitized Solar Cells: Red-Shifted Current Response Concomitant with Attenuated Charge Recombination." *J. Am. Chem. Soc., 133* (30), 11442–11445.

Barea, E.M., Zafer, C., Gultekin, B., Aydin, B., Koyuncu, S., Icli, S., Santiago, F.F. and Bisquert, J. (2010). "Quantification of the Effects of Recombination and Injection in the Performance of Dye-Sensitized Solar Cells Based on N-Substituted Carbazole Dyes." *J. Phys. Chem. C, 114* (46), 19840–19848.

Becke, A.D. (1988). "Density-functional exchange-energy approximation with correct asymptotic behavior." *Phys. Rev. A*, *38* (6), 3098–3100.

Becke, A.D. (1993). "A new mixing of Hartree-Fock and local density-functional theories." *J. Chem. Phys*, *98* (2), 1372–1377.

Bisquert, J. (2001). "Theory of the Impedance of Electron Diffusion and Recombination in a Thin Layer." *J. Phys. Chem. B*, *106* (2), 325–333.

Cai, S., Tian, G., Li, X., Su, J. and Tian, H. (2013). "Efficient and stable DSSC sensitizers based on substituted dihydroindolo[2,3-b]carbazole donors with high molar extinction coefficients." *Journal of Materials Chemistry A*, *1* (37), 11295.

Cheema, H., Islam, A., Han, L. and El-Shafei, A. (2014). "Influence of Number of Benzodioxan-Stilbazole-based Ancillary Ligands on Dye Packing, Photovoltage and Photocurrent in Dye-Sensitized Solar Cells." *ACS Appl. Mater. Interfaces*, *6* (14), 11617–11624.

Cheema, H., Islam, A., Han, L., Gautam, B., Younts, R., Gundogdu, K. and El-Shafei, A. (2014). "Influence of mono versus bis-electron-donor ancillary ligands in heteroleptic Ru (II) bipyridyl complexes on electron injection from the first excited singlet and triplet states in dye-sensitized solar cells." *J. Mater. Chem. A*, *2* (34), 14228- 14235.

Cheema, H., Islam, A., Younts, R., Gautam, B., Bedja, I., Gupta, R.K., Han, L., Gundogdu, K. and El-Shafei, A. (2014). "More stable and more efficient alternatives of Z-907: carbazole-based amphiphilic Ru(II) sensitizers for dye-sensitized solar cells." *Phys. Chem. Chem. Phys.*, *16* (48), 27078-27087.

Chen, C.-Y., Wang, M., Li, J.-Y., Pootrakulchote, N., Alibabaei, L., Ngoc-le, C., Decoppet, J.-D., Tsai, J.-H., Grätzel, C., Wu, C.-G., Zakeeruddin, S.M. and Grätzel, M. (2009). "Highly Efficient Light-Harvesting Ruthenium Sensitizer for Thin-Film Dye-Sensitized Solar Cells." *ACS Nano*, *3* (10), 3103-3109.

Chen, R., Yang, X., Tian, H., Wang, X., Hagfeldt, A. and Sun, L. (2007). "Effect of Tetrahydroquinoline Dyes Structure on the Performance of Organic Dye-Sensitized Solar

Cells." *Chem. Mater.*, *19* (16), 4007-4015.

Chiba, Y., Islam, A., Watanabe, Y., Komiya, R., Koide, N. and Han, L. (2006). "Dye-Sensitized Solar Cells with Conversion Efficiency of 11.1%." *Japanese Journal of Applied Physics, 45* (No. 25), L638–L640.

Crosby, G.A. and Demas, J.N. (1971). "Measurement of photoluminescence quantum yields. Review." *J. Phys. Chem.*, *75* (8), 991-1024.

Deacon, G.B. and Phillips, R.J. (1980). "Relationships between the carbon-oxygen stretching frequencies of carboxylato complexes and the type of carboxylate coordination." *Coord. Chem. Rev.*, *33* (3), 227-250.

Deglmann, P., Furche, F. and Ahlrichs, R. (2002). "An efficient implementation of second analytical derivatives for density functional methods." *Chem. Phys. Lett*, *362* (5-6), 511-518.

Deglmann, P., May, K., Furche, F. and Ahlrichs, R. (2004). "Nuclear second analytical derivative calculations using auxiliary basis set expansions." *Chem. Phys. Lett*, *384* (1-3), 103-107.

Dev, P., Agrawal, S. and English, N.J. (2013). "Functional Assessment for Predicting Charge-Transfer Excitations of Dyes in Complexed State: A Study of Triphenylamine–Donor Dyes on Titania for Dye-Sensitized Solar Cells." *J. Phys. Chem. A*, *117* (10), 2114-2124.

Dreuw, A. and Head-Gordon, M. (2004). "Failure of Time-Dependent Density Functional Theory for Long-Range Charge-Transfer Excited States: The Zincbacteriochlorin−Bacteriochlorin and Bacteriochlorophyll−Spheroidene Complexes." *J. Am. Chem. Soc.*, *126* (12), 4007-4016.

El-Shafei, A., Hussain, M., Atiq, A., Islam, A. and Han, L. (2012). "A novel carbazole-based dye outperformed the benchmark dye N719 for high efficiency dye-sensitized solar cells (DSSCs)." *J. Mater. Chem.*, *22* (45), 24048-24056.

Fan, S., Lu, X., Sun, H., Zhou, G., Chang, Y.J. and Wang, Z.-S. (2015). "Effect of the co-sensitization sequence on the performance of dye-sensitized solar cells with porphyrin and organic dyes." *Phys. Chem. Chem. Phys.*, *18* (2), 932-938.

Grätzel, M. (2001). "Photoelectrochemical cells." *Nature*, *414* (6861), 338-344.

Grätzel, M. (2005). "Solar Energy Conversion by Dye-Sensitized Photovoltaic Cells." *Inorganic Chemistry*, *44* (20), 6841-6851.

Greenwald, Y.; Cohen, G.; Poplawski, J.; Ehrenfreund, E.; Speiser, S.; Davidov, D. (1996). "Transient Photoconductivity of Acceptor-Substituted Poly(3-butylthiophene). " *J. Am. Chem. Soc.*, 118, 2980-2984.

Gupta, A., Armel, V., Xiang, W., Bilic, A. and Evans, R.A. (2015). "New organic sensitizers using 4-(cyanomethyl)benzoic acid as an acceptor group for dye-sensitized solar cell applications." *Dyes Pigments*, *113* 280–288.

Hagberg, D.P., Marinado, T., Karlsson, K.M., Nonomura, K., Qin, P., Boschloo, G., Brinck, T., Hagfeldt, A. and Sun, L. (2007). "Tuning the HOMO and LUMO Energy Levels of Organic Chromophores for Dye Sensitized Solar Cells." *J. Org. Chem.*, *72* (25), 9550-9556.

Hagberg, D.P., Yum, J.-H., Lee, H., De Angelis, F., Marinado, T., Karlsson, K.M., Humphry-Baker, R., Sun, L., Hagfeldt, A., Grätzel, M. and Nazeeruddin, M.K. (2008). "Molecular Engineering of Organic Sensitizers for Dye-Sensitized Solar Cell Applications." *J. Am. Chem. Soc.*, *130* (19), 6259-6266.

Hagfeldt, A. and Graetzel, M. (1995). "Light-Induced Redox Reactions in Nanocrystalline Systems." *Chem. Rev.*, *95* (1), 49-68.

Han, L., Islam, A., Chen, H., Malapaka, C., Chiranjeevi, B., Zhang, S., Yang, X. and Yanagida, M. (2012). "High-efficiency dye-sensitized solar cell with a novel co-adsorbent." *Energy Environ. Sci.*, *5* (3), 6057-6060.

Han, L., Koide, N., Chiba, Y., Islam, A. and Mitate, T. (2006). "Modeling of an equivalent circuit for dye-sensitized solar cells: improvement of efficiency of dye-sensitized solar cells by reducing internal resistance." *Comptes Rendus Chimie*, *9* (5-6), 645-651.

Hasan, M.A. and Sumathy, K. (2010). "Photovoltaic thermal module concepts and their performance analysis: A review." *Renewable and Sustainable Energy Reviews*, *14* (7), 1845–1859.

Hara, K., Kurashige, M., Dan-oh Yasufumi, Kasada, C., Shinpo, A., Suga, S., Sayama, K. and Arakawa, H. (2003). "Design of new coumarin dyes having thiophene moieties for highly efficient organic-dye-sensitized solar cells." *New J. Chem.*, *27* (5), 783-785.

Hara, K., Wang, Z.-S., Sato, T., Furube, A., Katoh, R., Sugihara, H., Dan-oh Yasufumi, Kasada, C., Shinpo, A. and Suga, S. (2005). "Oligothiophene-Containing Coumarin Dyes for Efficient Dye-Sensitized Solar Cells." *J. Phys. Chem. B*, *109* (32), 15476-15482.

Hardin, B.E., Snaith, H.J. and McGehee, M.D. (2012). "The renaissance of dye-sensitized solar cells." *Nat Photon*, *6* (3), 162-169.

Hart, A.S., K. C., C.B., Subbaiyan, N.K., Karr, P.A. and D'Souza, F. (2012). "Phenothiazine-Sensitized Organic Solar Cells: Effect of Dye Anchor Group Positioning on the Cell Performance." *ACS Appl. Mater. Interfaces*, *4* (11), 5813-5820.

He, J., Guo, F., Li, X., Wu, W., Yang, J. and Hua, J. (2012). "New Bithiazole-Based Sensitizers for Efficient and Stable Dye-Sensitized Solar Cells." *Chem. Eur. J.*, *18* (25), 7903-7915.

Higashijima, S., Inoue, Y., Miura, H., Kubota, Y., Funabiki, K., Yoshida, T. and Matsui, M. (2012). "Organic dyes containing fluorene-substituted indoline core for zinc oxide dye-sensitized solar cell." *RSC Adv.*, *2* (7), 2721-2724.

Hong, Y., Iqbal, Z., Yin, X. and Cao, D. (2014). "Synthesis of double D-A branched organic dyes employing indole and phenoxazine as donors for efficient DSSCs." *Tetrahedron*, *70* (36), 6296-6302.

Hong, Y., Liao, J.-Y., Cao, D., Zang, X., Kuang, D.-B., Wang, L., Meier, H. and Su, C.-Y. (2011). "Organic Dye Bearing Asymmetric Double Donor-π-Acceptor Chains for Dye-Sensitized Solar Cells." *J. Org. Chem.*, *76* (19), 8015-8021.

Horiuchi, T., Miura, H. and Uchida, S. (2003). "Highly-efficient metal-free organic dyes for dye-sensitized solar cells." *Chem. Commun.*, (24), 3036–3037.

Horiuchi, T., Miura, H., Sumioka, K. and Uchida, S. (2004). "High Efficiency of Dye-Sensitized Solar Cells Based on Metal-Free Indoline Dyes." *J. Am. Chem. Soc.*, *126* (39), 12218-12219.

Huang, S.-T., Hsu, Y.-C., Yen, Y.-S., Chou, H.H., Lin, J.T., Chang, C.-W., Hsu, C.-P., Tsai, C. and Yin, D.-J. (2008). "Organic Dyes Containing a Cyanovinyl Entity in the Spacer for Solar Cells Applications." *J. Phys. Chem. C*, *112* (49), 19739-19747.

Hussain, M., Islam, A., Bedja, I., Gupta, R.K., Han, L. and El-Shafei, A. (2014). "A comparative study of Ru(II) cyclometallated complexes versus thiocyanated heteroleptic complexes: thermodynamic force for efficient dye regeneration in dye-sensitized solar cells and how low could it be?" *Phys. Chem. Chem. Phys.*, *16* (28), 14874–14881.

Hwang, S., Lee, J.H., Park, C., Lee, H., Kim, C., Park, C., Lee, M.-H., Lee, W., Park, J., Kim, K., Park, N.-G. and Kim, C. (2007). "A highly efficient organic sensitizer for dye-sensitized solar cells." *Chem. Commun.*, (46), 4887-4889.

Ito, S., Miura, H., Uchida, S., Takata, M., Sumioka, K., Liska, P., Comte, P., Péchy, P. and Grätzel, M. (2008). "High-conversion-efficiency organic dye-sensitized solar cells with a novel indoline dye." *Chem. Commun.*, (41), 5194-5196.

Ito, S., Zakeeruddin, S.M., Humphry-Baker, R., Liska, P., Charvet, R., Comte, P., Nazeeruddin, M.K., Péchy, P., Takata, M., Miura, H., Uchida, S. and Grätzel, M. (2006). "High-Efficiency Organic-Dye- Sensitized Solar Cells Controlled by Nanocrystalline-TiO_2 Electrode Thickness." *Adv. Mater.*, *18* (9), 1202-1205.

Ji, Z., Natu, G. and Wu, Y. (2013). "Cyclometalated Ruthenium Sensitizers Bearing a Triphenylamino Group for p-Type NiO Dye-Sensitized Solar Cells." *ACS Appl. Mater. Interfaces, 5* (17), 8641-8648.

Jose, R., Kumar, A., Thavasi, V. and Ramakrishna, S. (2008). "Conversion efficiency versus sensitizer for electrospun TiO2 nanorod electrodes in dye-sensitized solar cells." *Nanotechnology, 19* (42), 424004.

Jose, R., Kumar, A., Thavasi, V., Fujihara, K., Uchida, S. and Ramakrishna, S. (2008). "Relationship between the molecular orbital structure of the dyes and photocurrent density in the dye-sensitized solar cells." *Appl. Phys. Lett, 93* (2), 023125.

Jung, I., Lee, J.K., Song, K.H., Song, K., Kang, S.O. and Ko, J. (2007). "Synthesis and Photovoltaic Properties of Efficient Organic Dyes Containing the Benzo[b]furan Moiety for Solar Cells." *J. Org. Chem.*, *72* (10), 3652-3658.

Karlsson, K.M., Jiang, X., Eriksson, S.K., Gabrielsson, E., Rensmo, H., Hagfeldt, A. and Sun, L. (2011). "Phenoxazine Dyes for Dye-Sensitized Solar Cells: Relationship Between Molecular Structure and Electron Lifetime." *Chem. Eur. J.*, *17* (23), 6415-6424.

Kern, R., Sastrawan, R., Ferber, J., Stangl, R. and Luther, J. (2002). "Modeling and interpretation of electrical impedance spectra of dye solar cells operated under open-circuit conditions." *Electrochim. Acta, 47* (26), 4213-4225.

Kim, S., Choi, H., Kim, D., Song, K., Kang, S.O. and Ko, J. (2007). "Novel conjugated organic dyes containing bis-dimethylfluorenyl amino phenyl thiophene for efficient solar cell." *Tetrahedron, 63* (37), 9206–9212.

Kim, S., Lee, J.K., Kang, S.O., Ko, J., Yum, J.-H., Fantacci, S., Angelis, F. De, Censo, D. Di, Nazeeruddin, M.K. and Grätzel, M. (2006). "Molecular Engineering of Organic Sensitizers for Solar Cell Applications." *J. Am. Chem. Soc.*, *128* (51), 16701-16707.

Kitamura, T., Ikeda, M., Shigaki, K., Inoue, T., Anderson, N.A., Ai, X., Lian, T. and Yanagida, S. (2004). "Phenyl-Conjugated Oligoene Sensitizers for TiO2 Solar Cells." *Chem. Mater.*, *16* (9), 1806-1812.

Koide, N., Islam, A., Chiba, Y. and Han, L. (2006). "Improvement of efficiency of dye-sensitized solar cells based on analysis of equivalent circuit." *Journal of Photochemistry and Photobiology A: Chemistry, 182* (3), 296–305.

Koops, S.E., O'Regan, B.C., Barnes, P.R.F. and Durrant, J.R. (2009). "Parameters Influencing the Efficiency of Electron Injection in Dye-Sensitized Solar Cells." *J. Am. Chem. Soc., 131* (13), 4808-4818.

Koumura, N., Wang, Z.-S., Mori, S., Miyashita, M., Suzuki, E. and Hara, K. (2006). "Alkyl-Functionalized Organic Dyes for Efficient Molecular Photovoltaics." *J. Am. Chem. Soc., 128* (44), 14256-14257.

Lai, H., Hong, J., Liu, P., Yuan, C., Li, Y. and Fang, Q. (2012). "Multi-carbazole derivatives: new dyes for highly efficient dye-sensitized solar cells." *RSC Adv., 2* (6), 2427-2432.

Lan, C.-M., Wu, H.-P., Pan, T.-Y., Chang, C.-W., Chao, W.-S., Chen, C.-T., Wang, C.-L., Lin, C.-Y. and Diau, E.W.-G. (2012). "Enhanced photovoltaic performance with co-sensitization of porphyrin and an organic dye in dye-sensitized solar cells." *Energy Environ. Sci., 5* (4), 6460-6464.

Lee, C., Yang, W. and Parr, R.G. (1988). "Development of the Colle-Salvetti correlation-energy formula into a functional of the electron density." *Phys. Rev. B, 37* (2), 785-789.

Lee, K., Park, S.W., Ko, M.J., Kim, K. and Park, N.-G. (2009). "Selective positioning of organic dyes in a mesoporous inorganic oxide film." *Nat Mater, 8* (8), 665-671.

Li, G., Liang, M., Wang, H., Sun, Z., Wang, L., Wang, Z. and Xue, S. (2013). "Significant Enhancement of Open-Circuit Voltage in Indoline-Based Dye-Sensitized Solar Cells via Retarding Charge Recombination." *Chem. Mater., 25* (9), 1713-1722.

Li, H., Wu, Y., Geng, Z., Liu, J., Xu, D. and Zhu, W. (2014). "Co-sensitization of benzoxadiazole based D–A–π–A featured sensitizers: compensating light-harvesting and retarding charge recombination." *J. Mater. Chem. A, 2* (35), 14649-14657.

Li, Q., Lu, L., Zhong, C., Shi, J., Huang, Q., Jin, X., Peng, T., Qin, J. and Li, Z. (2009). "New Indole-Based Metal-Free Organic Dyes for Dye-Sensitized Solar Cells." *J. Phys. Chem. B, 113* (44), 14588–14595.

Liang, M., Xu, W., Cai, F., Chen, P., Peng, B., Chen, J. and Li, Z. (2007). "New Triphenylamine-Based Organic Dyes for Efficient Dye-Sensitized Solar Cells." *J. Phys. Chem. C, 111* (11), 4465-4472.

Lin, J.T., Chen, P.-C., Yen, Y.-S., Hsu, Y.-C., Chou, H.-H. and Yeh, M.-C.P. (2009). "Organic Dyes Containing Furan Moiety for High-Performance Dye-Sensitized Solar Cells." *Org. Lett., 11* (1), 97-100.

Liu, B., Liu, Q., You, D., Li, X., Naruta, Y. and Zhu, W. (2012). "Molecular engineering of indoline based organic sensitizers for highly efficient dye-sensitized solar cells." *J. Mater. Chem., 22* (26), 13348-13356.

Liu, W.-H., Wu, I.-C., Lai, C.-H., Lai, C.-H., Chou, P.-T., Li, Y.-T., Chen, C.-L., Hsu, Y.-Y. and Chi, Y. (2008). "Simple organic molecules bearing a 3,4-ethylenedioxythiophene linker for efficient dye-sensitized solar cells." *Chem. Commun.*, (41), 5152-5154.

Lu, X., Feng, Q., Lan, T., Zhou, G. and Wang, Z.-S. (2012). "Molecular Engineering of Quinoxaline-Based Organic Sensitizers for Highly Efficient and Stable Dye-Sensitized Solar Cells." *Chem. Mater., 24* (16), 3179-3187.

Magne, C., Urien, M. and Pauporté, T. (2013). "Enhancement of photovoltaic performances in dye-sensitized solar cells by co-sensitization with metal-free organic dyes." *RSC Adv., 3* (18), 6315-6318.

Mao, J., Guo, F., Ying, W., Wu, W., Li, J. and Hua, J. (2012). "Benzotriazole-Bridged Sensitizers Containing a Furan Moiety for Dye-Sensitized Solar Cells with High Open-Circuit Voltage Performance." *Chem. Asian J., 7* (5), 982-991.

Marszalek, M., Nagane, S., Ichake, A., Humphry-Baker, R., Paul, V., Zakeeruddin, S.M. and Grätzel, M. (2011). "Tuning spectral properties of phenothiazine based donor–π–acceptor dyes for efficient dye-sensitized solar cells." *J. Mater. Chem., 22* (3), 889-894.

Mathew, S., Yella, A., Gao, P., Humphry-Baker, R., Curchod, B.F.E., Ashari-Astani, N., Tavernelli, I., Rothlisberger, U., Nazeeruddin, M.K. and Grätzel, M. (2014). "Dye-sensitized solar cells with 13% efficiency achieved through the molecular engineering of porphyrin sensitizers." *Nat Chem, 6* (3), 242-247.

Meng, F.S., Yao, Q.H., Shen, J.G., Li, F.L., Huang, C.H., Chen, K.C. and Tian, H. (2003). "Novel Cyanine Dyes with Multi-carboxyl Groups and their Sensitization on Nanocrystalline TiO2 Electrode." *Synthetic Metals, 137* (1–3), 1543-1544.

Menzel, R., Ogermann, D., Kupfer, S., Weiß, D., Görls, H., Kleinermanns, K., González, L. and Beckert, R. (2012). "4-Methoxy-1,3-thiazole based donor-acceptor dyes: Characterization, X-ray structure, DFT calculations and test as sensitizers for DSSC." *Dyes Pigments, 94* (3), 512-524.

Mishra, A., Fischer, M.K.R. and Bäuerle, P. (2009). "Metal-Free Organic Dyes for Dye-Sensitized Solar Cells: From Structure: Property Relationships to Design Rules." *Angew. Chem. Int. Ed., 48* (14), 2474-2499.

Mikroyannidis, J.A., Kabanakis, A., Balraju, P. and Sharma, G.D. (2010). "Novel Broadly Absorbing Sensitizers with Cyanovinylene 4-Nitrophenyl Segments and Various Anchoring Groups: Synthesis and Application for High-Efficiency Dye-Sensitized Solar Cells." *J. Phys. Chem. C, 114* (28), 12355–12363.

Nazeeruddin, M. K.; Péchy, P.; Renouard, T.; Zakeeruddin, S. M.; Humphry-Baker, R.; Comte, P.; Liska, P.; Cevey, L.; Costa, E.; Shklover, V.; Spiccia, L.; Deacon, G. B.; Bignozzi, C. A.; Grätzel, M. (2001) "Engineering of Efficient Panchromatic Sensitizers for Nanocrystalline TiO_2-Based Solar Cells. " *J. Am. Chem. Soc.*, 123, 1613-1624.

Nazeeruddin, M. K.; Zakeeruddin, S. M.; Humphry-Baker, R.; Jirousek, M.; Liska, P.; Vlachopoulos, N.; Shklover, V.; Fischer, C.-H.; Grätzel, M. (1999) " Acid−Base Equilibria of (2,2‘-Bipyridyl-4,4‘-dicarboxylic acid)ruthenium(II) Complexes and the Effect of Protonation on Charge-Transfer Sensitization of Nanocrystalline Titania" *Inorg. Chem.*, 38, 6298-6305.

Nazeeruddin, M.K., Humphry-Baker, R., Liska, P. and Grätzel, M. (2003). "Investigation of Sensitizer Adsorption and the Influence of Protons on Current and Voltage of a Dye-Sensitized Nanocrystalline TiO_2 Solar Cell." *J. Phys. Chem. B, 107* (34), 8981-8987.

Nazeeruddin, M.K., Kay, A., Rodicio, I., Humphry-Baker, R., Mueller, E., Liska, P., Vlachopoulos, N. and Graetzel, M. (1993). "Conversion of light to electricity by cis-X2bis(2,2'-bipyridyl-4,4'-dicarboxylate)ruthenium(II) charge-transfer sensitizers (X = Cl-, Br-, I-, CN-, and SCN-) on nanocrystalline titanium dioxide electrodes." *J. Am. Chem. Soc., 115* (14), 6382-6390.

Nazeeruddin, M.K., Péchy, P. and Grätzel, M. (1997). "Efficient panchromatic sensitization of nanocrystallineTiO2 films by a black dye based on atrithiocyanato–ruthenium complex." *Chem. Commun.*, (18), 1705-1706.

Neale, N.R., Kopidakis, N., Lagemaat, J. van de, Grätzel, M. and Frank, A.J. (2005). "Effect of a Coadsorbent on the Performance of Dye-Sensitized TiO2 Solar Cells: Shielding versus Band-Edge Movement." *J. Phys. Chem. B, 109* (49), 23183-23189.

Ning, Z. and Tian, H. (2009). "Triarylamine: a promising core unit for efficient photovoltaic materials." *Chem. Commun.*, (37), 5483-5495.

Ning, Z., Fu, Y. and Tian, H. (2010). "Improvement of dye-sensitized solar cells: what we know and what we need to know." *Energy Environ. Sci., 3* (9), 1170-1181.

Ning, Z., Zhang, Q., Wu, W., Pei, H., Liu, B. and Tian, H. (2008). "Starburst Triarylamine Based Dyes for Efficient Dye-Sensitized Solar Cells." *J. Org. Chem., 73* (10), 3791-3797.

Numata, Y., Islam, A., Chen, H. and Han, L. (2012). "Aggregation-free branch-type organic dye with a twisted molecular architecture for dye-sensitized solar cells." *Energy Environ. Sci., 5* (9), 8548-8552.

O'Regan, B. and Grätzel, M. (1991). "A low-cost, high-efficiency solar cell based on dye-sensitized colloidal TiO2 films." *Nature, 353* (6346), 737-740.

Oskam, G., Bergeron, B.V., Meyer, G.J. and Searson, P.C. (2001). "Pseudohalogens for Dye-Sensitized TiO_2 Photoelectrochemical Cells." *J. Phys. Chem. B, 105* (29), 6867-6873.

Park, S.S., Won, Y.S., Choi, Y.C. and Kim, J.H. (2009). "Molecular Design of Organic Dyes with Double Electron Acceptor for Dye-Sensitized Solar Cell." *Energy Fuels*, *23* (7), 3732-3736.

Peach, M.J.G., Benfield, P., Helgaker, T. and Tozer, D.J. (2008). "Excitation energies in density functional theory: An evaluation and a diagnostic test." *The Journal of Chemical Physics*, *128* (4), 044118.

Pei, K., Wu, Y., Islam, A., Zhang, Q., Han, L., Tian, H. and Zhu, W. (2013). "Constructing High-Efficiency D-A-π-A Featured Solar Cell Sensitizers: a Promising Building Block of 2,3-Diphenylquinoxaline for Antiaggregation and Photostability." *ACS Appl. Mater. Interfaces*, *5* (11), 4986-4995.

Perdew, J.P. (1986). "Erratum: Density-functional approximation for the correlation energy of the inhomogeneous electron gas." *Phys. Rev. B*, *34* (10), 7406-7406.

Qu, P. and Meyer, G.J. (2001). "Proton-Controlled Electron Injection from Molecular Excited States to the Empty States in Nanocrystalline TiO2." *Langmuir*, *17* (21), 6720-6728.

Qu, S., Wang, B., Guo, F., Li, J., Wu, W., Kong, C., Long, Y. and Hua, J. (2012). "New diketo-pyrrolo-pyrrole (DPP) sensitizer containing a furan moiety for efficient and stable dye-sensitized solar cells." *Dyes and Pigments*, *92* (3), 1384-1393.

Ren, X., Jiang, S., Cha, M., Zhou, G. and Wang, Z.-S. (2012). "Thiophene-Bridged Double D-π-A Dye for Efficient Dye-Sensitized Solar Cell." *Chem. Mat.*, *24* (17), 3493-3499.

Schäfer, A., Huber, C. and Ahlrichs, R. (1994). "Fully optimized contracted Gaussian basis sets of triple zeta valence quality for atoms Li to Kr." *J. Chem. Phys.*, *100* (8), 5829-5835.

Sharma, G.D., Patel, K.R., Roy, M.S. and Misra, R. (2014). "Characterization of two new $(A–\pi)_2–D–A$ type dyes with different central D unit and their application for dye sensitized solar cells." *Organic Electronics*, *15* (8), 1780–1790.

Sharma, G.D., Reddy, M.A., Ganesh, K., Singh, S.P. and Chandrasekharam, M. (2013). "Indole and triisopropyl phenyl as capping units for a diketopyrrolopyrrole (DPP) acceptor central unit: an efficient D–A–D type small molecule for organic solar cells." *RSC Adv.*, *4* (2), 732-742.

Shi, D., Cao, Y., Pootrakulchote, N., Yi, Z., Xu, M., Zakeeruddin, S.M., Grätzel, M. and Wang, P. (2008). "New Organic Sensitizer for Stable Dye-Sensitized Solar Cells with Solvent-Free Ionic Liquid Electrolytes." *J. Phys. Chem. C*, *112* (44), 17478-17485.

Shi, J., Chen, J., Chai, Z., Wang, H., Tang, R., Fan, K., Wu, M., Han, H., Qin, J., Peng, T., Li, Q. and Li, Z. (2012). "High performance organic sensitizers based on 11,12-bis(hexyloxy) dibenzo[a,c]phenazine for dye-sensitized solar cells." *J. Mater. Chem.*, *22* (36), 18830-18838.

Sirimanne, P.M. and Tributsch, H. (2004). "Parameters determining efficiency and degradation of TiO2|dye|CuI solar cells." *Journal of Solid State Chemistry*, *177* (6), 1789-1795.

Sirohi, R., Kim, D.H., Yu, S.-C. and Lee, S.H. (2012). "Novel di-anchoring dye for DSSC by bridging of two mono anchoring dye molecules: A conformational approach to reduce aggregation." *Dyes Pigments*, *92* (3), 1132-1137.

Takechi, K., Kamat, P.V., Avirah, R.R., Jyothish, K. and Ramaiah, D. (2008). "Harvesting Infrared Photons with Croconate Dyes." *Chem. Mater.*, *20* (1), 265-272.

Tang, J., Hua, J., Wu, W., Li, J., Jin, Z., Long, Y. and Tian, H. (2010). "New starburst sensitizer with carbazole antennas for efficient and stable dye-sensitized solar cells." *Energy Environ. Sci.*, *3* (11), 1736-1745.
Tang, J., Hua, J., Wu, W., Li, J., Jin, Z., Long, Y. and Tian, H. (2010). "New starburst sensitizer with carbazole antennas for efficient and stable dye-sensitized solar cells." *Energy Environ. Sci.*, *3* (11), 1736-1745.

Tefashe UM, Rudolph M, Miura H, Schlettwein D, Wittstock G. 2012." Photovoltaic characteristics and dye regeneration kinetics in D149-sensitized ZnO with varied dye loading and film thickness". *Phys Chem Chem Phys*; 14: 7533-42.

Tian, H., Yang, X., Chen, R., Pan, Y., Li, L., Hagfeldt, A. and Sun, L. (2007). "Phenothiazine derivatives for efficient organic dye-sensitized solar cells." *Chem. Commun.*, (36), 3741-3743.

Tian, H., Yang, X., Chen, R., Zhang, R., Hagfeldt, A. and Sun, L. (2008). "Effect of Different Dye Baths and Dye-Structures on the Performance of Dye-Sensitized Solar Cells Based on Triphenylamine Dyes." *J. Phys. Chem. C, 112* (29), 11023-11033.

Tsao, M.-H., Wu, T.-Y., Wang, H.-P., Sun, I.-W., Su, S.-G., Lin, Y.-C. and Chang, C.-W. (2011). "An efficient metal-free sensitizer for dye-sensitized solar cells." *Materials Letters, 65* (3), 583-586.

Wan, Z., Jia, C., Zhang, J., Duan, Y., Lin, Y. and Shi, Y. (2012). "Triphenylamine-based starburst dyes with carbazole and phenothiazine antennas for dye-sensitized solar cells." *Journal of Power Sources, 199* 426-431.

Wang, Q., Moser, J.-E. and Grätzel, M. (2005). "Electrochemical Impedance Spectroscopic Analysis of Dye-Sensitized Solar Cells." *J. Phys. Chem. B, 109* (31), 14945-14953.

Wang, Y., Chen, B., Wu, W., Li, X., Zhu, W., Tian, H. and Xie, Y. (2014). "Efficient Solar Cells Sensitized by Porphyrins with an Extended Conjugation Framework and a Carbazole Donor: From Molecular Design to Cosensitization." *Angew. Chem., 126* (40), 10955-10959.

Wang, Z.-S., Cui, Y., Dan-oh Yasufumi, Kasada, C., Shinpo, A. and Hara, K. (2007). "Thiophene-Functionalized Coumarin Dye for Efficient Dye-Sensitized Solar Cells: Electron Lifetime Improved by Coadsorption of Deoxycholic Acid." *J. Phys. Chem. C, 111* (19), 7224-7230.

Wang, Z.-S., Cui, Y., Hara, K., Dan-oh Y., Kasada, C. and Shinpo, A. (2007). "A High-Light-Harvesting-Efficiency Coumarin Dye for Stable Dye-Sensitized Solar Cells." *Adv. Mater., 19* (8), 1138-1141.

Wang, Z.-S., Koumura, N., Cui, Y., Takahashi, M., Sekiguchi, H., Mori, A., Kubo, T., Furube, A. and Hara, K. (2008). "Hexylthiophene-Functionalized Carbazole Dyes for Efficient Molecular Photovoltaics: Tuning of Solar-Cell Performance by Structural Modification." *Chem. Mater., 20* (12), 3993-4003.

Wu, G., Swaminathan, V., Mitra, S. and Kumar, R. (2014). Online video session progress prediction using low-rank matrix completion. In 2014 IEEE International Conference on Multimedia and Expo Workshops (ICMEW), pp 1-6.

Wu, Y., Marszalek, M., Zakeeruddin, S.M., Zhang, Q., Tian, H., Grätzel, M. and Zhu, W. (2012). "High-conversion-efficiency organic dye-sensitized solar cells: molecular engineering on D–A–π-A featured organic indoline dyes." *Energy Environ. Sci., 5* (8), 8261-8272.

Xu, W., Peng, B., Chen, J., Liang, M. and Cai, F. (2008). "New Triphenylamine-Based Dyes for Dye-Sensitized Solar Cells." *J. Phys. Chem. C, 112* (3), 874-880.

Yang, C.-J., Chang, Y.J., Watanabe, M., Hon, Y.-S. and Chow, T.J. (2012). "Phenothiazine derivatives as organic sensitizers for highly efficient dye-sensitized solar cells." *J. Mater. Chem., 22* (9), 4040-4049.

Yella, A., Lee, H.-W., Tsao, H.N., Yi, C., Chandiran, A.K., Nazeeruddin, M.K., Diau, E.W.-G., Yeh, C.-Y., Zakeeruddin, S.M. and Grätzel, M. (2011). "Porphyrin-Sensitized Solar Cells with Cobalt (II/III)–Based Redox Electrolyte Exceed 12 Percent Efficiency." *Science, 334* (6056), 629-634.

Zhang, M., Liu, J., Wang, Y., Zhou, D. and Wang, P. (2011). "Redox couple related influences of π-conjugation extension in organic dye-sensitized mesoscopic solar cells." *Chem. Sci., 2* (7), 1401-1406.

Zhang, X.-H., Cui, Y., Katoh, R., Koumura, N. and Hara, K. (2010). "Organic Dyes

Containing Thieno[3,2-b]indole Donor for Efficient Dye-Sensitized Solar Cells." *J. Phys. Chem. C, 114* (42), 18283-18290.

Zhu, W., Wu, Y., Wang, S., Li, W., Li, X., Chen, J., Wang, Z. and Tian, H. (2011). "Organic D-A-π-A Solar Cell Sensitizers with Improved Stability and Spectral Response." *Adv. Funct. Mater., 21* (4), 756-763.

List of publications

Papers published / communicated to international journals

[1] **Dickson D. Babu**, Gachumale, S.R., Anandan, S. and Adhikari, A.V. (2015). "New D-π-A type indole based chromogens for DSSC: Design, synthesis and performance studies." *Dyes and Pigments, 112* 183–191.

(**Ranked 4th among 25 hottest articles published by the journal of "*Dyes and Pigments*" between July-September 2014)**.

[2] **Dickson D. Babu**, Adhikari, A.V., "Molecular Engineering and Theoretical Investigation of Metal-Free Organic Chromophores for Dye-Sensitized Solar Cells." *Advanced Science Letters*, **In press**.

[3] **Dickson D. Babu**, Cheema, H., Elsherbiny, D., El-Shafei, A. and Adhikari, A.V. (2015). "Molecular Engineering and Theoretical Investigation of Novel Metal-Free Organic Chromophores for Dye-Sensitized Solar Cells." *Electrochimica Acta, 176* 868–879.

[4] **Dickson D. Babu**, Elsherbiny, D., Cheema, H., El-Shafei, A. and Adhikari, A.V. (2015). "Highly Efficient Panchromatic Dye-Sensitized Solar Cells: Synergistic Interaction of Ruthenium Sensitizer with Novel Co-sensitizers Carrying Different Acceptor Units." Revised manuscript submitted to *Journal of Power Sources*.

[5] **Dickson D. Babu**, Su, R., El-Shafei, A. and Adhikari, A.V. (2016). "From Molecular Design to Co-sensitization; High performance novel photosensitizers for dye-sensitized solar cells.'' Revised manuscript submitted to *Electrochimica Acta*.

[6] **Dickson D. Babu**, Su, R., El-Shafei, A. and Adhikari, A.V. (2016). "New indole based co-sensitizers for dye sensitized solar cells exceeding 10% efficiency.'' Communicated to *RSC Advances.*

[7] **Dickson D. Babu**, Su, R., El-Shafei, A. and Adhikari, A.V. (2016). "Synthesis and photovoltaic performance of a novel asymmetric dual-channel co-sensitizer for dye-sensitized solar cell exceeding 10% efficiency'' Communicated to *New Journal of Chemistry (RSC).*

Research papers presented in conferences

[1] **Dickson D. Babu**, Airody Vasudeva Adhikari, ‘’Design and Synthesis of Metal-Free Organic Chromophores for Dye-Sensitized Solar Cells’’. ***International Conference on Advanced Functional materials (ICAFM-2014)***. CSIR-National Institute for Interdisciplinary Science and Technology (NIIST), Thiruvananthapuram, Kerala, India. February 19-21, 2014.

[2] **Dickson D. Babu**, Airody Vasudeva Adhikari, “Molecular Engineering and Theoretical Investigation of Metal-Free Organic Chromophores for Dye-Sensitized Solar Cells.” ***Emerging Materials: Characterization & Application-2014 (EMCA-2014)***, CSIR-Central Glass & Ceramic Research Institute, Kolkata, December 4-6, 2014.

[3] **Dickson D. Babu**, Airody Vasudeva Adhikari, “Novel D-π-A Organic Dyes for Highly Efficient Dye-Sensitized Solar Cells. **Advanced Materials for Energy and Environmental Applications *(*AMEEA-2015*)***, Bharathiar University, Coimbatore, March 18-20, 2015. (***Honored with Best poster Presentation award)***.

[4] **Dickson D. Babu**, Airody Vasudeva Adhikari, “Synthesis and DFT Studies of New *n*-type Dyes for Dye-Sensitized Solar Cells.’’ ***Nascent Developments in Chemical Sciences: Opportunities for Academia-Industry Collaboration (NDCS-2015)***, Birla Institute of Technology and Science, Pilani, Rajasthan, October 16-18, 2015.

[5] **Dickson D. Babu**, Adhikari, A. V. “High performance organic photosensitizers for dye-sensitized solar cells”. A **Paper** Presented at the **International Conference on Advances in Chemical Engineering (ICACE-2015),** NITK, Surathkal, December 20-22, 2015.

[6] **Dickson D. Babu,** Adhikari, A. V. “Tailor-Made Co-adsorbents for Highly Efficient DyeSensitized Solar Cells”. A **Paper** Presented at the **National Conference on Recent Trends In Chemical Sciences** (**NCRTCS-2016**) MIT, Manipal, January 11-12, 2016.

Dickson D. Babu

PhD. Research Scholar
Department of Chemistry
National Institute of Technology, Karnataka
Surathkal, Mangalore-575 025, India.

Residential Address: Agarsen Nagar
Plot no. E-44-A
Churu, Rajasthan -331001

PERSONAL

Name	:	**Dickson D. Babu**
Age & Date of Birth	:	26 years; June 29, 1989
Mobile	:	+91 7795531415
Email	:	dickson.babu@yahoo.com

RESEARCH EXPERIENCE

1. **Research Fellow:** Department of Chemistry, National Institute of Technology Karnataka, Surathkal, Mangalore 575025, India. ***July 2012 - till date***.

   Advisor: Prof. Airody Vasudeva Adhikari

2. **Visiting Research Fellow:** CSIR-National Institute for Intersdisciplinary Science and Technology (CSIR-NIIST), Trivandrum, Kerala, India. ***May-July 2015.***

   Advisor: Dr. Joshy Joseph

3. **Project Assistant:** Apotex Pharmachem India Pvt. Ltd., Bangalore, India, ***December 2011.***

   Advisor: Dr. Anitha Varghese

Area of Specialization:

1. Design and development of organic sensitizers for dye sensitized solar cells
2. Synthetic organic chemistry
3. Structural characterization of compounds.

Achievements:

1. **University topper** in MSc. Chemistry (**Gold medalist**).
2. **Topper in BSc.** with **92.16%** in chemistry.

3. **100%** marks in Organic Chemistry in BSc.

4. CGPA of **9.54** in PhD. Course work.

5. Guided **four** M.Sc. and **one** M.Tech students in order to complete PG project.

Summary of Publications:

(i)	Research papers (in journals)	:	3
(ii)	Research papers (in symposia)	:	9

List of Publications:

1. **Dickson D. Babu**, Gachumale, S. R., Anandan, S., & Adhikari, A. V. "New D-π-A type indole based chromogens for DSSC: Design, synthesis and performance studies.'' *Dyes and Pigments*, **2014**, *112*, 183–191 **(Ranked 4th among 25 hottest articles published by the journal of "*Dyes and Pigments*" between July-September 2014).**
2. **Dickson D. Babu**, Cheema, H., Elsherbiny, D., El-Shafei, A., & Adhikari, A. V. "Molecular Engineering and Theoretical Investigation of Novel Metal-Free Organic Chromophores for Dye-Sensitized Solar Cells." *Electrochimica Acta*, **2015**, *176*, 868–879.
3. **Dickson D. Babu**, & Adhikari, A. V. "Molecular Engineering and Theoretical Investigation of Metal-Free Organic Chromophores for Dye-Sensitized Solar Cells." *Advanced Science Letters*, 2015, **Accepted manuscript.**
4. **Dickson D. Babu**, Elsherbiny, D., Cheema, H., El-Shafei, A. and Adhikari, A.V. (2015). "Highly Efficient Panchromatic Dye-Sensitized Solar Cells: Synergistic Interaction of Ruthenium Sensitizer with Novel Co-sensitizers Carrying Different Acceptor Units." Revised manuscript submitted to *Journal of Power Sources*.
5. **Dickson D. Babu**, Su, R., El-Shafei, A. and Adhikari, A.V. (2016). "From Molecular Design to Co-sensitization; High performance novel photosensitizers for dye-sensitized solar cells.'' Revised manuscript submitted to *Electrochimica Acta*.
6. **Dickson D. Babu**, Su, R., El-Shafei, A. and Adhikari, A.V. (2016). "New indole based co-sensitizers for dye sensitized solar cells exceeding 10% efficiency.'' Communicated to *RSC Advances.*
7. **Dickson D. Babu**, Su, R., El-Shafei, A. and Adhikari, A.V. (2016). "Synthesis and photovoltaic performance of a novel asymmetric dual-channel co-sensitizer for dye-sensitized solar cell exceeding 10% efficiency'' Communicated to *New Journal of Chemistry (RSC).*

Papers/Posters Presented in National and International Conferences:

1. **Dickson D. Babu**, Airody Vasudeva Adhikari, "Design and Synthesis of Metal-Free Organic Chromophores for Dye-Sensitized Solar Cells''. ***International Conference***

on Advanced Functional materials (ICAFM-2014). CSIR-National Institute for Interdisciplinary Science and Technology (NIIST), Thiruvananthapuram, Kerala, India. February 19-21, 2014.

2. **Dickson D. Babu**, Airody Vasudeva Adhikari, "Molecular Engineering and Theoretical Investigation of Metal-Free Organic Chromophores for Dye-Sensitized Solar Cells." ***Emerging Materials: Characterization & Application-2014 (EMCA-2014)***, CSIR-Central Glass & Ceramic Research Institute, Kolkata, December 4-6, 2014.

3. **Dickson D. Babu**, Airody Vasudeva Adhikari, "Novel D-π-A Organic Dyes for Highly Efficient Dye-Sensitized Solar Cells." **Advanced Materials for Energy and Environmental Applications *(*AMEEA-2015*)***, Bharathiar University, Coimbatore, March 18-20, 2015. (***Honored with Best poster Presentation award)***.

4. **Dickson D. Babu**, Airody Vasudeva Adhikari, "Synthesis and DFT Studies of New *n*-type Dyes for Dye-Sensitized Solar Cells.'' ***Nascent Developments in Chemical Sciences: Opportunities for Academia-Industry Collaboration (NDCS-2015)***, Birla Institute of Technology and Science, Pilani, Rajasthan, October 16-18, 2015.

5. **Dickson D. Babu**, Adhikari, A. V. "High performance organic photosensitizers for dye-sensitized solar cells". A **Paper** Presented at the **International Conference on Advances in Chemical Engineering (ICACE-2015),** NITK, Surathkal, December 20-22, 2015.

6. **Dickson D. Babu**, Adhikari, A. V. "Tailor-Made Co-adsorbents for Highly Efficient Dye Sensitized Solar Cells". A **Paper** Presented at the **National Conference on Recent Trends In Chemical Sciences** (**NCRTCS-2016**) MIT, Manipal, January 11-12, 2016.

7. Naik, P., **Dickson D. Babu** & Adhikari, A. V. "Design, Synthesis and Computational Modelling Of a New Metal-Free Organic Chromophore for Dye-Sensitized Solar Cell Application." A **Poster** Presented at the **National Conference on Recent Trends In Chemical Sciences** (**NCRTCS-2016**) MIT, Manipal, January 11-12, 2016.

8. Naik, P., **Dickson D. Babu** & Adhikari, A. V. "Design and Synthesis of new Metal-Free Organic Chromophores for Dye-Sensitized Solar Cell application". A **Poster** Presented at the **International Conference on Advances in Chemical Engineering (ICACE-2015),** NITK, Surathkal, December 20-22, 2015.

9. Naik, P., **Dickson D. Babu** & Adhikari, A. V. "Design and Synthesis of new Metal-Free Organic Chromophores for Dye-Sensitized Solar Cell application". A **Poster** Presented at the ***10th Mid-Year CSRI* symposium in chemistry.** National Institute of Technology, Trichy, India, July 23-25, 2015.

Academic Background:

Course	Subjects	Board / University	Year of passing	Percentage
M.Sc (CHEMISTRY)	Chemistry	Christ University, Bangalore	2012	**82.32%**
B.Sc (CHEMISTRY)	Chemistry (Main), Physics & Mathematics	Mahatma Gandhi University, Kottayam	2010	**87.1%**

RESEARCH SKILLS

Analytical skills

(i) Synthesis and characterization of organic molecules. Good at handling Schlenk line and using glove box techniques.

(ii) Study of photophysical properties of organic molecules using steady-state and time-resolved techniques.

(iii) Experience in working with and maintaining various types of equipments including time correlated single photon counting system (TCSPC), fluorescence spectrophotometers, UV-Visible-NIR spectrophotometer, cyclic voltammeter (CV), TG and DSC measurements.

(iv) Handling and working with single crystal x-ray diffraction (SCXRD) instrument. Solving structures of Varity of organic and inorganic compounds.

(v) DFT calculations using TURBOMOLE (powerful Quantum Chemistry program package), X'.

Computer skills:

Adapt knowledge in using various computer programs such as MS Office Programs, Chem-Draw, Origin, End-Note and Turbomole Molecular Calculation Software.

Languages: Fluent in English, Hindi and Malayalam.